BERICHTE
aus dem Fachbereich Geowissenschaften
der Universität Bremen

No. 266

Bohrmann, G., A. Bahr, F. Brinkmann, M. Brüning, S. Buhmann, V. Diekamp, K. Enneking, D. Fischer, A. Gassner, G. von Halem, D. Huettich, S. Kasten, S. Klapp, M. Nasir, N. Nowald, W.-T. Ochsenhirt, T. Pape, V. Ratmeyer, R. Rehage, J. Rethemeyer, M. Reuter, P. Rossel, M. Saleem, W. Schmidt, C. Seiter, S. Stephan, K. Thomanek, N. Wittenberg, M. Yoshinaga, K. Zonnefeld

REPORT AND PRELIMINARY RESULTS OF R/V METEOR CRUISE M74/3, FUJAIRAH - MALE, 30 OCTOBER - 28 NOVEMBER, 2007. COLD SEEPS OF THE MAKRAN SUBDUCTION ZONE (CONTINENTAL MARGIN OF PAKISTAN).

Berichte, Fachbereich Geowissenschaften, Universität Bremen, No. 266, 161 pages, Bremen 2008

ISSN 0931-0800

The "Berichte aus dem Fachbereich Geowissenschaften" are produced at irregular intervals by the Department of Geosciences, Bremen University.

They serve for the publication of experimental works, Ph.D.-theses and scientific contributions made by members of the department.

Reports can be ordered from:

Monika Bachur

Forschungszentrum Ozeanränder, RCOM

Universität Bremen

Postfach 330 440

D 28334 BREMEN

Phone: (49) 421 218-65516

Fax: (49) 421 218-65515

e-mail: MBachur@uni-bremen.de

http://elib3.suub.uni-bremen.de/publications/diss/html

Citation:
Bohrmann, G., and cruise participants
Report and preliminary results of R/V Meteor Cruise M74/3, Fujairah – Male, 30 October - 28 November, 2007.
Cold Seeps of the Makran Subduction Zone (Continental Margin of Pakistan).
Berichte, Fachbereich Geowissenschaften, Universität Bremen, No. 266, 161 pages. Bremen, 2008.

ISSN 0931-0800

R/V METEOR
Cruise Report M74/3

Cold Seeps of the Makran Subduction Zone (Continental Margin of Pakistan)

M74, Leg 3
Fujairah – Male
30 October – 28 November, 2007

Cruise within the framework of the DFG financed Research Center Ocean Margins, project area E: "Fluid and gas seepage at ocean margins"

Edited by
Gerhard Bohrmann and Greta Ohling
with contributions of cruise participants

The cruise was performed by
MARUM Center for Marine Environmental Sciences

Universität Bremen

marum

R/V METEOR Cruise Report M74/3

Table of contents

Preface

R/V METEOR Cruise M74/3 investigated fluid venting at the sea floor along the Makran subduction zone (Continental slope of Pakistan). The expedition was strongly related to the previous cruise of METEOR M74/2, during which geophysical investigations on fluid seepage were conducted in the same area. Both cruises were planned together as part of research area E of the DFG Research Center Ocean Margins at the University of Bremen (RCOM). Fluid and gas seepage (cold seeps) at the sea floor is of global importance and leads to a major material exchange between sediments of the ocean, the hydrosphere and/or the atmosphere. Scientists from RCOM are currently working on various types of cold seeps to understand the mechanisms of fluid and gas exchange as well as to measure and estimate the amount of sea floor emissions and to learn about the influence of emissions to the environment.

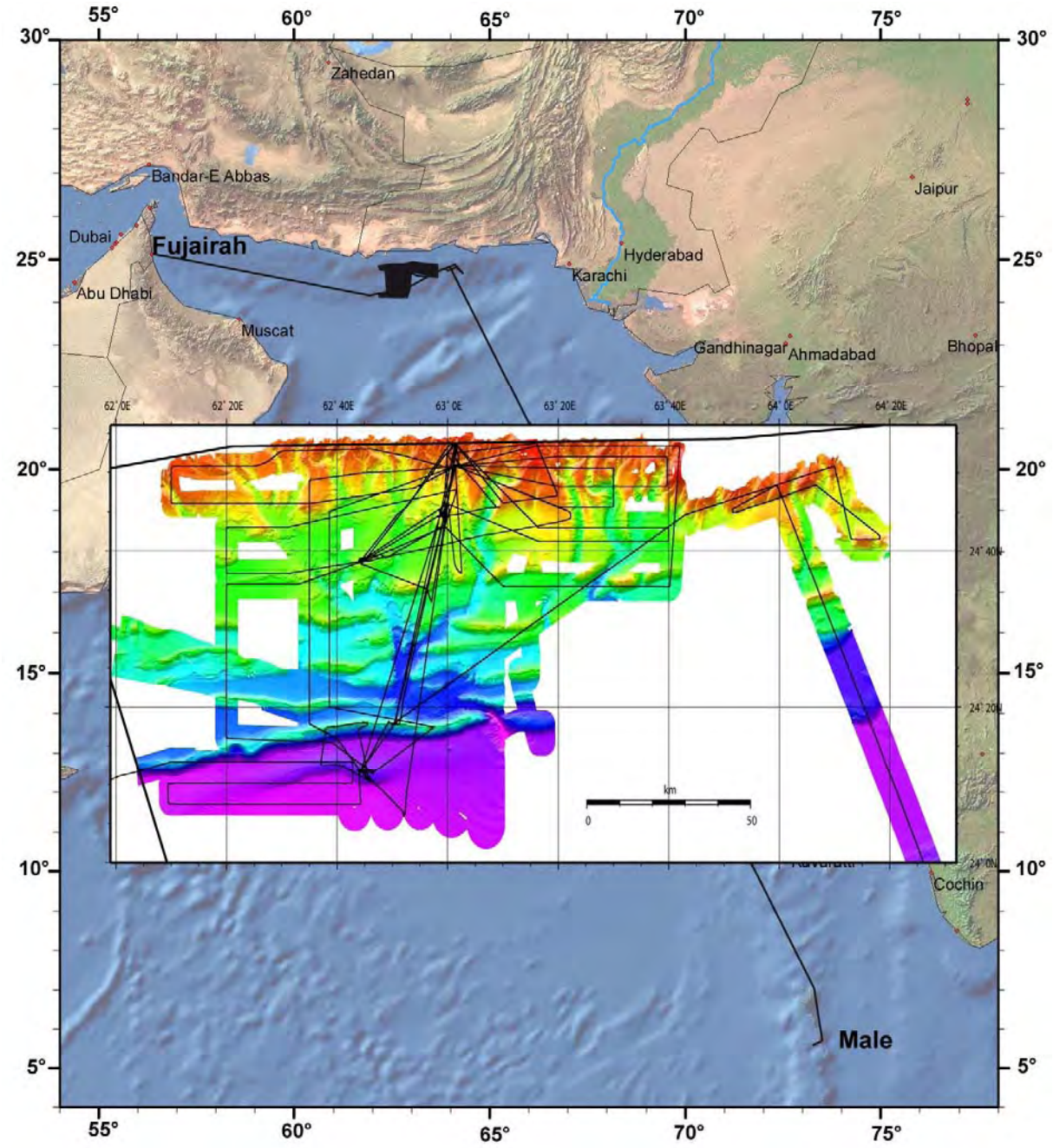

Fig. 1: Cruise track of R/V METEOR Cruise M74/3 starting in Fujairah (United Arab Emirates) sailing to Male (Maldives).

RCOM scientists had been limited so far to the study of the cold seeps at passive margin sites in the Gulf of Mexico, in the Mediterranean and the Niger deep sea fan. During this cruise research activities for the first time took place at an active margin where fluid and gas circulation by dewatering of sediments is characterized by the compression tectonic regime of the plate convergence. Thus in the investigation area the Arabic plate, and/or a micro plate is pushing against the continental slope of Pakistan, whereby very thick sediments in the collision zone are squeezed and should produce an intensive fluid and gas circulation within the accretionary wedge. R/V Meteor Cruise M74/3 brought together interdisciplinary groups from RCOM Research Areas B and E.

Fig. 2: Research vessel METEOR in the northern Indian Ocean (left). Preparation of ROV QUEST on the working deck; in the heat of the day parts of the ROV have been protected from direct sun light (right).

The cruise and the research programs were planned, coordinated and carried out by the Department of Earth Sciences and the MARUM Center for Marine Environmental Sciences of the University of Bremen. The National Institute of Oceanography of Pakistan NIO and the Office of Hydrographer of Pakistan Navy HPN helped in preparing the cruise and are involved in the scientific analyses and interpretation of the data.

Fig. 3: Important equipment for work within the oxygen minimum zone of the Arabic sea. Water sampling by hydro casts (left); fast treatment in the sediment laboratory is needed because of the rapid hydrate decomposition (right).

The German Embassy in Islamabad and the Ministry of Foreign Affairs in Berlin helped in obtaining the permission necessary to work within the EEZ of Pakistan. Thanks to all of them.

The cruise was financed in Germany by the German Research Foundation (DFG). The shipping operator (Reederei F. Laeisz GmbH, Bremerhaven) provided technical support on the vessel in order to accommodate the large variety of technical challenges required for the complex sea-going operations. We would like to especially acknowledge the master of the vessel, Walter Baschek, and his crew for the continued contribution to a pleasant and professional atmosphere aboard R/V METEOR.

Personnel aboard R/V METEOR M74/3

Table 1: Scientific crew.

Name	Working group	Affiliation
Gerhard Bohrmann	Chief scientist	RCOM
André Bahr	Sediments	RCOM
Florian Brinkmann	Carbonates	RCOM
Markus Brüning	Sidescan sonar	RCOM
Sitta Buhmann	ROV QUEST	MARUM
Volker Diekamp	Coring devices	RCOM
Karsten Enneking	Pore water	GeoB
David Fischer	Pore water	AWI
André Gassner	Pore water	RCOM
Gregor von Halem	GIS Mapping	RCOM
Daniel Huettich	ROV QUEST	MARUM
Sabine Kasten	Pore water	AWI
Stephan Klapp	Hydrates	RCOM
Muhammad Nasir	Observer	NIO
Nicolas Nowald	ROV QUEST	MARUM
Wolf-Thilo Ochsenhirt	Meteorology	DWD
Thomas Pape	Gas analyses	RCOM
Volker Ratmeyer	ROV QUEST	MARUM
Ralf Rehage	ROV QUEST	MARUM
Janet Rethemeyer	Biogeochemistry	RCOM
Michael Reuter	ROV QUEST	MARUM
Pamela Rossel	Biochemistry	RCOM
Monawwar Saleem	Lt. Commander	HPN
Werner Schmidt	ROV QUEST	MARUM
Christian Seiter	ROV QUEST	MARUM
Sebastian Stephan	Heat flow	GeoB
Kim Thomanek	Bubblemeter	HBVH
Nina Wittenberg	PARASOUND/bath.	GeoB
Marcos Yoshinaga	Biogeochemistry	RCOM
Karin Zonnefeld	Biochemistry	RCOM

Participating Institutions

AWI	Alfred-Wegener-Institut für Polar- und Meeresforschung, 27570 Bremerhaven, **Germany**
DWD	Deutscher Wetterdienst, Geschäftsfeld Seeschifffahrt, Bernhard-Nocht-Straße 76, 20359 Hamburg, **Germany**
GeoB	Fachbereich Geowissenschaften, University of Bremen, Klagenfurter Str., 28359 Bremen, **Germany**
HBHV	Hochschule Bremerhaven, An der Karlstadt 8, 27568 Bremerhaven, **Germany**
MPI	Max-Planck Institut für Marine Mikrobiologie, Celsiusstr. 1, 28359 Bremen, **Germany**
HPN	Office of Hydrographer of Pakistan Navy II, Liaquat Barracks, Karachi, **Pakistan**
NIO	National Institute of Oceanography, St 47, Block 1, Clifton, Karachi-75600, **Pakistan**
NOC	National Oceanographic Centre, University of Southampton, Waterfront Campus, European Way, Southampton SO14 3ZH, **UK**
RCOM	DFG-Forschungszentrum Ozeanränder University of Bremen, P.O.Box 30440, 28334 Bremen, **Germany**

Fig. 4: Scientists, technicians, and guests sailed during R/V METEOR Cruise M74/3.

Table 2: Crew members onboard R/V METEOR

Name	Work onboard	Name	Work onboard
Walter Baschek	Master	Günter Stängl	Seaman
Uwe-Klaus Klimeck	Ch-mate	Günther Ventz	Seaman
Jörg Suhnel	2nd Officer	Marco Tontsch	Seaman
Stefan Räbisch	2nd Officer	Andreas Gulich	Seaman
Klaus Rathnow	Doctor	Carsten Heitmann	Motorman
Peter Neumann	Chief Engineer	Jens Köhler	Motorman
Uwe Schade	2nd Engineer	Frank Sebastian	Motorman
Ralf Heitzer	2nd Engineer	Franz Grün	Chief Cook
Heinz Wentzel	Chief Electrician	Willy Braatz	2nd Cook
Michael Reiber	Electrician	Michael Booth	Chief Steward
Harry Schulz	Electr. Engineer	Peter Eller	2nd Steward
Katja Pfeiffer	System Manager	Irina Wartenberg	2nd Steward
Werner Sosnowski	Fitter	Seng Choon Ong	Laundryman
Peter Hadamek	Bosun	René Schroeter	Appr.
Pjotr Bussmann	Seaman	Nikolas Wöckner	Appr.
Bernd Neitzsch	Seaman	Matthias Klumb	Trainee
Eberhard Weiß	Seaman	Hartmut Bosch	Trainee

Participating Companies

Reederei F. Laeisz GmbH	"Haus der Schifffahrt", Lange Str. 1a, D-18055 Rostock, **Germany**

1 Introduction and Geological Background

1.1 Geology of the Makran Accretionary Wedge

(M. Saleem and M. Iqbal Nasir)

The accretionary wedge of the Makran subduction zone is one of the largest on earth and is forming at the plate boundary between the Eurasian Plate in the north to the Arabian Plate in the south. The Arabian plate is subducting at an angle of <2° and with a rate of 3-5 cm/a towards north under the Eurasian Plate. This subducting process is ongoing and active at least since Cretaceous times (DeJong, 1982). The Makran accretionary wedge developed throughout the Cenozoic period and its sequence was mainly influenced by Himalayan turbidites (Harms et al., 1984). Terrestrial sediment input created a sediment of thickness >7 km above the oceanic basement (White 1982).

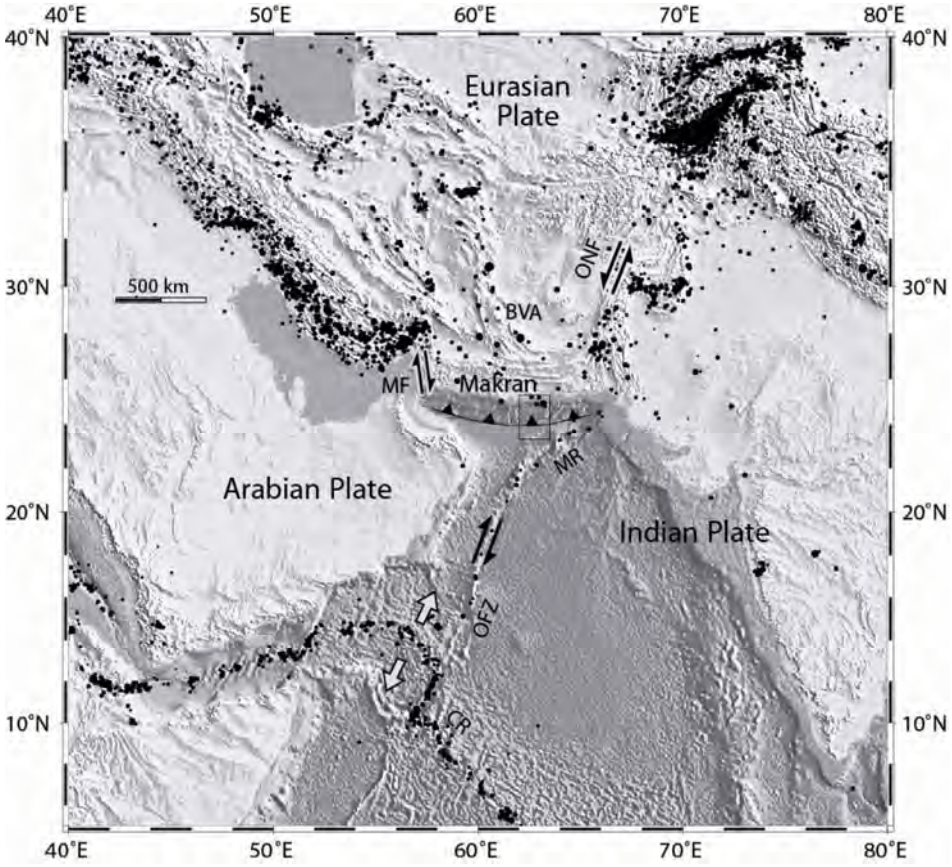

Fig. 5: Plate tectonic setting of the Arabian sea (from Kopp et al. 2000). Compared to surrounding plate boundaries, the Makran subduction is characterised by sparse earthquake activity (black dots). MF = Minab Fault system, MR = Murray Ridge, BVA = Baluchistan volcanic arc, ONF = Ornach-Nal Fault, OFZ = Owen Fracture Zone, CR = Carlsberg Ridge, rectangle = research area.

The extension of the total Makran accretionary wedge is approximately 800 km from east to west (Pakistan-Iran). Its southern offshore boundary is approximately 150 km where it reaches at the maximum depth 3200 m below sea level and it extends heights of 1500 m above sea level in the north approximately 500 km north of its deformation front. In the south and southwest the Oman abyssal plain is bounded by the Murray Ridge, which separates the Arabian and the Indian Plates (Fig. 5). To the east, the abyssal plain narrows due to

convergence of the Murray Ridge and the Makran accretionary wedge and disappears at about 65°30'E (Fig. 5).

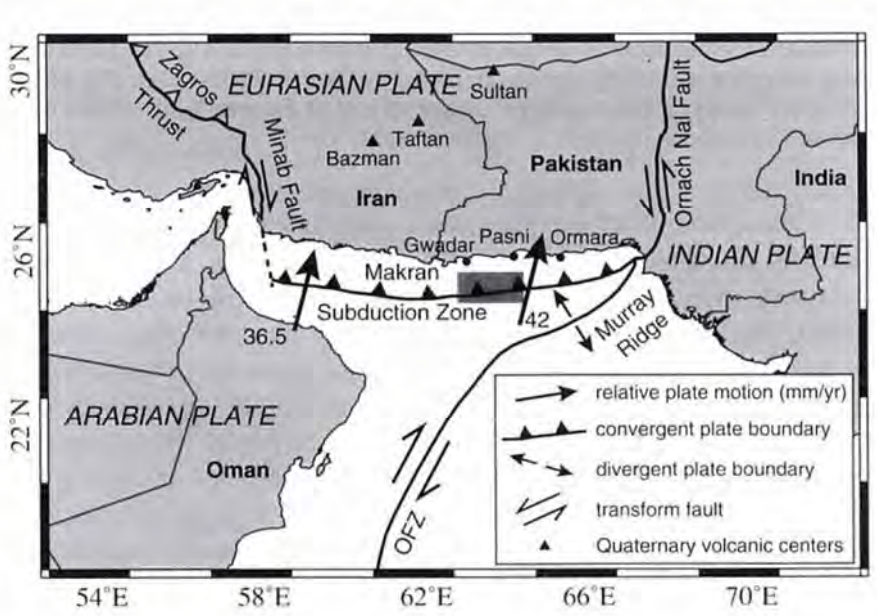

Fig. 6: Plate boundaries in the area of the Arabian-Indian-Eurasian convergence zone (from Kukowski et al. 2000). Direction of convergence is shown by arrows as well as the area (dark-shaded box) of swath mapping during Cruise SO-123.

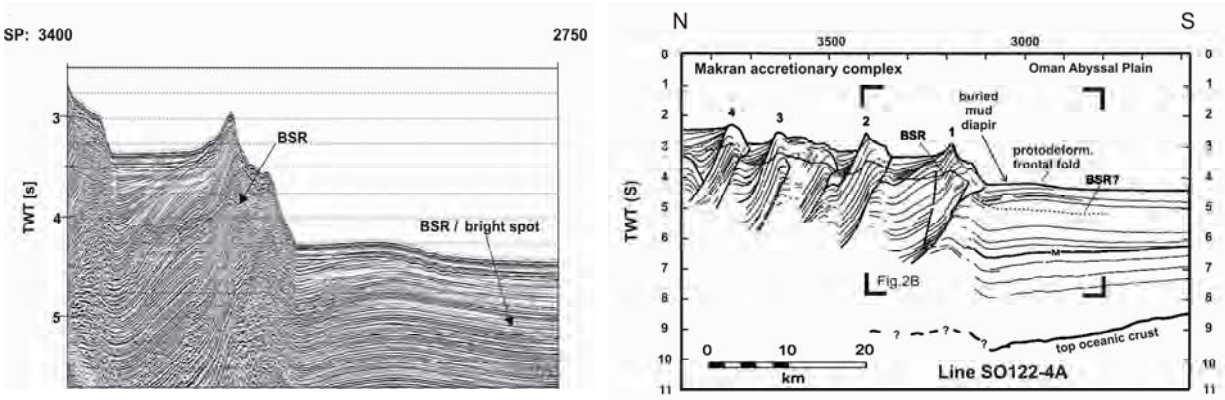

Fig. 7: Section of Multi-channel seismic profile SO 122-04A (from von Rad et al. 2000). Record covering First and Nascent Ridges (left). Interpretation of a larger part of the section (right).

Offshore, the Makran accretionary wedge consists of a number of ridges with long, narrow in parallel sequences, orientated from east to west. It can be divided into three sections: the upper slope, the mid-slope terrace and the lower slope. The upper slope is shallow, narrow and less steep than the lower slope (Pratson and Haxby, 1996), the accreted wedges continue in further north 400-500 km across the Iran and Pakistan. The deformation front of the Makran accretionary prism lies approximately 150 km south from the coast (Kukowski et al., 2000). Two major seasonal rivers (Shadi and Hingol) transport sediments onto the continental slope and turbidity currents form deep erosive canyons "Shadi and Save" (Underwood 1991, Gnibidenko and Sarichevskaya, 1983).

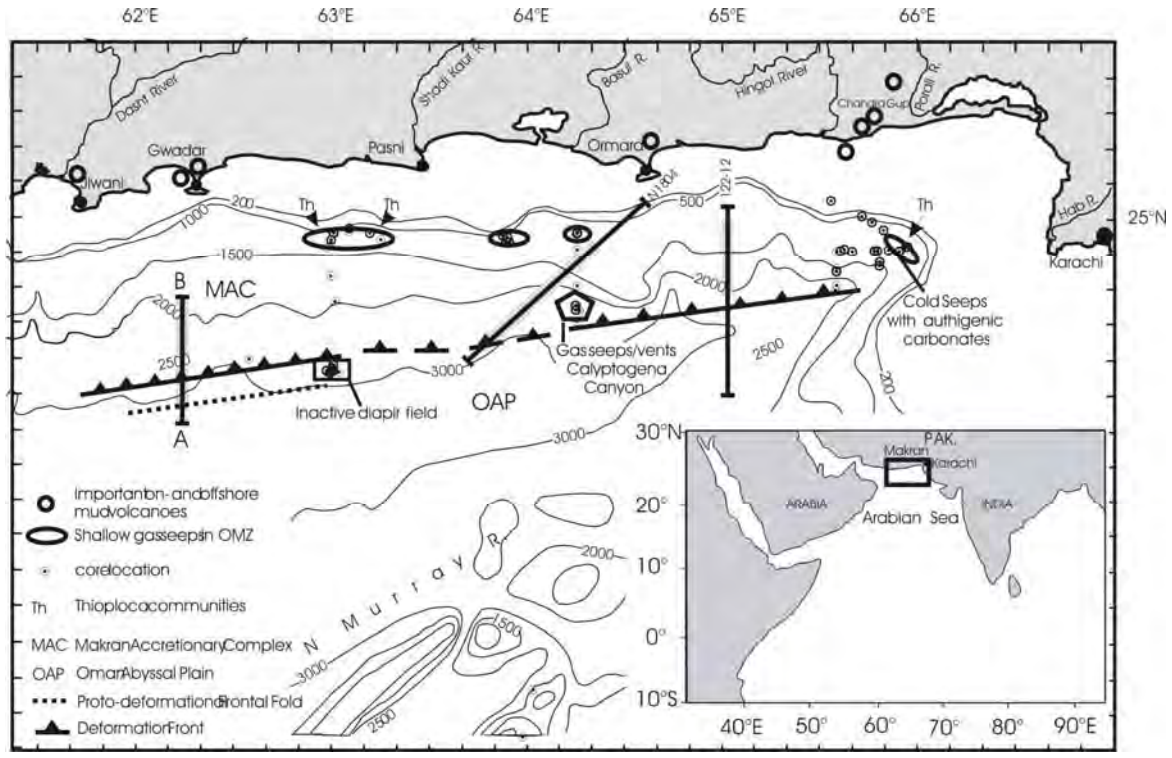

Fig. 8: Map taken from von Rad et al. (2000) showing main features of seepage recovered during SO 122/130 cruises.

The Northern Arabian Sea is the highest biological productive area in the world especially during the summer monsoon. High oxygen consumption due to organic matter degradation results in a stable and mid-water oxygen minimum zone (OMZ) between about 150-1100 m water depths in the Arabian Sea (Wyrtki, 1973). Productivity derived organic matter and terrestrial organic rich mud input lead to lamination of the ocean floor deposits. The sedimentation rate of the slope sediments is extremely high up to 0.2->1 mm/a (von Rad et al., 2000) because of rapid tectonic uplift, the narrow shelf, and the effective erosion of the hinterland because of the lack of extensive vegetation. The burial of organic matter in the sediments, particularly on continental margins also provides a unique palaeoenvironmental record as well as the main potential source for fossil fuels (Berner, 1989).

During bathymetry surveys of several cruises with the German research vessel SONNE in 1997 and 1998 (SO-122, SO-123, SO-124 and SO-130), gas seepage from shallow ridges near the OMZ were documented (von Rad et al., 2000). Associated to those seep sites a number of white microbial mats composed of large sulphur oxidizing bacteria (such as *Beggiatoa* and *Thioploca*) were found. Furthermore in a deeply incised submarine canyon at 2100-2500 m water depth seeps of methane and H_2S-rich fluids were found (von Rad et al. 2000). The fluid flux was explained by the tectonic stress within the zone of convergence. The occurrence of gas hydrates was shown by the presence of a well pronounced bottom-simulating seismic reflector (BSR) documented in most of the seismic profiles (Figs. 7 and 9). Driven by the dynamic of the accretionary wedge the landward part of the gas hydrate-bearing sediments are being progressively uplifted which should lead to progressively decomposition of gas hydrates since they move out of their stability field. At least enhanced seepage at sea floor above 800 m water depth was explained by this process (Fig. 9).

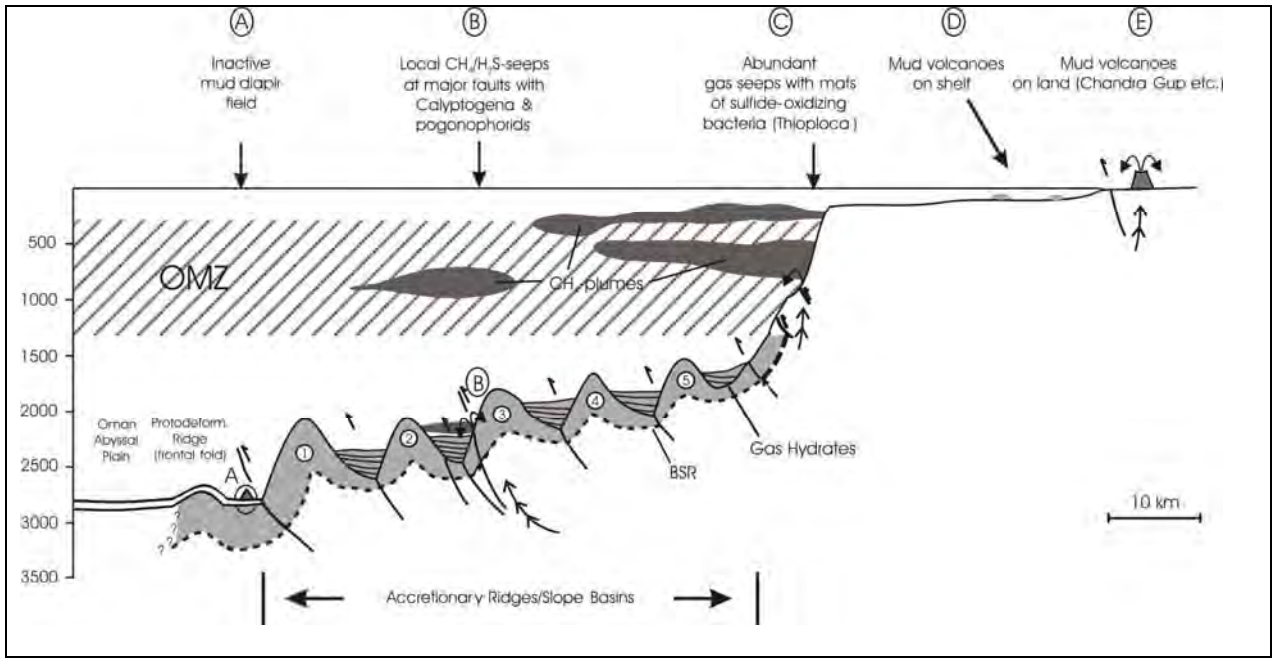

Fig. 9: Schematic cross section of the Makran accretionary margin summarizing seep related features in relation to the tectonic situation and the location of the oxygen minimum zone (from von Rad et al. 2000).

Furthermore mud volcanoes are a prominent feature of the coastal area of Makran. These mud volcanoes were exposed in the Makran coastal area during Plio- to Pleistocene age (Hunting Survey Corporation Ltd., 1960). Mud volcanoes are mostly found in the eastern part between the Hingol River and convergent zone Omach Nach fault, while some at Gwadar, Jiwani, Ormara were reported by Sondhi (1947) and Delisle (2004). In the eastern part of Ormara, a cluster of outstanding eroded muddy hills near the Bussey Pass (between Ormara and Hingol) is present, and in the western part enormous patches of carbonate shells (most likely *Calytopgena sp*.), soft muddy beds spread along the coastal (belt 5-10 km) between the two coastal cities (Pushukan to Gunz) west of Gwadar. In November 1945 three islands emerged in the shallow coastal area (off Pasni) during a strong earthquake with huge mud erupted simultaneously self ignited flame plume in atmosphere; within few months they submerged by wave activities (Sondhi, 1947).

Last year (8-10 June, 2007) an environmental survey of the Ormara coastal area observed gas bubbles erupting in the water column near the Ormara- headland area.

1.2 Objectives, Backgrounds and Research Program
(G. Bohrmann)

Main objective of the research cruise was to find seeps in different water depths along the continental slope in order to decipher key processes at those cold seeps. Ocean margins host large systems of circulating aqueous fluids. In some areas these are associated with hydrocarbon migration and focused emission of fluids, gases and muds at the sea floor. Some estimates suggest that the magnitude of upward flow through continental margins could be similar to that at hydrothermal systems. Associated with fluid outflow at seeps are chemosynthetic communities that utilize the chemical energy of reduced components such as H_2, H_2S, CH_4, and other hydrocarbons. The biomass of these communities is often several orders of magnitude greater than in the non-seep vicinity. The primary energy flow to these highly specialized communities comes from microbial turnover of sulfide, methane and other hydrocarbons. Cold seep ecosystems are recognized by distinct morphological features (e.g. pockmarks, chimneys, and irregular build-ups), specific biological communities, highly reduced chemical environments, high sulfide fluxes, mineral precipitates (e.g. authigenic carbonates, barite, and gas hydrates), and diagnostic stable-isotope signals in inorganic and organic phases.

Emissions of reduced compounds such as methane, hydrogen sulfide and iron-II affect the cycling of elements around seep locations in unique ways. Cold-seep environments may also serve as model systems for past perturbations of the carbon cycle that were presumably triggered by release of methane from subsurface reservoirs. Previous studies of seep environments were often concerned with local geologic features and/or specific biogeochemical processes such as the anaerobic oxidation of methane (AOM), a main sink for methane in the sea floor. Systematic approaches to an investigation of different seep systems (i.e., asphalt-, petroleum-, methane-, CO_2-, brine-seepage; carbonate-paved or fluid muds; methane- or sulfide based chemosynthesis; focused versus diffuse fluid flow, etc.) and their element fluxes have not yet been undertaken and form a focus of the RCOM.

Similar to hot vent ecosystems, cold seeps support enormous biomasses of tube worms, vesicomyid, mytilid, and solemyid bivalves, as well as mats of giant sulfide-oxidizing bacteria. These chemosynthetic communities are nourished by the chemical energy, i.e. methane and sulfide, rising from subsurface sources and forming the basis of cold-seep ecosystems. High chemoautrotrophic production at these habitats supports additional seep-associated organisms. In areas of high hydrocarbon fluxes, the benthic biomass fueled by chemosynthetic processes can be 1,000 to 50,000 times greater than the biomass of detritus-based deep-water ecosystems. Some recently discovered microbial communities at seep systems represent important barriers for the release of greenhouse gases and toxic substances. Examples are methanotrophic archaea mediating AOM, and various bacterial groups oxidizing sulfide with oxygen or nitrate. The role of iron, manganese and other metals in anoxic hydrocarbon and sulfur turnover is not well known. Also, little is known on the biogeography of seep-related microbial communities, the endosymbiotic chemosynthetic fauna and other seep fauna. Methane-seep deposits are typically dominated by authigenic carbonates, iron sulfides, barite, calcium sulfates, and gas hydrates. Mineral authigenesis is linked to biogeochemical cycling of carbon and sulfur. The anaerobic oxidation of methane

leads to an increase in alkalinity, which results in the precipitation of carbonate minerals including aragonite, calcite, and dolomite with low $\delta^{13}C$ values (as low as -69‰). The product of AOM, sulfide, interacts with iron and other sedimentary compounds. Mineral fabrics, stable isotopes, and lipid biomarkers track microbial processes in the formation of modern and ancient seep precipitates.

Investigations during former cruises along the Makran margin (see Chapter 1.1) did not show extensive seepage. Based on the huge thickness of the sediments which are squeezed due to the convergence, sea floor seepage should be much more pronounced than observed in past. Therefore, systematic seep search was conducted during M74/3 (chief scientist Volkhard Spiess) by using sidescan sonar TOBI, seismic multi-channel profiling, flare imaging with the PARASOUND system, and TV-sled investigations. The TOBI survey showed anomalously high backscatter areas linked to areas of sediment covered sea floor where fluids and/or gas are seeping. Distinct bubble flares have also been detected in the water column records of TOBI. Furthermore, several of those locations have been revisited and investigated by detailed Parasound analyses. By the end of the cruise 7 well defined flares (numbered from one to seven) have been found from shallow water depth down to 300 m water depth at distinct geological settings. Flares, backscatter anomalies and seismic records formed the basis for a detailed survey during our cruise. ROV QUEST was used as the main tool in order to map the sea floor and take samples at the potential seep sites. ROV QUEST also served as platform for the deployment and recovery of autonomous tools, e.g. bubble meter or in-situ pore water sampler.

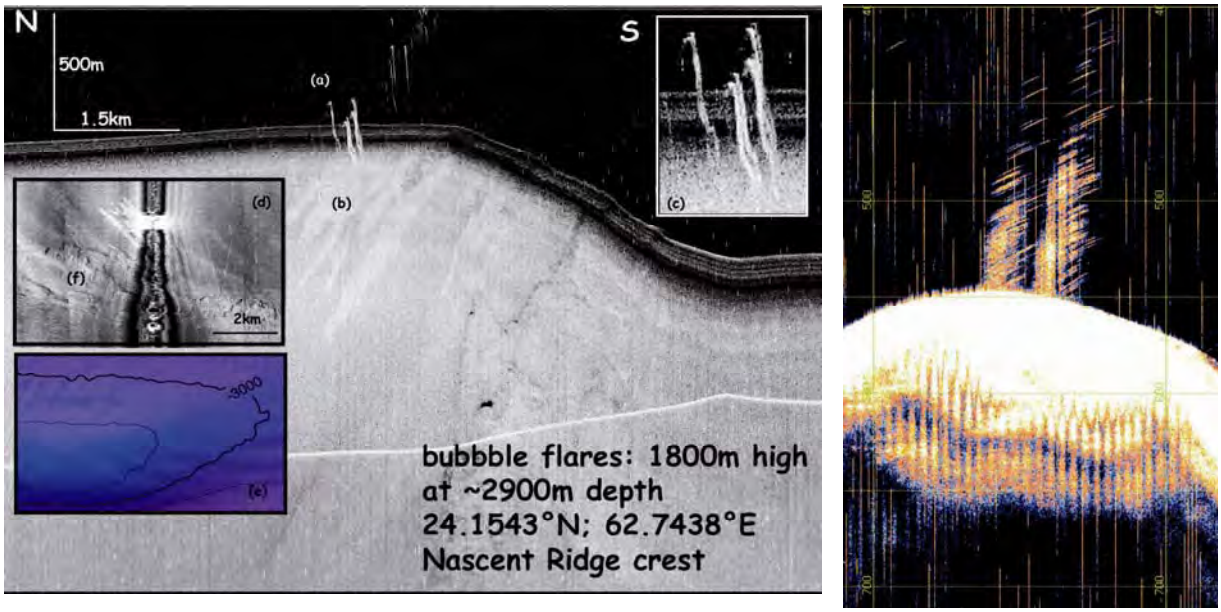

Fig. 10: TOBI sonargraph showing bubble flares (left) on nascent ridge crest (Flare 5). Two bubble flares observed during PARASOUND survey (right). Bubble ebullition was also documented by TV-sled observations at 550 m water depth within the OMZ; both images are from Cruise M74/2.

2 Cruise Narrative

(G. Bohrmann)

R/V METEOR sailed from the pier in the harbour of Fujairah (United Arab Emirates) at 7 p.m. local time on Tuesday 30 October. After 2.5 days in the port of Fujairah during which scientists and scientific devices were exchanged, R/V METEOR started its cruise. The new device on board, the ROV QUEST 4000, represents the main instrument of our cruise. A 30-hour transit began towards the area of activity in the south of Pakistan. After a 10-hour bathymetric survey at the proto-deformation front the first dive with ROV QUEST began on Friday 2 November on Nascent Ridge, a small ridge south of the first accretionary structure. Due to the brilliant result obtained during the cruise before, a place of free gas emanation was immediately found by the ROV. The site was characterized by one of several acoustically detected plumes in the water column which were found in sidescan-sonar (TOBI) and the PARASOUND records. We have been very lucky to find an active seep field just right at the beginning of the cruise. Beside numerous discharge positions of gas bubbles the seep area was characterized by a dark grey colour of the sediments as well as by a settlement of small tube worms in the centre and chemosynthetic clam shells at the edge. A gas and a push core sampling, as well as temperature measurements in the very fine-grained sediment performed the program of analyses, before we unfortunately had to break off the dive for technical reasons. In the evening we tried to sample the seep area by means of the gravity corer. We succeeded, the entire gravity core was filled with gas hydrates which had formed near the surface within the seep environment from ascending free gas. After a bathymetric survey during the night a second gravity core was taken for a detailed geochemical examination in the seep area. Afterwards we began in advance with a special sampling program for the investigation of the oxygen minimum zone, since further ROV dives had to be cancelled for a longer repair work time.

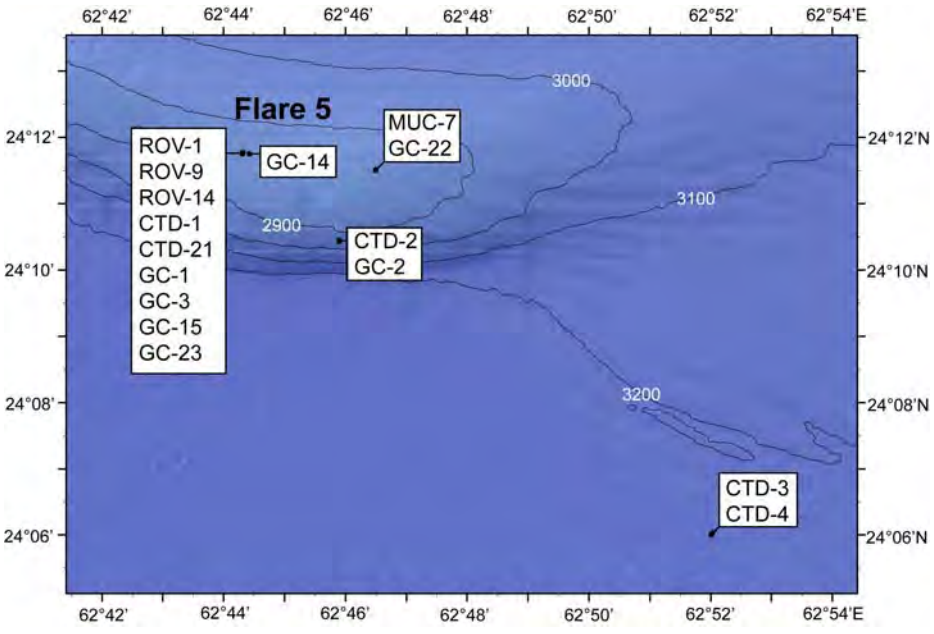

Fig. 11: Location sites of Cruise M74/3 in the deepest part of the accretionary margin at Nascent Ridge (for details see also station list Appendix 1).

On Sunday 4 November we used the time during the repair work of the ROV QUEST to accomplish our sampling program of the oxygen minimum zone (OMZ) along a transect over the margin. The water column was sampled using the CTD and hydro casts, and the sediments were sampled with multicorer and gravity corer at 660 m, 995 m, 1425 m and 1586 m water depth. The scientists will examine the samples and study the effects of the different oxygen concentrations on preservation of certain organic particles and substances, e.g. dinoflagellate cysts and biomarkers. The investigations are used for the evaluation of individual marine microfossils, as well as biogeochemical and geochemical proxies, so that their use for palaeoceanographic studies will be tested. Biogeochemical work on the organic material will be performed as well as pore water investigations of the sediments.

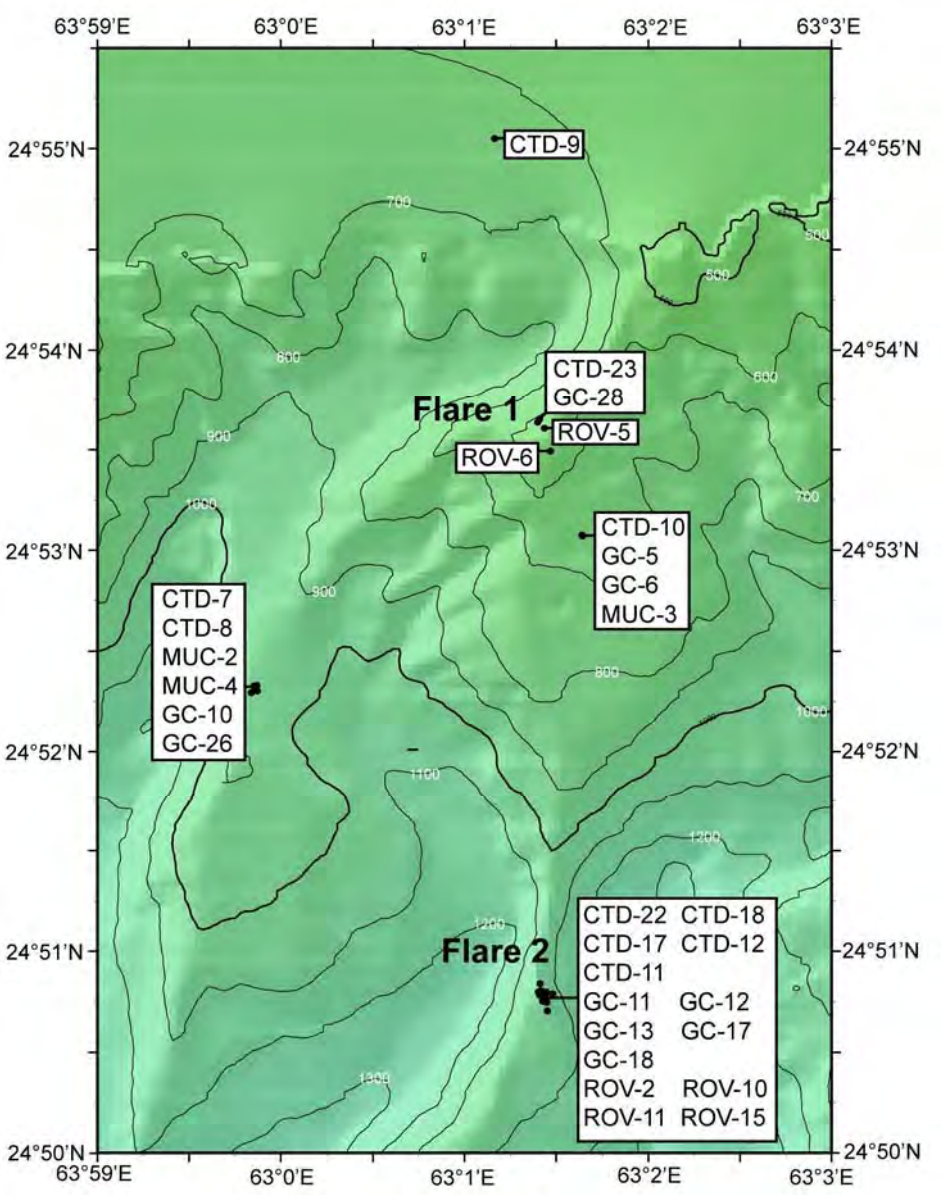

Fig. 12: Map of the shallow area with sample sites at Flares 1, 2 and 13 within the oxygen minimum zone (for details see also station list Appendix 1).

On Monday 5 November, the daily ROV dive began, and up to Saturday evening 7 dives were successfully performed. The dives examined scientifically spectacular and exciting information and samples. The fluid and gas seeps were dominantly characterized by bacterial mats in the OMZ. Other chemosynthetic organisms in addition appeared sometimes and their presence seemed to be related to small changes in oxygen content. This was especially the case at the lower boundary of the OMZ. On the crest at gas seep No. 7 in 1600 m water depth where a large area (300 x 1000 m) of high backscatter signals in the side-scan sonar measurements were found, we could observe widespread seep areas. The entire crest was covered by carbonate crusts several decimeters to several centimeters thick explaining the presence of high backscattering in the side-scan record. Large fields which are colonised by *Bathymodiolus* mussels and which usually are interrupted by tube worm colonies at the more active seep sites were particularly impressing. In several places we could repeatedly observe emanation of free gas, and with the pressure tight gas sampler we could analyse both, the gas flux and the gas composition. Detailed observations with the ROV showed that the tube worms root with their tubes underneath the carbonate crust, where they can find sufficient hydrogen sulphide for their symbiotic bacteria. In contrast, the *Bathymodiolus* mussels were sitting on the carbonate plate, and so far it is not clear which reduced substances are used by their symbionts and how is the mechanism of their transport.

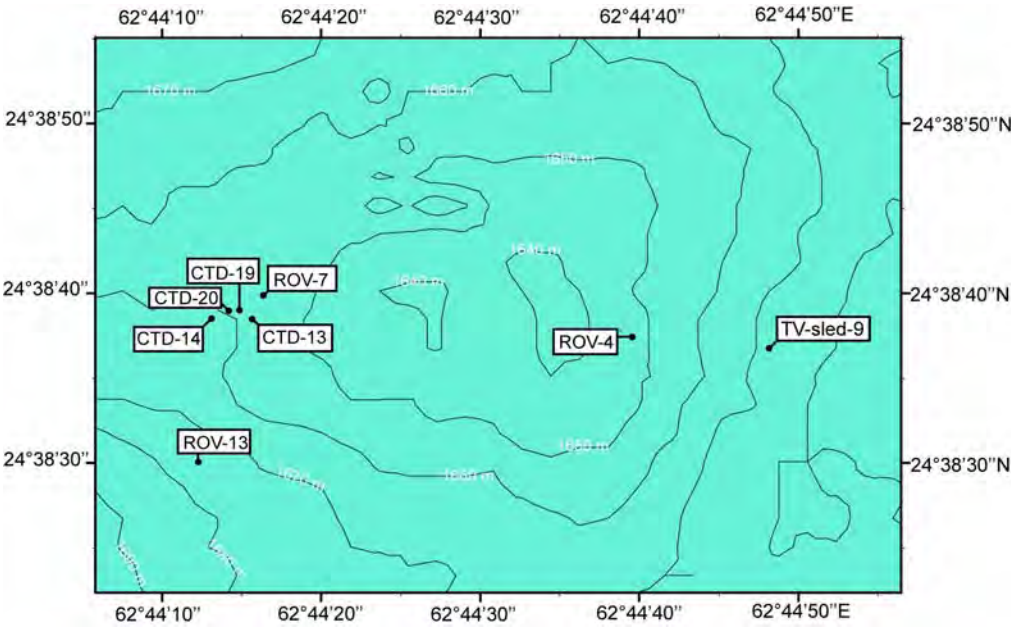

Fig. 13: Location sites sampled during M74/3 at Flare 7 at medium water depths (for details see also station list Appendix 1).

At the edge of the carbonate crust area fluid and gas seeps were characterized by nests of vesicomyide clams, which to a certain part were sitting in the sediment. These clams can become amazingly large; during Dive No. 185 we sampled 2 specimen of up to 18 cm in length. The variations of the seeps and especially the settlements by chemosynthetic organisms have been unexpectedly large. Nevertheless we could differentiate between several characteristic seep systems because of their position at the accretionary wedge of the Makran subduction zone, their geological structures and their level of oxygen. Such interdisciplinary

investigations at the bottom of the sea floor are impossible without a deep-diving ROV. In addition we had the good support by the crew on board R/V METEOR.

As before, the third week was characterized by ROV QUEST dives during the day, whereby in the early morning and late evening gravity corer, multicorer and CTD stations were performed. At the night locations with acoustically proven gas emanations were pre-examined with the TV-sled for potential ROV dives, or geologically interesting places were explored by the PARASOUND for further acoustic gas plumes. Thus we could find 5 well defined gas flares in addition to the 7 flare positions found during previous cruise M74/2. This mode of day and night shifts was productive and gave the scientists also sufficient time to work on their samples. This schedule also allowed the ROV pilots to accomplish their small repair work in the evening hours. On each morning after 2-hour preparation ROV QUEST was ready for the next dive. By support of the ROV dives we could understand clear differences of the fluid and gas discharge through the oxygen minimum zone (OMZ). The OMZ is characterized by oxygen concentrations of less than 0.05 ml/L between 150 - 1200 m water depth. In the environment of Flare No. 1 at 570 m water depth filaments of sulfure bacteria (very probable *Thioploka*) arose directly around the gas emission site. We have examined approximately 8-10 oval patches of white bacterial mats, often with orange coloured in the centre. Each of these patches had several holes where gas in various intensities bubbled out. Settlements by other benthic organisms were not to be proven, and are not to be expected due to the very small oxygen concentrations in the water. The seeps of Flare No. 2 at 1020 m water depth however showed clearly more benthic live, which appeared nevertheless very small-sized. So vesicomyide clams and other animals were found in clear distance to the gas discharge positions surrounded by bacterial mats. Such gradients in biological zonal colonization are well-known from other areas, where different hydrogen sulfide concentrations lead the chemosynthetic organisms to colonize according to their individual acceptance in H_2S concentrations. H_2S-content is probably very high around the gas discharge position due to the high rate of anaerobic methane oxidation which might be toxic for clams. In a greater distance however the H_2S-concentration is surely smaller, so that clams find ideal conditions to life. The pore water profiles of our push corer sampled with ROV QUEST will show whether this applies also here and which differences exist to the seeps known so far. This clear zoning around the actual gas bubble sites was found in 1000 m several times. We could prove an accumulation of these seeps along a 5-15 m wide and minimum 400 m long morphologic depression zone over a ridge just next to a slump area in the northeast. The elongated depression seems to belong to a normal fault system outcropping at the sea floor which should be part of the slump. Due to lateral expansion free gas can rise up in sediments to the sea floor, where the typical seep communities can start to grow because of high rates of AMO. Below the OMZ the seeps were characterized by the settlement of clearly larger seep organisms.

On Thursday, 15 November we accomplished two short dives. The first dive in the morning was performed at Flare No. 2 in order to quantify gas bubble emanation using the newly-developed bubblemeter. The principal aim of the equipment is an illumination which produces light over an area of 30 x 30 cm with a homogeneous intensity corresponding to the 1,5-fold of the sun exposure during a sunny day in Bremen. Ascending gas bubbles in front of this screen were recorded by a camera with very high resolution rate, so that most of the gas

bubbles could be determined with the help of a computer program. Both, the handling of the equipment, and the somewhat unusual adjustment to the ROV QUEST, worked very well, so that this dive could be finished around midday. The second dive was started within the area of Flare No. 3 in 1500 m water depth, but had to be terminated after short time due to a short-circuit of the electrical system of the ROV.

On Sunday 18 November the video mosaic was completed at Flare No. 2. Furthermore the in-situ pore water sampler was deployed, gas was sampled by pressure tight gas sampler and push cores have been taken. At Flare No. 2 we obtained the most complete data set and sample set of the cruise. The dive performed during the following day at Flare No. 11 was very exciting. As at many seeps in these water depths of 1500 m mytilide mussels were predominantly to find, which settled on hard substrates, predominantly above authigenic carbonates. Enormous large surfaces were settled by a dense population of galatheide crabs. This massive occurrence of closely sitting white crabs was fascinating for all of us on board, and many of us were reminded of a science fiction thriller published recently. It is unkown to us why these crabs do arise in such great quantities. We can only speculate that the large quantity of biomass usually formed at the fluid and gas seeps has somewhat to do with this phenomenon. Sampling of the water column directly above the discharge positions and sampling of the carbonates as well as the clams finished this fascinating dive.

The dive on Tuesday examined an area of the first accretionary ridge, where backscatter anomalies have been found during the TOBI survey. Since PARASOUND measurements could not prove an acoustic anomaly in the water column, the ROV investigations of that structure were postponed. This ridge is the youngest and tectonically most active ridge of the subduction zone, so that fluid circulation and seepage were of special interest. After an investigation with the video-sled during the night there were sufficient signs for active seepage, so that the dive on the crest of the very narrow ridge in 2000 m water depth was performed. The ridge has a very steep flank to the south of more than 1000 m height. So a constant slipping of rocks and sediments is expected related to the tectonic folding. Many extensive fresh outcrops were observed at this southern flank, which probably constantly rebuild very fast, so that they are not settled at all by organisms. Thus, we found our indicators for fluid seepage, the chemosynthetic organisms, only direct on top of the crest in small protected depressions. Again and again we searched along the steep southern flank, until we found very small holes at the bottom where fluids expulsions have been observed. Smallest differences in the density of the fluids showed us that these fluids mix with the bottom water very fast and then cannot be traced anymore.

The very small expulsion sites of less than a half cm in the diameter were to be seen only with the HD camera, which can be driven very near to the bottom. Since all other seeps which we examined so far on the cruise were characterized by free gas expulsion, here we could document a fluid outflow without free gas. The depths of the accretionary wedge from which the fluids ascend, will be clarified by the geochemical analyses of water samples which were taken by the KIPS sampler. The last dive (no. 18 of this cruise) was accomplished on Wednesday at a new location within the oxygen minimum zone (OMZ) at 750 m water depth. This diving work considerably extended our past spectrum of the OMZ seeps, since we could sample valuable carbonate chimneys at gas discharge positions, which develop as a precipitate

of biogeochemical methane transformation around the gas bubble sites. Beside the diving program we daily sampled with the gravity corer, multicorer and CTD.

The station work was terminated in the night from Wednesday to Thursday, and the 5-day transit to the south began. Only PARASOUND and the deep water multibeam echosounder registrated data up to the border of the research area. On Tuesday we entered the port of Male in the morning, where our scientific cruise ended. We returned to Bremen with a large treasure at samples, as well as with scientifically substantial new realizations and experiences. The expedition gave large pleasure to us for being able to accomplish research on highest technical and scientific level in this friendly and helpful atmosphere.

In total 18 ROV dives have been performed with sampling of 68 push cores, 18 gas bubble samplers, 9 temperature-stick measurements, 6 deployments of the in-situ pore water sampler, and deployments of the osmo-sampler and the bubblemeter. Scientific work includes also 31 gravity corer stations, 25 CTD/hydrocasts, 8 multiple corer stations and around 3330 nautical miles of PARASOUND and swath bathymetry mapping.

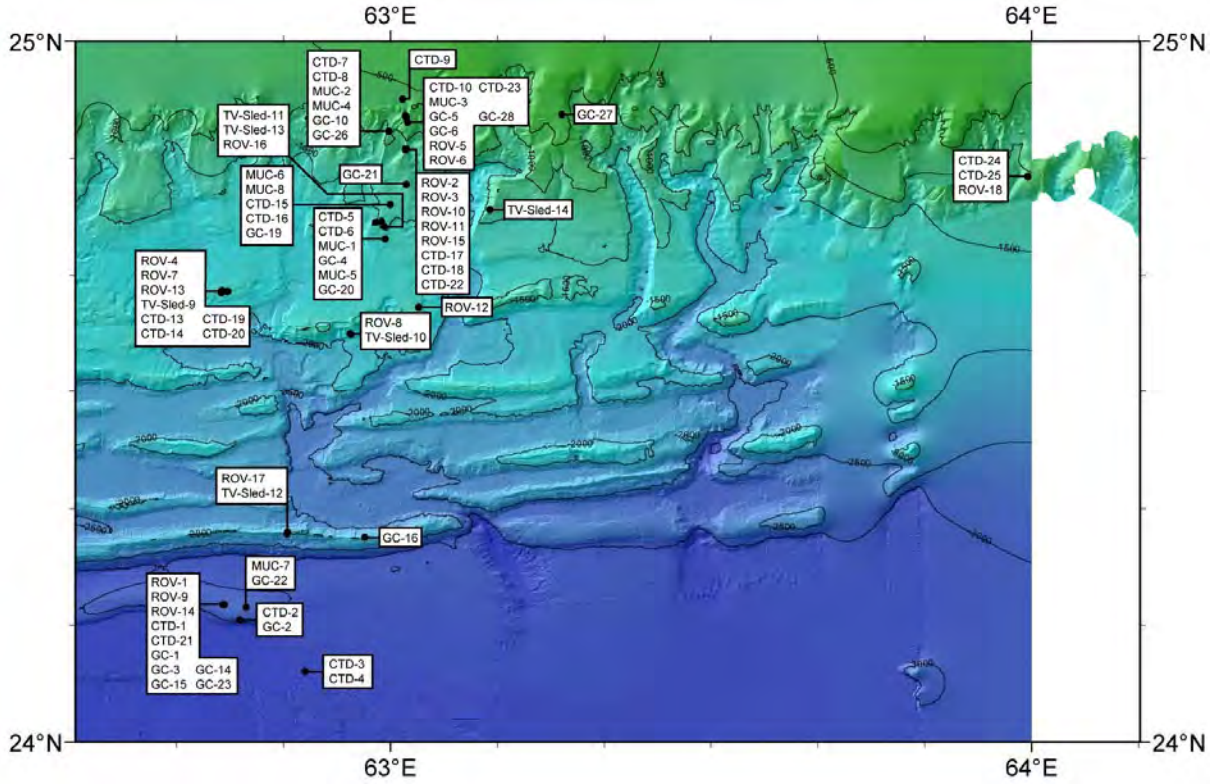

Fig. 14: Summary of all stations at the Makran continental margin from Cruise M74/3.

3 Multibeam Swathmapping

(M. Brüning, N. Wittenberg, and watchkeepers)

Knowledge of the bathymetry of the sea floor is essential for most of the investigations conducted during the cruise. Nina Kukowski provided a bathymetry grid covering the main part of the working area with a grid spacing of 200 m. It is a compilation of several cruises of R/V SONNE. For the purpose of the M74 cruise the resolution was too poor, and METEOR's echosounders increased it significantly during station work off Pakistan.

KONGSBERG SIMRAD EM 120 and EM 710 multibeam echosounders are installed in the hull of R/V METEOR. The EM 120 has a frequency of 12 kHz and can cover full ocean depth. The EM 710 has a frequency of 70 to 100 kHz and is optimised to survey with higher resolution in shallower water down to 1,000 m. As most of the working area was deeper, the EM 710 was not used very often. The SIMRAD EM 120 sends out 191 beams with a maximum opening angle of 140°. The mode was set to obtain equally spaced soundings on the sea floor. Yaw movements of the ship were compensated automatically by the software by transmitting the swath rather perpendicular to the track than to the ship's axis. The opening angle was limited either by the maximum angle possible, a maximum angle set, or a maximum coverage in metre on the sea floor. Those values were adjusted to the special survey task depending on the requirements. For TOBI lines, which were 5.5 km apart, the coverage was limited to get some overlap at the edges of profiles. During transits in areas, which were covered before by the SIMRAD, swath width were usually 6 km wide, on surveys over areas covered by Kukowski's grid, 7 km. Where no data were available at all, the full opening angle of 140° was run.

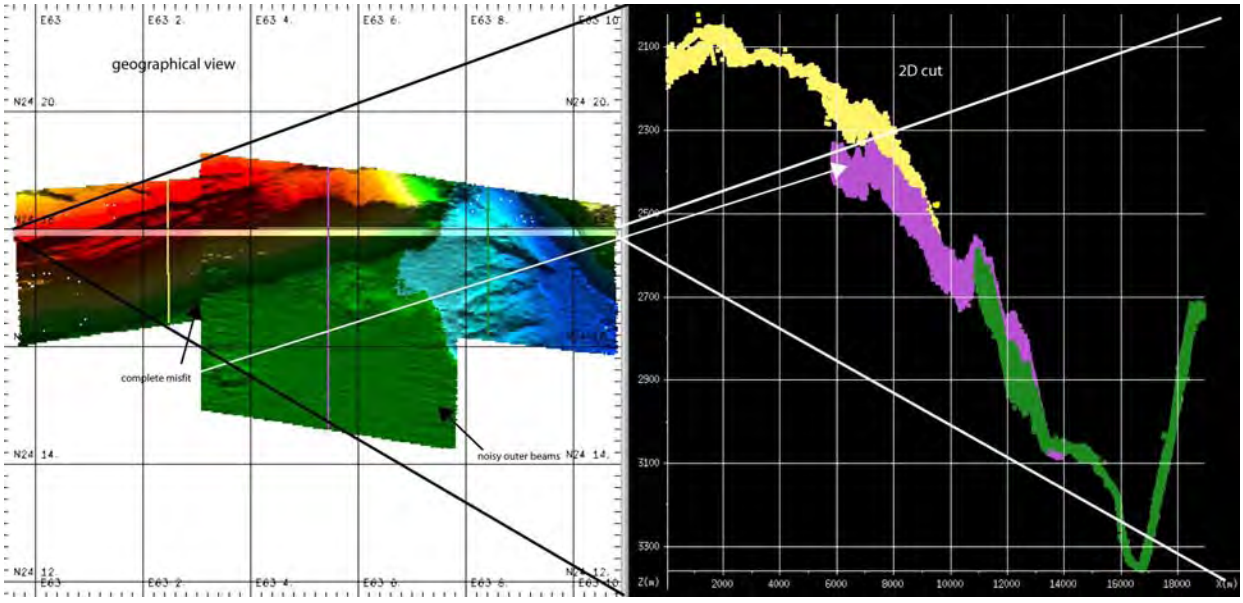

Fig. 15: Misfit of outer beams on a steep ridge. The data points underneath the bright line are presented as along-track-view on the right. Different colours represent different tracks. Yellow and pink data should overlap, which is not the case. Image from Odicce module in CARAIBES.

Ship speed varied between 2.5 kn during TOBI profiles, 5 kn during seismic profiles, 8 kn for bathymetry surveys, and 11 to 12 kn during transits. The first CTD station during M74/2, GeoB 12201, in 3000 m water depth delivered the sound velocity profile used during the

whole survey. At the beginning of M74/2 bathymetry processing was done parallel with different software packages: CARIS HIPS (Tim LeBas) and CARAIBES (Markus Brüning). Both delivered almost identical maps with quality increasing with the time spent on manual editing. Finally, the software MB System 5.0.9 (http://www.ldeo.columbia.edu/res/pi/MB-System/) served for processing the raw bathymetry data. The advantage of MB is its availability to all, free of charge, even though it is not as powerful in graphical issues as the two other commercial ones.

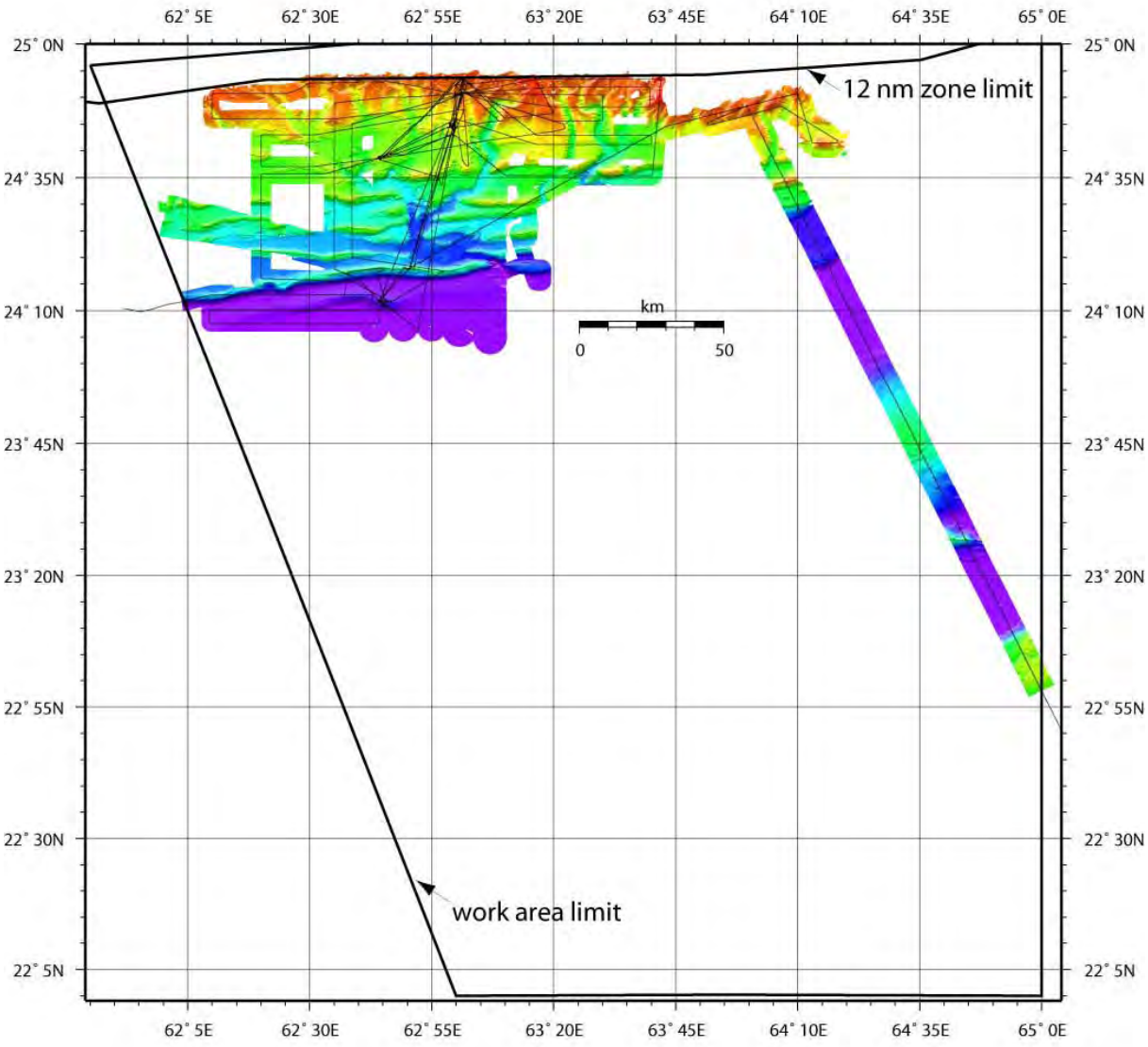

Fig. 16: Makran working area with bathymetry surveyed during Cruises M74/2 and M74/3. Tracklines of Leg 3 are shown.

Data were imported into MB system, filtered with a median spike filter, outer beams removed according to the profile's overlap and data quality, and manually edited. The grid was then calculated by omitting data where ships velocity was less then 2 km/h, because those soundings are generally of bad data quality. The grid cell size was 50 m. MB produced a netCDF grid, which was then visualized in GMT (Generic Mapping Tool, http://gmt.soest.hawaii.edu/) or further exported as ESRI GIS grid. It is important to note here that MB changes the value slightly, latitude and longitude differently, to fit the grid into the

given geographical limits. ESRI GIS expects identical increments in x and y, therefore a resampling (gridsample in GMT 4.1) was necessary to avoid distortion.

Systematically biased outer beams (see Fig. 15) produced problems in areas with large overlap of parallel profiles. An inappropriate sound velocity profile would cause bending up or down of outer beams. This was tested on a flat sea floor morphology. There was no significant error. Another possibility is a roll bias, but again, no improvement was possible in testing for different values. As the effect seems to be strongest on steep slopes, it might be a problem in yaw, which was not tried to be corrected for so far. By omitting outer beams or reducing the opening angle the problem was omitted.

Results

Results of swathmapping during Legs M74/2 and M74/3 are shown in Figs. 16-18. During M74/2 leg the central part of the working area was completely covered with new multi-beam data of 10 north-south running lines. Surveys conducted during M74/3 fill gaps and enlarge the mapping area at all sides. Fig. 16 shows the entire working area, limited by the 12 nm zone in the north. Tracklines give a representation of transits between station work at frequently re-visited sites, and newly covered areas further out. METEOR's lines were located to fill pre-existing gaps. Some of the gaps not filled during this expedition had already been mapped by earlier R/V SONNE cruises. Postprocessing work on land will also integrate the older data from previous cruises.

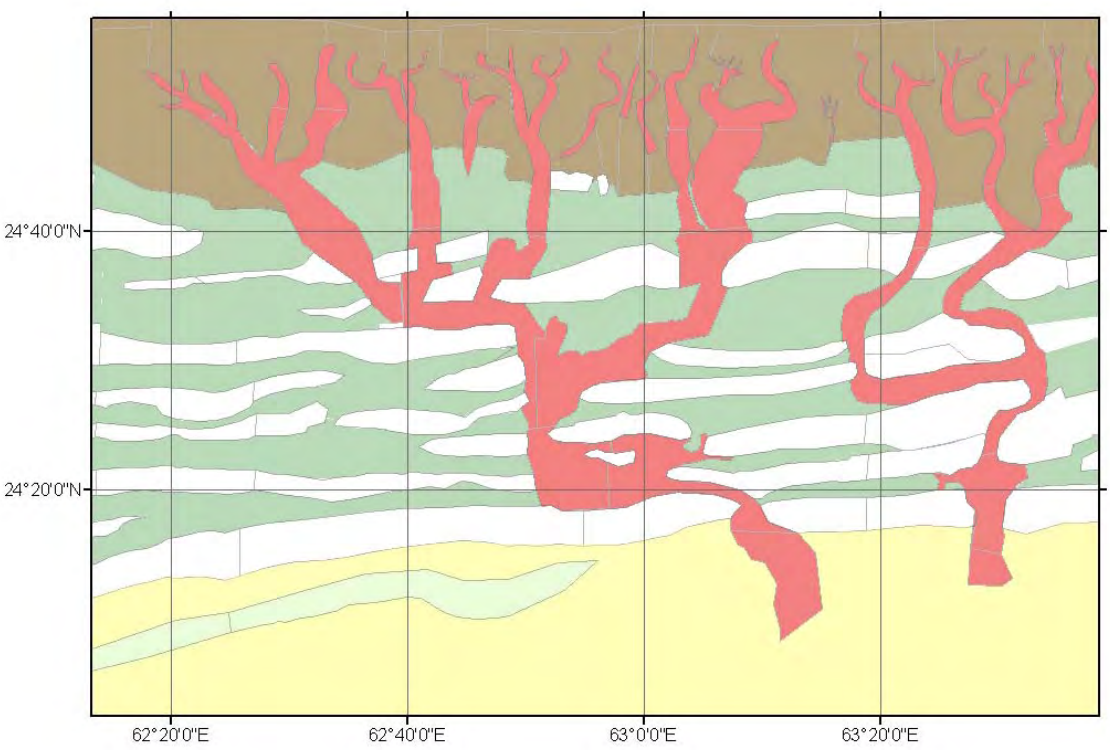

Fig. 17: Interpretation of R/V METEOR and R/V SONNE bathymetry data. Brown: upper steep slope, red: canyons / erosional channels, white: ridges, green: slope basins, yellow: oceanic plate, light green: nascent ridge.

Fig. 16 shows the area of research permission and the bathymetry measured during the cruise south of Pakistan. In the south the oceanic plate has water depths deeper than 3,000 m. The youngest up-doming ridge, or nascent ridge, around 24°10'N, is still only a small piece in lateral extend and elevation. The first accretionary ridge rises 1,000 m above the oceanic plate showing a slope angle of 20 degree. At 63°10'E a canyon breaks through the ridge. To the north five or six more ridges are following, depending on the location of the slope. They become shallower in elevation towards the north as the basins between become more and more filled with sediments. Several canyons run down from the steeper slopes, cutting ridges at many places (Fig. 17). The SONNE fault (Kukowski et al., 2001) running from the NW corner of the map southeastwards, is a major element controlling those erosional channels. The area covered before leaving to Male is about 10,000 km².

Fig. 17 is a simplified interpretation of the most prominent features identified on our bathymetry, in combination with earlier maps, collected during SONNE cruises. Fig. 18 shows a magnified portion, located roughly in the centre of Fig. 16. It is a slump, which is most probably related to fluid seepage.

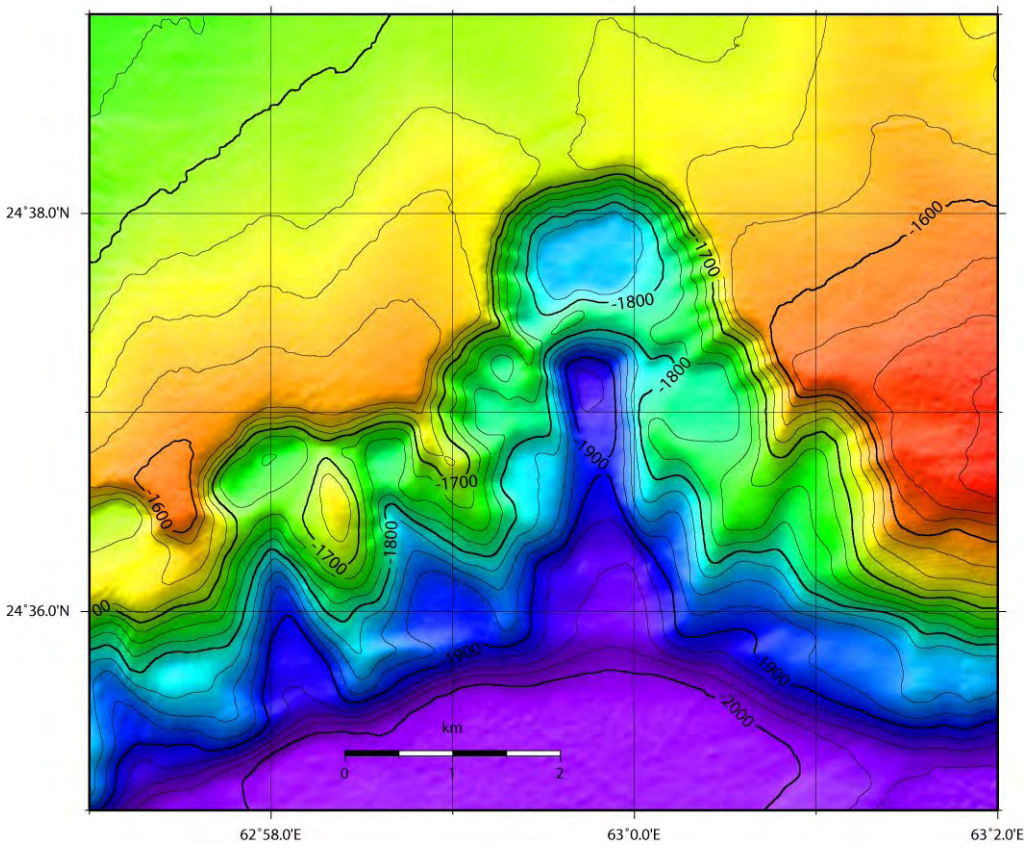

Fig. 18: Detailed view of a slump area probably evolving under the influence of fluid seepage.

4 Subbottom Profiling and Flare Imaging

N. Wittenberg, M. Brüning, S. Stephan, and watchkeepers

With the parametric echosounder ATLAS PARASOUND it was possible during the cruise to penetrate into the sea floor sediment to get information about the internal structure. It was also possible to visualize features within the water column e.g. like gas seeps (Figs. 19, 20) simultaneously.

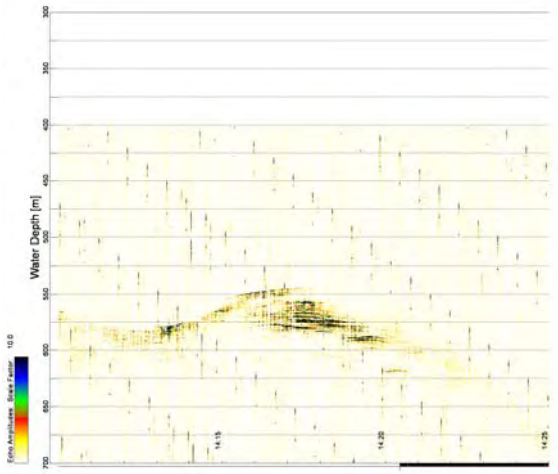

Fig. 19: Example of the subbottom profiling with 4 kHz frequency.

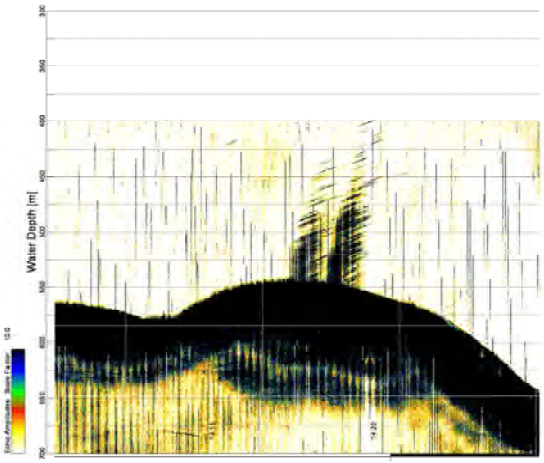

Fig. 20: Flare imaging with 18 kHz. Both images (Figs. 19 and 20) were taken during the same profiling.

The Primary High Frequency (PHF) is 18 kHz and allows the detection of gas venting into the water column (Bohrmann et al. 2007). Adding a secondary high frequency (22 kHz), a secondary low frequency (SLF) with 4 kHz is generated using the parametric effect. The 4 kHz is the frequency, which makes the subbottom visualization possible (Fig. 21). The beam of PARASOUND has an opening angle of 2°, therefore the footprint is in a first approximation 7% of the water depth. For online processing, the software ATLAS PARASTORE was used. ATLAS PARASTORE allows the colour-coded visualisation of the different frequency data in a freely chosen number of windows with different scales. Different processing algorithms can be performed. During the cruise three echogram windows were displayed, one PHF and one SLF window with 500 m window length in order to have a proper close-up of possible issuing gases and sediment structures. The third echogram window displayed the PHF again, but it shows the complete profile from the sea surface down to the sea floor. It turned out to be necessary, as some flares escape

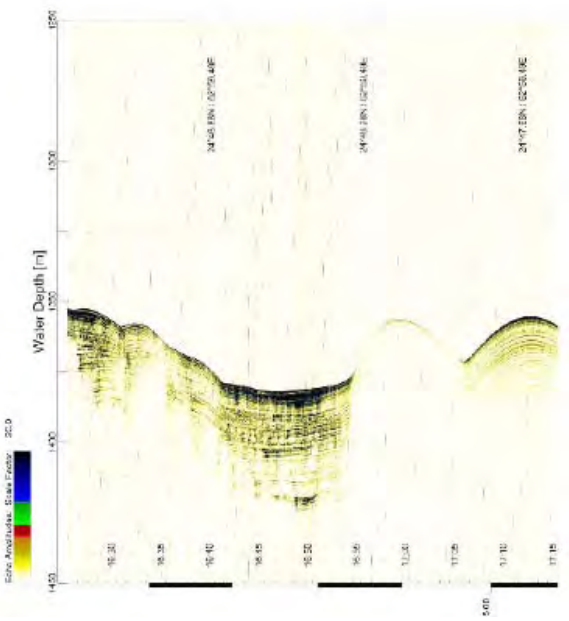

Fig. 21: Example of the subbottom profiling with the 4 kHz frequency. Sediment layers can be identified.

points on the sea floor which were not hit with PARASOUND's 7% footprint. Nevertheless, the flare rose in the water column in an oblique way, so that only upper parts returned reflections.

Two different transmission sequences (single pulse or pulse train) were run, depending on the speed of the ship. If the aim was to find flares in a certain area, the PARASOUND run in the single pulse mode. That means there was just one ping emitted, and the next one was sent out as soon as the first one was received back. This results in a complete visualisation of the water column, and therefore it was possible to detect a flare even if it is not connected to the sea floor. When the vessel is moving faster than 3 knots, single pulse mode got inefficient because the spatial resolution became very low. In this case the pulse train mode was performed, which means that there is more than one ping emitted in a short interval, which is automatically calculated.

In this mode, it is not possible to visualize the complete water column except in very shallow water. The water depth in the survey area ranges roughly from 300-3,200 m. 15 flare locations have been identified together with the findings from M74/2. The flares were found in various water depths (<200-2,850 m). The shapes and the heights of the plumes were very different (see Table 3). The heights of the flares range between 50 – 1,800 m.

Table 3: Basic data of acoustic flares detected during Cruises M74/2 and 3.

Flare No.	Date	Time (UTC)	Lat. °N	Long °E	Water depth (m)	Height of flare (m)
1a	09. Oct	14:17	24°53.64'	63°01.45'	550	100 - 150
1b	09. Oct.	14:17	24°53.62'	63°01.41'	550	100 - 150
1	13. Oct.	22:18	24°53.01'	63°01.59'	700	50 - 100
2	15. Oct.	13:14	24°50.80'	63°01.44'	1027	170
3	16. Oct.	23:06	24°37.23'	63°02.55'	1543	
4	11. Oct.	21:40	24°17.91'	62°50.25'	1955	450
5	23. Oct.	04:44	24°11.77'	62°44.38'	2871	1800
6	26. Oct.	09:13	24°34.89'	62°56.32'	1806	900
7a	20. Oct.	11:18	24°38.61'	62°44.64'	1644	850
7b	03. Nov.	20:21	24°38.58'	62°44.34'	1650	850
8	07. Nov.	21:50	24°51.75'	63°16.09'	467	100
9	08. Nov.	15:02	24°52.17'	63°09.25'	670	80
10	08. Nov.	18:20	24°53.40'	63°38.95'	200	70
11	10. Nov.	19:32	24°44.52'	63°58.71'	1475	100 - 150
12	13. Nov.	21:15	24°50.75'	62°34.25'	812	150
13	19. Nov.	17:07	24°51.87'	63°59.86'	910	50
14	19. Nov.	18:29	24°52.74'	63°04.66'	754	50 - 100
15	21. Nov.	01:10	24°48.42'	63°59.65'	733	100

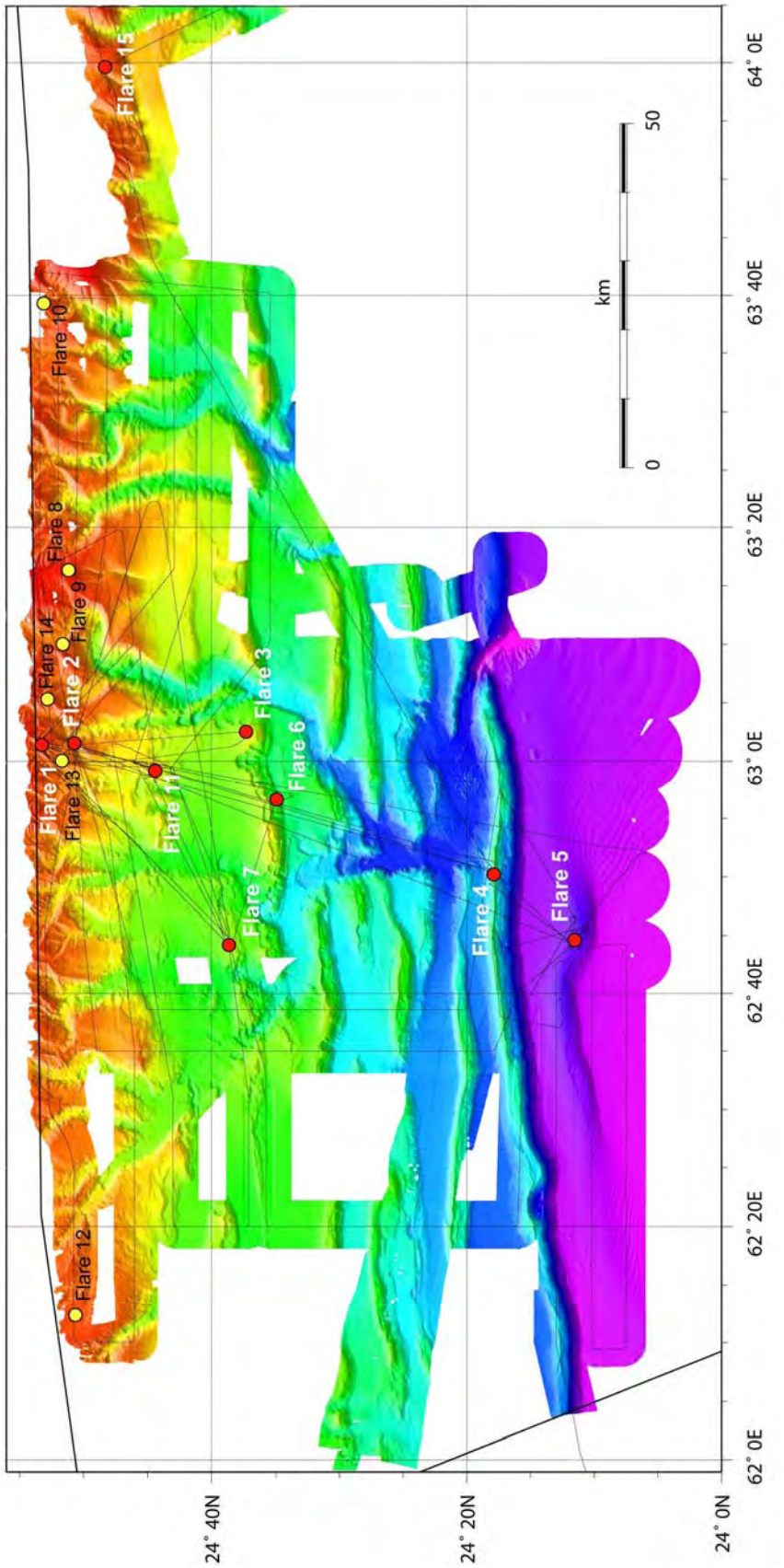

Fig. 22: Survey area at the Makran continental margin during R/V METEOR Cruise M74/2 and 3 and locations of flares found during PARASOUND surveys. Flares numbered as 1, 2, 3, 4, 5, 6, 7, 11, and 15 were investigated by ROV dives.

5 TV-sled Investigations

(M. Brüning, H. Sahling, N. Wittenberg, S. Stephan)

The TV-sled is a deployed frame with a black-and-white camera system that transmits in real time video images of the sea floor to the lab monitor. It is used to visually observe the sea floor at geological features identified in the bathymetric maps, TOBI sidescan sonar images, and at flare locations detected by PARASOUND. The prime target during this cruise was to find evidences for methane seepage with the objective of obtaining a general overview of how fluid seepage is distributed at the continental slope off Pakistan. Part of the identified sites were studied in greater detail with ROV QUEST during cruise M74/3.

The TV-sled is a towed black-and-white camera system transmitting energy to the sled and the analogue video signal from the sled through the ship's coax cable (W12). The main components are the video-data telemetry system consisting of an underwater and a deck unit, a black-and-white camera system and a halogen light. The black-and-white video signal transmitted by the video-data-telemetry system is displayed in real time on monitors and recorded by a VCR. The electronic components of the system were manufactures by the company Oktopus GmbH (Kiel) and are property of the University of Hamburg (working group Prof. Matthias Hort). The underwater system is mounted in a steel frame with a length, width, height of 120 x 80 x 120, respectively (Fig. 23). In order to determine the position of the TV-sled, the ship's ultra short baseline system (USBL) Posidonia was used. A Posidonia transponder (S/N 413) was mounted on the wire 50 m above the sled.

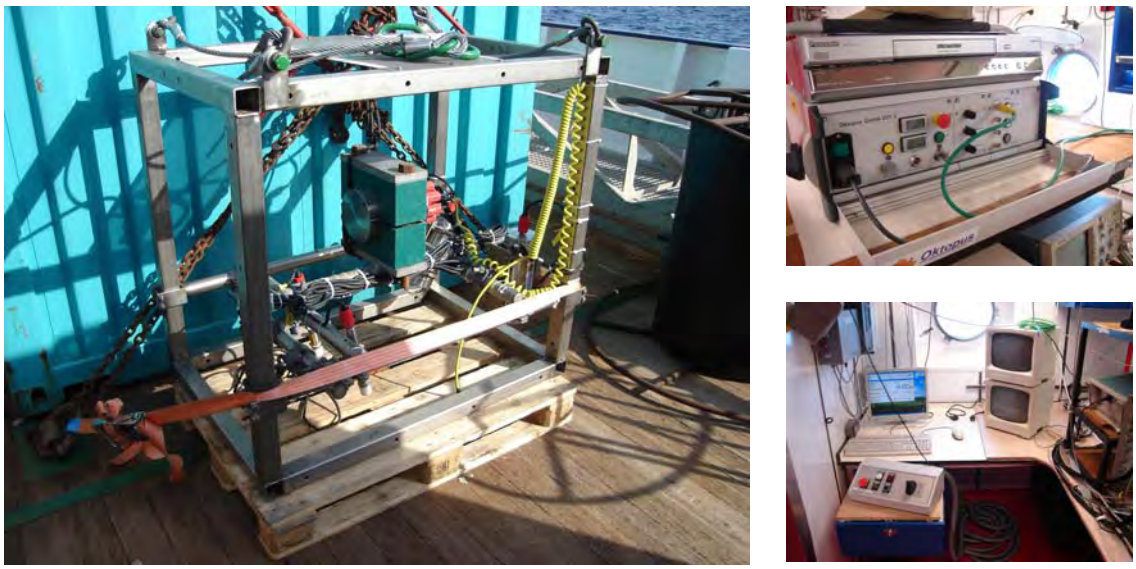

Fig. 23: TV-sled (left), deck unit (upper right) and workplace of the winch operator (lower right).

The sled was lowered on the side of R/V METEOR and towed at a speed of 0.5 to 1 knot at a distance of about 2 m above the ground. This distance is kept by a winch operator manually adjusting the cable length such that a weight suspended 2 m below the sled is flying just above the sea floor. The diameter of the weight is 6 cm.

Results

The strategy for finding seeps with the TV-sled is, generally, to observe the sea floor in the areas where there is evidence for fluid seepage, e.g., when gas bubbles are detected as hydroacoustic anomalies in the PARASOUND echosounding system. Furthermore, we used the TOBI sidescan maps to look at backscatter anomalies that may be a result of methane seepage. Indications of seepage are gas hydrates, chemosynthetic communities, or the precipitation of authigenic carbonates close to the sediment-seawater interface.

Table 4: Summary of TV-sled deployments during M74/3. Counting deployments continues after eight TV-sled deployments during M74/2.

GeoB 12310 / TV-sled 9 04.11.07 15:16 – 18:50 Flare 7	**Massive carbonates,** platy and dome-like shapes, extensive **mussel fields**
GeoB 12311 / TV-sled 10 4.11.07 21:29 – 00:02 Flare 6 and Pockmark	**Clams, mussels**, **and carbonates** south of flare position, no indications for fluid seepage at pockmark
GeoB 12323 / TV-sled 11 10.11.07 21:12 – 00:45 Flare 11, TOBI backscatter anomaly	**Inactive carbonate** structures have been found
GeoB 12325 / TV-sled 12 11.11.07 20:45 – 01:50 Flare 4, first ridge	**Massive carbonates, clams and mussels** found 500 m west of TOBI flare position
GeoB 12345 / TV-sled 13 18.11.07 19:56 – 21:08 Flare 11, TOBI backscatter anomaly	**Seep indicators** found along axis of the backscatter anomaly
GeoB 12346 / TV-sled 14 19.11.07 00:02 – 01:05 Canyonwall slump	**No indication for fluid seepage**

Seep-typical organisms are commonly used as evidence for sulphide-rich habitats, and may occur, in general, at methane seeps as well as in the oxygen minimum zone (OMZ). Their nutrition is largely based on reduced sulphide compounds (chemotrophy) which are produced when sulphate, rather than oxygen is used as electron acceptor (sulphate reduction). This can be either coupled to the process of methane oxidation (anaerobic oxidation of methane, AOM) or to organic matter degradation. In the OMZ both processes may co-occur whereas at methane seeps AOM generally dominates. The expected chemosynthetic organisms that thrive on sulphides are filamentous sulphide oxidizing bacteria (Thioploca, Beggiatoa) forming thick white mats at the sea floor, or invertebrate species that live in symbiosis with sulphur-oxidizing bacteria such as bivalves or vestimentiferan tube worms. Depending on the geochemical setting and the water depths one or the other species may prevails at a sulphide-rich site.

The filamentous sulphur oxidizing bacteria Thioploca was found in the OMZ off Pakistan (Schmaljohann et al. 2001). These bacteria can cope with low oxygen concentrations by using nitrate as electron acceptor. The filamentous sulphur oxidizing bacteria Beggiatoa and invertebrate species such as vesicoymid clams or mytilid mussels are expected to be present at methane seeps below the OMZ.

Authigenic carbonate precipitation at the sea floor is additional evidence for methane seepage. AOM produces carbonate ions which can then precipitate as calcium carbonate ($CaCO_3$) using seawater calcium (and to minor extent magnesium). The carbonates may

cement the sediments or precipitate in the water column forming so-called chemoherms that can reach several meters in height. In total, six TV-sled profiles have been conducted during the R/V METEOR cruises (Table 4, Fig. 24).

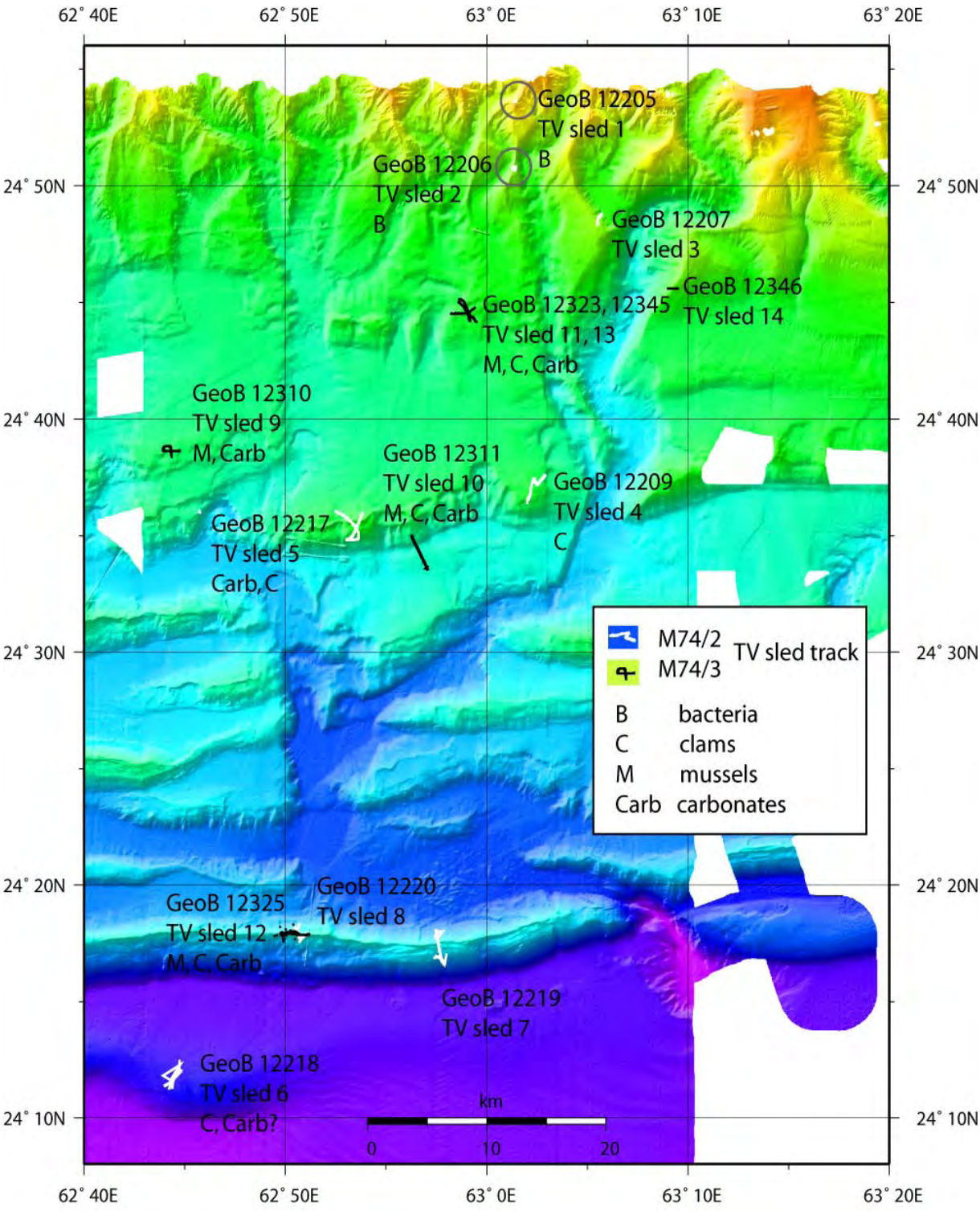

Fig. 24: Overview of TV-sled deployments during cruises M74/2 (white) and M74/3 (black).

GeoB 12310, TV-sled 9

During recording of TOBI profiles one flare was discovered, which motivated to do another more detailed flare imaging campaign in the area. After discovery of a second flare, the first flare position was not active at that time, TV-sled 9 gave an impression of the appearance of the sea floor. Coincident with a TOBI backscatter anomaly of higher backscatter intensity, repeatedly carbonate structures and mussel fields of 10s of metres in extend were found, which became the target for some ROV dives.

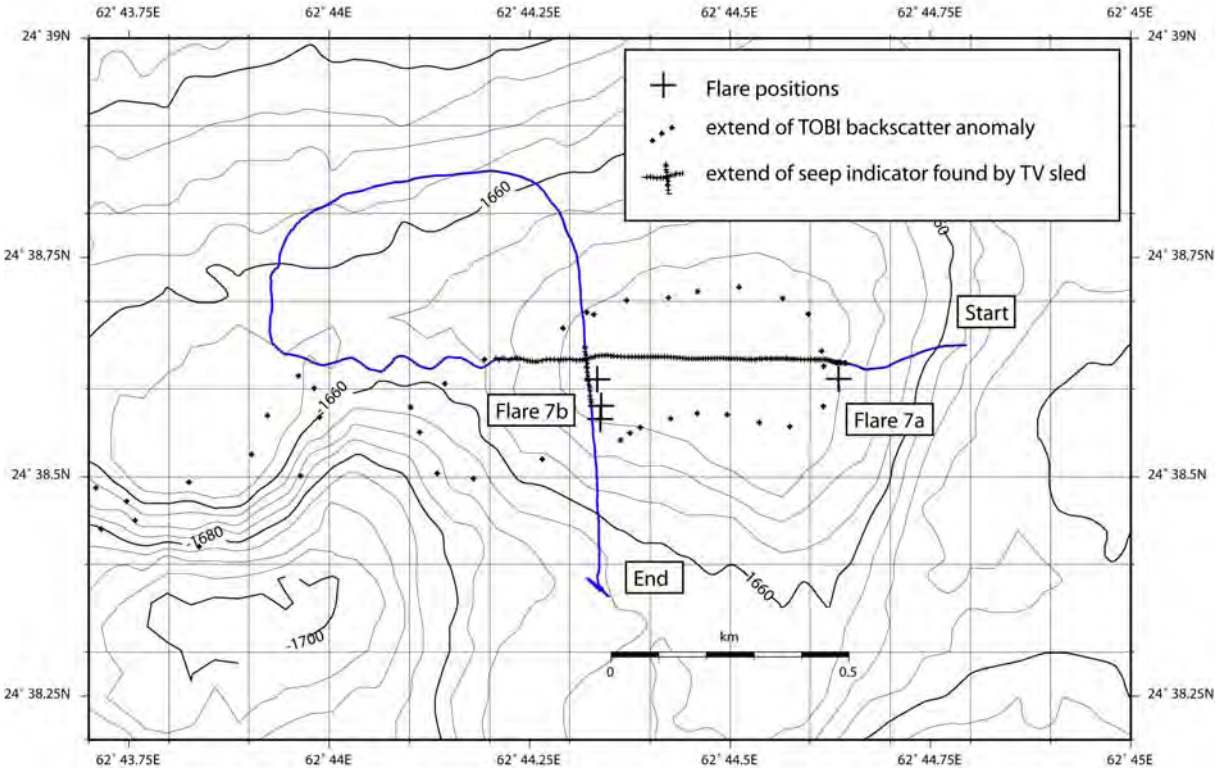

Fig. 25: (GeoB 12310) Tracks of TV-sled 9 at Flare 7.

GeoB 12311, TV-sled 10

TV-sled 10 started north upslope of the position, where the strongest signal of Flare 6 was seen on PARASOUND records. It passed the flare-position and continued further downslope to have a look into a pockmark found during Leg M74/2. Right south below the flare position indicators for seepage appeared on the sea floor: clams, mussels, and carbonates. Their extend correlates well with the TOBI backscatter anomaly of increased value in that area. Between the foot of the steep slope and the pockmark innumerable sea urchins settled. The pockmark did not show any indication of present or past seep activities in the video observation.

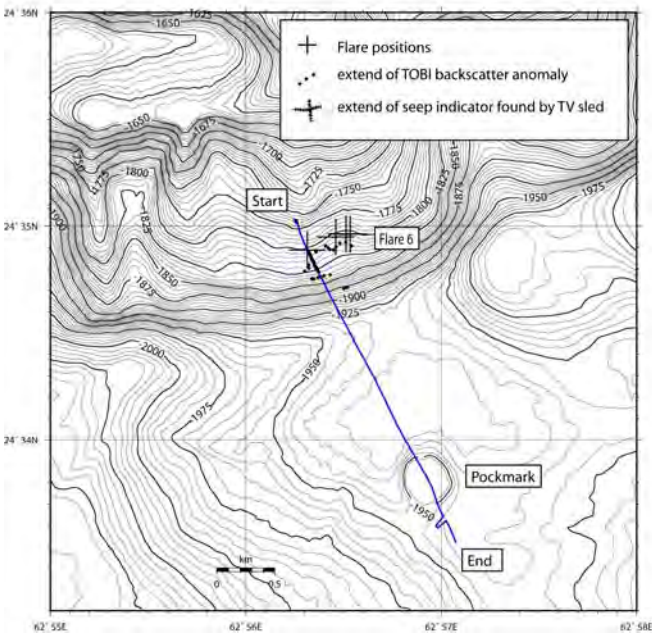

Fig. 26: (GeoB 12311) Track of TV-sled 10 at Flare 6 and through the pockmark.

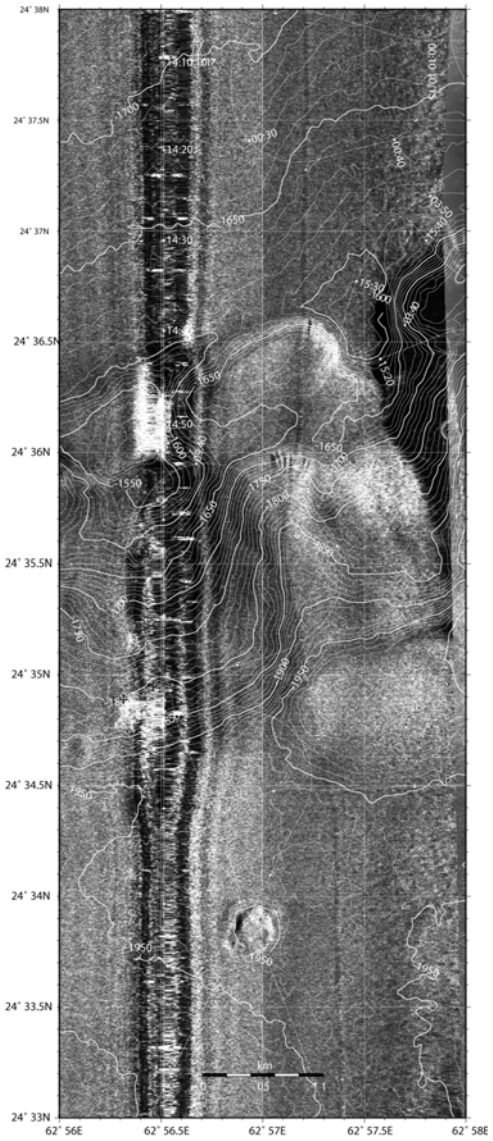

Fig. 27: TOBI side scan image. High backscatter is in light colours, low backscatter dark.

GeoB 12323, TV-sled 11

TV-sled 11 intended to cross a backscatter anomaly recorded by TOBI, shown in Fig. 28. It is a large area with high backscatter, and two neighbouring smaller ones. Arriving in the area, the main anomaly was passed very slowly by R/V METEOR to look for flares, which were found (Flare 11 a and b). A crossing of the two small areas and then several crossings of the main part, including the flare positions, moving westwards were planned. Due to a problem with the ship's cable, which needed to speed up with 2 kn northwards of the end of the first profile, and tight schedule, only two lines were possible.

Two structures of carbonate blocks of metre size were found, one in the south-eastern backscatter anomaly, one far north, not corresponding to the TOBI image. Both did not show signs of recent activity like mussels or other biota.

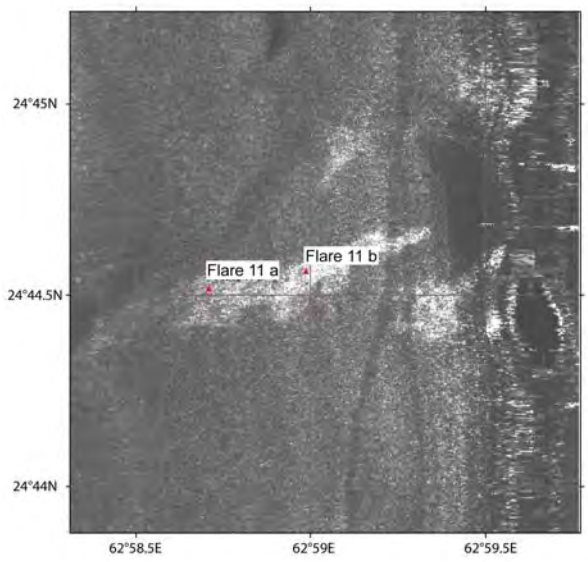

Fig. 28: TOBI backscatter anomaly investigated by TV-sled 11 and 13. High backscatter is light, low backscatter dark.

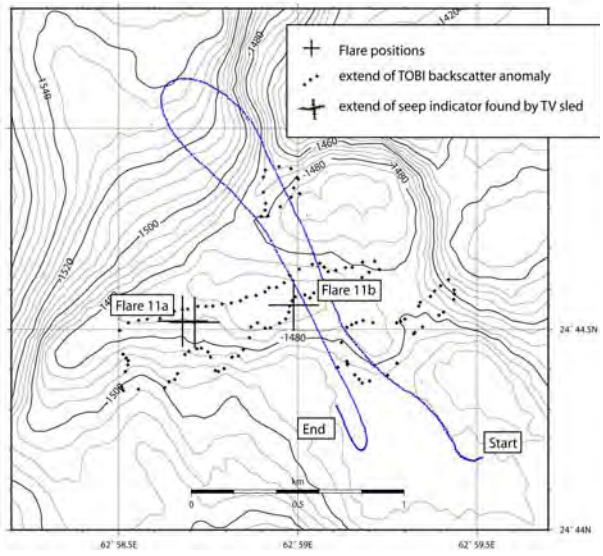

Fig. 29: (GeoB 12323) Track of TV-sled 11 at a TOBI backscatter anomaly and flare 11. Two inactive carbonate blocks were discovered. Shortage of time did not allow more crossings of the structure.

GeoB 12325, TV-sled 12

TV-sled 12 is an extension of TV-sled 8. TOBI had indicated a flare on the first ridge, but TV-sled 8 did not reveal any indicators for seep-activity on the sea floor. As the first ridge was a new setting which was not explored by ROV at that time, one more try was taken to find the root of the flare. It focused on the part of the ridge west of the old flare position. PARASOUND showed flare 4 500 m west of TOBI's position as can be seen in Fig. 30. A 500 m long transect of seep indicators: clams, mussels, and carbonates fits well to the two flares seen on PARASOUND. Between those two the biology appeared highly active.

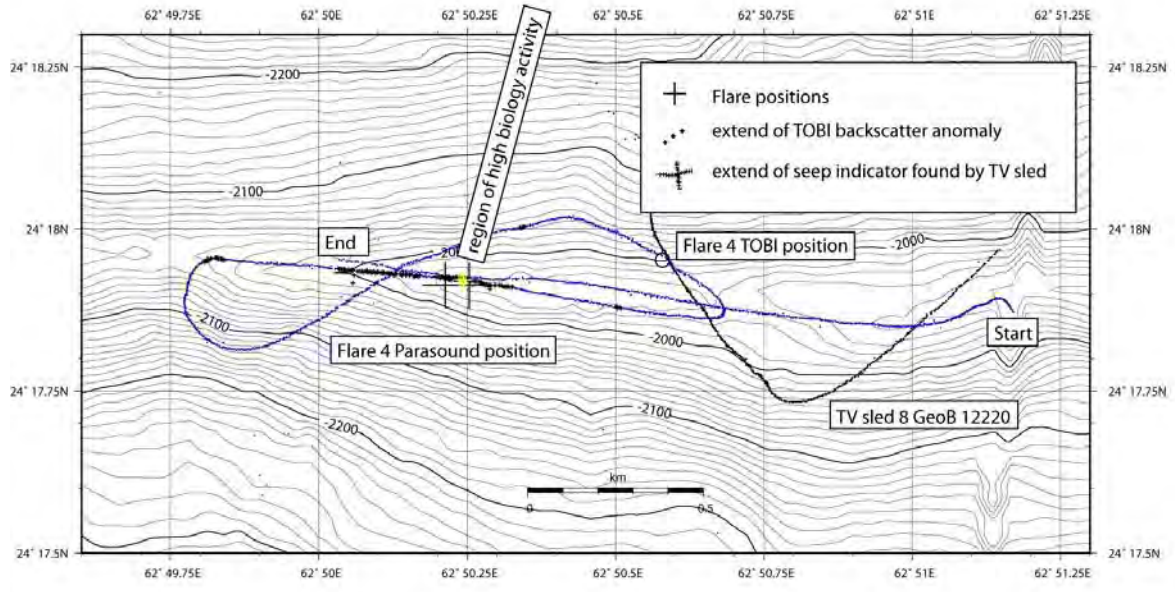

Fig. 30: (GeoB 12325) Track of TV-sled 12 next to GeoB 12220 TV-sled 8. A flare was found with PARASOUND 500 m west of TOBI's flare position (circle). Seep-related organisms as observed correlate well with those new flare positions.

GeoB 12345, TV-sled 13

TV-sled 13 followed the preceding TV-sled 11. It travelled along the prolate backscatter anomaly passing both Flare positions 11 a and b. Starting 100 m east of Flare 11 b a 500 m long strip with seep indicating clams, mussels, and carbonates was detected. 150 m ahead of Flare 11 a it ended, and nothing special was seen at Flare 11 a or west of it.

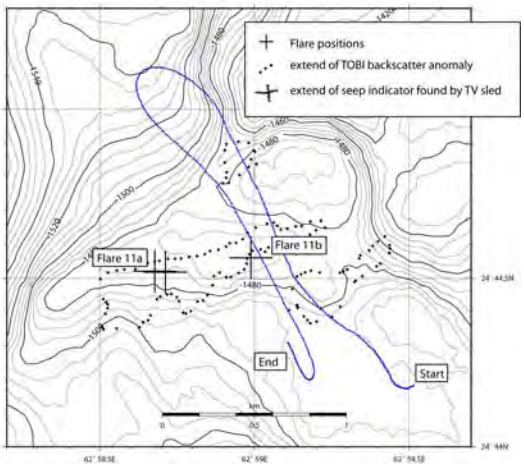

Fig. 31: (GeoB 12345) Track of TV-sled 13. This second TV-sled at Flare 11 was more successful in finding active seep communities and carbonate on the sea floor.

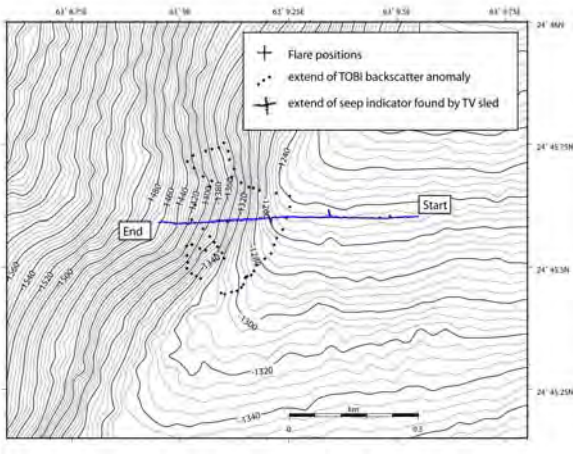

Fig. 32: (GeoB 12346) TV-sled 14 followed a canyon wall edge and downslope a fresh slump scarp.

GeoB 12346 TV-sled 14

TV-sled 14 ought to find seepage at a water depth of 1200 m to fill a gap in the overall M74/3 ROV program in that depth. A slump which was indicated by high backscatter on the upper part of a canyonwall was chosen for that. It showed high backscatter at the crest above the slump. Flare 2 which was investigated during several ROV dives showed seepage in a similar location from a crack parallel to a steep drop down into a canyon.

Opposite to indications in the backscatter the video observation did not show anything else than plain sea floor.

6. Remotely Operated Vehicle (ROV) QUEST

6.1. Technical Description and System Performance

(V. Ratmeyer, S. Buhmann, D. Huettich, N. Nowald, R. Rehage, M. Reuter, W. Schmidt, C.Seiter)

The deepwater ROV (remotely operated vehicle) "QUEST 4000m" used during M74/3 aboard R/V METEOR, is installed and operated at MARUM, Center for Marine Environmental Sciences at the University of Bremen, Germany. The ROV QUEST is based on a commercially available 4,000 m rated deepwater robotic vehicle designed and built by Schilling Robotics, Davis, USA. Since installation at MARUM in Mai 2003, it was designed as a truly mobile system specially adapted to the requirements of scientific work aboard marine research vessels for worldwide operation. Today, QUEST has a total record of 196 dives, including this cruise.

During M74/3, QUEST performed a total of 18 dives to depths between 550 and 2,950 m (Tabs. 5a and 5b). Except for one, all dives with a total of 135 hours bottom time allowed successful scientific sampling and observation at different sites. QUEST was operated by a team of 8 pilots/technicians on a daily basis with a mean dive time of 12 hrs. One dive had to be cancelled and two other dives were interrupted for technical reasons due to an isolation and a compensation, which both could be instantly repaired after recovery.

Fig. 33: ROV QUEST being deployed from R/V METEOR (left). View inside the QUEST control van during carbonate sampling (Dive 196; right).

Close cooperation between ROV team and ships crew on deck and bridge allowed a quick gain of experience for the handling procedures during deployment and recovery. During diving, this cooperation allowed precise positioning and navigation of both ship and ROV, which was essential for accurate sampling and intervention work such as instrument deployment and recovery. The ROV team is very grateful for this kind of steady support from the entire ships crew during the cruise.

QUEST System Description

The total QUEST system weighs about 45 tons (including the vehicle, control van, workshop van, electric winch, 5000-m umbilical, and transportation vans) and can be transported in four standard ISO 20-foot vans. Using a MacArtney Cormac electric driven storage winch to

manage the 5000 m of 17.6 mm NSW umbilical, no additional hydraulic connections are necessary to host the handling system.

Table 5a: Data from Dives 179-188.

Dive number/ GeoB	Dive 179 / 12301	Dive 180 / 12313	Dive 181 / 12315	Dive 182 / 12317	Dive 183 / 12319
Area	Nascent Ridge	Flare 2	Flare 2	Flare 7	Flare 1
Scientist	v. Halem	Gassner	Brinkmann	Brüning	Klapp
Water depth (m)	2800 - 2900	1000 - 1100	1000 - 1100	1660 - 1640	550 - 600
Date	02 Nov 07	05 Nov 07	06 Nov 07	07 Nov 07	08 Nov 07
Start at bottom (UTC)	06:22	10:04	05:14	09:30	04:37
End at bottom (UTC)	10:31	15:41	15:02	16:22	07:39
Bottom time (h:m)	04:09	05:37	09:48	06:52	03:02
MiniDVD tapes	5 A + 5 B	6 A + 6 B	10 A + 10 B	7 A + 7 B	4 A + 4 B
HDCam tapes	2	2	4	3	-
Push cores (no.)	4	8	8	1	
GBS (no.)	1	2	1	1	
Net		Sed + clams			
T-stick	2				1
Marker		No 9			
ISPS		deployed	recovered		yes
KIPS					
Carbonate		1		1	
Others			Osmo deplo.		

Dive number/ GeoB	Dive 184 / 12320	Dive 185 / 12322	Dive 186 / 12324	Dive 187 / 12326	Dive 188 / 12328
Area	Flare 1	Flare 7	Flare 6	Nascent Ridge	Flare 2
Scientist	Bohrmann	Pape	Von Halem	Bahr	Brinkmann
Water depth (m)	550 - 600	1660 - 1640	1850 - 1800	2800 - 2900	1000-1100
Date	9 Nov 07	10 Nov 07	11 Nov 07	12 Nov 07	13 Nov 07
Start at bottom (UTC)	05:29	06:04	06:58	05:37	05:39
End at bottom (UTC)	15:49	15:28	16:43	15:47	15:00
Bottom time (h:m)	10:20	09:24	09:45	10:10	09:29
MiniDVD tapes	12 A + 12 B	9 A + 9 B	10 A + 10 B	11 A + 11 B	10 A + 10 B
HDCam tapes	3	2	2	1	2
Push cores (no.)	8	2	8	8	8
GBS (no.)	2	1		2	1
Net					
T-stick	1		3		
Marker				No 1 + 8	
ISPS	yes		yes	yes	
KIPS	2	2			
Carbonate			1		
Others		Bubblemeter			Osmo recov.

The QUEST uses a Doppler Velocity Log (DVL, 1200 kHz) to perform Stationkeep, Displacement, and other auto control functions. The combination of 60-kW propulsion power with DVL -based auto control functions provides exceptional positioning capabilities at depth. Designed and operated as a free-flying vehicle, QUEST system exerts such precise control over the electric propulsion system that the vehicle maintained relative positioning accuracy within decimeters. Although these data were not used for absolute navigation, they are an essential

Table 5b: Detailed informations from Dives 189-196.

Dive number/GeoB	Dive 189 / 12333	Dive 190 / 12334	Dive 191 / 12338	Dive 192 / 12339	Dive 193 / 12343
Area	Flare 2	Flare 3	Flare 7	Flare 5	Flare 2
Scientist	Tomanek	Klapp	Rossel	Brüning	Yoshinaga
Water depth (m)	1000 - 1100	1550-1600	1640-1660	2800-2900	1000 - 1100
Date	15 Nov 07	15 Nov 07	16 Nov 07	17 Nov 07	18 Nov 07
Start at bottom (UTC)	05:12	10:40	06:29	06:26	05:47
End at bottom (UTC)	07:45	11:12	16:01	14:21	14:22
Bottom time (h:m)	02:00	01:32	09:30	07:55	08:25
MiniDVD tapes	3 A + 3 B	2 A + 2 B	10 A + 10 B	7 A + 7 B	9 A + 9 B
HDCam tapes	1	1	3	1	2
Push cores (no.)				8	
GBS (no.)	1		1	2	1
Net			2 x sediment		
T-stick					1
Marker					
ISPS					1
KIPS			6		
Carbonate			4		
others	BM				

Dive number/GeoB	Dive 194 / 12348	Dive 195 / 12352	Dive 196 / 12353	Total dives
Area	Flare 11	Flare 4	Flare 15	**18**
Scientist	Bohrmann	Bahr	Klapp	
Water depth (m)	1450	1950-2050	700	
Date	19 Nov 07	20 Nov 07	21 Nov 07	
Start at bottom (UTC)	08:08	07:39	09:54	
End at bottom (UTC)	13:08	15:05	16:53	
Bottom time (h:m)	05:00	07:25	06:59	**135:22**
MiniDVD tapes	5 A + 5 B	8 A + 8 B	7 A + 7 B	**270**
HDCam tapes	4	4	1	**46**
Push cores (no.)		1	4	**68**
GBS (no.)			1	**18**
Net		sediment	sediment	**5**
T-stick		1		**9**
Marker				**3**
ISPS				**6**
KIPS		6		**16**
Carbonate	1		5	**13**
others				**1 + 2**

tool for vehicle control during flight and dynamic positioning on the sea floor, especially during situations with higher currents. Absolute GPS-based positioning is performed using the shipboard IXSEA POSIDONIA USBL positioning system. Performance of the USBL system reached an absolute accuracy in the range of 5-10 m.

The QUEST SeaNet telemetry and power system provides a convenient way to interface all types of scientific equipment, with a current total capacity of 16 video channels and 60 RS-232 data channels. The SeaNet connector design allows easy interface to third-party equipment, particularly to prototype sensor and sampling devices, by combining power-, data- and video-distribution plus compensation fluid transport all through one single cable-connector setup. This ease of connection is especially important in scientific applications,

where equipment suites and sensors must be quickly changed between dives. When devices are exchanged, existing cables can be kept in place, and are simply mapped to the new devices, which can consist of video, data, or power transmission equipment.

The space inside the QUEST 5 toolskid frame allows installation of mission-specific marine science tools and sensors. The initial vehicle setup includes two manipulators (7-function and 5-function), 7 color video cameras, a digital still camera (inside SCORPIO, 3.3 Megapixel), a light suite (with various high-intensity discharge lights, HMI lights, lasers, and dimmable incandescent lights), a CTD, a tool skid with drawboxes, an acoustic beacon finder and a 675 kHz scanning sonar. Total lighting power is almost 3 kW. Total additional auxiliary power capacity is 8 kW.

For extremely detailed video closeup filming, a near-bottom mounted broadcast quality (>1000 TVL) 3CCD HDTV video camera was used (inside ZEUS). Spatial Resolution of this camera is 2.2 MegaPixel at 59.94 Hz interlaced. Recording was performed on demand onto tapes in broadcast-standard digital SONY HDCAM format, using uncompressed 1.5 Gbit HD-SDI transmission protocols. Continuous PAL video footage was recorded on MiniDV tapes with two colorzoom cameras (inside PEGASUS or DSPL Seacam 6500). In order to gain a fast overview of the dive without the need of watching hours of video, video is continuously frame-grabbed and digitized at 5 sec intervals, covering both PAL and HD video material.

The QUEST control system provides transparent access to all RS-232 data and video channels. The scientific data system used at MARUM feeds all ROV- and ship-based science and logging channels into a commercial, adapted real-time database system (DAVIS-ROV). During operation, data and video including HD are distributed in real-time to minimize crowding in the control van. Using the existing ship's communications network, sensor data can be distributed by the real-time database via TCP/IP from the control van into various client laboratories, regardless of the original raw-data format and hardware interface. This allows topside processing equipment to perform data interpretation and sensor control from any location on the host ship.

Additionally, the pilot's eight-channel video display is distributed to client stations into the labs on the ship via simple CAT7 cable. This allows the simple setup of detailed, direct communication between the lab and the ROV control van. Thus, information from the pilot's display is distributed to a large number of scientists. During scientific dives where observed phenomena are often unpredictable, having scientists witness a "virtual dive" from a laboratory rather than from a crowded control van allows an efficient combination of scientific observation and vehicle control.

Post-cruise data archival will be hosted by the information system PANGAEA at the World Data Center for Marine Environmental Sciences (WDC-MARE), which is operated on a long-term base by MARUM and the Alfred Wegener Institute for Polar and Marine Research, Bremerhaven (AWI).

During M74/3, the following scientific equipment suite was handled with QUEST:
ROV based tools, installed on vehicle:

Push cores, max. 8 (geochemistry and geology)

T-Stick (continuous sediment temperature measurements)

KIPS II discrete 38 sample water probe (water and fluid chemistry)

Slurp gun (8 samples) (installed but not used)
ROV drawbox basket (carbonate sampling)
Manipulator handnet
Manipulator gas catcher
2 Quantitative gas pressure samplers
Simple buoancy markers
Autonomous T-loggers
Realtime Sea and Sun CTD with turbidity sensor
Bubblemeter (in situ video based gas measurements)

In situ instruments, intervention/operation by vehicle:

ISPS Rhizone porewater sampler
Osmo sampler

In addition, the permanently installed KONGSBERG 675 kHz Type 1071 forward looking scanning sonar head provided acoustic information of bottom morphology and was regularily used for detection of gas emissions. Also, a BENTHOS 1600 type dual frequency sidescan sonar was permanently installed and used for mapping of sea floor structures and detection of seep sites.

As a new approach, two new computers were setup in the science lab to improve the access to both the remote sidescan sonar control as well as extended planning and dive tracking using GIS. In accordance to GIS data preparation using ArcGIS by the science party, the IFREMER - developed software tool MIMOSA was very successfully used for the first time to display and follow ROV and ship tracks upon GIS based map layers in realtime. The efficiency of such information display and access instantly during a dive allowed the science lab a higher level of planning, realtime participation and documentation than during earlier cruises.

6.2 Dive Observations and Protocols

6.2.1 Dive 179 (GeoB 12301)

Area:	Nascent Ridge, Pakistan		
Responsible scientist:	Gregor von Halem		
Date:	Friday, 2 November 2007		
Start/end at bottom (UTC):	06:22/10:31		
Total bottom time:	4 h, 9 min		
Start at the bottom:	24°11.750’N	62°44.308’E	2830 m water depth
Start ascend:	24°11.741’N	62°44.258’E	2872 m water depth

Scientist schedule:	**Scientist 1/Scientist 2/Navigator in the lab**
06:00 – 08:00	Gregor von Halem/Gerhard Bohrmann/Florian Brinkmann
08:00 – 10:00	Gregor von Halem/Florian Brinkmann/Gerhard Bohrmann
10:00 – 12:00	Florian Brinkmann/Stephan Klapp/Gregor von Halem

Table 6: Instruments and tools deployed during ROV Dive 179.

GeoB	Tool/instrument	Start	Lat. [°N]	Long. [°E]	Depth (m)	Remarks
12301-1	GBS 1	09:03	24°11.748	62°44.307	2876	
12301-2	T-stick 1	09:19	24°11.750	62°44.309	2876	
12301-3	Push core 1	09:26	24°11.749	62°44.308	2876	PC 11
12301-4	Push core 2	09:29	24°11.749	62°44.308	2876	PC 28
12301-5	Push core 3	09:32	24°11.750	62°44.308	2876	PC 35
12301-6	Push core 4	09:35	24°11.750	62°44.308	2876	PC 29
12301-7	T-stick 2	09:40	24°11.750	62°44.308	2876	Marker 4

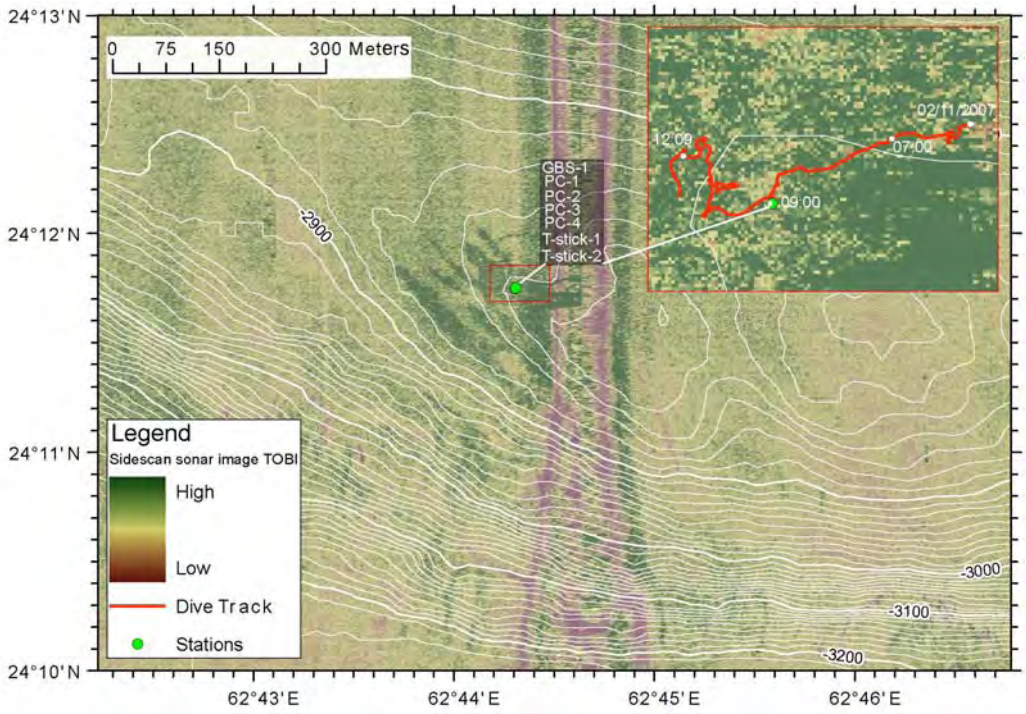

Fig. 34: Sidescan sonar map (high backscatter in green) overlaid by the ROV 179 dive track (see insert red rectangle top right corner) and stations.

The dive time was limited to five hours due to an oil pressure loss of the ROV. Nevertheless the area of Flare 5 was surveyed by using the horizontally-directed sonar system mounted on the ROV in combination with a georeferenced sidescan sonar map. A high backscatter signature was quickly identified at the area of Flare 5. The actual bubble escape site was identified by following the high backscatter signature on the sonar screen and the bubble flare on the HD/TV screen to the sea floor. The sea floor around the bubble escape site looked smooth and perforated. The perforated area was enclosed by little elevations surrounded by dead clams (Fig. 35). Living tube worms have been identified close to the bubble escape sites, as well as sea-stars and crustacaea. The bubble escape site itself was composed of several bubble streams along a linear trend, giving the impression of a curtain of bubbles (Fig. 35). After surveying the area the gas bubble sampler (GBS) was used for gas sampling (Fig. 36). Furthermore two T-stick measurements were made. The first T-stick was set in 1.4 m distance to the bubble escape site (Fig. 35) and the second one into the bubble escape site. Additionally 4 push cores have been taken parallel to the linear bubble escape site and Marker 4 was set (Fig. 36). Finally the survey continued in SW direction and the horizontally-directed sonar was again used to look for gas flares. Another high backscatter signature was recorded by the

forward looking sonar but due to the time restriction it was not possible to find the bubble stream and identify that bubble escape site on the sea floor.

Fig. 35: Sampling and surveying at Flare 5. Perforated and smooth surface around the bubble escape site (left). T-stick measurement 1.4 m away from the bubble escape site (right).

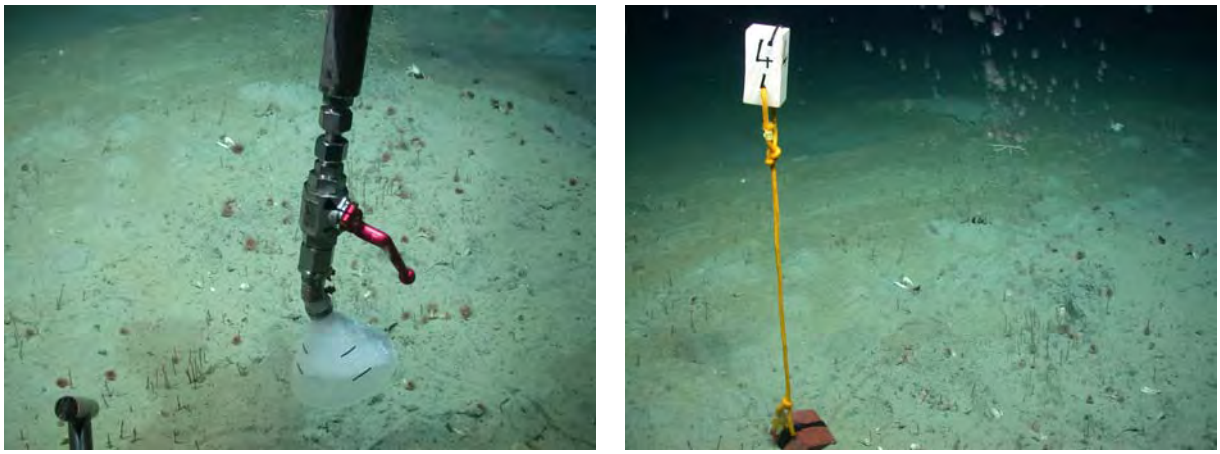

Fig. 36: Sampling and surveying at Flare 5. Gas bubble sampler measurement (left). Marker 4 set at Flare 5 close to the bubble escape (right).

6.2.2 Dive 180 (GeoB 12313)

Area:	Flare 2 in 1000 m water depth on top of a slide		
Responsible scientist:	André Gassner		
Date:	Monday, 5 November 2007		
Start /end at bottom (UTC):	10:04/15:41		
Total bottom time:	5 h, 37 min		
Start at the bottom:	24°50.787'N	63°01.483'E	1032 m water depth
Start ascend:	24°50.829'N	63°01.419'E	1038 m water depth

Scientist schedule:	**Scientist 1/Scientist 2/Navigator in the lab**
10:00 – 12:00	Gerhard Bohrmann/André Gassner/Gregor von Halem
12:00 – 14:00	Gregor von Halem/Marcos Yoshinaga/Stefan Klapp
14:00 – 15:35	Florian Brinkmann/Sabine Kasten/Gregor von Halem

Table 7: Instruments and tools deployed during ROV Dive 180.

GeoB	Tool/instrument	Start	Lat. [°N]	Long. [°E]	Depth (m)	Remarks
12313-1	ISPS	10:39	24°50.787	63°01.419	1023	Deployment of ISPS
12313-2	Push core 1	10:49	24°50.787	63°01.419	1023	PC 21
12313-3	GBS 2	11:41	24°50.799	63°01.420	1024	
12313-4	BC	12:06	24°50.799	63°01.420	1023	
12313-5	Push core 2	14:34	24°50.827	63°01.420	1038	PC 14
12313-6	Push core 3	14:37	24°50.827	63°01.420	1038	PC 3
12313-7	Push core 4	14:41	24°50.827	63°01.419	1038	PC 4
12313-8	GBS 3	14:57	24°50.827	63°01.419	1038	
12313-9	Marker 9	15:08	24°50.828	63°01.420	1038	
12313-10	Push core 5	15:20	24°50.828	63°01.420	1038	PC 7
12313-11	Push core 6	15:25	24°50.828	63°01.419	1038	PC 15
12313-12	Push core 7	15:26	24°50.828	63°01.419	1038	PC 33
12313-13	Push core 8	15:34	24°50.829	63°01.419	1038	PC 24
12313-14	Net	15:38	24°50.829	63°01.419	1038	

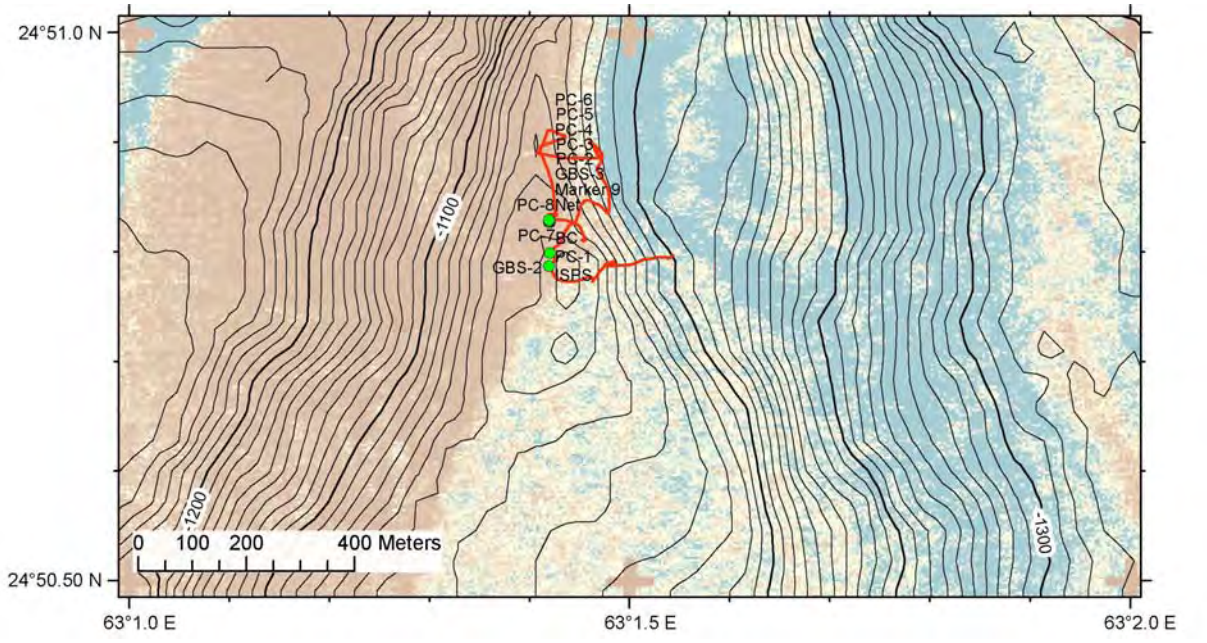

Fig. 37: Track of QUEST Dive 180.

The main objective of Dive 180 was to deploy the In Situ Pore Water Sampler (ISPS, Fig. 38), two pressure tight gas bubble samplers and 8 push cores. Additionally, exploration and gas bubble survey with the forward looking sonar of QUEST was performed. A site with no gas- or fluid seepage should be found to deploy the ISPS. After approx. 25 minutes flight to the west over hemipelagic seabed with a steep slope, the ROV reached the top of the small ridge. After having parked QUEST, the ISPS (GeoB 12313-1, Fig. 38) was successfully deployed in the sediment. A push core (GeoB 12313-2, Fig. 38) was taken at this reference site for the ISPS approx. 30 cm beside to compare both profiles. After the deployment of the tools, QUEST ascended 20 m above the sea floor for gas bubble search using the forward looking sonar. After 5 minutes gas bubbles were detected in the water column and a corresponding seep site was discovered on the bottom. This site was a kind of tiny caldera with a rim, covered with tube worms, polychaets and bacteria. With the gas bubble sampler

(GeoB 12313-3, Fig. 38) and a gas bubble catcher, gas and vent fauna were sampled. Afterwards QUEST flew for sonar survey to and around WP1. A high backscatter on the sonar screen was observed to the west in direction of WP 1. At the sea floor, patches of bacterial mats (most possibly Thioploca mats, Fig. 39) were found. At a Thioploca mat with an escape of free gas, tube worms, other worms (Polychaets?) and mussels have been observed. After having parked QUEST, a larger amount of gas bubbles escaped. 3 push cores (GeoB 12313-5/ -6/ -7) were taken from the fluffy sediment covered with the bacterial mat, whereas a strong gas expulsion due to a penetrating push core was observed. Additionally the second gas bubble sampler (GeoB 12313-8) and a marker (No. 9, GeoB12313-9) were deployed. After having sampled the Thioploca mat, the ROV moved towards the clam field, surrounding the bacteria for taking 3 more push cores (GeoB 12313-10/ -11/ -12) from the clam field. While penetrating the push cores into the sea floor, no gas bubble escape was observed. One push core (GeoB 12313-13) was deployed at the very border of the clam field. At least the net (GeoB 12313-14, Fig. 39) was deployed to sample the clams and the worms (Fig. 39).

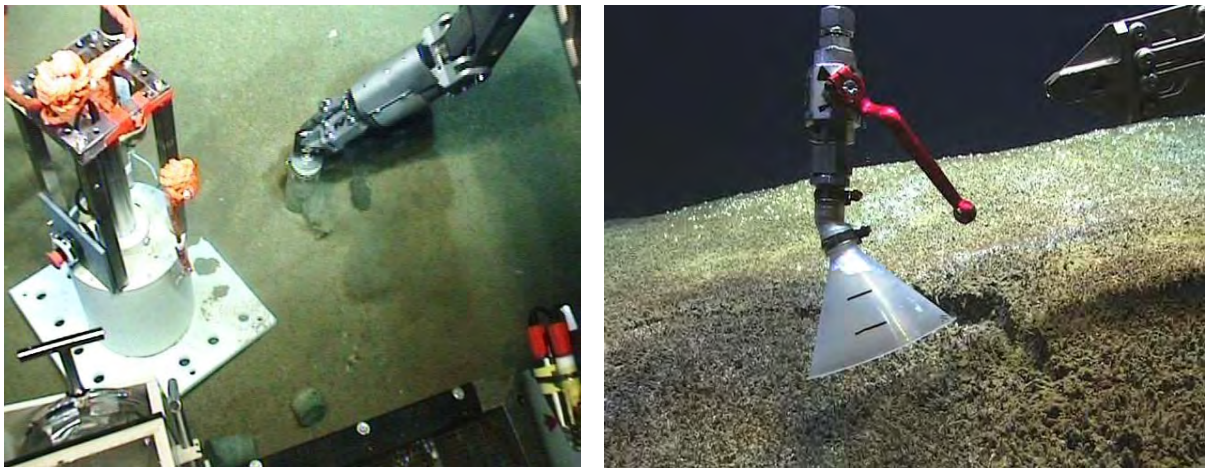

Fig. 38: ISPS and PC deployment in background area (left). Gas bubble sampler deployment over seep area covered with worms and bacteria (right).

Fig. 39: Thioploca mat surrounded by worms and clams (left). ROV collecting worms and clams with the Net (right).

6.2.3 Dive 181 (GeoB 12315)

Area:	Flare 2 in about 1000 m water depth on top of a slide		
Responsible scientist:	Florian Brinkmann		
Date:	Tuesday, 6 November 2007		
Start/end at bottom (UTC):	05:14/15:02		
Total bottom time:	9 h, 48 min		
Start at the bottom:	24°50.796'N	63°01.440'E	1025 m water depth
Start ascend:	24°50.786'N	62°01.424'E	1015 m water depth

Scientist schedule:	**Scientist 1/Scientist 2/Navigator in the lab**
09:00 – 11:00	Florian Brinkmann/Stephan Klapp/Gregor von Halem
11:00 – 13:00	Gerhard Bohrmann/André Bahr/Markus Brüning
13:00 – 15:00	Markus Brüning/Pamela Rossel/Gregor von Halem
15:00 – 17:00	Gregor von Halem/Sebastian Stephan/Florian Brinkmann
17:00 – 19:00	Florian Brinkmann/Sabine Kasten/Gregor von Halem

Table 8: Instruments and tools deployed during ROV Dive 181.

GeoB	Tool/instrument	Start	Lat. [°N]	Long. [°E]	Depth (m)	Remarks
12315-1	OS	05:36	24°50.753	63°01.436	1025	
12315-2	GBS-4	06:24	24°50.753	63°01.436	1025	Yellow GBS
12315-3	Carbonate 1	13:22	24°50.784	63°01.422	1025	
12315-4	Push core 1	13:53	24°50.753	63°01.439	1025	PC 36
12315-5	Push core 2	13:57	24°50.753	63°01.439	1025	PC 19
12315-6	Push core 3	14:03	24°50.753	63°01.439	1025	PC 5
12315-7	Push core 4	14:24	24°50.753	63°01.439	1025	PC 28
12315-8	Push core 5	14:29	24°50.753	63°01.439	1025	PC 11
12315-9	Push core 6	14:34	24°50.753	63°01.439	1025	PC 2
12315-10	Push core 7	14:39	24°50.753	63°01.439	1025	PC 23
12315-11	Push core 8	14:51	24°50.789	63°01.417	1025	PC 22
12315-12	ISPS	14:55	24°50.789	63°01.417	1025	

Main emphasis of this survey was the investigation of an elongated depression that was discovered on top of the ridge structure (Fig. 40) during the dive before, Dive 180. This depression, showing a northwest/southeast extension, could be followed easily by means of the forward looking sonar (Fig. 41 left). But also visual observation allowed investigations of this crack-like structure (Fig. 41 right). The dimension of the depressions varies quite strongly. The flanks are mostly less than one meter in height and the diameter of the structure ranges from a few to more than ten metres. Bacterial mats with associated faunal assemblages are very abundant in the central parts. They mark the most characteristic feature and show a clear concentric appearance (Fig. 42 left and right). The faunal clearly bears a longish concentric distribution. The central part is dominated by bacterial mats which show distinctive colours, ranging from white over pale pink to bright orange. They might be Beggiatoa, or Thioploca mats (as it has been reported for the Makran Accretionary Ridge). Two subsequent outer rims comprise small tube worms (undefined polychaeta) and small clams (very likely vesicomyids). The surrounding areas are dominated by much bigger clams (possibly Calyptogena). Often the mats were very extensive (Fig. 43 left) and densely covered with

long filaments (Fig. 43 right). All structures and fauna were documented by means of HD videos in detail.

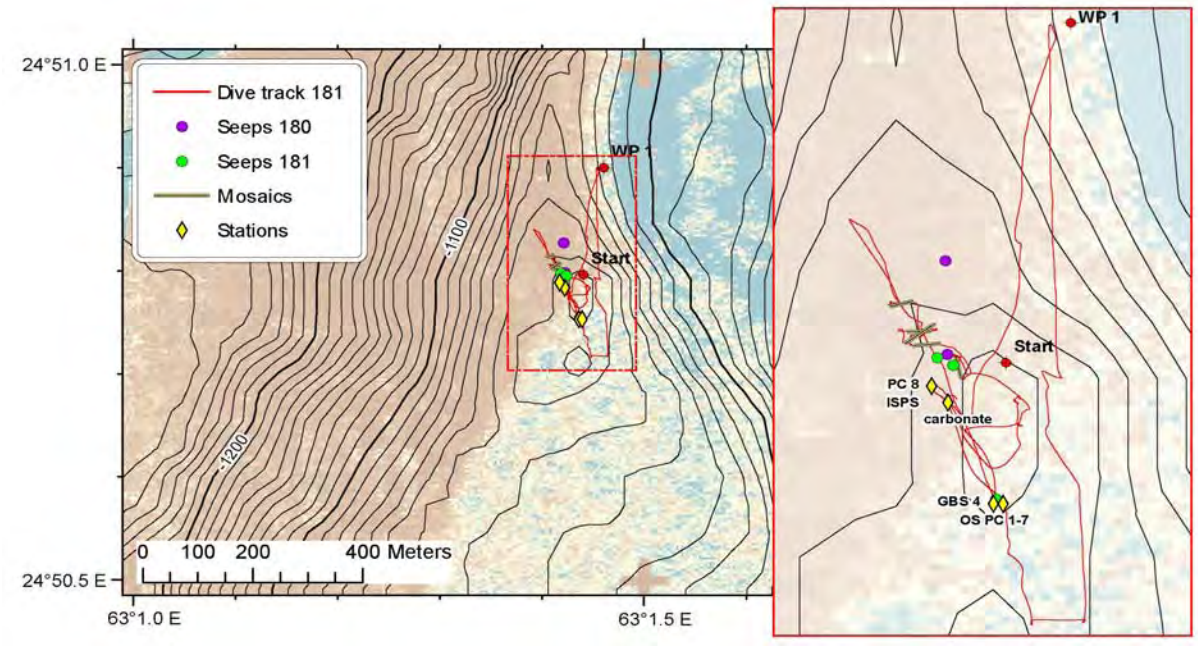

Fig. 40: Sidescan sonar map comprising a projection of the ROV dive track 181 and the waypoints. Red insert marks a zoom into the central part of the dive track. In this case, distinction between high (greenish) and low (brownish) backscatter might be a shadow effect due to the ridge structure. The centre part of the surveyed area is dominated by a ridge structure. On top of the ridge a depression, running more or less parallel to the ridge, was examined and a few photo mosaic sequences were performed.

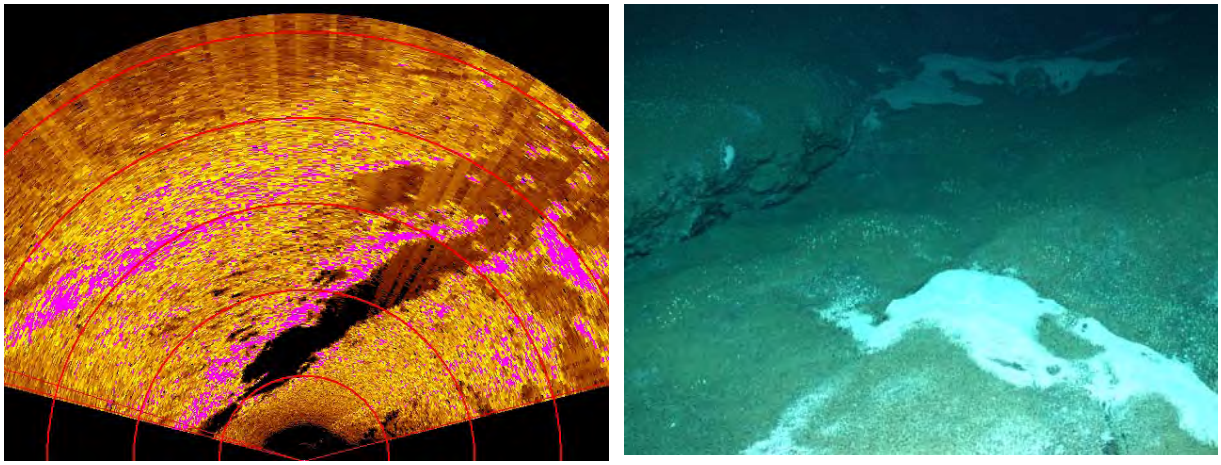

Fig. 41: Survey documentation at Flare 2. Approaching the depression from the south east using forward looking sonar (one circle equals 10 metres) (left). Visual appearance of the depression on top of the investigated ridge. White patches are bacterial mats (right).

Two other main objectives were the recovery of the In Situ Pore water Sampler, ISPS (Fig. 44 left) and the deployment of the Osmo Sampler The Osmo Sampler was deployed at an active seep site over an extensive bacterial mat (Fig. 44 left). Additionally, the gas bubbles were sampled with a Gas Bubble Sampler (Fig. 44 right). A carbonate crust sample was taken at one of the flanks surrounding the depression (Fig. 45 left). Furthermore, 3 push cores were

taken at the tube worm zone (TW) surrounding the bacterial mat where the Osmo Sampler was deployed (Fig. 45 right), and 4 directly in the bacterial mat (Fig. 46 left). After a last push core was taken next to the ISPS, the pore water sampler was recovered (Fig. 46 right) and the dive was completed.

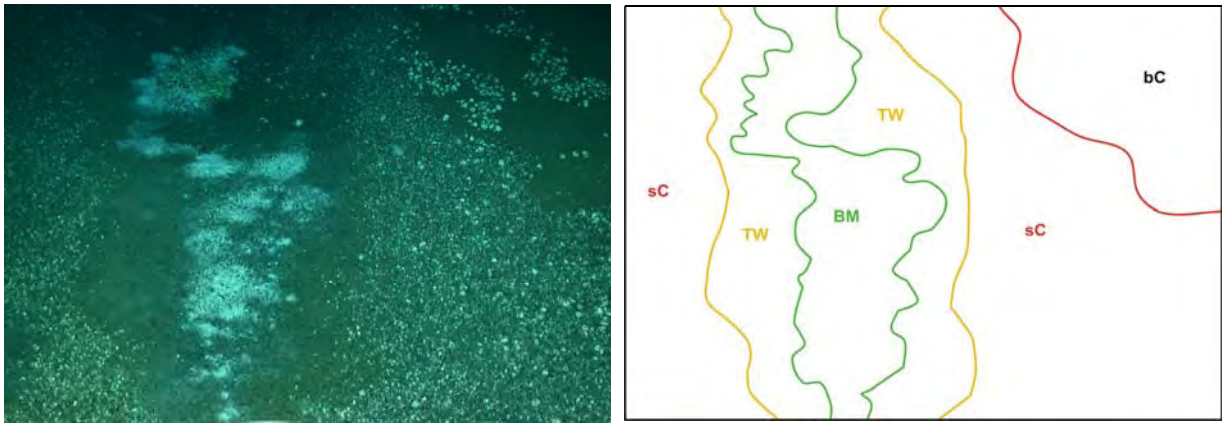

Fig. 42: Survey documentation at Flare 2. Concentric structures of involved biota on the top of the ridge. Whereby the central part is dominated by bacterial mats two subsequent outer rims comprise small tube worms and small clams. The surrounding areas are dominated by much bigger clams (left). Sketch of the concentric structure. Abbreviations: BM bacterial mat, TW tube worms (undefined polychaeta), sC small clams (very likely vesicomyids), bC big clams (possibly calyptogena) (right).

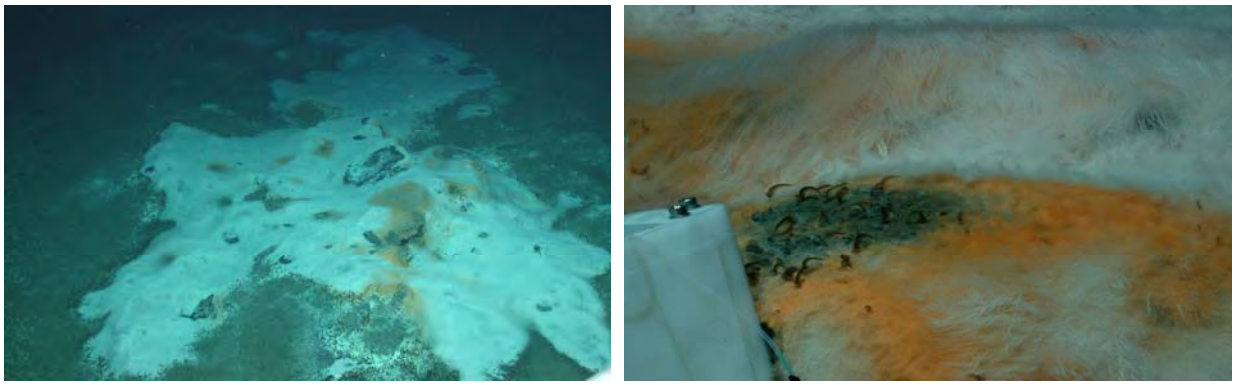

Fig. 43: Survey documentation of Flare 2. At some spots the covering bacterial mats are very extensive and dense (left). Details of a bacterial mat. The bacteria form long filaments in different colours ranging from white over pale pink to bright orange. The dark patch which is not covered with bacteria bears a few of the polychaets (right).

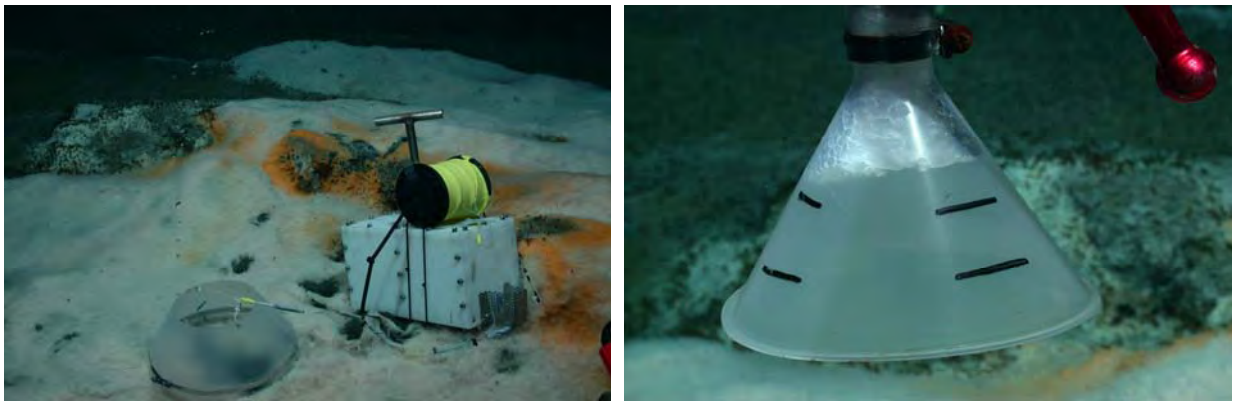

Fig. 44: Sampling at Flare 2. Funnel of the Osmo Sampler placed over an active bubble stream. The actual osmotic pump device samples the bottom water within the funnel at fixed intervals over a certain time period (left). The bubble stream at the Osmo Sample was additionally sampled by means of a Gas Bubble Sampler (GBS) (right).

Fig. 45: Sampling at Flare 2. Carbonate Crust was recovered from one of the flanks of the depression (left). 3 push cores were taken with the tube worm zone (TW) around the bacterial patch where the Osmo Sampler was deployed (right).

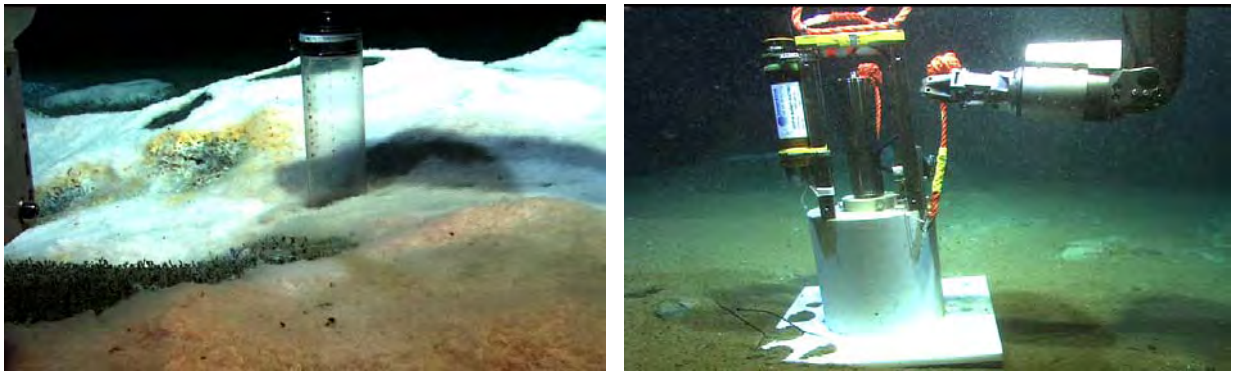

Fig. 46: Sampling at Flare 2. 4 push cores were taken within the bacterial mat (left). Recovery of the ISPS (right).

6.2.4 Dive 182 (GeoB 12317)

Area:	Flare 7 high-backscatter hilltop		
Responsible scientist:	Markus Brüning		
Date:	Wednesday, 7 November 2007		
Start/end at bottom (UTC):	09:30/16:22		
Total bottom time:	6 h, 52 min		
Start at the bottom:	24°38.624'N	62°44.660'E	1652 m water depth
Start ascend:	24°38.633'N	62°44.644'E	1651 m water depth

Scientist schedule:	**Scientist 1/Scientist 2/Navigator in the lab**
09:24 – 10:34	Markus Brüning/Thomas Pape/Gregor von Halem
10:34 – 12:00	Gerhard Bohrmann/Mohammad Nasir/Markus Brüning
12:00 – 14:00	Gregor von Halem/David Fischer/Gerhard Bohrmann
14:00 – 16:22	Florian Brinkmann/Sabine Kasten/Markus Brüning

Table 9: Instruments and tools deployed during ROV Dive 182.

GeoB	Tool/instrument	Start	Lat. [°N]	Long. [°E]	Depth (m)	Remarks
12317-1	GBS-5	13:56	24°38.649	62°44.254	1654	yellow GBS
12317-2	PC-1	15:49	24°38.633	62°44.645	1651	PC-14
12317-3	Clams	16:22	24°38.633	62°44.644	1651	

ROV Dive 182 on 07 November 2007 explored a hilltop at 24°38.6'N 62°44.5'E which was passed once on its eastern edge during M74/2 and revealed a flare (Flare 7) on PARASOUND records. During two night programs of M74/3 PARASOUND flare imaging and TV-sled surveys showed further evidence for seepage (Flare 7b), seep-communities and carbonates on the sea floor. ROV Dive 182 started at the eastern end, near the first flare position at 09:27 and 24°38.625'N 62°44.662'E. The first view showed a hemipelagic sea floor with little elevations and lighter colours in places caused by bioturbation. A first exposed carbonate block of metre size was passed at 09:35 at 24°38.627'N 62°44.652'E. It showed no signs of present fluid escapes. Appearing out of the sediment a carbonate platform ended after several metres, followed by a 50 cm step to the following lower sea floor covered with several white shells. At least one clam field had living individuals. A tube worm is growing close to it.

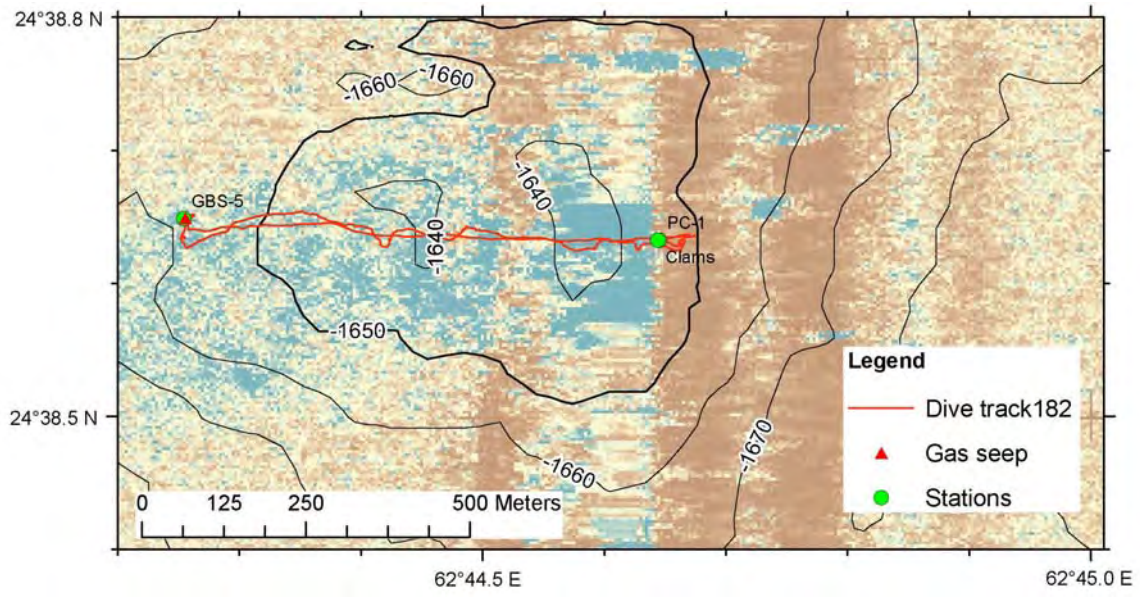

Fig. 47: Map of Dive 182: the dive started from the east, imaging the sea floor, creating an irregular track. From the westernmost point back to the starting point the side scan sonar data were recorded.

Flying westwards, until 09:56 the sea floor was bare but for a few blocks of carbonate of decimetre size. Then another clam field with tube worms in front of large carbonate plates appeared, several metres across. The carbonate plate was fully covered with sediment on top. The underpart was sparsely settled by barnacles, and possibly by bacteria forming 5 cm large half-spheres hanging from the ceiling. The ROV followed the rim of the carbonate structure westwards.

Here more layers were built on top of the main plate, with similar height between the different storeys (Fig. 48). Colonisation by *Bathymodiolus*, tube worms, white sponges, galatheid crabs and a large pink crab have been observed on the rim of the carbonate structure. On the way further westwards, after about 20 m of carbonate plates with several floors, sediment with carbonate blocks and clams followed for the next 50 m. Another step up onto a carbonate platform, similar to the first one was passed. A dense field of brown *Bathymodiolus* mussels of about 15 m diameter with irregular boundaries was followed by another sediment area with irregular loose distribution of white clams. Close to the hilltop a

third step of carbonate plate appeared. Further on, a crack in the carbonate plate was filled with tubes of tube worms, which seem to be dead, and barnacles with tube-like bases. Several steps with carbonate outcrops overhanging the sea floor followed, intersected by large strips of sediment loosely covered with shells. In places shells are lined up or gathered in nests.

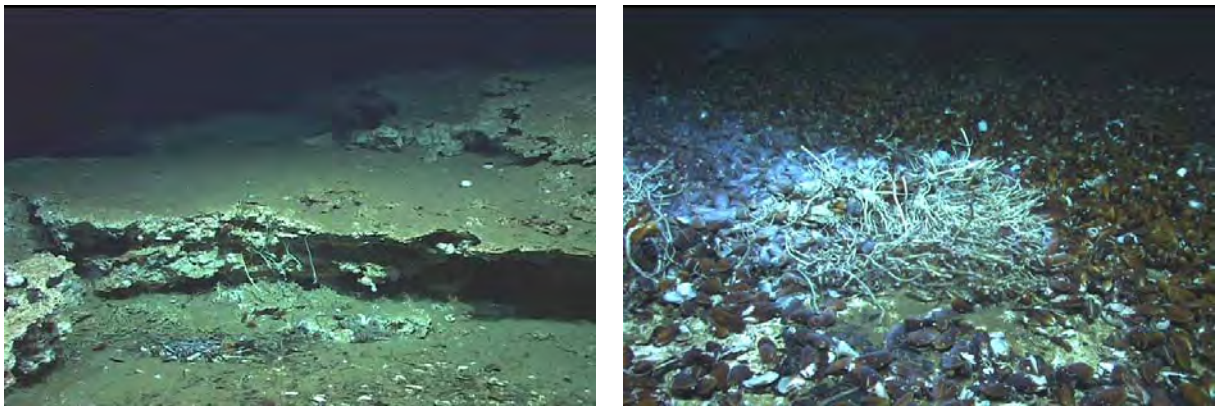

Fig. 48: Outcrop of a carbonate plate. The step from the foreground up to the background is about 50 cm high. Around the step of exposed carbonate a teeming fauna settles. The carbonate plate is covered by hemipelagic sediment. On the right-hand-side of the picture another step-up can be seen (left). Mussel field with vestimentiferan tubeworms on the carbonate plate. Parts of the mussels and tubeworms have a white coating, possibly bacteria (right).

At 10:38 the ROV reached a field of about 20 m extend in E-W direction of *Bathymodiolus*, and some other bivalves and sponges. After another section with plain sediment and few clams and small steps of carbonate outcrops downwards, at 11:11 one more field of *Bathymodiolus*, followed by several storeys of carbonate plates leading down to plain hemipelagic sediment. At 11:28 the centre of a large *Bathymodiolus* field contained a bunch of living tube worms and neighbouring clams had a whitish cover (Fig. 48 right). The site was observed in detail with HD-camera. On the way further westwards the sea floor was flat with only few clams covering the sediment. At 12:05 a *Bathymodiolus* field with loose settlement and sediment visible between mussels was passed. For the next half hour the ROV flew over sea floor with occasional white shells and small carbonate bits.

At the westernmost point, WP5 24°38.646’N 62°44.319’E, the ROV ascended into the water column to detect bubbles using the forward looking sonar. A bubble-stream was found (Flare 7c), emanating from a *Bathymodiolus* field. A sample of the gas was collected with the gas bubble sampler (GBS-5, Fig. 47). To start a flight with sidescan sonar the ROV rose to 15 m above sea floor and shifted to a position 20 south of the previous track on the sea floor. Running the sonar the ROV returned to the eastern point, where the dive started. This survey took from 14:21 till 15:26. Back on the sea floor it was intended to sample the earlier seen living clam fields with push cores at the end of the dive. Due to the hard sea floor, probably carbonate under the soft surface-sediment, only one push core could be filled (PC-1, GeoB 12317-2). To prevent destroying the plastic tubes of another push core, a net was filled with clams instead (Geo B12327-3). The dive ended at 16:22 UTC.

6.2.5 Dive 183 (GeoB 12319)

Area:	Flare 1		
Responsible scientist:	Stephan Klapp		
Date:	Thursday, 8 November 2007		
Start/end at bottom(UTC):	04:38/07:39		
Total bottom time:	3:01 hours		
Start at the bottom:	24°53.619'N	63°01.410'E	575 m water depth
Start ascend:	24°53.631'N	63°01.422'E	572 m water depth

Scientist schedule:	**Scientist 1/Scientist 2/Navigator in the lab**
04:38 – 07:00	Gerhard Bohrmann/Monawar Saleem/Gregor von Halem
07:00 – 07:39	Stephan Klapp/Janet Rethemeyer/Gerhard Bohrmann

Table 10: Instruments and tools deployed during ROV Dive 183.

GeoB	Tool/instrument	Start	Lat. [°N]	Long. [°E]	Depth (m)
12319-1	T-Stick	06:44	24°53.629	63°1.418	572
12319-2	ISPS	07:23	24°53.631	63°01.423	572

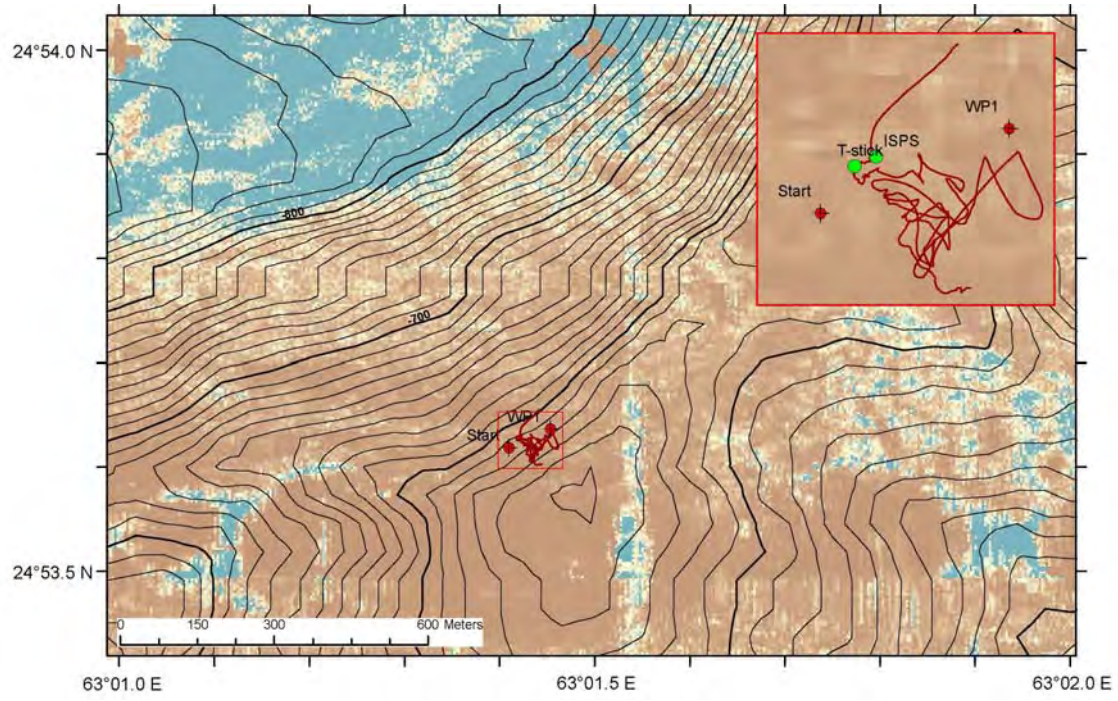

Fig. 49: Dive track of ROV-Dive 183 / GeoB 12319.

The very short dive (3 hours bottom time) had to be terminated early due to a leakage of a hydraulic oil valve. The dive had the objective to characterize the sea floor at the Flare 1. It is located at about 600 m water depth and hence at conditions where no gas hydrates form. The tasks were to detect bubble streams by forward looking sonar and sidescan sonar running across the crest (Fig. 49) and in case of positive findings, seep documentation and samplings were planned.

The survey started with a sonar flight; two spots were discovered by sonar, where bubbles escaped. However, the signals were too weak to see bubbles in the water and to locate these sites. After 1,5 hours, the ROV went down to the sea floor to watch out for bubble escape at the bottom. At 24°53.630'N/63°01.423'E, a bacterial mat came into view, but no bubbles were discernable at this site. The deployment of the ISPS was planned. Prior to that, the temperatures of the subsurface were recorded by the T-stick. They are about 12,3°C, the gradient in the first 45 cm is 0,293°C/m. The ISPS was launched off the bacterial mat but in close vicinity to gain background data. It was recovered during the subsequent Dive ROV-184 (GeoB 12320), about 32 hours later. After the deployment, pictures were taken of the tool and the bacterial mat. At the same location, the broken valve was detected and the vehicle immediately commenced the ascent.

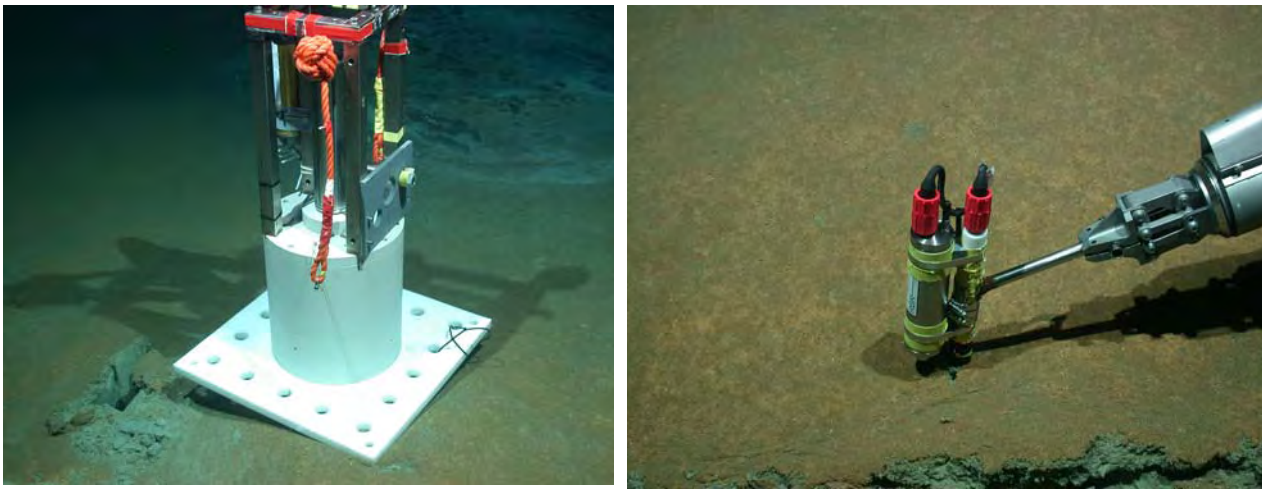

Fig. 50: ISPS on sediment. Bacterial mat is seen in the background (left). T-stick deployed by ROV-Orion arm (right).

6.2.6 Dive 184 (GeoB 12320)

Area:	Flare 1		
Responsible scientist:	Gerhard Bohrmann		
Date:	Friday, 9 November 2007		
Start/end at bottom (UTC):	05:29/15:49		
Total bottom time:	10:20 hours		
Start at the bottom:	24°53.491'N	63°01.469'E	552 m water depth
Start ascend:	24°53.630'N	63°01.425'E	580 m water depth

Scientist schedule:	**Scientist 1/Scientist 2/Navigator in the lab**
05:00 – 07:00	Stefan Klapp/Janet Rethemeyer/Gregor von Halem
07:00 – 09:00	Gerhard Bohrmann/Karin Zonneveld/Stefan Klapp
09:00 – 11:00	Gregor von Halem/Kim Thomanek/Gerhard Bohrmann
11:00 – 13:00	Florian Brinkmann/Nina Wittenberg/ Gregor von Halem
13:00 – 15:49	Gerhard Bohrmann/Sabine Kasten/ Florian Brinkmann

Table 11: Instruments and tools deployed during ROV Dive 184.

GeoB	Tool/Instrument	Start	Lat. [°N]	Long. [°E]	Depth (m)	Remarks
12320-1	T-stick	08:29	24°53.636	63°01.405	592	
12320-2	GBS-6	09:23	24°53.636	63°01.406	591	red GBS
12320-3	GBS-7	11:17	24°53.633	63°01.405	590	yellow GBS
12320-4	PC-1	14:04	24°53.634	63°01.404	551	PC 22
12320-5	PC-2	14:08	24°53.634	63°01.404	551	PC 21
12320-6	PC-3	14:10	24°53.634	63°01.404	551	PC 20
12320-7	PC-4	14:12	24°53.634	63°01.404	551	PC 15
12320-8	PC-5	14:22	24°53.634	63°01.404	551	PC 3
12320-9	PC-6	14:25	24°53.634	63°01.404	551	PC 29
12320-10	PC-7	14:26	24°53.634	63°01.404	551	PC 32
12320-11	KIPS-1	14:55	24°53.631	63°01.405	557	bubble site
12320-12	KIPS-2	15:17	24°53.631	63°01.405	557	water column
12320-13	PC-8	15:36	24°53.630	63°01.425	580	PC 7
12319-2	ISPS	15:38	24°53.630	63°01.425	580	recovery of ISPS from ROV-183

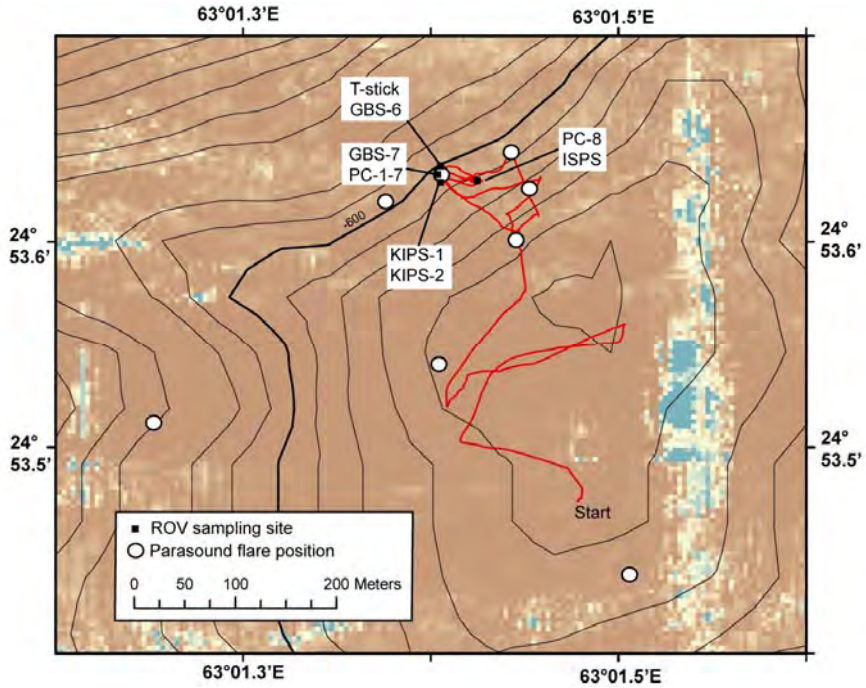

Fig. 51: Dive Track and sampling positions of ROV Dive 184 at Flare 1 within the OMZ.

Fig. 52: Seep sites at acoustic Flare 1. White and often orange bacterial maps are surrounding gas bubble escape sites.

Because Dive 183 the day before was finished due to technical problems, ROV Dive 184 was planned to visit the same seep area at Flare 1. Several acoustic anomalies have been documented so far in the area and seep structures on the sea floor have not been documented during the previous dive. Same target points on the sea floor have been used and the dive started just south of the top of the hill in 550 m water depth (Fig. 51). ROV QUEST moved along the sea floor to the top of the elevation. Since no gas seeps have been found, the vehicle started to fly higher up in westwards direction during which the forward looking sonar was used to detect potential bubbles. Since no gas bubbles have been found the ROV moved towards to three other potential gas seeps detected by flares in the water column (Fig. 51). Close to the last two flare positions QUEST could detect bubbles in the forward looking sonar, which could be attributed to bubble streams discharging from the sea floor. Each bubble stream was surrounded by a patch of whitish bacterial map, which in most cases became orange in its central part (Fig. 52). Sediments below the bacterial mats are of very dark colour because of the very fine disseminated sulphide particles. No other benthic organisms have been observed in the nearly oxygen-free bottom water. Just a few fishes have been observed by the ROV.

Fig. 53: Dark sulfide-enriched sediment becomes excavated below the white bacterial map of a gas bubble site (left). Detailed view of a distinct gas discharge site (right).

About a dozen of those seep patches (Fig. 53) have been found in a small area of about 30-50 m^2. At all patches discharging gas bubbles have been observed which moved out of holes from the sea floor (Fig. 53). We took a temperature probe measurement by the T-stick and a gas sample with the GBS at the first seep patch. A second gas sample was taken just a few meters away at a second bubble stream. After two hours exploring many of those seep patches one patch was chosen for a detailed sampling by push cores. After two water samples have been taken by the KIPS sampler ROV QUEST moved ca. 30 m to the east to the site where was deployed the day before. Before the ISPS was recovered from the sea floor a push core was taken in order to calibrate the pore water data from both profiles. After > 10 hours bottom time the ROV started his ascent to come to the surface.

6.2.7 Dive 185 (GeoB 12322)

Area:	Flare 7 (location from earlier ROV Dive 182)		
Responsible scientist:	Thomas Pape		
Date:	Saturday, 10 November 2007		
Start/end at bottom (UTC):	06:05/15:28		
Total bottom time:	9.5 hours		
Start at the bottom:	24°38.638'N	62°44.262'E	1632 m water depth
Start ascend:	24°38.565'N	62°44.398'E	1637 m water depth

Scientist schedule:	**Scientist 1/Scientist 2/Navigator in the lab**
06:00 – 07:00	Gerhard Bohrmann/Kim Thomanek/Gregor von Halem
07:00 – 09:00	Thomas Pape/Kim Thomanek/Stephan Klapp
09:00 – 11:30	Gregor von Halem/Kim Thomanek/Thomas Pape
11:30 – 13:00	Thomas Pape/André Bahr/Gerhard Bohrmann
13:00 – 15:30	Florian Brinkmann/Sabine Kasten/Thomas Pape

Table 12: Instruments and tools deployed during ROV Dive 185.

GeoB	Tool/instrument	Start	Lat. [°N]	Long. [°E]	Depth m	Remarks
12322-3	Bubblemeter	12:10	24°38.664	62°44.273	1657	
12322-1	Kips 1	12:28	24°38.643	62°44.261	1652	
12322-2	Kips 2	12:34	24°38.643	62°44.261	1652	
12322-4	GBS	12:56	24°38.644	62°44.260	1652	yellow GBS
12322-5	Push core 1	14:30	24°38.610	62°44.303	1649	PC 11
12322-6	Push core 2	15:14	24°38.579	62°44.344	1649	PC 19

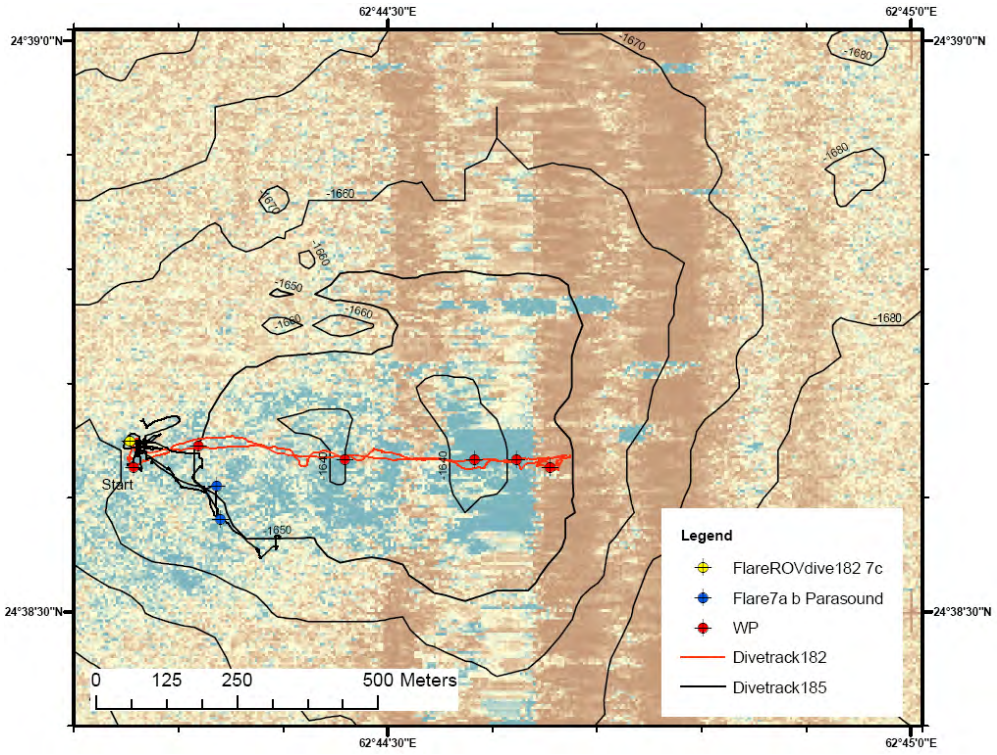

Fig. 54: Sidescan sonar map (high backscatter in blue) overlaid by the ROV 185 dive track. Yellow flag shows the location of the marker as well as the position of the identified bubble escape site. The yellow and red points indicate flare positions identified with PARASOUND.

The target area (area of Flare 7) of Dive 185 was investigated first during Dive 182. Using PARASOUND during the cruise several sites feeding gas flares in the water column could be found in the area of Flare 7, and seepage from the sea floor was already documented during Dive 182. Major task during Dive 185 was to recover known bubble emission sites in order to deploy the bubblemeter. Additionally, it was planned to collect gas, water and sediment samples using the gas bubble sampler, the KIPS, and push cores. In the meantime, a detailed habitat documentation of seepage should be accomplished.

Near-seabottom work during Dive 185 was started close to the seep site of Flare 7c. Search for gas flares was performed using the horizontally-directed sonar and flying QUEST in about 20 to 25 m above sea floor. However, backscatter anomalies in the sonar attributed to bubbles in the water column, occasionally occurred and vanished again. Sometimes even single bubbles could be observed in the water column, but tracking them to the sea floor failed. After one hour, QUEST left the area of Flare 7c heading for flares documented at locations 7a and 7b. Since indications for bubble release were not observed at both flare areas during that time, QUEST was moved back to Flare 7c.

Fig. 55: Seep site at flare area 7c settled by Bathymodiolus-like clams and crustacea in high density. Note the conspicious staining of shells of those clams living close to the seep site (left). Positioning of the bubblemeter mounted at the porch of ROV QUEST. Same emission site as in the figure left. Note three gas bubbles in front of the left side of the screen (right).

Having searched for bubbles at Flare 7c for about two hours, relatively strong, but small-sized signals suddenly appeared in the sonar image. This series could be detected over a time span of several minutes and individual signals were assumed to originate from single bubbles or small bubble clusters, which were directed towards QUEST by the bottom water current during ascent. By carefully following the signal, QUEST was lowered to the sea floor and a seep site providing single bubbles or short bubble chains every 17 to 20 seconds was discovered. The entire emission site was strongly colonized by alive clams, probably related to the genus Bathymodiolus, and diverse crustaceans. During photo and video documentation of the site the bubble release frequency diminished down to 83 seconds. Having studied the site for about 30 min, a relatively strong gas release suddenly commenced and bubbles continuously escaped the sea floor with a periodicity lower than 2 seconds for some while. It was decided to deploy the bubblemeter and subsequently the KIPS sampling system at this

site, but both devices did not work accurately due to technical problems. The gas bubble sampler was used to recover a pressurized water sample close to the bubble site. After comprehensive habitat photo- and video documentation, including high-resolution sequences of a giant crustacean, the site was left heading southeast towards Flares 7a and 7b for benthic survey. In that course, some stopovers were performed for detailed documentation of the distributions of diverse clam species, tube worms, and carbonate crusts. Furthermore, two giant Calyptogena clams were sampled by using of push cores (Fig. 56). Ascent of QUEST was started after about 9.5 hours bottom time from a site about 75 m southeast of Flare 7b.

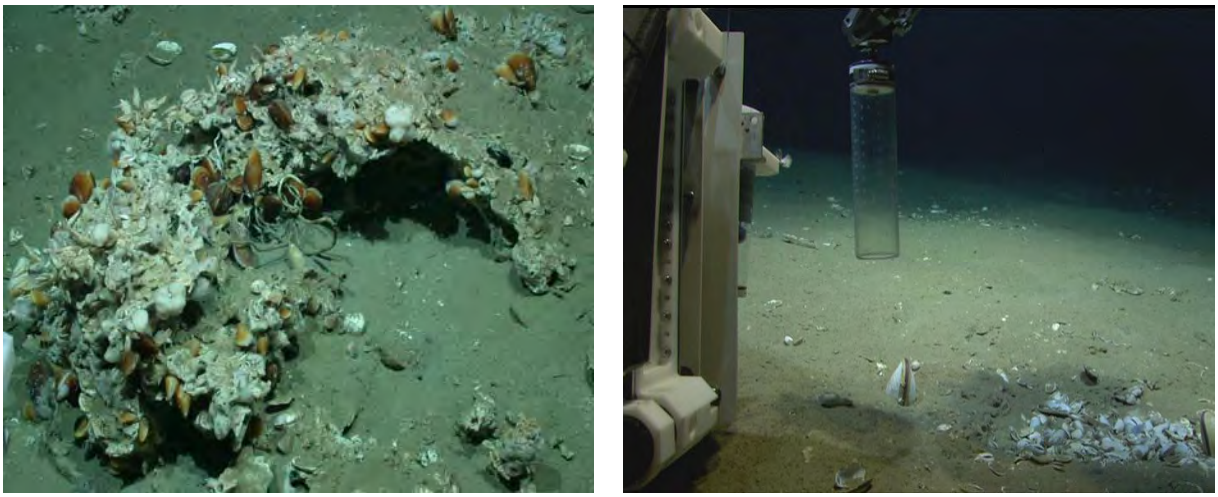

Fig. 56: Carbonate crust colonized by clams, barnacles and tube worms near flare area 7b (left). Sampling of a Calyptogena-like clam by use of a push core close to the site shown in the picture left (right).

6.2.8 Dive 186 (GeoB 12324)

Area:	Flare 6, Pakistan		
Responsible scientist:	Gregor von Halem		
Date:	Sunday, 11 November 2007		
Start/end at bottom (UTC):	06:48/16:53		
Total bottom time:	10:05 hours		
Start at the bottom	24°34.97'N	62°56.30'E	1600 m water depth
Start ascend	24°34.85'N	62°56.30'E	1800 m water depth

Scientist schedule:	**Scientist 1/Scientist 2/Navigator in the lab**
06:00 – 08:00	Gregor von Halem/André Gassner/Gerhard Bohrmann
08:00 – 10:00	Florian Brinkmann/Sebastian Stephan/Stephan Klapp
10:00 – 12:00	Gregor von Halem/Pamela Rossel/Thomas Pape
12:00 – 14:00	Gerhard Bohrmann/Mohammad Nasir/Gregor von Halem
14:00 – 17:00	Stefan Klapp/Sabine Kasten/Florian Brinkmann

Table 13: Instruments and tools deployed during ROV Dive 186.

GeoB-Nr.	Tool/instruments	Start	Lat. [°N]	Long. [°E]	Depth (m)	Remarks
12324-1	ISPS	08:53	24°34.820	62°56.305	1822	
12324-2	Carbonate	09:34	24°34.808	62°56.324	1823	3 carbonate pieces
12324-3	T-stick 1	12:14	24°34.809	62°56.325	1823	
12324-4	T-stick 2	13:28	24°34.841	62°56.522	1835	
12324-5	T-stick 3	14:22	24°34.840	62°56.522	1835	
12324-6	PC-1	14:47	24°34.840	62°56.522	1835	PC 21
12324-7	PC-2	14:55	24°34.839	62°56.521	1835	PC 22
12324-8	PC-3	14:56	24°34.840	62°56.521	1835	PC 15
12324-9	PC-4	15:00	24°34.840	62°56.521	1835	PC 20
12324-10	PC-5	15:34	24°34.841	62°56.525	1836	PC 36
12324-11	PC-6	15:35	24°34.842	62°56.524	1836	PC 7
12324-12	PC-7	15:37	24°34.840	62°56.524	1836	PC 5
12324-13	PC-8	15:39	24°34.840	62°56.523	1836	PC 17

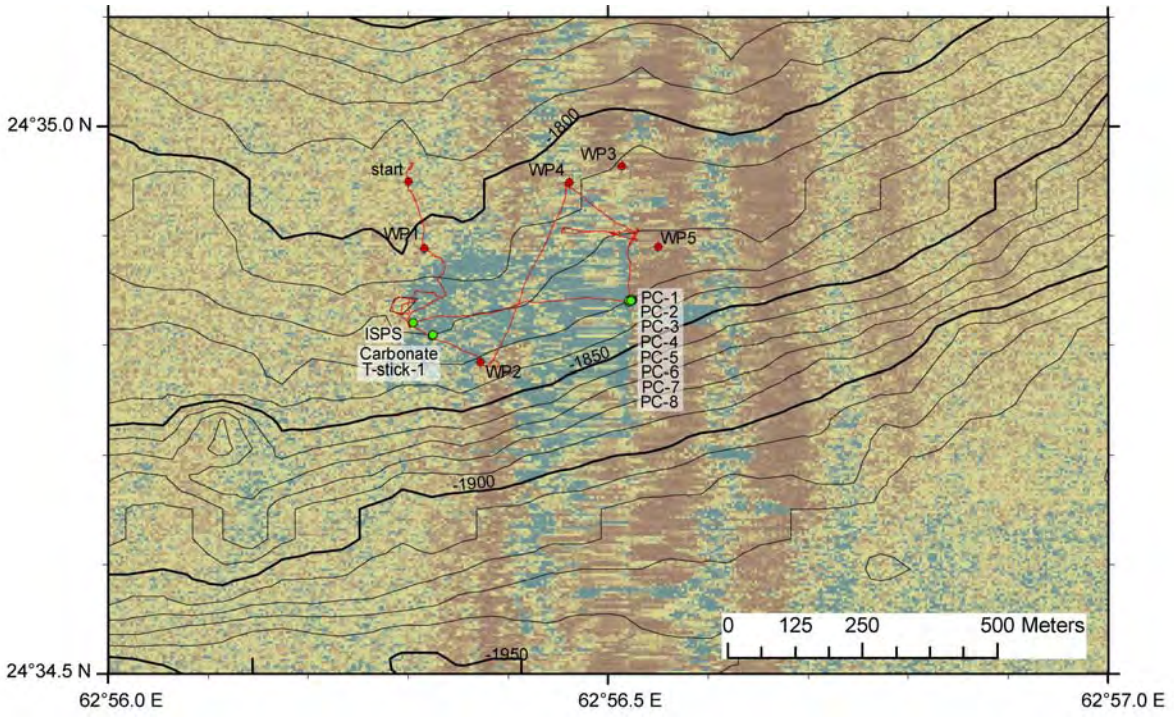

Fig. 57: Sidescan sonar map overlaid by the ROV track 186. Points show the sample positions. Points marked with WP are waypoints.

Flare 6 is located at the base of a 400 m high ridge in a water depth of about 1850 m. The scientific program started with a 360 degree flare imaging survey at WP2 using the forward directed sonar system. No acoustic anomalies have been detected. Further during the dive the work continued with the sea floor in view to find a suitable position for deploying the ISPS. A suitable site was found in southern direction after circling around a hill and following the interface between high and low backscatter intensity on the dive map. It turned out that the interface between high and low backscatter intensity on the dive map coincides very well with carbonate crusts and clam/mussel fields (high backscatter) and the low backscatter signature with a smooth seabed with very little carbonate crusts or clams/mussels at the sea floor. Unfortunately the ISPS deployment close to a Calyptogena nest failed due to the hard sea

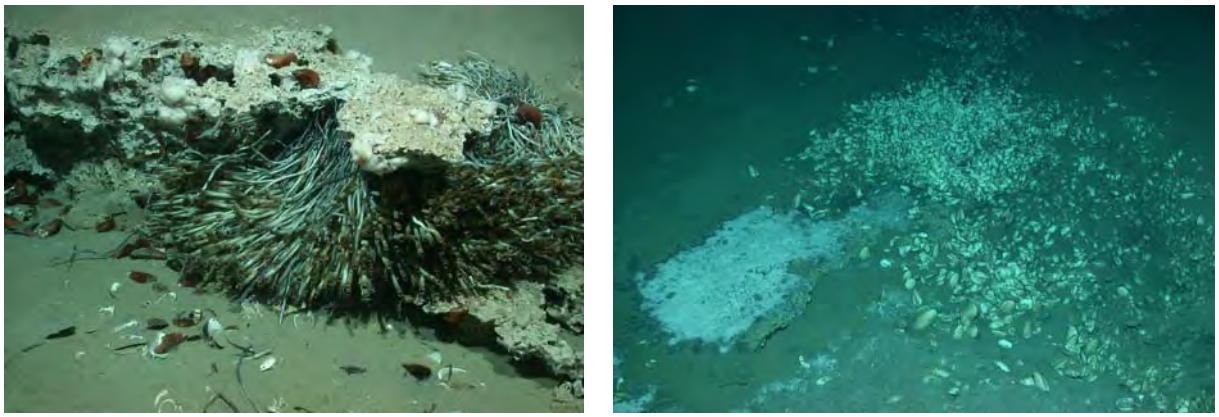

Fig. 58: *C*arbonate crusts with dead tube worms and white sponges (left); patch with vesicomyid clams and bacterial mats (right).

floor. The device could only penetrate about 10 cm into the sea floor but not deeper. Therefore the device was left behind and later picked up. The ROV headed SE to WP2 and crossed areas with carbonate crusts and tube worms as well as smooth featureless areas. Three carbonate samples have been taken ca. 50 m NW of WP2 (Fig. 57). From WP2 the ROV headed for WP4 in the NE to survey the sea floor which shows a more diffusive backscatter pattern on the sidescan sonar image of the dive map. It turned out, that the sea floor is predominantly smooth with occasional carbonate crusts and some smaller clam/mussel fields. After resultless flare imaging between WP4 and WP5 the flare imaging continued in western direction (120 m) to search for a flare which has been identified with PARASOUND. But no gas bubbles have been found. Further on a mussel patch was surveyed at the sea floor on the way back to WP5 and the T-stick was used to measure the in-situ temperature within the patch. However, the sea floor could not be penetrated by the T-stick and the measurement was stopped. From WP5 the dive continued in southern direction. The sea floor looks smooth with occasional occurring patches and nests of living and dead clams/mussels. The flight in southern direction stopped at a microbial mat with clams/mussels. Two T-stick measurements have been performed at this site and 8 push cores have been recovered before the ROV dive continued in western direction to pick up the ISPS. Dive 186 ended at 16:40 UTC with the recovery of the ISPS.

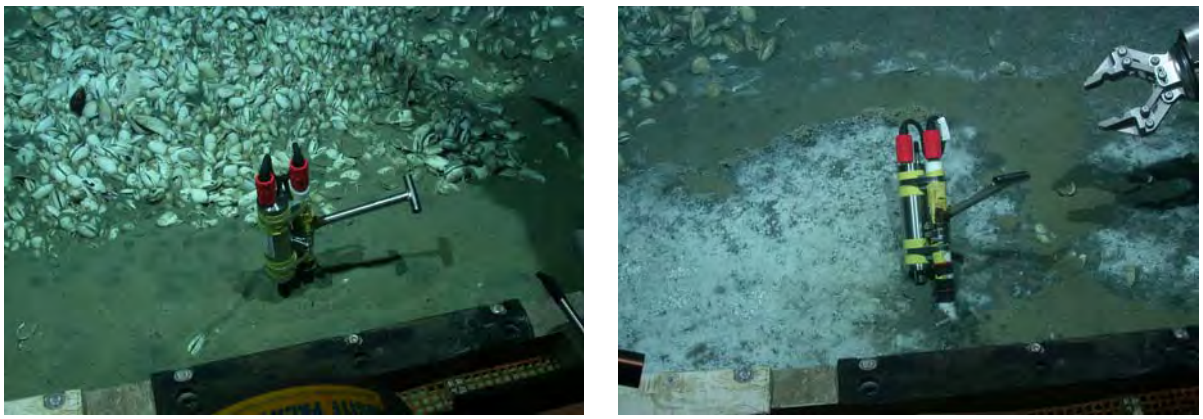

Fig. 59: Temperature measurements with the T-stick close to a patch of vesicomyid clams (left) and bacterial mats (right).

Fig. 60: Push core sediment samples close to the bacterial mat (left) and close to the vesicomyid clam field (right).

6.2.9 Dive 187 (GeoB 12326)

Area:	Flare 5, Nascent Ridge (location from earlier ROV Dive 179)		
Responsible scientist:	André Bahr		
Date:	Sunday, 12 November 2007		
Start/end at bottom (UTC):	05:50/15:52		
Total bottom time:	10 hours		
Start at the bottom:	24°11.771'N	62°44.324'E	2876 m water depth
Start ascend:	24°11.744'N	62°44.308'E	2875 m water depth

Scientist schedule:	**Scientist 1/Scientist 2/Navigator in the lab**
10:00 – 12:00	Gregor von Halem/André Bahr/Stefan Klapp
12:00 – 14:00	Gerhard Bohrmann/Monawwar Salem/Gregor von Halem
14:00 – 16:00	André Bahr/Janet Rethemeyer/Florian Brinkmann
16:00 – 18:00	Florian Brinkmann/Nina Wittenberg/Gerhard Bohrmann
18:00 – 20:00	Thomas Pape/Sabine Kasten/André Bahr

Table 14: Instruments and tools deployed during ROV Dive 187.

GeoB	Tool/instruments	Start	Lat. [°N]	Long. [°E]	Depth[m]	Remarks
12326-1	ISPS	6:09	24°11.745	62°44.306	2876	
12326-2	GBS-9	8:44	24°11.750	62°44.418	2874	
12326-3	Marker 1	8:59	24°11.749	62°44.418	2874	
12326-4	GBS-10	9:45	24°11.745	62°44.424	2873	
12326-5	Marker 8	10:08	24°11.746	62°44.424	2873	
12326-6	PC-1	14:03	24°11.750	62°44.420	2873	PC 2
12326-7	PC-2	14:07	24°11.749	62°44.420	2873	PC 28
12326-8	PC-3	14:14	24°11.740	62°44.421	2873	PC 24
12326-9	PC-4	14:20	24°11.749	62°44.420	2873	PC 1
12326-10	PC-5	15:01	24°11.743	62°44.307	2875	PC 11
12326-11	PC-6	15:07	24°11.743	62°44.306	2875	PC 32
12326-12	PC-7	15:10	24°11.742	62°44.306	2875	PC 33
12326-13	PC-8	15:20	24°11.742	62°44.307	2875	PC 13

Fig. 61: Sidescan sonar map (high backscatter in pink) overlain by the ROV 187 dive track (see insert for a close-up of the dive track). Yellow stars show the location of the Markers 1 and 8 as well as the positions of identified bubble escape sites.

Dive 187 was planned as the continuation of Dive 179, which had to be terminated early due to technical problems. The objectives of this dive were to find Marker 4 located at the bubble site during Dive 179, deploy the ISPS, and then search for, document and sample other flare sites based on pre-survey results of TOBI and PARASOUND (see Fig. 61).

The first target, the bubble curtain at Marker 4, was found without problems and the ISPS was deployed aside the major bubble stream. After completing this task, the ROV was directed in a sonar flight towards the suspected flare in the southeast, however, when the vehicle reached the position about 2 hours after starting work on the sea floor, no bubbles could be found despite a 360° sonar survey. QUEST was then steered towards the northwest into the direction of the next suspected flare position. After 30 minutes two distinct gas bubble signals were detected in the sonar and traced to the sea floor. At the first bubble emission site, the smooth sea floor is covered with linear areas colonized by anemones, tube worms, vesicomyid clams surrounding whitish bacteria covered patches. Interestingly, the bubble emission (Flare 5b, Fig. 62) is taking place outside of these populated areas; the direct surrounding of the bubble-releasing holes is almost barren of any fauna. After sampling the bubble stream with the GBS and deploying Marker 2, this flare site was left and the sonar flight continued heading northwest towards the second flare site recognized in the foreward looking sonar which was found after 20 minutes of flight (Flare 5c, Fig. 63). The morphology on that location is slightly rougher than at the previous site and dominated by elongated ridges and valleys. White bacterial patches (including abundant clams) are mostly confined to the "valleys" and are surrounded by rims of vesicomyid clams, anemones and occasional pogonophora. Seepage occurs at this site also along linearly oriented bubble-spots, but directly within the centre of the whitish patches. From this site a GBS was taken and a marker set (Marker 8).

The following program of the dive has been characterised by an extensive sea floor survey which was first directed towards the northernmost waypoint, then towards the southwest in a

track rectangular to the striking of the linear structures visible on the sidescan backscatter plot and finally back to Flare 5b. The main objective was to groundtruth the nature of the backscatter pattern also by using the ROV-mounted sidescan sonar. The sea floor on this track was mainly smooth with occasional burrows and grazing traces, interrupted by areas currently colonized by bacteria, tube worms, clams and/or anemones in an environment characterized by smooth hills (Fig. 64), presumably representing the high-backscatter patches. After 3 h 20 min of sea floor survey Marker 1 was reached again and 4 pushcores taken, retrieving some clams and anemones. The dive ended at the start point (Marker 4) where another 4 pushcores were taken next to the marker in a field inhabited by pogonophora. Finally, the ISPS was successfully recovered and the ascent of the ROV back to the surface began.

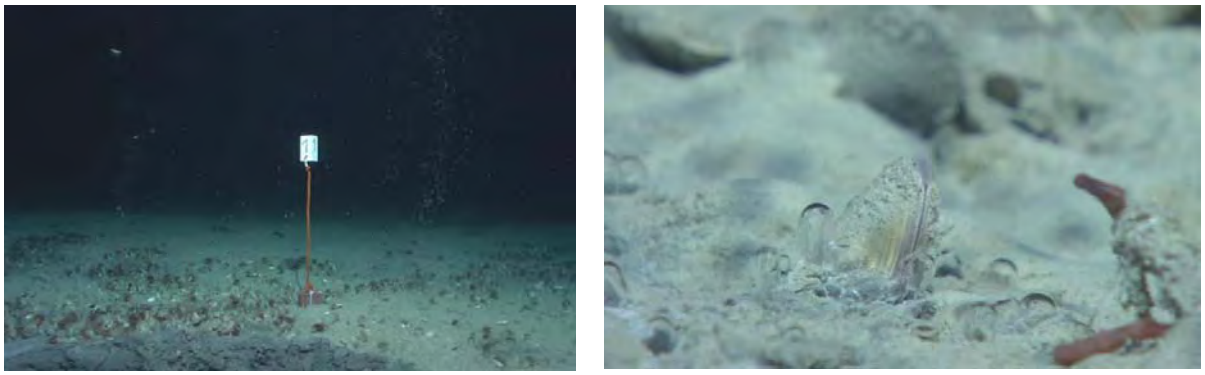

Fig.62: Flare 5b at Marker 1 (left), Close-up on a bubble emanating spot in Flare 5b (right).

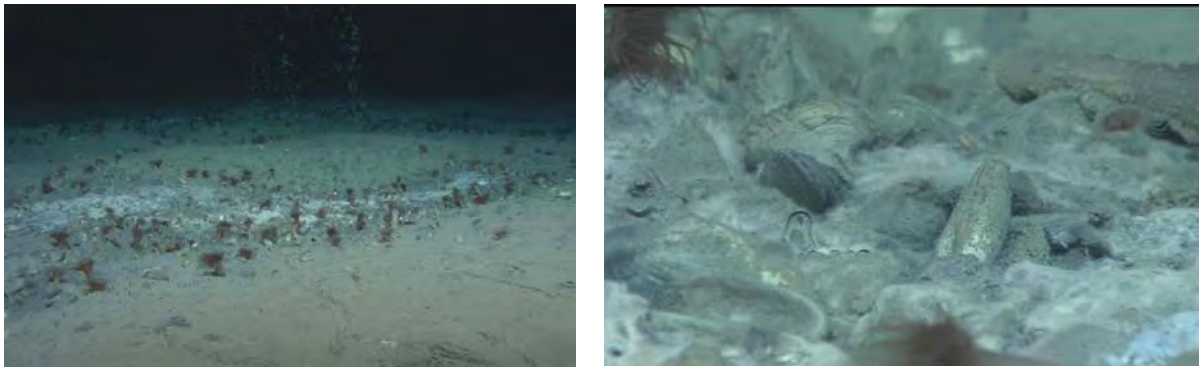

Fig. 63: Surroundings of Flare 5c (left) and sea floor close-up (right); note the thicker bacterial cover in comparison to Fig. 62 right.

Fig.64: Non-flat sea floor morphology in high- backscatter area (left); scattered dead clam shells on the sea floor close by (right).

6.2.10 Dive 188 (GeoB 12328)

Area:	Flare 2 in about 1000 m water depth on top of a slide		
Responsible scientist:	Florian Brinkmann		
Date:	Tuesday, 13 November 2007		
Start/end at bottom (UTC):	05:40/15:00		
Total bottom time:	9 h, 20 m		
Start at the bottom:	24°50.796'N	63°01.447'E	1025 m water depth
Start ascend:	24°50.754'N	62°01.436'E	1015 m water depth

Scientist schedule:	**Scientist 1/Scientist 2/Navigator in the lab**
09:00 – 11:00	Gregor von Halem/Marcos Yoshinaga/Stefan Klapp
11:00 – 13:00	Florian Brinkmann/Karin Zonneveld/André Bahr
13:00 – 15:00	Stefan Klapp/David Fischer/Gregor von Halem
15:00 – 17:00	Markus Brüning/Sebastian Stephan/Florian Brinkmann
17:00 – 19:00	Florian Brinkmann/Sabine Kasten/Markus Brüning

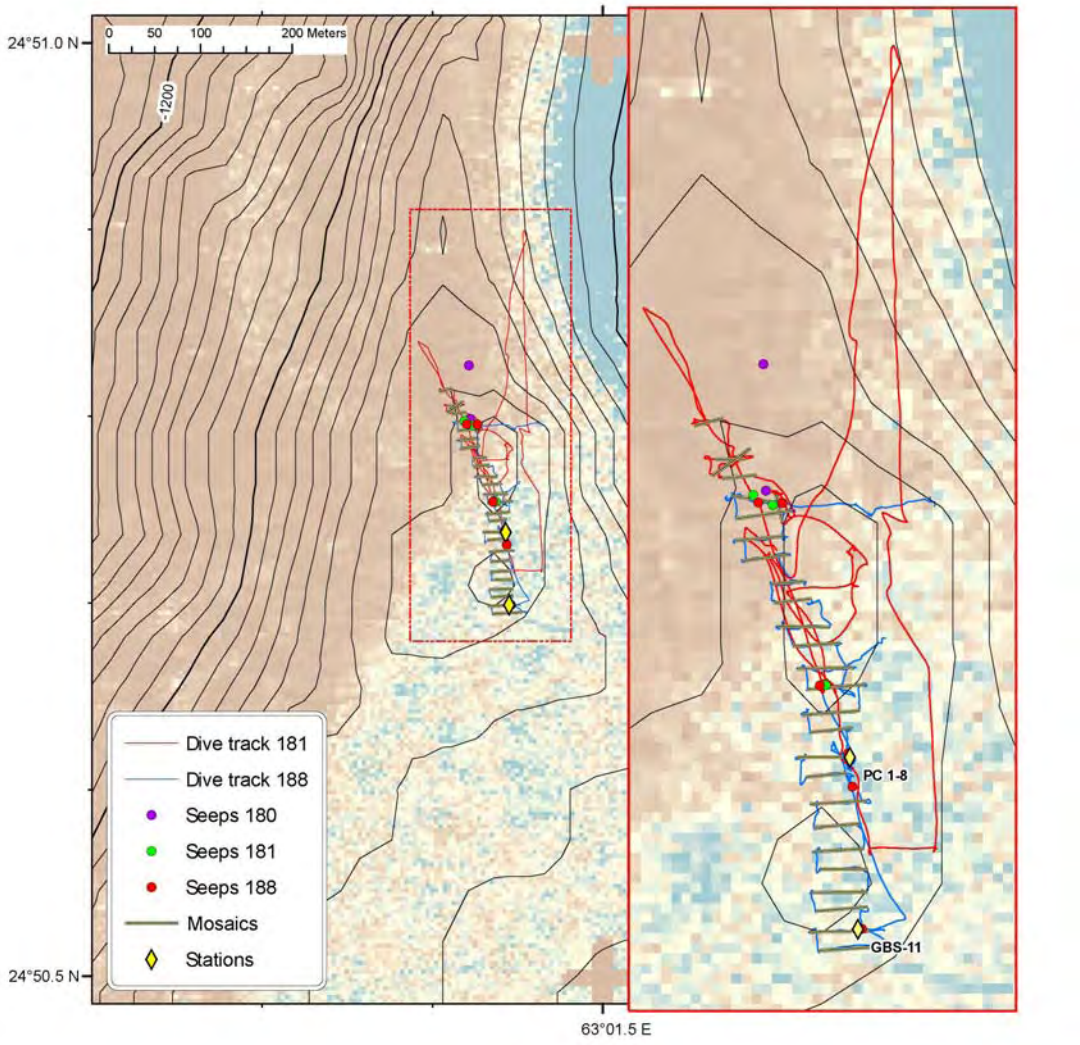

Fig. 65: Sidescan sonar map of the working area. Insert marks a zoom into the dive track. Background colours indicate backscatter intensity. The photo mosaics along the depression on top of the ridge that were started during Dive 181, were continued during Dive 188.

Table 15: Instruments and tools deployed during ROV Dive 188.

GeoB	Tool/instrument	Start	Lat. [°N]	Long. [°E]	Depth (m)	Remarks
12328-1	GBS-11	12:42	24°50.699	63°01.445	1028	
12328-2	PC-1	14:22	24°50.738	63°01.443	1025	PC 36
12328-3	PC-2	14:25	24°50.738	63°01.443	1025	PC 7
12328-4	PC-3	14:30	24°50.738	63°01.443	1025	PC 15
12328-5	PC-4	14:33	24°50.738	63°01.443	1025	PC 20
12328-6	PC-5	14:44	24°50.738	63°01.443	1025	PC 17
12328-7	PC-6	14:44	24°50.738	63°01.443	1025	PC 21
12328-8	PC-7	14:42	24°50.738	63°01.443	1025	PC 9
12328-9	PC-8	14:41	24°50.738	63°01.443	1025	PC 22

Main objective of the survey was to continue the photo mosaic survey that was started during Dive 181. In addition to the five mosaics from Dive 181, 17 further mosaics (Fig. 65) will help observing seep distribution along the north-south extension of the depression. The photograph sequences were taken by the ROV flying from the east to west or from the west to the east, respectively. Flying along the depression a mosaic was performed every 10 metres, heading southwards. Each sequence covers a track of about 20 metres. At the beginning and at the end of each track a screenshot of the forward looking sonar (Fig. 66 left) was saved as a further tool to analyse the structure of the depression. The structure of this distinctive feature is dominated by clear flanks in the north (Fig. 66 right), whereas more diffuse and rather flat borders (Fig. 67 left) are characteristic in the south. But bacterial patches are still situated along a clearly defined morphological structure. The typical elongated concentric bacterial mats as observed during Dive 181 were also found all along the depression throughout the entire mosaicing profile.

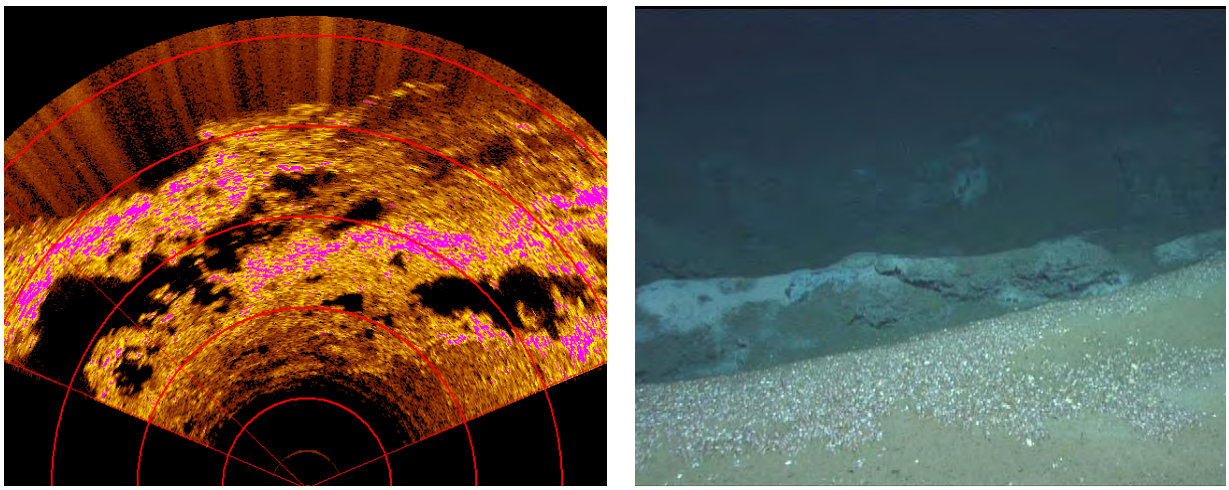

Fig. 66: Screenshot of the forward looking sonar showing the structure of the depression (one circle equals 5 metres) (left). Visual appearance of the depression on top of the investigated ridge. Prominent flanks enclose the depression in the northern parts (right).

Additionally, gas bubbles at the southernmost seep were sampled with a gas bubble sampler (Fig. 67 right). As a further objective, push cores were taken at a very distinctive bacterial patch (Fig. 68 left). To get pore water profiles in faunal zones of the patch, 8 push cores were taken; two in the zone of worms surrounding the bacterial mat (BM), 2 in the outer part dominated by the small vesicomyid clams (sC), and 4 directly within the bacterial mat

(Fig. 68 right). As a last task, the osmo sampler, which was deployed at an active seep site above an extensive bacterial mat during Dive 181, was recovered and the dive was completed.

Fig. 67: In the southern parts of the depression the flanks are more diffuse and rather flat (left). But the bacterial patches are still lined along a clearly defined structure; Bubbles at the southernmost seep within the mosaicing profile were sampled by the gas bubble sampler (right).

Fig. 68: Faunal zones of a bacterial patch to outside (left). From the centre to the outer zones: bacterial mat, small worms, small clams, background sediment with larger clams in lower density; four push cores were taken directly within the bacterial mat. Two further ones were taken in the zone dominated by small worms and two in the outer zone characterized by small clams, respectively (right).

6.2.11 Dive 189 (GeoB 12333)

Area:	Flare 2		
Responsible scientist:	Kim Thomanek		
Date:	Thursday, 15 November 2007		
Start/end at bottom (UTC):	05:09/07:12		
Total bottom time	2 hours		
Start at the bottom:	24°50.745'N	63°01.448'E	1029 m water depth
Start ascend:	24:50.800'N	63:01.421'E	1024 m water depth

Scientist schedule:	**Scientist 1/Scientist 2/Navigator in the lab**
09:00 – 11:00	Gerhard Bohrmann/Kim Thomanek/Florian Brinkmann
11:00 – 13:00	Markus Brüning/Kim Thomanek/Gregor von Halem

Table 16: Instruments and tools deployed during ROV Dive 189.

GeoB	Tool/instrument	Start	Lat. [°N]	Long. [°E]	Depth(m)
12333-1	Bubblemeter 2	06:17	24°50.797	63°01.420	1023
12333-2	GBS 12	06:52	24°50.797	63°01.420	1024

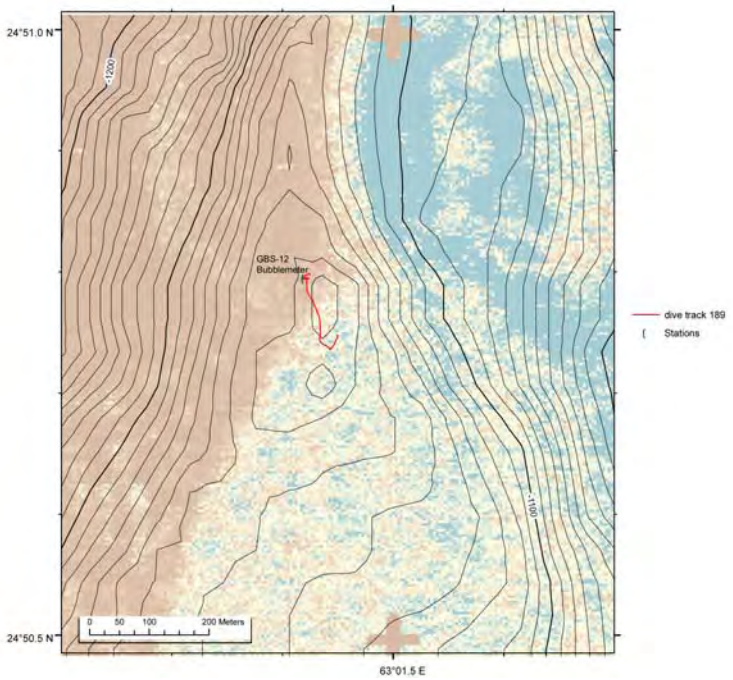

Fig. 69: Track of Dive 189.

After descend the ROV headed towards a pre-selected seep site which was active during Dive 188 (24°50.739'N 63°01.443'E, 05:17UTC). Because the site did not show active bubble release another site was searched and was found at 24°50.797'N, 63°01.419'E; at 05:45UTC. After completion of measurements the ROV left bottom to surface at 24°50.8000'N, 63°01.421'E; 07:12UTC.

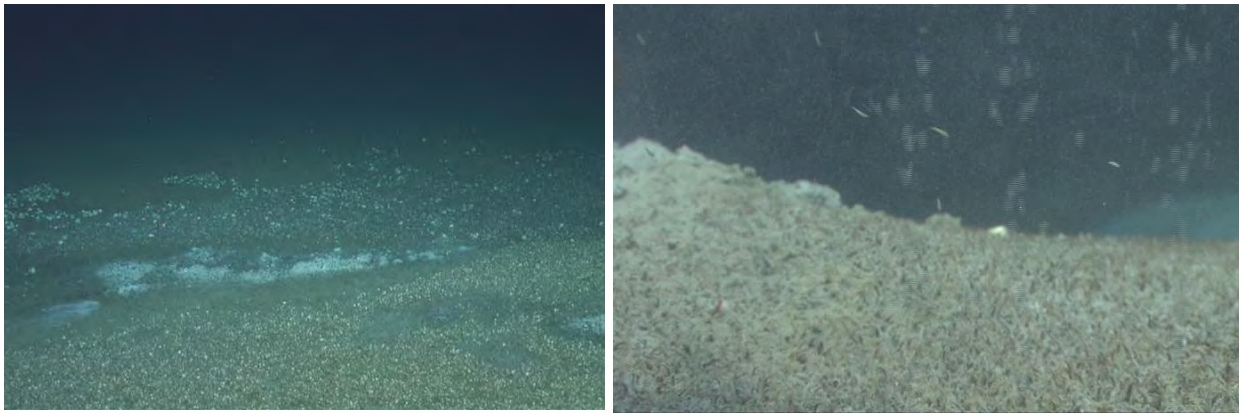

Fig 70: The pre-selected active seep location known from dive 188 was inactive at time of arrival (left). The selected bubble seep was observed with the field of observation parallel to the line alignment of the orifices (right).

The active gas seep showed strong acoustic signals in the Parasound - as well as in the forward looking sonar system. The ground structure was mostly flat with some slight elevations. The bottom was partially covered with soft sediment. Patches of bacterial mats were visible within the area of the gas seep. Four gas orifices were readily visible using all three ROV cameras (Fig. 70). Three orifices were bundled within close distance Fig. 70 right), the fourth orifice was separated approximately 0.5 m away from the others. Using laser distance comparison, the three orifices were found to be aligned along a line separated approx 5cm from each other. The field of view was planar to the line of bubble seeps.

The Bubblemeter was centre positioned on top of the bundle with an approximate object distance of 85 cm. It was triggered then and a sequence of 2 seconds had been recorded with a time resolution of 500 fps and a spatial resolution of 1280 x 1024 pixel. After storing the used tools, the ROV was shifted 0.5 m towards port side maintaining the same heading. That way the high resolution camera was able to zoom directly on to the vents. For an auxiliary gas flux quantification the gas bubble sampler was used to measure the time required for filling a defined volume. In order to determine possible major changes in gas flux rates during observation, the high resolution camera recorded the filling process as well as an additional 8 minutes post gas sampling. For size calibration the finger action tool of the Orion was held into the plain of view aligned with the bubble stream (Fig. 71 right). At 07:01 UTC the sampling was completed and preparations for surfacing commenced.

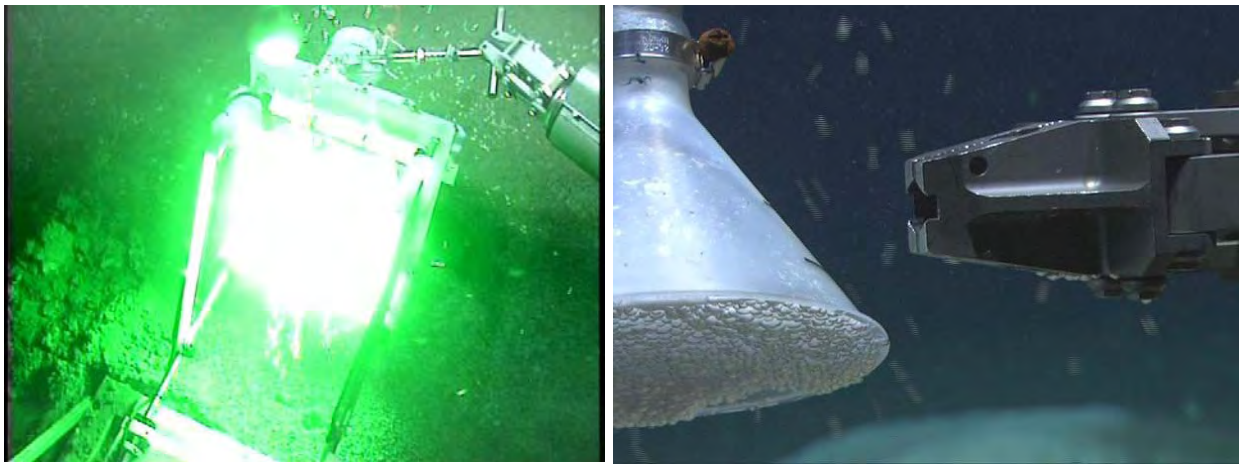

Fig 71: After acoustic detection of an active seep, the device was precisely positioned and recorded rising bubbles for 2 s for quantification purposes (left). Additional gas sampling and quantification was conducted using the GBS (right).

6.2.12 Dive 190 (GeoB 12334)

Area:	Flare 3		
Responsible scientist:	Stephan A. Klapp		
Date:	Thursday, 15 November 2007		
Start/end at bottom (UTC):	10:40/11:45		
Total bottom time	1:05 hours		
Start at the bottom:	24°37.267’N	63°02.617’E	1552 m water depth
Start ascend:	24°37.219’N	63°02.530’E	1539 m water depth

Scientist schedule: **Scientist 1/Scientist 2/Navigator in the lab**
10:40 – 11:45 Gregor von Halem/Markus Brüning/Stephan A. Klapp

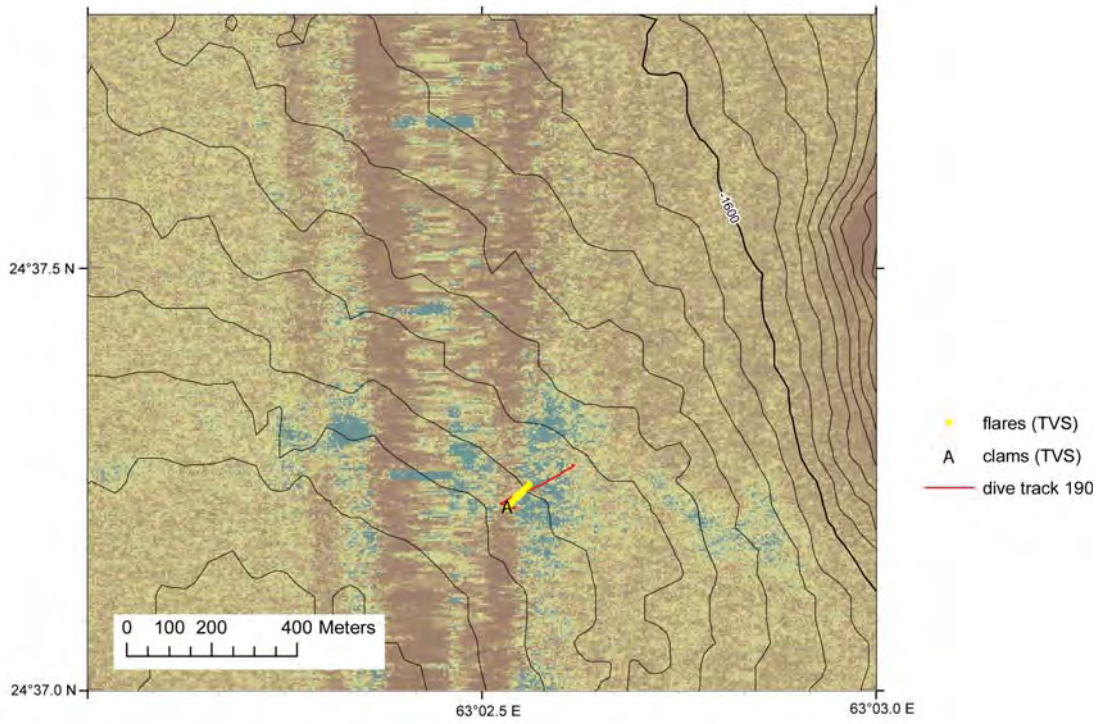

Fig. 72: Map of dive track ROV 190.

The objective of Dive 190 was to characterize seeps at Flare 3. However, due to a malfunction of the ROV the dive needed to be terminated after a bit more than an hour. A short distance from the starting point, a large clam field was discovered. The field comprised "nests" of living brown Bathymodiolus mussels indicating recent seepage. HD camera records were taken at this site as well as high-resolution images. In close vicinity, another similar field of Bathymodiolus mussels was found. Along the way between the two fields a few large crabs have been observed. Adjacent to the Bathymodiolus nest a large area of dead Calyptogena clams was seen and in between patches of living mussels. Next to a nest of Bathymodiolus mussels, the ROV set down to explore the ground for sampling and taking temperature measurements, but a malfunction occurred and the vehicle needed to ascent immediately.

Fig. 73: Nests of living Bathymodiolus mussels at Flare 3 point to recent seepage (left). Dead calyptogena clams scattered on the sea floor (right).

6.2.13 Dive 191 (GeoB 12338)

Area:	Flare 7 high-backscatter hilltop		
Responsible scientist:	Pamela Rossel		
Date:	Friday, 16 November 2007		
Start/end at bottom (UTC):	06:29/16:01		
Total bottom time:	9:32 h		
Start at the bottom:	24°38.504'N	62°44.205'E	1669 m water depth
Start ascend:	24°38.649'N	62°44.253'E	1875 m water depth

Scientist schedule:	**Scientist 1/Scientist 2/Navigator in the lab**
06:28 – 07:12	Stefan Klapp/Pamela Rossel/Gregor von Halem
07:12 – 09:15	Florian Brinkmann/Marcos Yoshinaga/Pamela Rossel
09:15 – 11:45	Markus Brüning/Pamela Rossel/Stephan Klapp
11:45 – 13:07	Gerhard Bohrmann/Mohammed Nasir/Florian Brinkmann
13:07 – 15:01	Florian Brinkmann/Sabine Kasten/Markus Brüning
15:01– 16:01	Markus Brüning/Pamela Rossel/Stephan Klapp

Table 17: Instruments and tools deployed during ROV Dive 191.

GeoB	Tools/instrument	Start	Lat. [°N]	Long. [°E]	Depth (m)
12338-1	Carbonate-1	7:01	24°38.544	62°44.241	1656
12338-2	Carbonate-2	7:51	24°38.556	62°44.246	1656
12338-3	Carbonate 3	8:10	24°38.556	62°44.246	1656
12338-4	Net	8:58	24°38.617	62°44.257	1652
12338-5	KIPS-1	10:27	24°38.649	62°44.255	1654
12338-6	KIPS-2	10:41	24°38.649	62°44.254	1654
12338-7	KIPS-3	10:48	24°38.649	62°44.254	1654
12338-8	KIPS-4	11:02	24°38.649	62°44.254	1654
12338-9	KIPS-5	11:11	24°38.649	62°44.253	1654
12338-10	KIPS-6	11:23	24°38.648	62°44.254	1654
12338-11	GBS 13	11:50	24°38.649	62°44.253	1654
12338-12	BC-1	12:40	24°38.650	62°44.253	1654
12338-13	Carbonate-4	12:49	24°38.563	62°44.286	1656

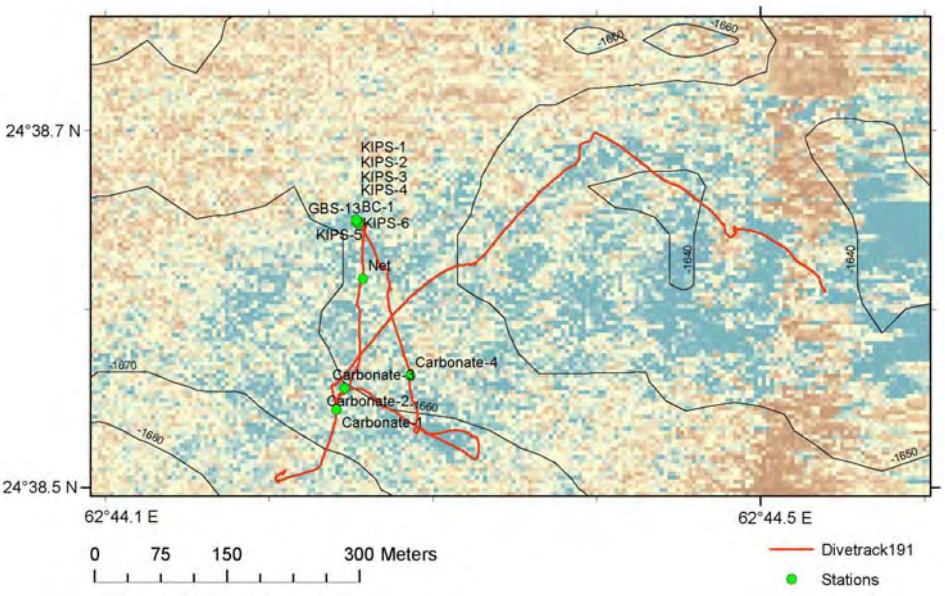

Fig. 74: Sidescan sonar map (high backscatter in blue) overlaid by the ROV 191 Dive track including positions of the stations where the samples collected.

The Dive 191 was a long dive with approximately 10 h of duration. During the beginning of the dive the area from the start point in direction to Flare 7 was surveyed. During this time we observed tube worms, fishes and dead clams close to a carbonate crust from where the first three samples were collected (7:01-7:08). The samples of collected carbonates presented two types of organisms associated, tube worms (from a structure 25 cm long) and sponges. At 7:41 a new place (eastward of the first site) was visited. This site was characterized by a big field of Bathymodiolus over a carbonate crust (high backscatter observed in the sonar).

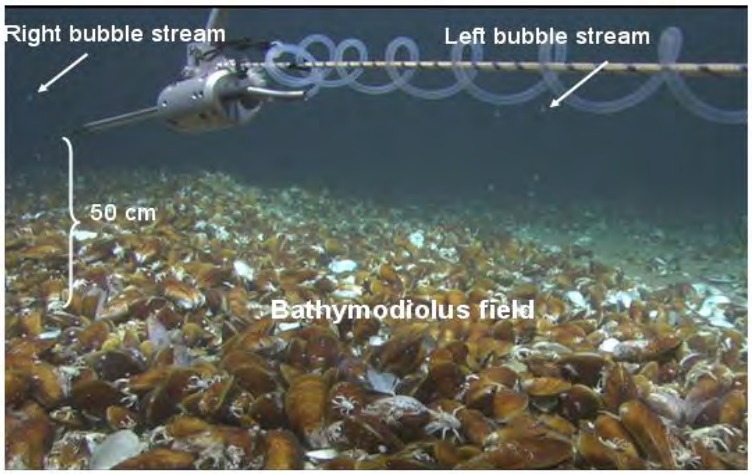

Fig. 75: scheme showing the sample area where the KIPS sampler was used over the Bathymodiolus field.

Around the carbonate crust fishes, crustaceous, barnacles and crabs were observed. The samples collected the with arm of the ROV and by the net (largest piece) contain mainly carbonate and Bathymodiolus mussels. At 09:15 flying in the direction of the flares observed in the previous dives of this site was observed a new flare named as 7 c in a Bathymodiolus site. At this new flare the KIPS sampler was used (9:43) that at the beginning didn't work properly (KIPS# 2, 3, 4 and 5). After a reset of all the systems the problem was solved (10:15). At this site 15 water samples were collected. In detail samples were obtained close to two different bubble streams (three samples from each bubble stream), background area (with no mussels, three more samples) and a vertical profile (20, ~ 50, ~ 100 cm, two samples each) over the Bathymodiolus field (Fig. 75) for later geochemical analysis. Water sampled with

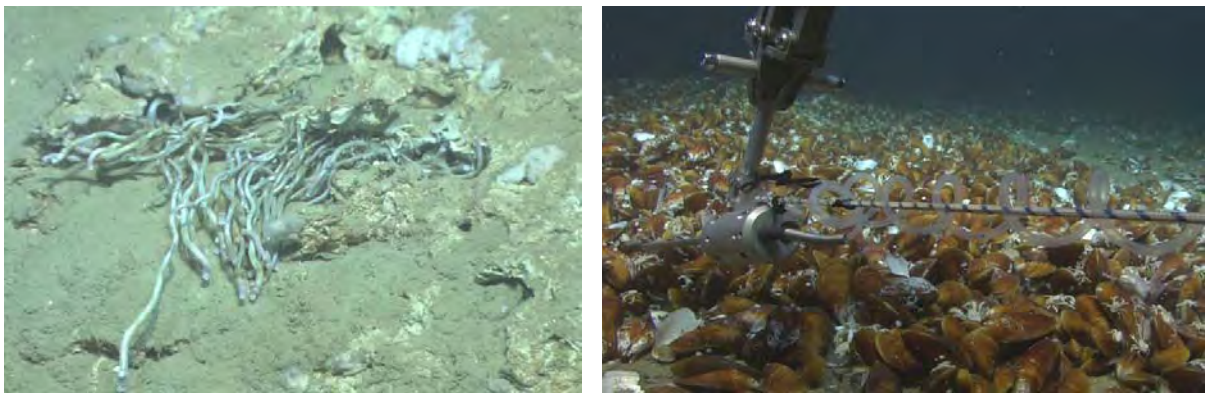

Fig. 76: First site where carbonate with tube worms and sponges collected (left). KIPS sampler in an area where bubble streams in a Bathymodiolus field can be observed (right).

KIPS was finished in this station at 11:31. Later on (12:04) the gas bubble sampler was used for ~ 20 min in the bubble stream of the same area, the bubbles collected presented hydrate skins. At 12:10 continuing the flying close to sea floor in direction to WP 2 with high backscatter we collected some stained Bathymodiolus mussels (12:35) and not far away a new piece of carbonate with several organisms (barnacles and sponges) was sampled. Close by the first try of push cores (14:01) in Bathymodiolus field was done, however due to the hard carbonates present below the mussels it was impossible to collect samples in this site. At 15:56 in direction to WP 3 very young mussels together with old ones were observed. At 16:01 the dive was finished.

Fig. 77: Bathymodiolus and carbonate pieces collected with the net (left). Background area close to the bubble stream used for KIPS sampler (right).

Fig. 78: Carbonate sample with sponges and barnacles (left). Gas bubble sampler over the same bubble stream where KIPS sampler was used (right).

6.2.14 Dive 192 (GeoB 12339)

Area:	Nascent Ridge at Flare 5 location, Makran accretionary wedge		
Responsible scientist:	Markus Brüning		
Date:	Saturday, 17 November 2007		
Start/end at bottom (UTC):	06:30/14:30		
Total bottom time:	8 h		
Start at the bottom:	24°11.746’N	62°44.307’E	2876 m water depth
Start ascend:	24°11.740’N	62°44.301’E	2875 m water depth

Scientist schedule:	**Scientist 1/Scientist 2/Navigator in the lab**
06:00 – 08:00	Gregor von Halem/Karin Zonneveld/Stefan Klapp
08:00 – 10:00	Gerhard Bohrmann/Monawwar Salem/Markus Brüning
10:04 – 12:11	Markus Brüning/Janet Rethemeyer/Florian Brinkmann
12:11 – 14:00	André Bahr/Nina Wittenberg/Gerhard Bohrmann
14:00 – 14:26	Markus Brüning/Sabine Kasten/Gregor von Halem

Table 18: Instruments and tools deployed during ROV Dive 192.

GeoB	Tool	Start	Lat. [°N]	Long. [E]	Depth (m)	Remarks
12339-1	GBS-14	13:12	24°11.742	62°44.301	2875	yellow GBS
12339-2	GBS-15	13:38	24°11.742	62°44.301	2875	red GBS, sampled water
12339-3	PC-1	13:49	24°11.742	62°44.300	2875	PC-24
12339-4	PC-2	13:51	24°11.742	62°44.302	2875	PC-6
12339-5	PC-3	14:03	24°11.741	62°44.300	2875	PC-28
12339-6	PC-4	14:06	24°11.740	62°44.301	2875	PC-11
12339-7	PC-5	14:09	24°11.741	62°44.300	2875	PC-22
12339-8	PC-6	14:13	24°11.740	62°44.301	2875	PC-9
12339-9	PC-7	14:16	24°11.740	62°44.300	2875	PC-13
12339-10	PC-8	14:18	24°11.740	62°44.301	2875	PC-29

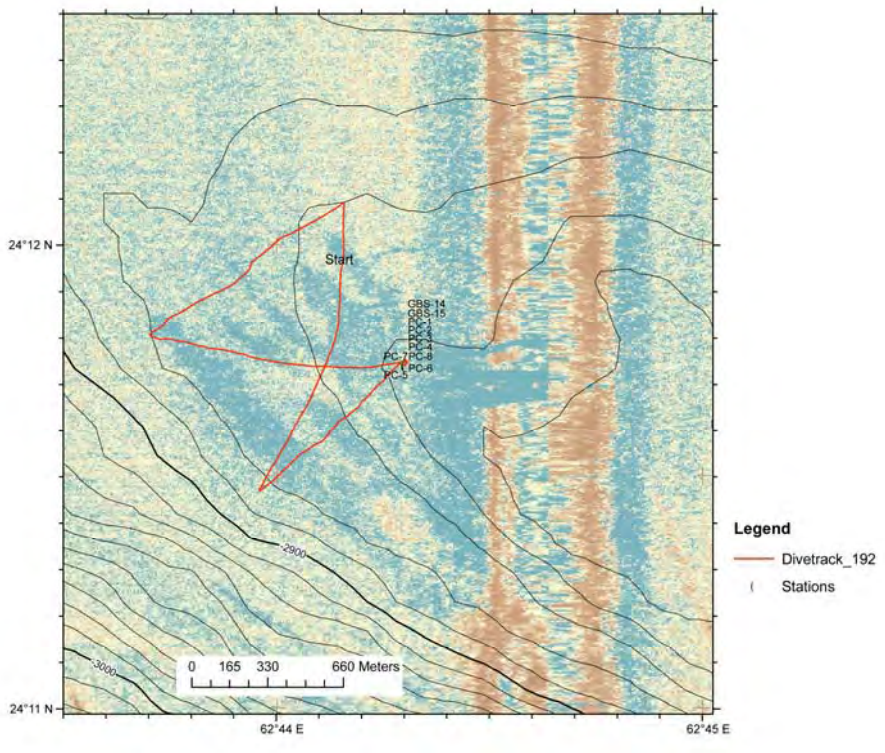

Fig. 79: Map, track and sample sites of Dive 192.

ROV Dive 192 took place at Nascent Ridge on 17 November 2007. It reached the sea floor at 06:26 close to Marker 4 at the well known bubble site. After observation of the bubble escape the ROV flew to SW which is perpendicular to the elongated backscatter anomalies recorded by TOBI (Fig. 79). The sea floor was flat and patchy in colouring with few shells (~3-4 per m²), starfishes and traces of moving biology. At 06:40 and 06:46 black-blue snails about 40 cm long were passed. At 06:55 photos of a nest of living shells and mussels were

taken. Next to the bivalves nest on two square metres 10 cm long, millimetre thick syphons, possibly tube worms, pierced out of the sea floor. An area with denser distribution of shells which were dead was seen at 07:01. The siphons were then continuously seen. Around 07:05 the density of biology decreased. An upright standing paint-bucket marks human activity offshore Pakistan. At 07:12 an uplifted area of 50 m^2 consisting of three connected mounds appeared. Behind, siphons and shells were increased in number, while the mounds themselves were bare. For most of the rest of the track south-west-wards, the sea floor had less reportable features than during the first part. Reaching the end of the track at 08:07, the ROV ascended to 10 m altitude and a side scan survey was run. Nothing was to be seen with the cameras, and videos were switched off. The profile started in a direction of 25°, later changed to almost 0°. The aim was to see if TOBI and ROV recorded backscatter anomalies align. When the endpoint at 09:53 was reached, the ROV returned to the sea floor to fly towards the SW and compare the far ends of the TOBI backscatter anomaly with visual observation. The sea floor in this region had many small hills like molehills. No signs of seepage were found along the track. At 11:41 the search on backscatter anomalies ended and the ROV headed directly to the flare site 1000 m east. At 11:58 some siphons of 20 cm length and a smooth morphological depression of 6 m diameter was passed. At 13:05 Marker 4 was reached and escaping gas was sampled by the gas bubble sampler (GBS-14, GeoB12339-1). A second gas bubble sampler was filled with water by just opening the valve and closing it again (GBS-15, GeoB 12339-2). Eight push cores, partly containing those siphons or tube worms observed all over Nascent Ridge, were collected. The dive ended at 14:22.

6.2.15 Dive 193 (GeoB 12343)

Area:	Flare 2 in 1000 m water depth on top of a slide		
Responsible scientist:	Marcos Yoshinaga		
Date:	Sunday, 18 November 2007		
Start/end at bottom (UTC):	05:47/14:22		
Total bottom time:	8:35 h		
Start at the bottom:	24°50.705'N	63°01.453'E	1031 m water depth
Start ascend:	24°50.692'N	63°01.450'E	1030 m water depth

Scientist schedule:	**Scientist 1/Scientist 2/Navigator in the lab**
05:30 – 07:00	Gregor von Halem/André Gassner/Marcos Yoshinaga
07:00 – 09:00	Gerhard Bohrmann/Marcos Yoshinaga/André Bahr
09:00 – 11:00	Stefan Klapp/Janet Rethemeyer/Florian Brinkmann
11:00 – 13:00	André Bahr/Marcos Yoshinaga/Markus Brüning
13:00 – 14:30	Florian Brinkmann/Sabine Kasten/Gregor von Halem

Table 19: Instruments and tools deployed during ROV Dive 193.

GeoB	Tools/instrument	Start	Lat. [°N]	Long. [°E]	Depth (m)
12343-1	T-Stick -1	06:08	24°50.697	63°01.446	1030
12343-2	ISPS	06:18	24°50.696	63°01.446	1030
12343-3	GBS-16	09:18	24°50.844	63°01.415	1040

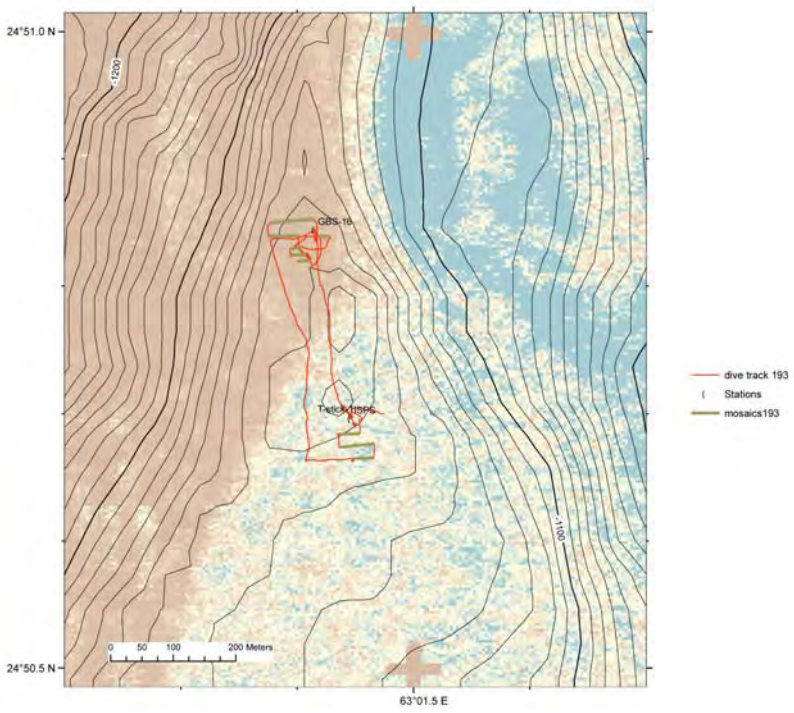

Fig. 80: Sidescan sonar map of Flare 2 and dive track performed during Dive 193.

The aim of the 5th dive at Flare 2 was to map more detailed the area, extending westwards the former mosaic surveys (Dives 181 and 188) using similar strategies (see Dive 188 report for detailed information on mosaic performance) (Fig. 80). Few minutes after reaching the sea floor, in between a clam field and a bacterial mat, the T-Stick was deployed in the sediments and nearby the ISPS was deployed (Fig. 81 left). The ISPS was left in this area, whereas the T-Stick was recovered, and the ROV started the mosaic survey (~06:45 UTC) to the south of the valley-like geological feature, which was investigated in previous dives (see Fig. 78). After the 3th mosaic survey (~07:45 UTC), it was decided to head to the north, towards the western flank of this geological feature. Mostly, during mosaicing the western flank, the sea floor was covered by filter feeders sea pens, with no signal for active seepage (Fig. 81 right), although slope-like and wave-like sea floor was commonly found in the area. In the northernmost area visited during this dive (Fig. 80), a new seepage location was found by the forward-looking sidescan sonar and sampled using the GBS (Fig. 82 left). As well as in other seep areas at Flare 2 (Fig. 80, on the right), a dense bacterial carpet covered the venting spot. While surveying the area for mosaics, now heading southwards from the seep site discovered during this dive, the ROV documented a vertebrate carcass of approximately 80 cm (Fig. 82 right).

After mosaic #6 (~11:30 UTC), it was decided to move northwards back to the seep location in order to survey westwards from that site found earlier during this dive. Mosaics # 7, 8 and 9 (from 11:50 to 13:17 UTC) were conducted in the northern flank of the Flare 2 area, until the ROV started looking for the gravity corer lost during recovery at station GeoB 12342-1 (GC-27, see M74/3 stations list). Surprisingly, the only evidence that the gravity corer was still nailed in the sediments was the plastic liner hanging out above the sea floor (Fig. 83 left, ~13:25 UTC). Not only this specific site, but also other areas surveyed later on during this dive were characterized by the presence of a hilly sea floor bearing thick carbonate

crust hosting dense bacterial mats (Fig. 83 right). After an unsuccessful carbonate sampling with the Orion arm (~13:51 UTC), the vehicle headed south towards the ISPS. At 14:22 UTC the ISPS was recovered and the ROV QUEST started ascending.

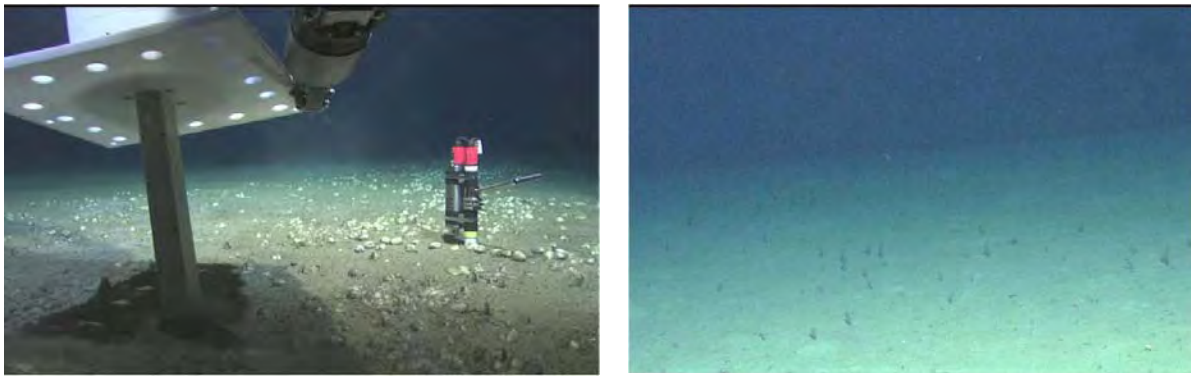

Fig. 81: ISPS coring and the T- Stick cored in a clam field area (left); Sea pens inhabiting background sediments (i.e. non-seep areas; right).

Fig. 82: GBS sampling streams of bubbles seeping out of the sea floor (left); a vertebrate carcass laying on the seabed (right).

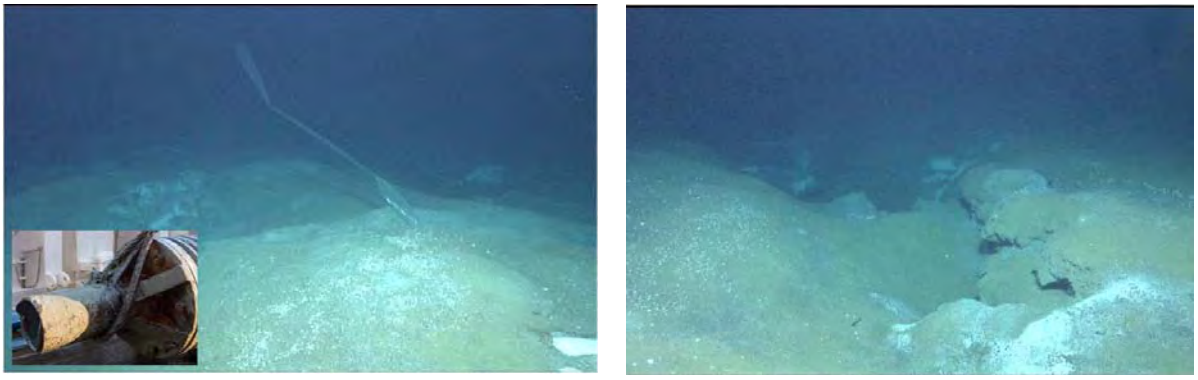

Fig. 83: Plastic liner from a gravity corer unsuccessfully recovered during M74/3 cruise (in detail, the broken gravity corer brought onboard – Photo by Volker Diekamp; left); Hilly sea floor bearing carbonate crusts covered by dense bacterial mats (right).

The Flare 2 area was extensively studied during the M74/3 cruise (Fig. 80). Visited 4 times prior to this dive, the location is characterized by interesting features such as intense seepage sites, dense bacterial mats, widespread clam fields, and carbonate-bearing sediments. Three out of five dives were devoted to mosaic surveying the area, covering the central and the

western flank of the valley-like geological feature. It is worth noting that almost all tools available for ROV-based sampling were used at this site, including the Osmo-Sampler and the Gas Bubble Meter (Dive 181 and 189, respectively). The information gathered during the 5 dives performed at Flare 2 will certainly provide a solid scientific foundation to further insights on methane seepage in this area.

6.2.16 Dive 194 (GeoB 12348)

Area:	Flare 11		
Responsible scientist:	Gerhard Bohrmann		
Date:	Monday, 19 November 2007		
Start/end at bottom (UTC):	08:08/13:08		
Total bottom time:	05:00h		
Start at the bottom:	24°44.515'N	62°58.639'E	1465 m water depth
Start ascend:	24°44.548'N	62°58.914'E	1463 m water depth

Scientist schedule:	**Scientist 1/Scientist 2/Navigator in the lab**
08:00 – 10:00	Gregor von Halem/Gerhard Bohrmann/Stefan Klapp
10:00 – 14:00	Florian Brinkmann/David Fischer/Gregor von Halem
14:00 – 16:00	Gerhard Bohrmann/Mohammed Nasir/Florian Brinkmann

Table 20: Instruments and tools deployed during ROV Dive 194.

GeoB	Tools/instrument	Start	Lat. [°N]	Long. [°E]	Depth (m)
12348-1	Carbonate 1	10:03	24°44.476	62°58.633	1475
12348-2	Carbonate 2	10:39	24°44.486	62°58.683	1475
12348-3	Carbonate 3	11:09	24°44.520	62°58.731	1469

ROV Dive 194 was planned on the crest of a ridge in 1500 m water depth in an area where several slides are influencing the detailed morphology of the sea floor. TV-sled 13 (Chapter 5) investigation revealed few indications for fluid venting in the very shallow parts of the track. Based on these findings and the more precise positions of the PARASOUND Flares 11a (24°44.519'N; 62°58.712'E) and 11b (24°44.561'N; 62°58.989'E) the ROV dive was planned around these two positions.

Unfortunately the navigation during the dive failed and the no correct positions of underwater navigation was available. The dive started at the western flare position and large fields of Bathymodiolus mussels were found that seem to settle on carbonate crusts (Figs. 84 and 85). In some areas the mussels have been covered by white crabs (Fig, 84) in a density which astonished all of us. This population was carefully documented by video imaging, photographing and carbonate samples have been taken three times (Tab. 20).

Furthermore, a sidescan sonar track was performed over the carbonate paved sea floor in the area of the huge colonization by chemosynthetic mussels and many video documentations were run in the area. Bubbles sites have also been observed at locations of stained mussels, very similar as at Flare 7 (Fig. 84 right). At the end of the dive, fields of Calyptogena-type

clams have also been observed and documented (Fig. 85 right). Due to technical problems (e.g. navigation) we decided to end the dive and ROV QUEST started ascend at 13:08.

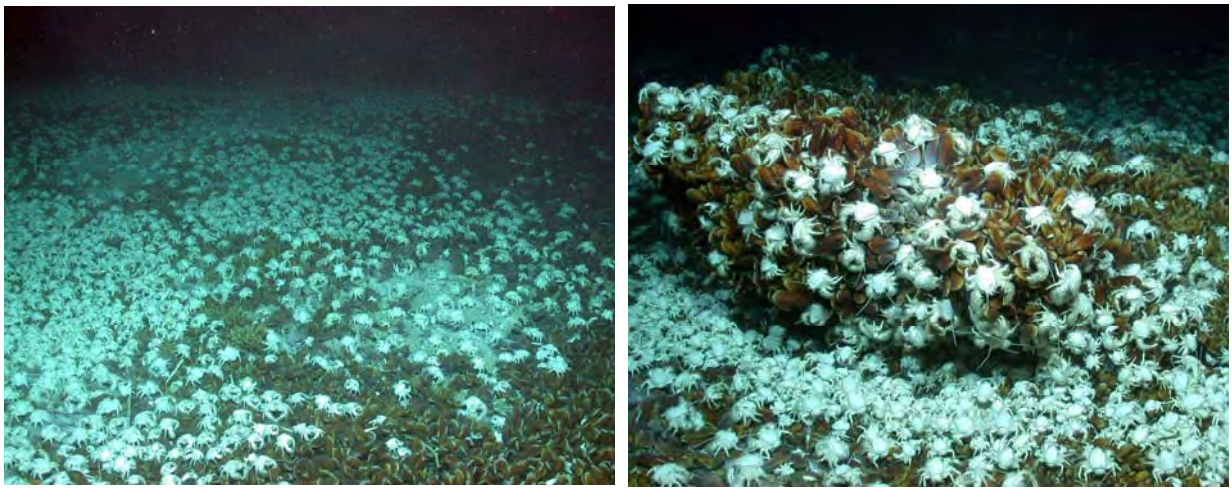

Fig. 84: Impression from Bathymodiolus mussel field at the rim of the dense crab population (left). Dense mussel accumulation and crabs colonize a possibly carbonate edifice (right), notice the staining of the mussels in the middle.

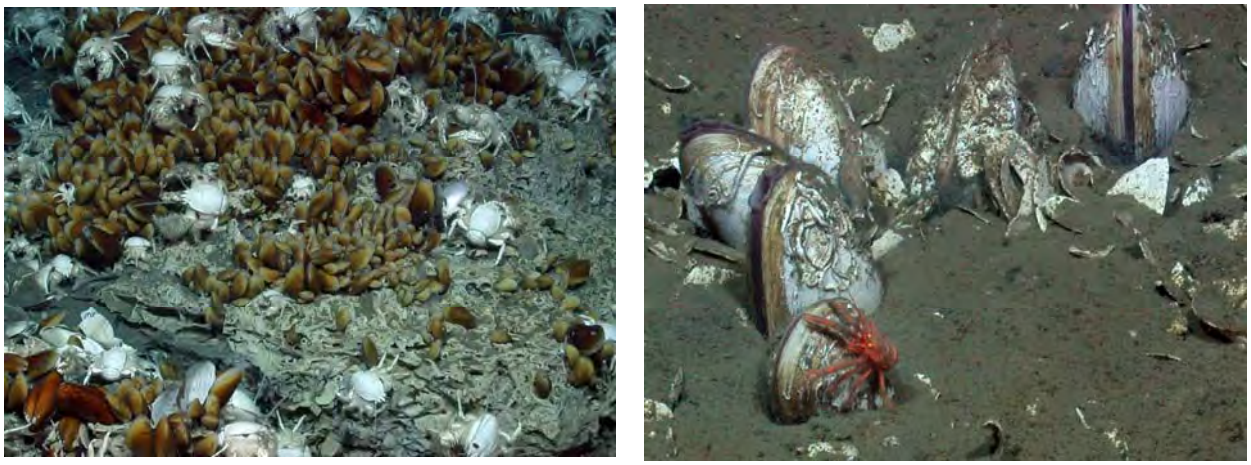

Fig. 85: Detail of mussels settling on authigenic carbonate rocks (left).Detail image from clam field (right).

6.2.17 Dive 195 (GeoB 12352)

Area:	Flare 4 on first ridge (seen by TOBI)		
Responsible scientist:	André Bahr		
Date:	Tuesday, 20 November 2007		
Start/end at bottom (UTC):	7:39/15:27		
Total bottom time:	7 h, 48 m		
Start at the bottom:	24°17.909'N	62°50.412'E	1946 m water depth
Start ascend:	24°17.929'N	62°50.098'E	1983 m water depth

Scientist schedule:	**Scientist 1/Scientist 2/Navigator in the lab**
12:00 – 14:00	Gregor von Halem/André Bahr/Stefan Klapp
14:00 – 16:00	Florian Brinkmann/Pamela Rossel/Gregor von Halem
16:00 – 18:00	Stefan Klapp/Sebastian Stephan/Florian Brinkmann
18:00 – 20:00	Markus Brüning/Monawar Saleem/André Bahr

Table 21: Instruments and tools deployed during ROV Dive 195.

GeoB	Tools/instrument	Start	Lat. [°N]	Long. [°E]	Depth[m]	Remarks
12352-1	Kips-1	10:38	24°17.932	62°50.081	1985	Sample 1
12352-2	Kips-2	10:40	24°17.933	62°50.081	1984	Sample 3
12352-3	Kips-3	10:47	24°17.934	62°50.081	1984	Sample 4
12352-4	Kips-4	11:10	24°17.934	62°50.081	1984	Samples 5, 6
12352-5	Kips-5	11:21	24°17.933	62°50.081	1984	Samples 7, 8, 9
12352-6	Kips-6	11:28	24°17.934	62°50.082	1984	Samples 10, 11
12352-7	PC-1	11:41	24°17.933	62°50.082	1984	PC 17
12352-8	BC-1	13:57	24°17.930	62°50.098	1983	
12352-9	T-stick-1	14:28	24°17.929	62°50.098	1983	
12352-10	GBS-17	15:15	24°17.929	62°50.097	1983	GBS red

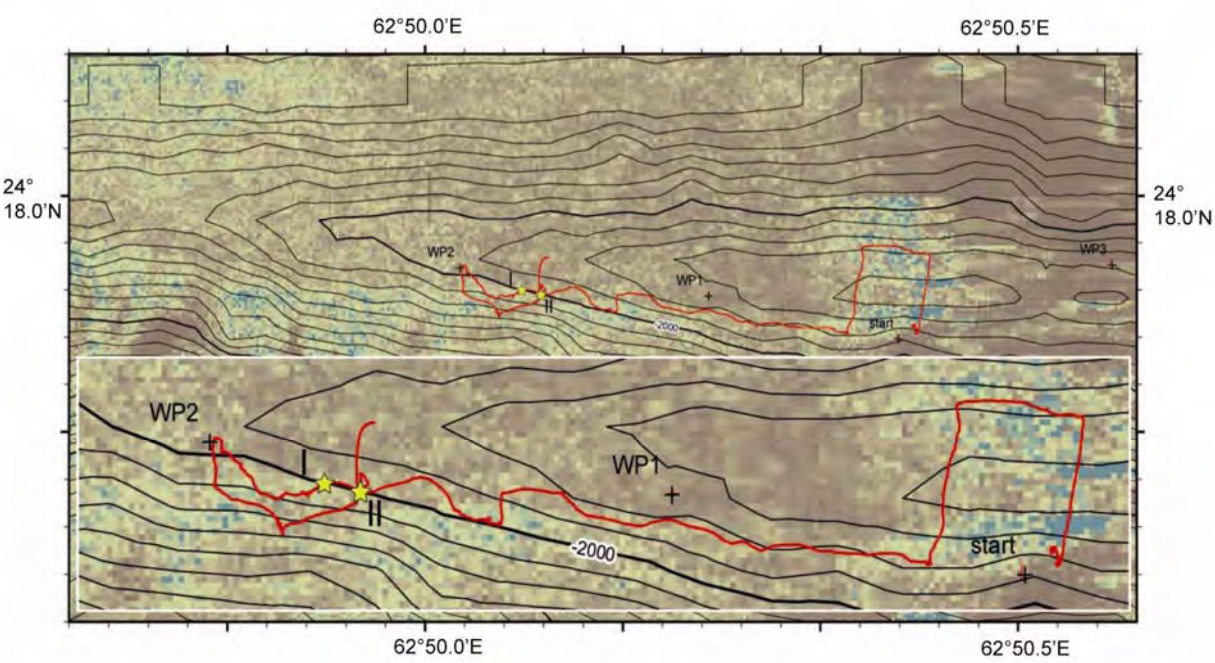

Fig. 86: Dive map with sampled fluid vent sites; the insert shows a close-up of the dive track with the sample sites (stars) I (KIPS, push coring) and II (sediment sampled with the bubble catcher, T-stick, GBS).

The purpose of Dive 195 was to ground-truth high backscatter patches observed in a previous Tobi survey, to look out for a gas bubble flare found in the Parasound record (WP 3) and to find and survey clam fields seen in a video slide track (WP 1 to W P2; Fig. 86). The dive began with a survey of a high-backscatter area north of the starting point. This was done by heading northward after bottom contact close to the start point and then, after approximately 100 m, redirecting in an eastward direction for another 100 m. However, no seep-indication or other phenomenon explaining the high backscatter patches could be found,

the sea floor looked rather smooth with some small hills indicating bioturbation by crustaceans (Fig. 87 left). In the next move Quest was directed southward again until it reached the very narrow crest of the ridge where it was planned to follow the crest in the direction of the assumed clam fields between WP 1 and WP 2. A search for the flare at WP 3 was skipped because of the inaccuracy of the Parasound-derived coordinates. After ca. 370 m of the first clam fields of living and dead clams were found, ca. 2 meters below the crest on the southern side of the ridge. These clams were partly found to form small nest-like clusters (Fig. 87 right). A patchy cover of bacterial biomass is only locally observed (Fig. 88 left), gas bubbling could not be found. After another approximately 130 m of survey to the west, a ca. 5 cm high crack along the ridge flank could be seen, apparently related to some faulting and/or slumping activity. On the downslope direction below the crack, whitish hills, some dm high, with small openings on the top were discovered (Fig. 88 right), often with cm-scale chimney-like tubes on top. From these holes a stream of apparently suspension-loaded fluid emanated (Fig. 89 left), in some cases also from the chimneys, which seemed to be inactive on the first glance. The fluid and background samples were then taken with the KIPS sampler (site I in Fig. 86). After finishing the KIPS sampling, sediment were planned to be taken with push cores. Because of the very powder-like fabric of the sediment, push coring turned out to be extremely difficult and only one sample could be successfully recovered. During coring, a number of polychaetes were observed escaping from the holes in the whitish hills and later disappearing into them again. Heading towards WP 2 the survey continued, however, aside from occasional bacterial patches and a Calyptogena-“nest”, no structure of particular interest has been found. After reaching WP 2, the survey continued towards the south and then further to the west towards the location of the newly discovered fluid venting site. Next to this site, along a very steep slope, another deposit of the powder- like material with the characteristic chimneys has been present, partly eroded, so that the abundant tubes were clearly visible (Fig. 89 right). The dive ended close to the initially discovered vent site (site II in Fig.86), where a sediment sample could be retrieved from one of the whitish hills using the bubble catcher. Finally, the T-stick and GBS have been deployed at a small reddish mound with a fluid-expelling hole next to a larger whitish mount.

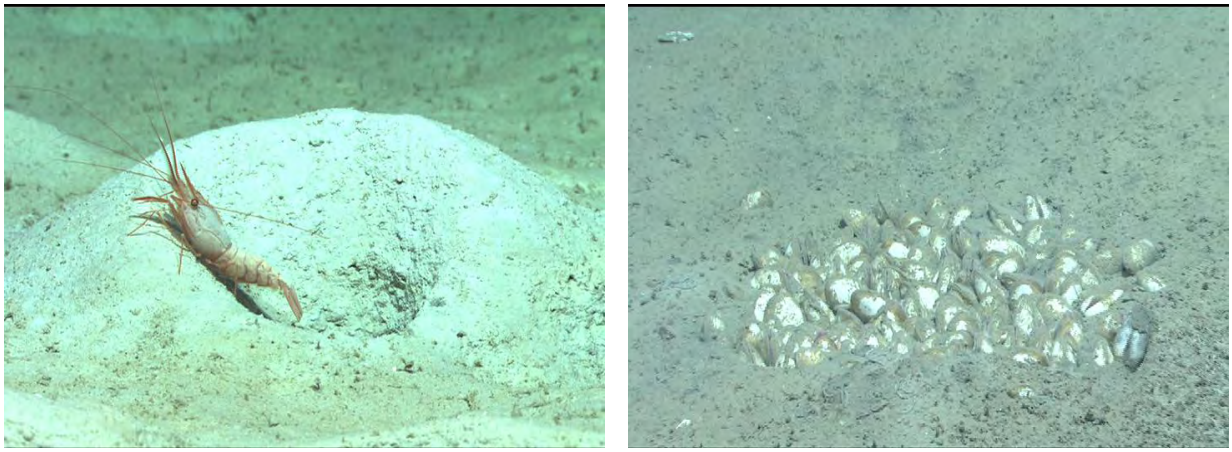

Fig. 87: Crustacean in entrance of its burrow (left); nested clams (right).

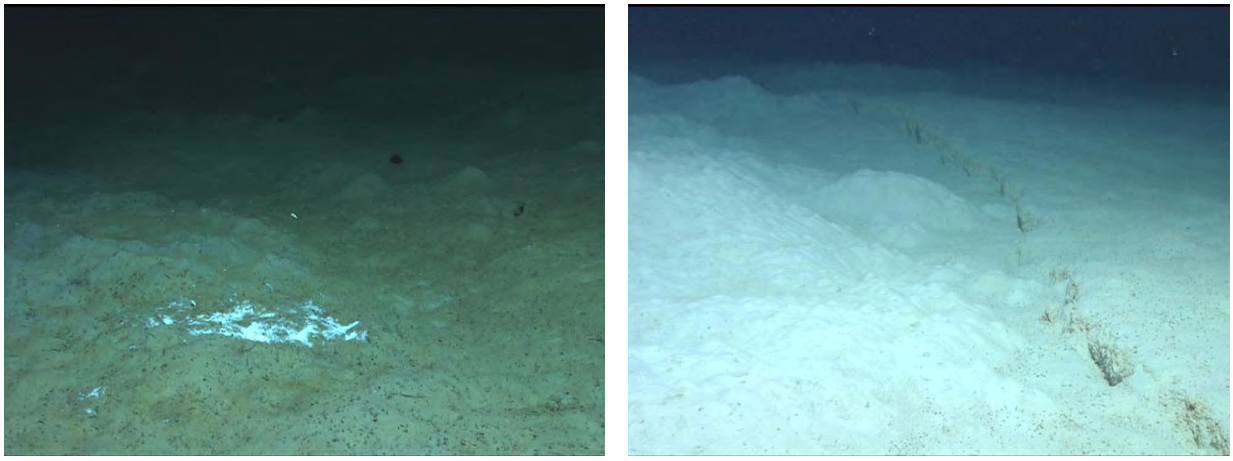

Fig. 88: Bacterial patch; (left); hilly morphology where fluid venting can be observed (right).

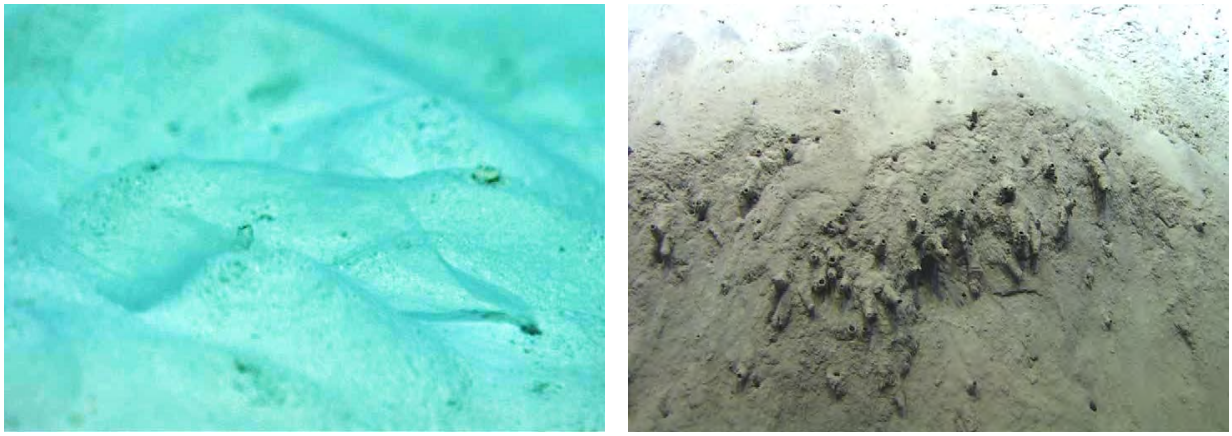

Fig. 89: Close-up on one of the fluid-venting holes on top of the whitish hills in Fig. 88 right (left); calcareous tubes exhumed at a very steep wall in proximity to the location shown in Fig. 88 right (right).

6.2.18 Dive 196 (GeoB 12353)

Area:	Flare 15		
Responsible scientist:	Stephan A. Klapp		
Date:	Wednesday, 21 November 2007		
Start/end at bottom (UTC):	09:54/16:53		
Total bottom time:	6:59 h		
Start at the bottom:	24°48.409'N	63°59.650'E	733 m water depth
Start ascend:	24°48.445'N	63°59.646'E	734 m water depth

Scientist schedule:	**Scientist 1/Scientist 2/Navigator in the lab**
09:54 – 12:02	Stephan A. Klapp/Thomas Pape/Gregor von Halem
12:02 – 14:02	Gregor von Halem/Karin Zonneveld/Florian Brinkmann
14:02 – 16:53	Florian Brinkmann/Nina Wittenberg/Stephan A. Klapp

Table 22: Instruments and tools deployed during ROV Dive 196.

GeoB	Tools/Instrument	Start	Lat [°N]	Long. [°E]	Depth (m)	Remarks
12353-1	Net	11:32	24°48.463	63°59.649	730	
12353-2	GBS-18	14:07	24°48.458	63°59.649	732	GBS yellow
12353-3	PC-1	14:42	24°48.458	63°59.649	732	PC 15
12353-4	PC-2	14:44	24°48.457	63°59.649	732	PC 4
12353-5	PC-3	14:48	24°48.457	63°59.649	732	PC 6
12353-6	PC-4	14:49	24°48.458	63°59.650	732	PC 2
12353-7	Carbonate-1	15:22	24°48.457	63°59.654	731	
12353-8	Carbonate-2	15:34	24°48.459	63°59.654	731	
12353-9	Carbonate-3	15:54	24°48.467	63°59.650	730	
12353-10	Carbonate-4	16:09	24°48.467	63°59.647	731	
12353-11	Carbonate-5	16:30	24°48.445	63°59.644	734	

ROV 196 was special in that it was undertaken at seep 15, which is ca. 60 nm east of the other seeps investigated during cruise M74/3.

The flight started at 09:54 h UTC from 24°48.409'N / 63°59.650'E with a short sonar survey 20 m above ground to detect gas bubbles in the water column, which were previously found by PARASOUND. At 10:38 UTC, bubbles were spotted and the ROV descended to the sea floor, where many bacterial mats were found (Figs. 91). A larger survey of these bacterial mats commenced with the objectives to document the mats, discover bubble escape sites and find appropriate sites for sampling. Additionally, HD recordings were done both during the survey flight to document the impression of the sea floor and the extension of the bacterial mats field and the HD Zeus camera also recorded during the inspections of individual mats. High-resolution pictures with the Scorpio camera were done at most of the bacterial mats.

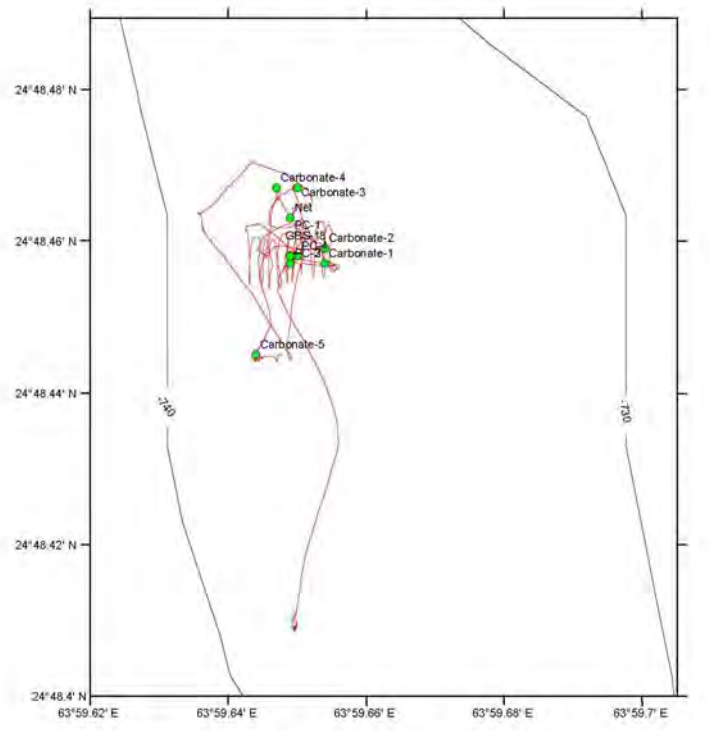

Fig. 90: Dive map of ROV 196 (unlike dives ROV 179-195, for Flare 15 exits no TOBI-backscatter map).

Thioploca bacteria most likely form the mats as a very soft layer on the sediment surface, which is white with a yellow center. The sediments in the area of Flare 15 are very soft with only very few carbonate crusts. Unlike other dives in the western part of the working area, for Flare 15 exists no backscatter map which could have been explored, and since many small Thioploca patches we found in the vicinity of the starting point, there was no reason to leave the area. Instead, the ROV stayed at the bacterial mats field for the entire dive.

After photo and video documentation of many bubble escape sites and bacterial mats (Figs. 91), background samples were taken of the soft sediment close to a crack along the sea floor by the net. After that, about 2 hours of the dive had passed. Then, the bacterial mat area was imaged by video mosaicing. In total, 10 mosaic tracks were recorded in ca. 2 hours.

After the very detailed imaging and documentation of the area, within one hour further samples were taken both for gas and pore water chemistry (see Table 22): The gas bubble sampler (GBS) was filled at a large bacterial mat where seepage occurred (Fig. 91 left), also, push cores were taken at the same location. The remaining time was spent to find hard carbonates (Figs. 92), which turned out to be a difficult enterprise as sediments at Flare 15 are rather soft. After 1,5 hours, 5 carbonate samples were recovered at different locations (see table 22) and the dive was finished.

Remark: As dive 196 /GeoB 21353 was the last dive on METEOR Cruise M74/3, within the last 1,5 hours of bottom time there was the chance for crew and some scientists to take over the pilot's place and fly the ROV for some time.

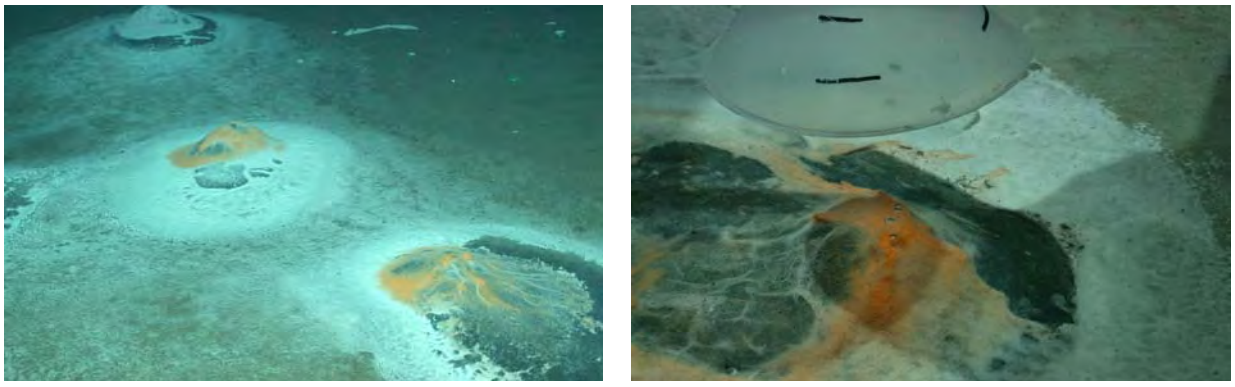

Fig. 91: The area of Flare 15 is covered by many bacterial mats (left). The mats are very thin, bubbles escaped at some of the mats (right).

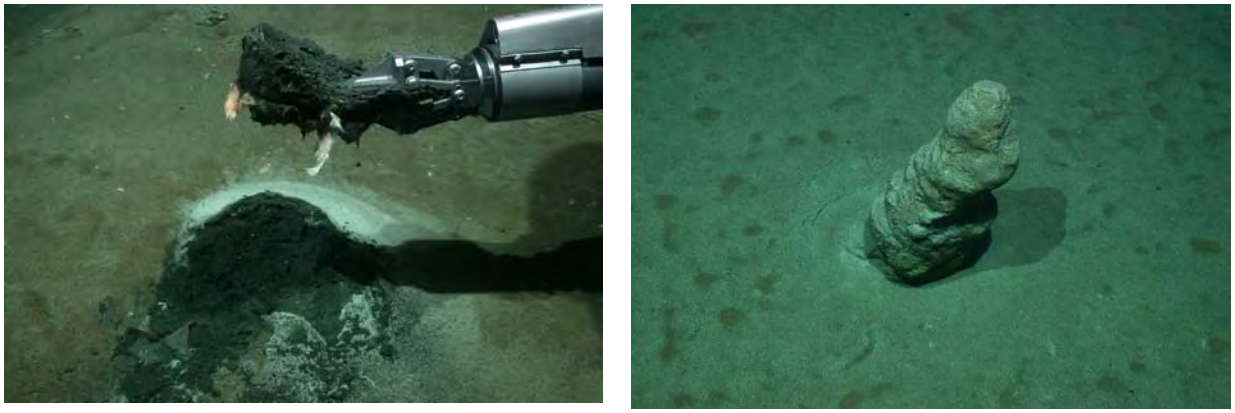

Fig. 92: Some carbonates were sampled at bacterial mats (left). Few carbonates were also present outside the immediate bacterial mats (right).

6.3 Bubblemeter

(K. Thomanek)

Photo optical systems are common in marine sciences and have been extensively used in coastal and deep sea research. The present design for an in-situ high speed image acquisition and automated data processing system, referred as “bubblemeter” has been deployed at the Makran accretionary wedge during Leg 3 of the METEOR Cruise 74. The objective was to prove the technical feasibility of measurering bubble size and rise velocity as well as determining the gas flux at single seep sites under in-situ conditions.

Determining the fate of methane bubbles emerging from seepage is highly motivated from a variety of disciplines in marine sciences. Gas seeps enable bacteria to form colonies on seabed in the immediate vicinity of vents and utilize methane as energy source. Methane may also be dissolved within intermediate layers of deep water and subject to oxidation. Furthermore methane bubbles may rise even higher and enter the mixed layer or even surface and therefore contribute to the greenhouse effect of the atmosphere. The fate of methane bubbles is inevitably related to parameters such as gas flux, bubble size and rise velocity as well as water temperature, hydrostatic pressure, bulk water methane concentration and the presence of surface active substances. Thus quantifying methane gas flux of single seepage along with its bubble size distribution and rise velocity represents a key element for estimating the impact of methane to the hydro- and atmosphere.

The gas bubbles are recorded rising in front of the homogenously illuminated screen using backlight illumination (Fig. 93 left). The camera records a sequence of 2 s duration acquiring a total of 1000 frames at a resolution of 1280 x 1024 pixel. Each frame is then automatically processed and analyzed with respect to bubble segmentation, size and rise velocity measurement as well as flux computation. The bubblemeter is deployed using the ROV being positioned exactly over a specified gas vent orifice.

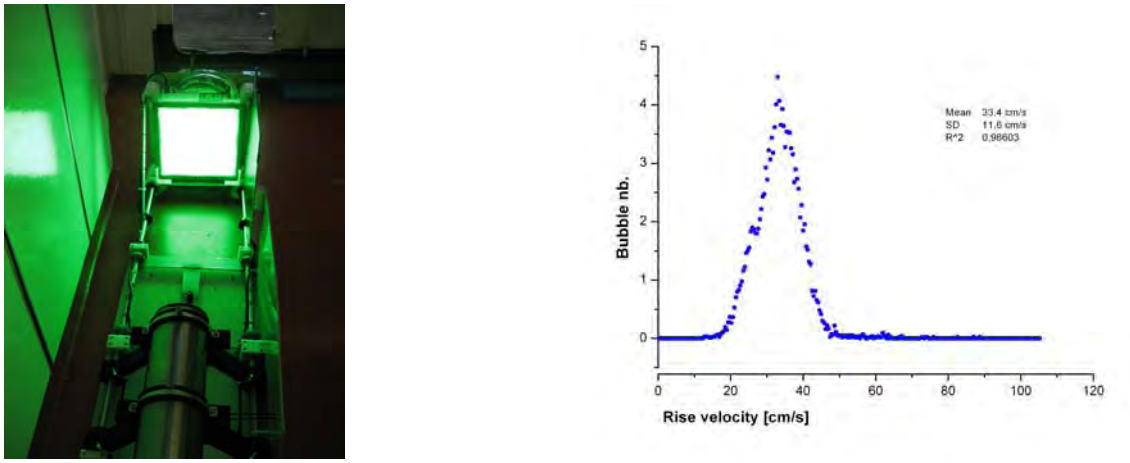

Fig 93: Pre-dive system test. Bubbles will be recorded in front of high intensity screen (left). Rise velocity distribution shows a distinct peak at 33,4 cm/s (right).

The device was deployed twice during the cruise. During Dive 185 at Flare 7 the system failed to trigger due to an electrical capacity change within the sub sea cable. However, the

system could then successfully be applied during Dive 189 at Flare 2 in a water depth of 1023 m. As a reference, an alternative method for quantifying the gas flux was used deploying the gas bubble sampler (for technical details see chapter 10.2) at the same site.

In total 1020 frames have been analyzed. Approximately 55.000 bubble measurements have been conducted. Bubbles could be tracked in successive frames with a success rate of 94%, yielding reliable statistics for size and velocity distribution. Fig. 93 right shows the rise velocity distribution with a mean of 33,4 cm/s and a standard deviation of 11,6 cm/s. The bubble size is described by the major and minor axis elongation (see Figs. 94). The major axis distribution shows 3 distinct peaks at x1=2,8mm σ=0,7mm, x2=3,8mm σ=0,4mm and x1=6,8mm σ=2,3mm. Whereas the minor axis peaks twice in y1=1,9mm σ=0,5mm an y1=3,5mm σ=1,7mm.

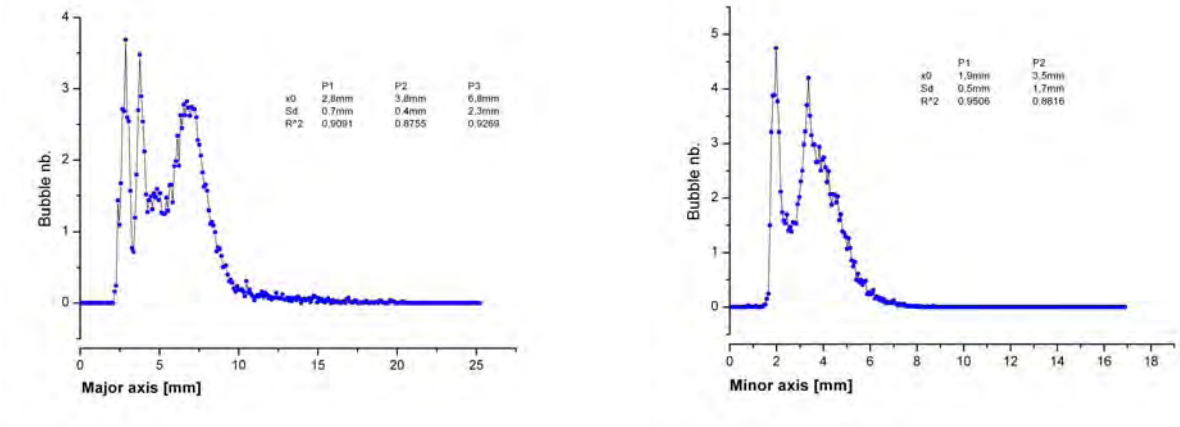

Fig. 94: Major axis distribution of bubble size showing 3 (left). Minor axis distribution of bubble distinct peaks size showing 2 distinct peaks (right).

The flux measurement yielded 133 bubbles passing a specified cross section during observation transporting a total volume of 4,7 ml of gas in-situ. Thus a momentary flux of 142 ml/min and an error of 10% can be deducted.

7 Temperature Measurements

(S. Stephan)

As seepage is conducted by the ascent of warm fluids, temperature anomalies can be caused at the sea floor and in the bottom water. These temperature anomalies can be detected and quantified by in situ measurements. Temperature measurements provide information of the strength and the nature of seepage and can be used to estimate the boundaries and the position of the gas hydrate stability zone within the sediment. Therefore in situ measurements were performed during R/V METEOR Cruise M 74/3 in shallow sediment depth (up to 0.6 m with the temperature lance) and in the bottom water.

The temperature-lance (Fig. 95) used on this cruise is manufactured by RBR Ltd. and is equipped with a data-logger (model RBR XR420). The temperature lance is capable to measure temperatures in depths up to 0.6 m below sea floor. The lance is equipped with eight equidistant spaced (3.3 cm) thermistors; the diameter of each sensor is 0.5 cm. The logging unit is usually set up to register the data from the thermistors every ten seconds during the whole dive. The precision of the measurements is ± 2 mK. The lance is pushed into the sediment by using the manipulator arm ("Orion") of the ROV "Quest 4000 m", which can grab the lance on a so-called T-handle. The lance penetrates the sediment to depths up to 0.6 m while staying in the sediment for at very least 7 minutes to reach equilibrium temperatures. During the temperature measurement, the ROV has no direct contact to the lance to avoid disturbances caused by movement of the ROV. The real equilibrium temperature is estimated by extrapolation of the measurement.

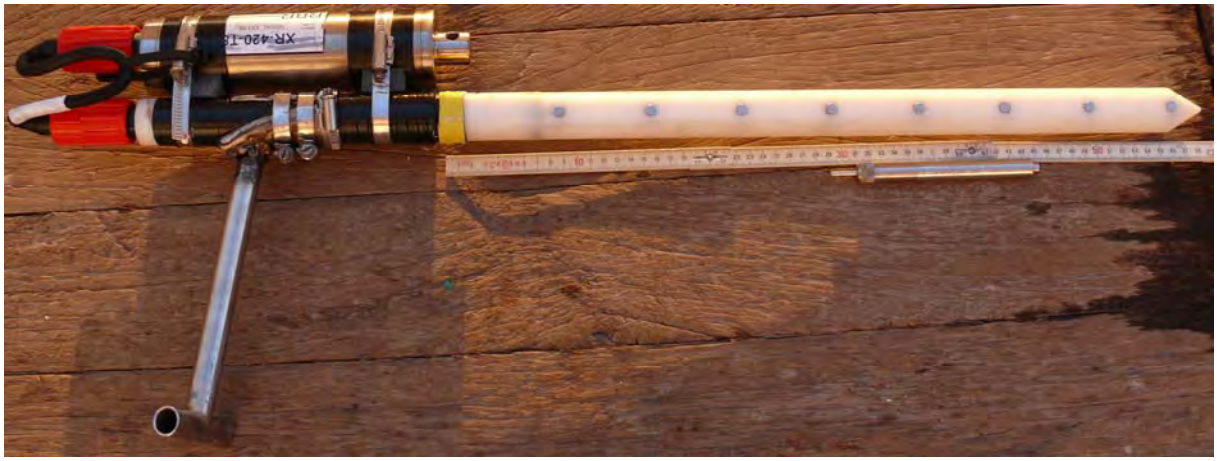

Fig. 95: Temperature lance manufactured by RBR Ltd.

For the measurements in the water column an autonomous data logger (miniaturized temperature logger - MTL) from Antares Datensysteme GmbH was used (Fig. 96). The MTL was directly attached to the frame of „ROV Quest 4000 m" on the port side (Fig. 97). In general, the relative resolution of the MTLs is 0.6 mK, which allows highly accurate relative temperature measurements. The absolute precision of the MTLs is ± 0.1 K, due to missing calibration with a high precision reference. For calibration purposes the MTLs were all on the ROV during the first dive, so that they could be calibrated relatively among each other. For initial relative calibration, the sensors were mounted on the lower frame on the port board side

of the ROV „Quest 4000 m" on a so called prism (Fig. 98). The MTL data loggers are used to record the bottom water temperature, especially the relative change of temperature.

Fig. 96: MTL (Miniaturized Temperature Logger) by ANTARES Datensysteme.

Fig. 97: Mounting position of MTL on ROV "QUEST 4000 m".

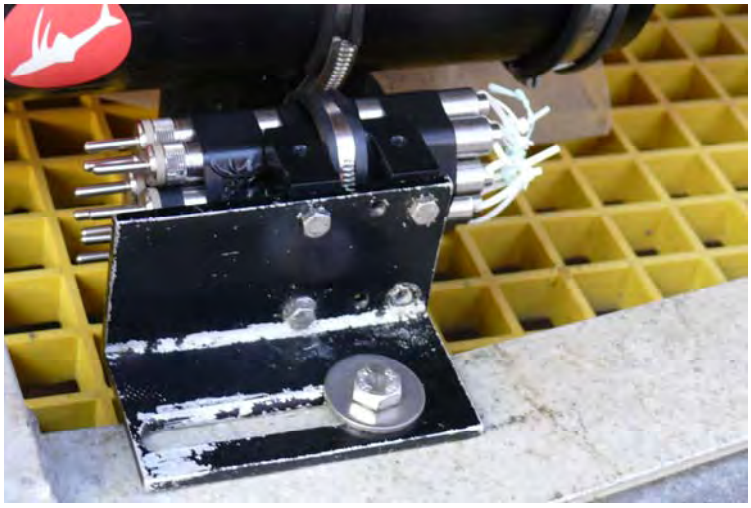

Fig. 98: Mounting of MTLs during calibration dive.

Preliminary results

The **in situ temperature measurements** were mainly taken to identify temperature anomalies in the sediment caused by seepage of warm fluids (for duration and positions see Tab. 23). The preliminary data processing shows no gradients indicating strong temperature anomalies over the measured depth interval. The differences in temperatures between bottom-water and sediment are too low for temperature influence caused by seepage. Fig. 99, right, shows an anomaly in the calculated gradient, which is assumed to be related to gas ebullition. Fig. 99, left, shows a gradient which is very low, this may be caused by infiltration of bottom water in the sediment. Fig. 100 shows the temperature over time for the specific measurement. The deepest sensor in the sediment is sensor #1.

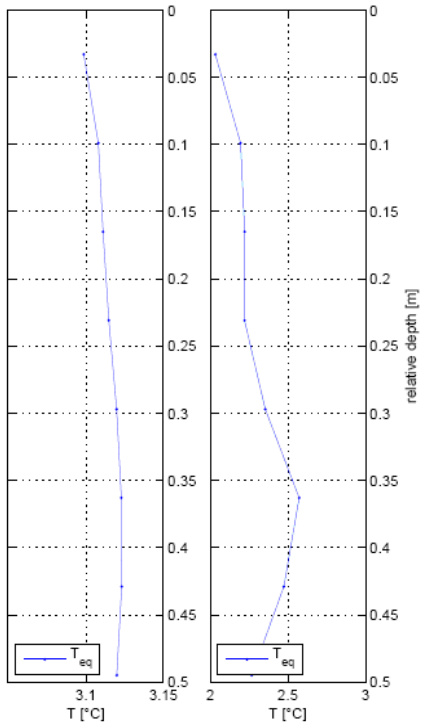

Fig. 99: The blue line shows the gradient calculated from the estimated equilibrium temperatures. Each dot represents a measurement in a certain depth below sea floor. Left: low gradient due to infiltration of bottom water. Right: Dive 179, anomaly in gradient at 0.3 m penetration depth related to gas ebullition.

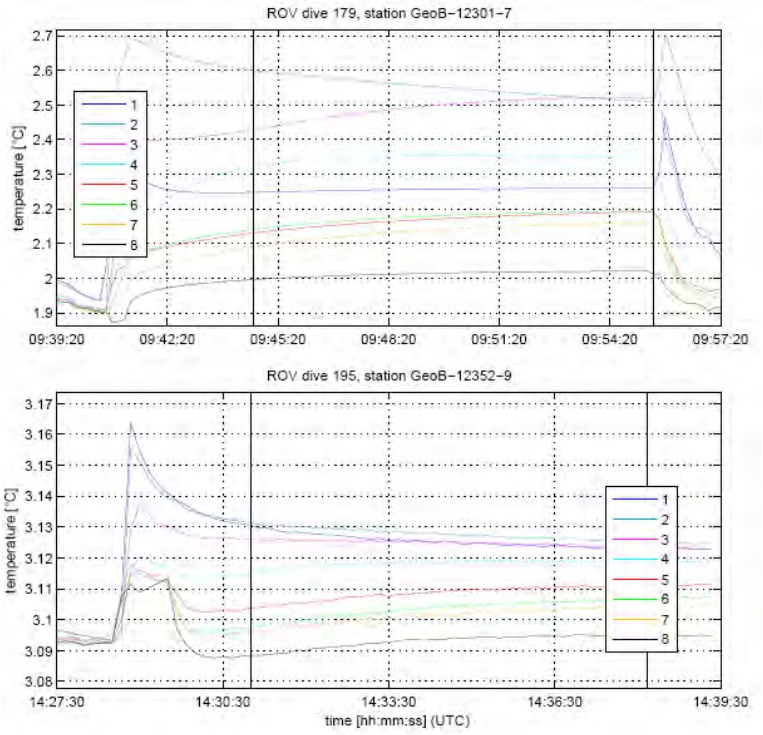

Fig. 100: Temperature over time for each sensor while penetration (sensor 1: deepest in sediment) for station GeoB-12301-7 (gradient: Fig. 99, right) and station GeoB-12352-9 (gradient: Fig. 99, left).

Table 23: List of measurements with T-lance.

Date	St. No. GeoB	Instruments	Location	Start Program	End Program	Water depth (m)	Latitude N°	Longitude E°	Recovery Remarks
2.11	12301-2	T-stick-1	Nasc. Ridge	09:19	09:38	2876	24:11.750	62:44.309	Dive 179 / T1: 65 cm
2.11	12301-7	T-stick-2	Nasc. Ridge	09:40	09:55	2876	24:11.750	62:44.308	Dive 179 / T1: 62 cm
8.11	12319-1	T-stick	Flare 1	06:44	06:54	572	24:53.629	63:01.418	Dive 183 / T1: 53 cm
9.11	12320-1	T-stick	Flare 1	08:29	08:49	592	24:53.636	63:01.405	Dive 184 / T1: 23 cm
11.11	12324-3	T-stick-1	Flare 6	12:14	12:15	1823	24:34.809	62:56.325	No pen. / no data
11.11	12324-4	T-stick-2	Flare 6	13:28	13:38	1835	24:34.841	62:56.522	Dive 185 / 45°; 55cm
11.11	12324-5	T-stick-3	Flare 6	14:22	14:38	1835	24:34.840	62:56.522	Dive 185 / T1: 50 cm
18.11	12343-1	T-stick-1	Flare 2	06:08	06:20	1030	24:50.697	63:01.446	Dive 193 / T1: 49 cm
20.11	12352-9	T-stick-1	Flare 4	14:28	14:40	1983	24:17.929	62:50.098	Dive 195 / T1: 48 cm

The **bottom water temperature** was logged by the CTD of ROV "QUEST 4000 m" and by a separate mounted MTL. The response of the MTL is very sensible and shows a more detailed pattern than the on-board CTD. Very small bottom-water anomalies can be observed over bacterial mats (i.e. during Dive 180). Fig. 101, middle, shows a temperature anomaly of 0.1°C at about 14:45. The red crosses represent the estimated bottom water temperature calculated from the gradient of the water temperature in the water column belonging to the actual depth measured by the ROV. At 14:45 the ROV was taking a gas sample with the GBS over a bacterial mat (Fig. 102). The gas seepage might be conducted to slightly warmer fluids which may cause the bottom water anomaly.

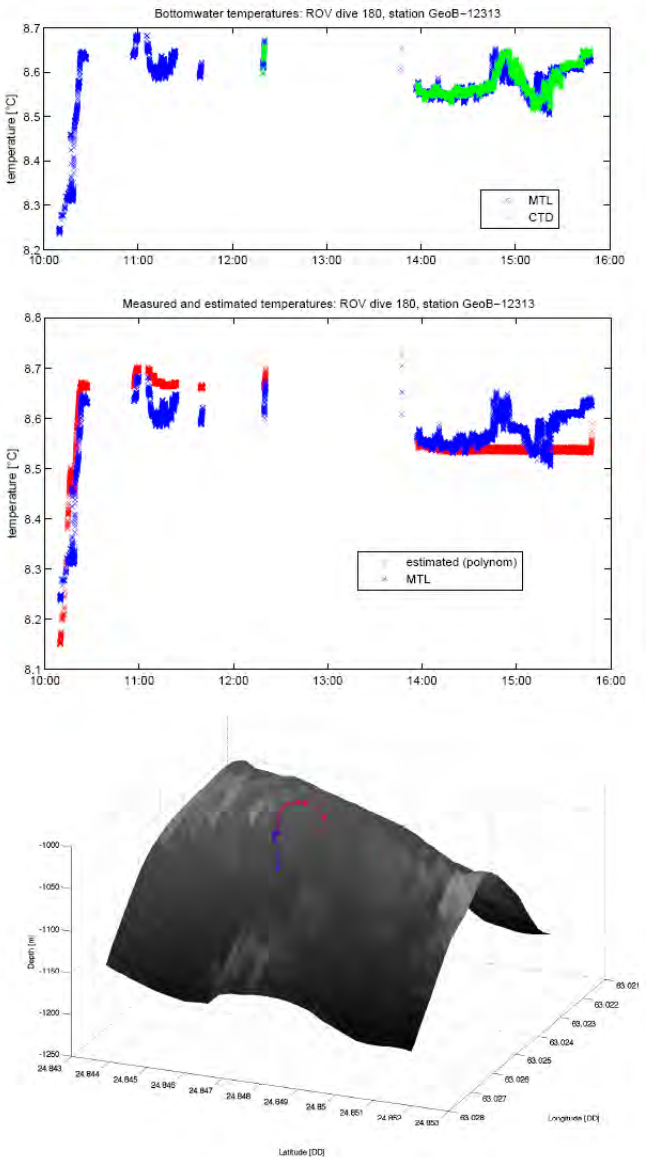

Fig. 101: Top: measured bottom water temperatures. green: CTD blue: MTL (temperature interval: 0.5°C) middle: estimated bottom water temperature in red and measured bottom water temperature in blue are showing an anomaly of about 0.1°C at 14:45. bottom: dive track over bathymetry. Coloring of dive track according to measured temperatures.

Fig. 102: ROV activity at 14:45 - picture copyright by MARUM, University of Bremen.

8 Water Properties of the Makran Area during the Intermonsoonal Period of November 2007

(K. Zonneveld)

8.1 Introduction

The northeastern Arabian Sea is characterised by climatically related high bioproductivity in the surface waters and the occurrence of a stable oxygen minimum zone at intermediate water depths. On the southern shelf and slope region of Pakistan (Makran) numerous locations with gas seepage have been discovered (e.g. von Rad et al., 1996). Until now no information is present in how far this methane rich gas contributes to development of the oxygen minimum zone next to the high bioproduction rates and the ocean circulation in the region. To obtain more insight into this detailed information is required about the characteristics of the water column in the direct vicinity of the seepage sites as well as on the regional characteristics of the water column.

As result of the presence of a stable oxygen minimum zone and high sedimentation rates in the area, the sediments within the region are known as excellent palaeoceanographic and palaeoclimatic archives that allow high resolution palaeoenvironmental studies. However, to unravel the complex interaction between changing oceanic circulation, chemistry, life and climate change and to obtain insight into the nature of positive and negative feedback mechanisms, detailed and quantitative information is required about individual control parameters. While direct observations only exist for the last decades, so called “proxy records” that are derived from isotopic, biological, chemical and physical properties of marine sediments, reach back millions of years. For a sound application of proxies it is essential to obtain insight in the usability and limitations of them. To achieve this, information on the basic processes that control the various proxies is required.

Consideral parts of the presently used proxies are plankton based. For instance the isotopic composition and elemental chemistry of carbonatic microfossils often form the backbone of palaeoceanographic and palaeoclimatic studies. Foraminifera have been most widely used as a result of their abundance in the sediments and the ease in which monospecific samples can be picked. However, biological factors such as the migration of several planktonic species through different water masses, the influence of calcite shell isotopic composition by photosynthetic activity of symbionts and consumption of other organisms and the ontogeny of individual species can hamper the interpretation of these signals (Bemis et al. 1998). Consequently, specific species equations of photosynthetic organisms, that form their calcite walls at a stable position within the water column, might overcome some of these problems.

Recent studies for the use of primary producers such as the photosynthetic dinoflagellate cyst *Thoracosphaera heimii* give promising results (Zonneveld 2004; Zonneveld et al. 2007). Cysts can relatively easily be isolated from sediments. Calculated temperatures based on the palaeotemperature equation for inorganic calcite precipitation generally reflect mean annual temperatures at thermocline (Deep Chlorophyll Maximum) depths, which is suggested to represent its preferred depth habitat (Zonneveld 2004). However, until now information about its preferred depth habitat is available for the equatorial and southern Atlantic Oceans only.

Acantharia are planktonic organisms whose skeletons consist of celestite ($SrSO_4$). Bernstein et al. (1992) proposed that the dissolution of acantharian-derived celestite which contains considerable amounts of barium ($BaSO_4/SrSO_4$ ratios in the order of 0.003) represents one of the major sources of productivity-related barium or barite. However, due to the fragile nature of these organisms and their susceptibility to rapid disintegration and dissolution of the celestite spines in the water column a clear relationship between the abundance and downward flux of acantharia and so-called “biogenic” or “marine” barite has not yet been established.

To obtain insight into the oceanographic properties of the water column and to gain information about the production and depth habitat of the calcareous dinoflagellate cyst *T. heimii* and Acantharien and to relate acantharian abundances to barium contents in the sediments, detailed information about the temperature, salinity, oxygen concentration, chlorophyll-a concentration and turbidity has been gathered. Apart from the investigations of the complete water column, special attention has been given to the photic zone properties, hence the upper 150 m.

8.2 Ocean Circulation

The oceanic circulation of the Arabian Sea is strongly influenced by the semi-annual reversal of wind patterns; the southwest (SW) monsoon in the boreal summer, and northeast (NE) monsoon in the boreal winter. In summer, differential heating of the continental and oceanic regions leads to low atmospheric pressure above the Asian Plateau and high atmospheric pressure over the relatively cool southern Indian Ocean. This results in the development of a strong low-level jet stream, the Findlater Jet (Smith et al. 1991). The response of the ocean to these southwestern winds includes the development of the southwestern Somali Boundary Current, with a north-northeastward current speed of about 150 cm/s (Brock et al. 1992; Bruce 1974; Bruce 1979). The speed decreases to about 10 cm/s at 100m depth. Development of this current leads to upwelling along the Somali and Arabian coasts, bringing relatively cold, nutrient-rich waters to the surface. In the Arabian Sea region north of the Findlater Jet a large area of open oceanic upwelling develops (Bauer et al. 1991; Brock et al. 1991; Currie et al. 1971). To the south, enhanced deepening of, and vertical motion in, the mixed-layer associated with Ekman pumping can be observed (Bauer et al., 1991). Both upwelling and processes associated with Ekman pumping result in increased nutrient availability and consequently enhanced bioproduction in surface waters of the Arabian Sea (Jochem et al. 1993; Qasim 1982).

During the NE monsoon both wind and surface circulation patterns are reversed. However, current speeds are not as high as during the SW monsoon, and over the year a net northward flow of 20-30 cm/s can be observed. Cold winds from the northeast induce increased mixing and cooling of waters near the Gulf of Oman and on the Pakistan shelf, which results in high bioproduction in this region (Qasim, 1982; Smith et al., 1991).

Arabian Sea subsurface waters consist of Red Sea and Gulf of Oman outflow waters that spread slowly southward at a depth of ± 200 m – 500 m and mix eventually with other water masses (Barton and Hill 1989; Johnson et al. 1991a; Johnson et al. 1991b; Shapiro and

Meschanov 1991; Wyrtki 1971). Bottom waters enter the Somali Basin from the south. Probably part of this water leaves the Somali basin in the North by passing the Owen Fracture Zone to become part of a southwestward flow along the Carlsberg Ridge.

The research area is located within the vicinity of the outlet of the Indus river which drains large parts of the Indian subcontinent. Presently the Indus forms an estuary during the SW monsoonal season only (Schubel 1984). This results in enhanced nutrient supply and mixing of the upper water column during this season. However, in the last decades the Indus outflow has been reduced dramatically due to increased utilisation of the flow of the Indus River for agriculture and damming/channelling of the river. Mean annual water and suspended sediment discharge load has dropped between 1950 and 1960 from about 90 km^3/yr and 200 Mt. to about 60 km^3/yr and less than 100 Mt. respectively (Milliman et al. 1984). Before 1950 the region near the Indus outlet was, however, characterised by well mixed surface waters throughout the year.

8.3 Materials and Methods

Detailed information about the temperature, conductivity and oxygen of the water column have been carried out with a CTD – Rosette combination (Seabird 911+) with additional oxygen sensor. Chlorophyll-a measurements and turbidity measurements have been carried our with a Wetlab CHL sensor and Dr. Haard turbidity sensor. The Rosette contains 18 bottles with a volume of 10 l.

To investigate the distribution of *T .heimii* cells and acantharien in the upper water column, water samples have been collected on a depth transect over the deep chlorophyll maximum. Directly after recovery, samples have been gently filtered through a 20µm and 10µm sieve and counted, to avoid dissolution of the acantharian. Counts have been carried out using an Axiovert microscope (Zeiss) under 400x magnification.

8.4 Results

Positions and timing of the preformed CTD casts are given in Appendix 2.
The water column properties reflect inter-monsoonal conditions with a strongly stratified upper water column (Fig. 103).

Subsurface waters bear a signal of the Gulf of Oman outflow waters that are characterised by high salinity and slightly better ventilation compared to waters above and below (Figs. 104 and 105). Based on the oxygen concentrations two zones with sub-oxic conditions can be observed between about 100 m and 350 m depth and between 900 m and 1200 m water depth (Fig. 106). Well ventilated waters can be observed below about 1600 m water depth.

Enhanced turbidity and chlorophyll-a concentrations can be observed in the upper part of the water column (Figs. 107 and 108). A deep chlorophyll maximum can be observed in the upper 50 m of the water column.

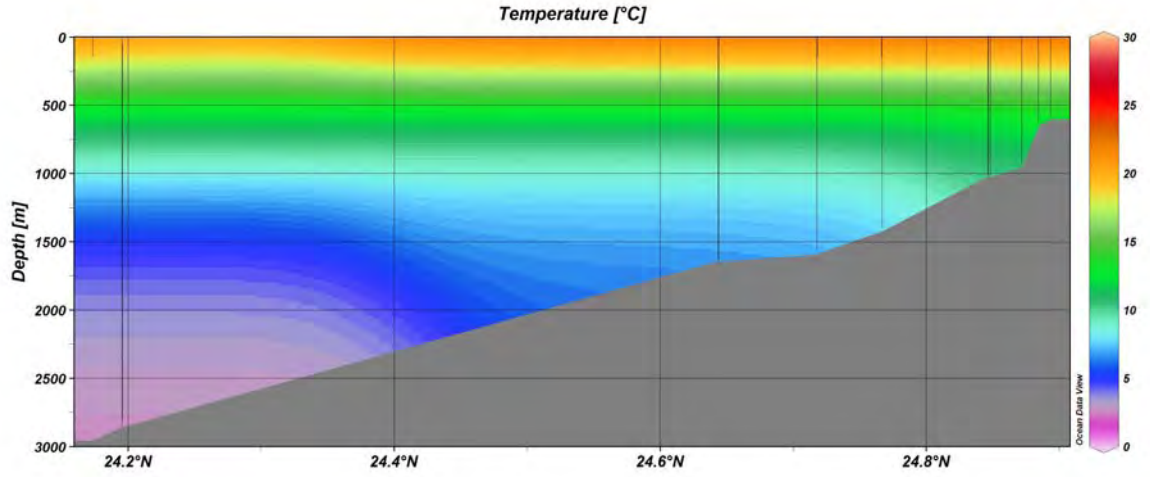

Fig. 103: Temperature (°C) compiled from all stations listed in Appendix 2.

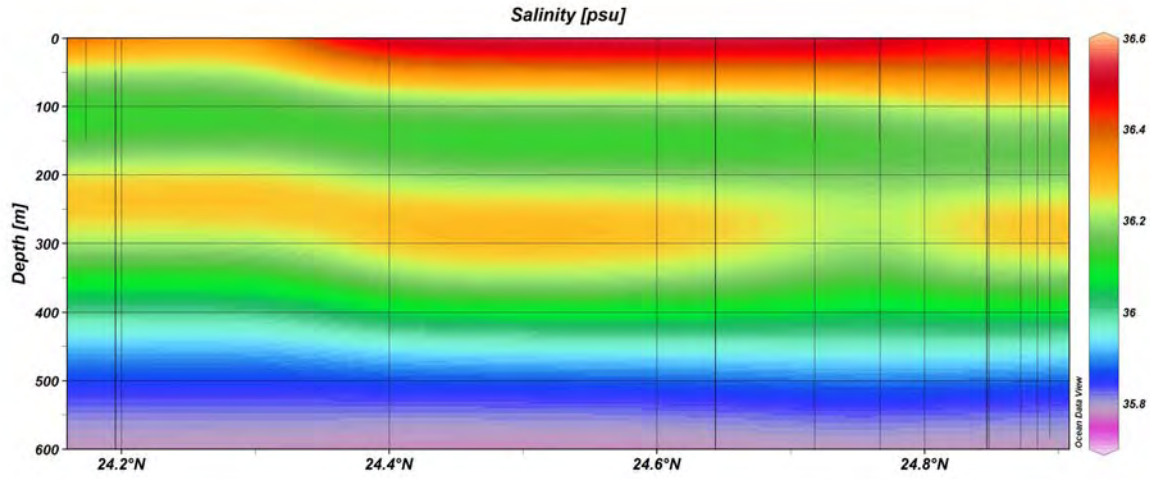

Fig. 104: Salinity (psu) of the upper 600m compiled from all stations listed in Appendix 2.

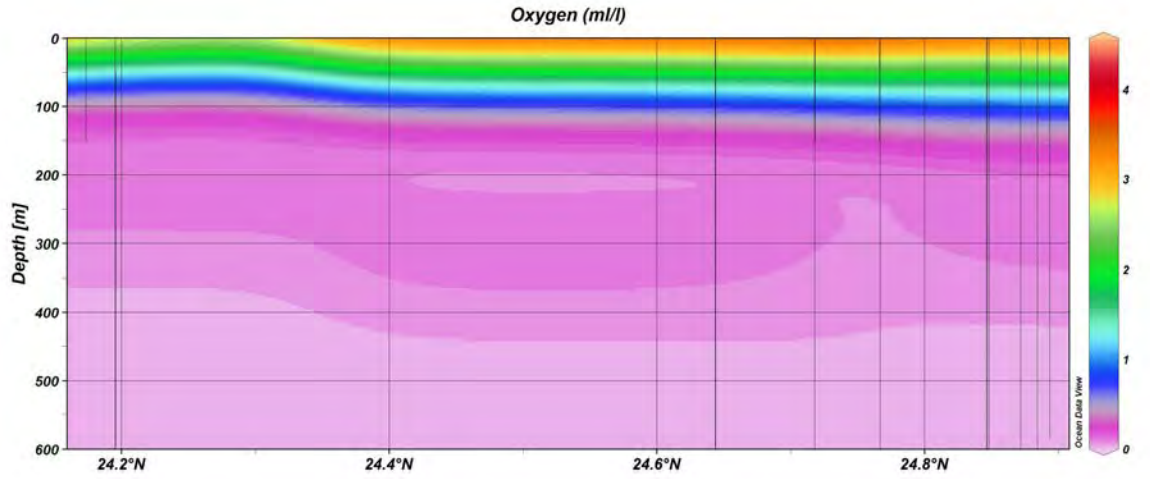

Fig. 105: Oxygen concentrations (ml/l) of the upper 600m compiled from all stations listed in Appendix 2.

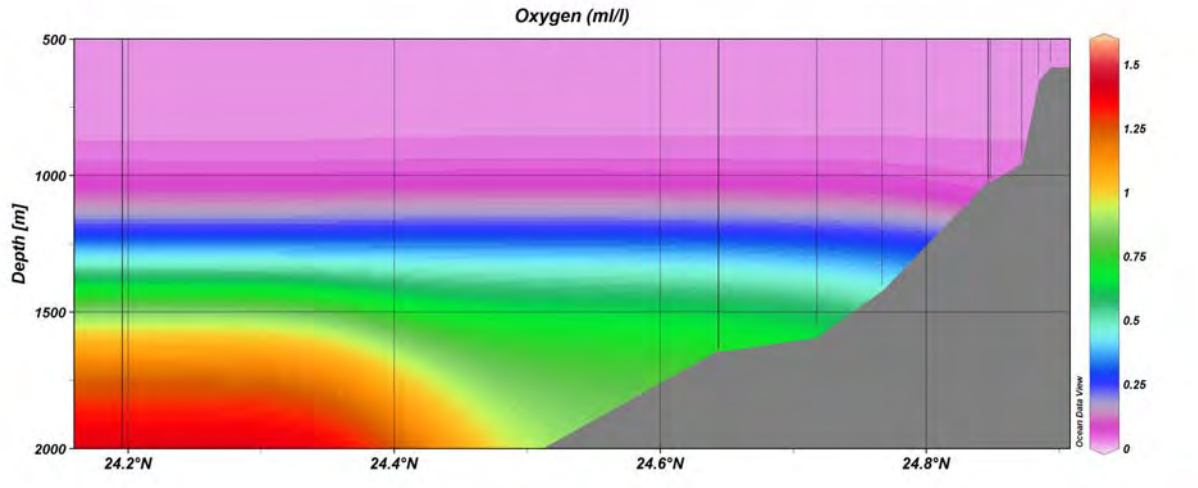

Fig. 106: Oxygen concentrations (ml/l) between 500m and 2000m water depth, compiled from all stations listed in Appendix 2.

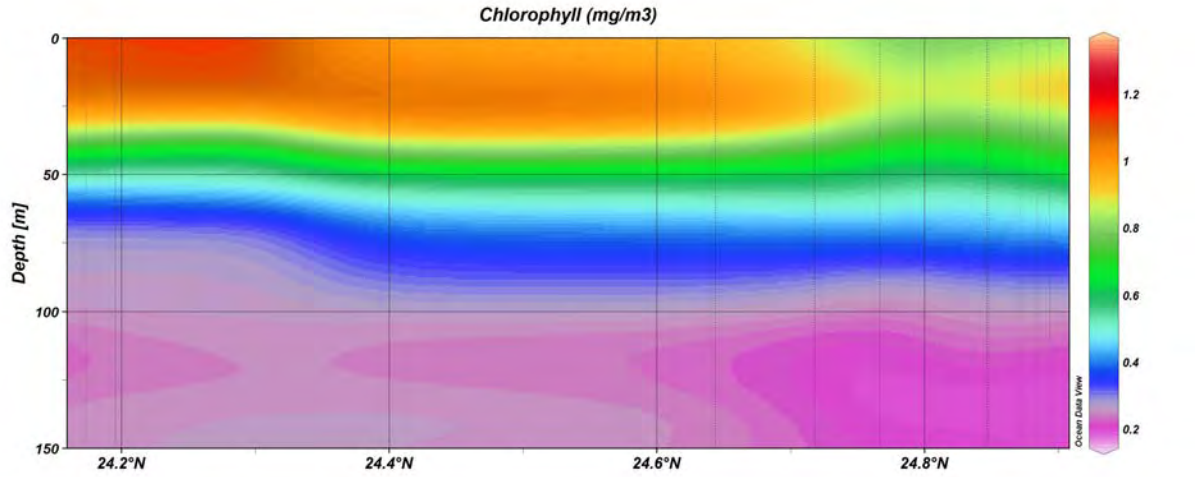

Fig. 107: Chlorophyll-a concentrations (mg/m3) in the upper 150 m of the water column compiled from all stations listed in Appendix 2.

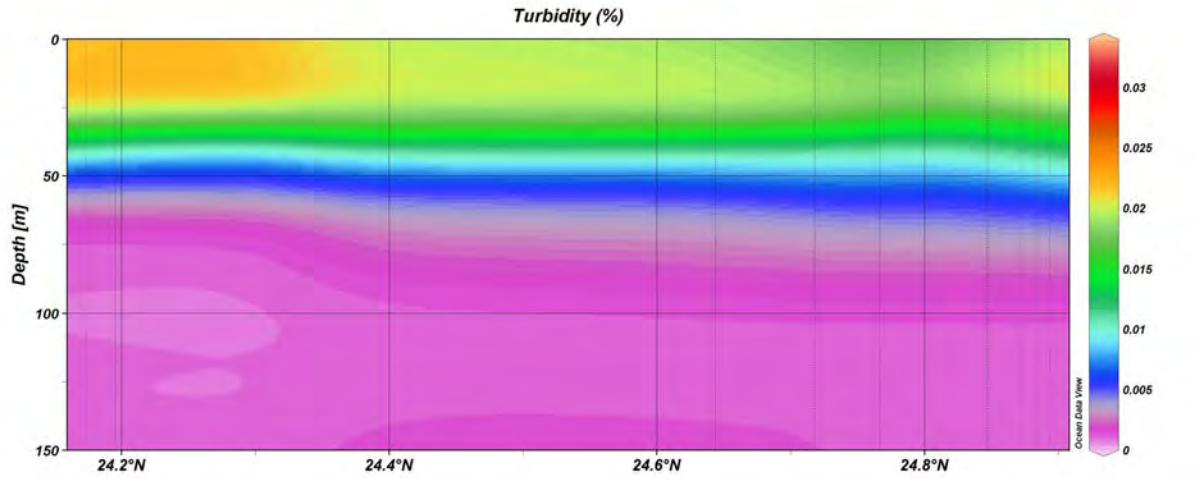

Fig. 108: Turbidity (%) in the upper 150 m of the water column compiled from all stations listed in Appendix 2.

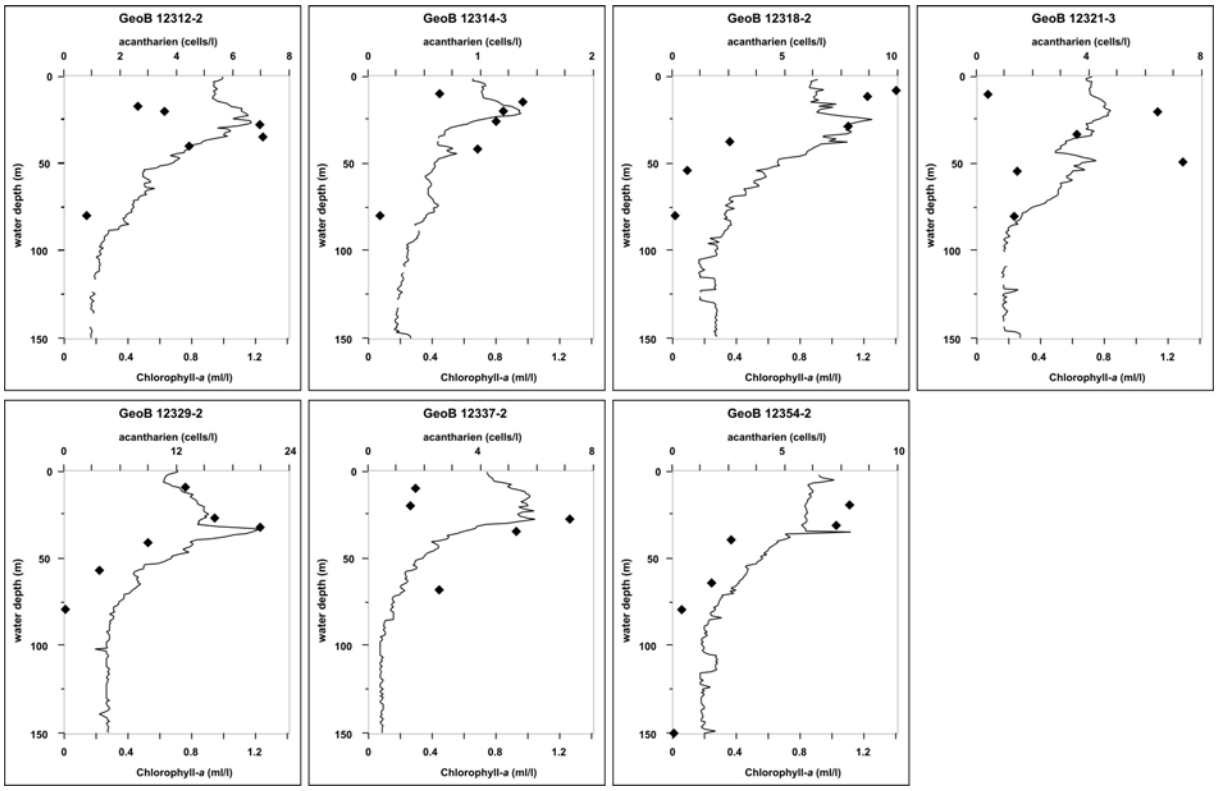

Fig. 109: Acantharien per liter water (diamonds) and chlorophyll-a concentrations in the upper 150 m of the water column.

The abundance of living acantharien per liter sea water reflects the chlorophyll-a concentration in the upper water masses (Fig. 109). However, although this holds for the individual sites, no significant relationship between the abundance of cells in the water column and chlorophyll-a concentrations can be found when data of all stations are combined.

9 Geological Sampling and Sedimentology

9.1 Geological Sampling Equipment

(A. Bahr, S.A. Klapp, S. Kasten)

One of the major objectives during R/V METEOR Cruise M74/3 has been the recovery of geological samples. Depending on the sampling target different coring devices have been used, i.e. a gravity corer with up to 6 m length (Appendix 3) and a shorter multicorer (Appendix 4) with a maximum core length of 50 cm.

Gravity cores (GC) were either deployed with a 6 m or a 3.5 m-core barrel, both with an outer diameter of 14 cm and an inner diameter of 13.2 cm. The coring was conducted either with a PVC liner or with a soft plastic hose inside, which has been used if gas hydrates were the target of the sampling site, since the soft hose allows the fast sampling of the hydrates, minimizing their dissociation during recovery. On R/V METEOR, winch W 11 was used for the deployment of the gravity corer. The winch speed was commonly set to 1.0 m/s to slack and 1.3 m/s to heave the GC in the water column, heaving out of the sediment was done with 0.2 to 0.5 m/s. The head was equipped with approximately 1155 kg of lead.

The **multicorer (MUC)** was used to sample undisturbed surface sediments. The MUC is equipped with a head for the deployment of 8 liners with a diameter of 10 cm and 4 liners with diameters of 6 cm, all of them with a length of 50 cm. For the deployment again R/V METEOR's winch W 11 was used. The slacking was set to 0.7 m/s and lifting speed was set to 1.0 m/s; depending on the sediment, the coring speed varied from 0.3 m/s to 0.7 m/s.

To achieve an optimal sampling precision, GC and MUC stations were run with the POSIDONIA (USBL) underwater navigation system when flare and gas hydrate sites were the target.

9.2 Sedimentological Description

(A. Bahr, J. Rethemeyer)

The appearance of sediments of the Makran Margin area is strongly affected by their location, i.e. whether they were situated within the oxygen minimum zone or were subjected to hydrocarbon seepage. Since bioturbation is severely limited or absent at water depths with minimum oxygen content (ca. 350 to 1150 m water depth, see CTD results) a sub-mm scale lamination of dark and lighter lamina could be preserved for Holocene sediments. Von Rad et al. (1999) proposed that the organic-rich lamina were deposited during the SW monsoon (June-August) when upwelling enhances phytoplankton productivity, while the lighter coloured lamina are dominated by terrigeneous (fluvial and aeolian) material representing the winter monsoon period with low primary productivity. This type of finely laminated sediments is well-documented in cores from stations between 957 – 592 m water depth (see MUC-3,-4, GC-31 in Fig. 110). Otherwise oxygen contents are high enough to promote (endo)benthic life and bioturbation has led to an homogenisation of the sediments (as in GC-26, MUC-1 and -6 in Fig. 110). The sediments are commonly clayey to silty clayey, with

occasional turbidite deposits showing higher sand contents. A particular feature observed in cores from the oxygen minimum zone (OMZ) are light grey layers within the finely laminated sediments. The origin of these layers has been debated, von Rad et al. (1999) suggested that they represent events of sediment plunging while Staubwasser and Sirocko (2001) proposed based on Nd and Pb isotope analysis that these layers are made of mud volcanic sediments, deposited when a newly build mud volcano on the shelf is eroded and the sediment is distributed over the shelf and slope.

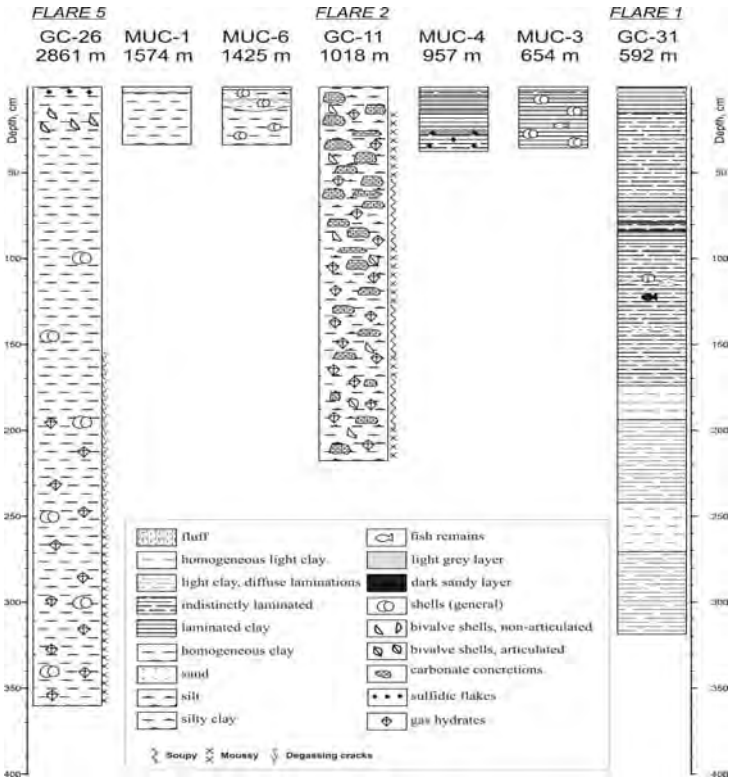

Fig. 110: Slope transect with representative core profiles from different water depths.

A comparison of the laminations in the MUCs GeoB 12312-3 (654 m water depth) and GeoB 12309-4 (957 m water depth) shows similarities in the pattern of the laminations (Fig. 111). However, GeoB 12309-4 is less distinctly laminated and exhibits some patchy light intervals, which might represent periods, when the oxygen deficit has not been as pronounced in that depth as today, promoting bioturbation. Considering that the oxygen depletion is highest in water depths between ca. 350 and 750 m, the less well developed laminations in the core from 957 m water depth seems to reflect the less ideal preservation conditions for sediment-microstructures in that depth. Based on the visual comparison of both cores, the sedimentation rates seem to be quite uniform on the middle slope. Following the suggestion that the light/dark lamina couplets are varves (von Rad et al.1999) and thus represent one year each, visual layer counting based on the photos taken gives an approximate sedimentation rate of 100 cm/kyr (without subtracting event deposits), which is most likely an overestimation since badly developed laminae might be overlooked without the aid of microscopy and radiographic imaging.

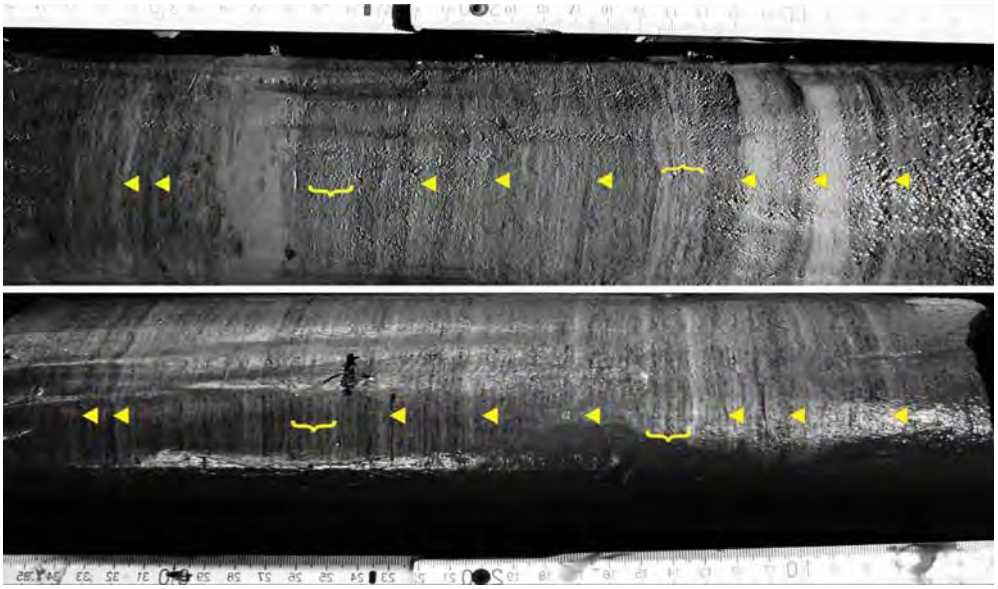

Fig. 111: Contrast-enhanced photographs of GeoB 12309-4 (left) and GeoB 12312-3 (right), showing similar sedimentation patterns (triangles, bracket).

Gas hydrate-bearing sediment cores are characterized by a destruction of any primary structure due to gas hydrate formation and dissociation forming sediment structures called descriptively “moussy” (Photo) or “soupy” (Fig. 112). Accordingly these structures were observed in cores where clathrates were present. Usually hydrate occurrence is restricted to the lower parts of the cores, although in some cases hydrates were found only a few cm below the core top (GeoB 12316-3 and 12316-4). Interestingly, there seems to be a correlation of grain size to hydrate occurrence, as observed in e.g. GC-26 (Fig. 110) where hydrates were only observed in sediments (clay to silty clay) containing noticable amounts of sand-sized biogenic components (particularly foraminifera). Due to the general small grain size (clay to silty clay) hydrates are either finely dispersed or form chips and tabular structures that follow certain sediment structures (e.g., turbidites or sediment laminae) and/or features like gas cracks and faults. In GeoB 12316-3 hydrates with bubble fabric were observed indicating that free gas was present within the sediment initiating hydrate growth.

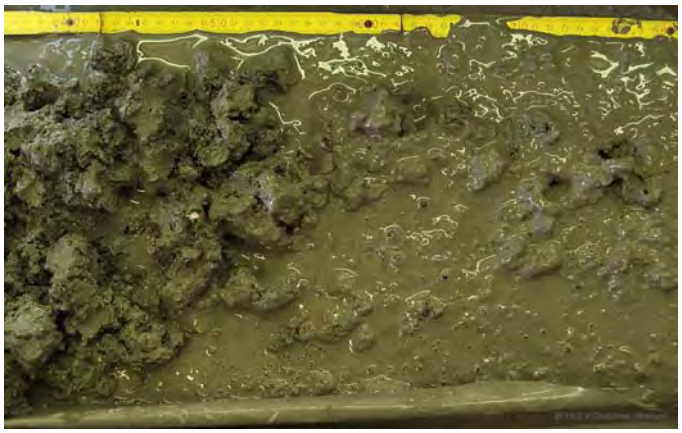

Fig. 112 Typical moussy (left part) and soupy (right) sediment structures in GeoB 12316-3, a result of the presence of gas hydrates.

Carbonates were only cored in samples from Flare 2 (Fig. 110), where gravity coring has been severely hampered by the high abundance of carbonate pieces. A more detailed description of the authigenic carbonates will be presented in the following Chapter.

9.3 Carbonates

(F. Brinkmann, A. Bahr)

Further distinctive geological features occurring within sediments at the Makran Accretionary Ridge are authigenic carbonates. They form due to an increase in alkalinity caused by microbial oxidation of CH_4 (Boetius et al., 2000). The methane is oxidized via anaerobic oxidation of methane (AOM) by a consortium of sulphate-reducing bacteria and methane-oxidizing archaea. The produced bicarbonate leads to precipitation of carbonate minerals, which consequently act as a sink for methane leaving the sea floor subsurface. Often high amounts are utilised before the methane can leave the sea floor and reach the atmosphere (Hinrichs and Boetius, 2000).

Hence, authigenic carbonate precipitates, also called seep carbonates, influence the global carbon budget and reveal an excellent archive of the biogeochemical processes that led to their formation. They have been documented during the last two decades both as modern occurrences and ancient sites going back in earth´s history up to the Devonian. Modern occurrences comprise locations in the North Sea (Hovland et al., 1987), the Black Sea (Peckmann et al., 2001), the Mediterranean (Aloisi et al., 2000), and at Hydrate Ridge (Bohrmann et al., 1998), Congo deep-sea fan (Pierre and Fouquet, 2007). A good review of the geographical distribution of known occurrences of ancient seep sites was prepared by Campbell (2006). Peckmann and Thiel (2004) reviewed the knowledge about biogeochemical processes within seep-influenced environments. Authigenic carbonates at the Makran accretionary Ridge have been reported once before, by von Rad et al. (1996).

Fig. 113: Recovery of a carbonate sample from an extensive active mytilid field at Flare 11 by means of the manipulator arm of the ROV QUEST. (GeoB 12348-1, left); Carbonate crust recovered from Flare 7 covered with a faunal assembling of mytilids, sponges, and many “Entenmuscheln”. (GeoB 12338-13, right).

During this cruise carbonate samples were recovered in different ways, i.e. by means of gravity corers, with push cores taken with the ROV QUEST, and predominantly with the

manipulator arm of QUEST, which was by far the most precise and effective way to obtain samples. Altogether 48 individual carbonate samples were recovered (Appendix 5), most of which are rather small. Only a few big pieces of the crusts and chimneys were retrieved.

Fig. 114: Sub-recent carbonate crust exposed to the sea water at Flare 11. (GeoB 12348-1, left); Sub-recent carbonate sample recovered from Flare 11. (GeoB 12348-1, right).

Seep carbonates principally occurred as small nodules and pieces within the upper sediment layers (mainly underneath areas covered with bacterial mats), as crusts densely covered by mytilids (mytilid shells are also incorporated in the crusts), as likely sub-recent, rather extensive crusts which seem to be exposed due to erosion (occasionally as fractional slabs), and within the OMZ as small dome-like structures.

Authigenic carbonates were most abundant at seep sites in a water depth between about 1500 and 1800 m. At Flare 11 (1460 m), Flare 3 (1500 m), Flare 7 (1650 m), and Flare 6 (1820 m) the carbonates occurred as crusts and fractional slabs that were mainly associated with mytilid bivalves (Fig. 113 left), of which the shells are often found to be incorporated into the carbonates. The crusts vary in thickness, ranging from several centimetres to a few decimetres. Samples of these rather extensive and massive crusts could be grabbed by means of the ROV QUEST quite easily. Most samples have a size similar to a small loaf of bread (Fig. 113 right). At other places sub-recent crusts are exposed due to erosion (Figs. 114).

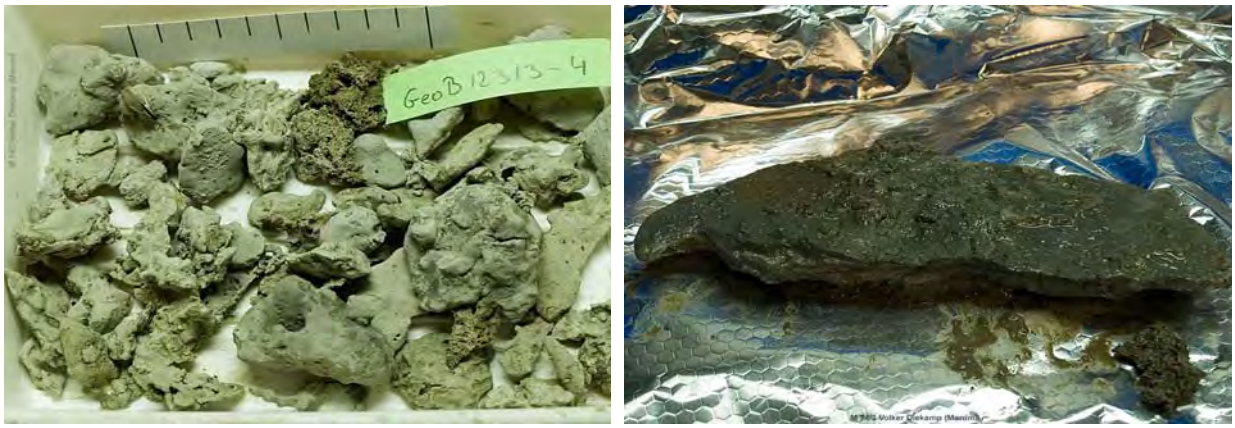

Fig. 115: Small carbonate pieces that were recovered from an area that was dominated by very small tube worms and bacterial mats. They were recovered by means of the bubble catcher, which was sometimes used to recovered sediment samples (GeoB 12313-4, Flare 2, left); Thin plate of the first carbonate grabbed by means of the manipulator arm of the ROV QUEST. Texture is very homogenous and surface rather smooth. Scale bar 5 cm. (GeoB 12315, Flare 2, right).

Carbonates did not occur at the deeper seeps that were investigated. Even though sites of active gas (Flare 5, nascent ridge, 2870 m) and active fluid seepage (Flare 4, 2000 m) were found, no indications for carbonates were discovered at this depth.

At Flare 2, which is situated at the lower border of the Oxygen Minimum Zone (OMZ), in a depth of about 1025 metres, carbonates were found directly underneath bacterial mats (recovered with push cores), mainly occurring as small nodules and aggregates (Fig. 115 left). Only one piece of carbonate, a thin (about 1 cm), rather dense, smooth, and homogenous plate, could be grabbed by means of the ROV (Fig. 115 right). In two gravity cores rather thick and cavernous crusts were found (Fig. 116 left). In two other ones, in contrast, smaller carbonate pieces were found throughout the whole cores, up to a depth of 120 cm (Fig. 116 right).

Fig. 116: Cavernous black carbonate crusts found on top of a gravity core at Flare 2 (GeoB 12314-1, left); Small carbonate pieces found in 53 to 56 cm within a gravity core from Flare 2 (GeoB 12316-2, right).

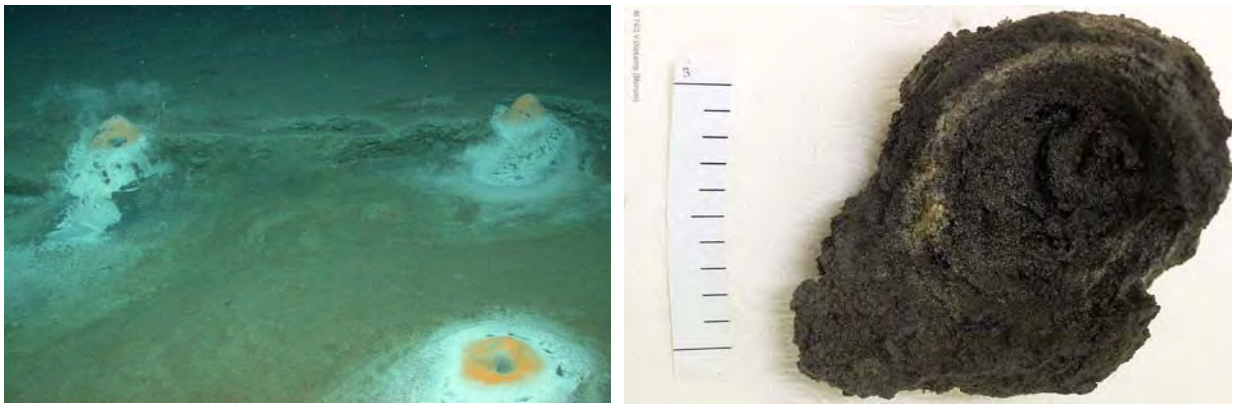

Fig. 117: Small “fried egg” bacterial patches at Flare 15. The positive relief of the orange part is caused by a dome-like precipitate. The structure on the top right was sampled as ”precipitate dome #3” (GeoB 12353-9, left); Cap of ”precipitate dome #1”. View from the bottom, ergo from the inside of the dome. The precipitate is rather organic rich, showing distinctive layers with an organic content (GeoB 12353-7, Flare 15, right).

In the shallower OMZ waters comprising depths of 575 (Flare 1) and 730 metres (Flare 15) the bacterial patches were dominated by two concentric zones. A yellow centre part and an outer white rim, which made us call them “fried egg” patches. Whereby no carbonates were discovered at Flare 1, the centre parts of many patches at Flare 15 showed a positive relief which turned out to be formed by mineral precipitates (Fig. 117 left). These domes seem to be

formed as subsequent layers of carbonate precipitates. Every layer likely represents one microbial generation overlain by a younger one (Fig. 117 right). There is no conduit within these structures. Consequently the term “chimney” does not fit. The structures are more or less towers of thin, dome-like, convex carbonate layers. Besides 4 smaller domes that were covered with the bacterial mats, a big “tower” (Figs. 118) was found as a singular feature surrounded by normal sea floor sediments. The smaller domes showed a rather blackish colour indicating occurrence of iron sulphide minerals. Compared to the big structure, which is quite strongly lithified, the small domes are very fragile and seem to have a much higher content of organic matter. The big “tower” was, as directed by destiny, found in the very last minute of the last ROV dive, and could be recovered just in time. Its strong lithification could already be guessed, as the structure was rather hard to break (with the manipulator arm of QUEST).

Fig. 118: A “tower-like” precipitate on the sea floor at Flare 15. It is about 50 cm high and was very hard to break and recover (GeoB 12353-11, left); The carbonate tower from Flare 15 is dominated by dome-like convex thin mineral layers. Many generations of precipitates formed a structure of 50 cm in height (GeoB 12353-11, right).

9.4 Gas Hydrates

(S. A. Klapp, G. Bohrmann, T. Pape, A. Bahr)

At cold seeps in a few hundred meters of water depth or deeper, gas might precipitate as gas hydrate as a part of seepage process. Gas hydrates are ice-like solids that are made of crystals formed by rigid cages of water molecules, each of which hosts a gas molecule. The cage structure, which leads to the formation of gas hydrates, forms only under limited conditions, e.g. elevated pressure, that occurs at some hundred meters of water depth, and low temperatures as in deep waters. At low pressure and warm temperature, gas hydrates dissolve. Because both gas seepage as well as all of these physical conditions are realized at the Makran accretionary wedge, the Makran area is an ideal place to study gas hydrates.

Depending on the gas molecules, which flocculate with water to gas hydrate, different cages and subsequently, different structures will form (Sloan and Koh 2007). Three gas hydrate structures are known to occur in nature, structures I and II (sI and sII) have been known since a while whereas the third structure H has been found very recently in nature (Lu et al. 2007). All of these structures have different stabilities. Methane is considered to account

for most gas hydrate occurrences on earth (Kvenvolden 1995) and is also the major sI gas hydrate former (von Stackelberg 1954).

Unlike vivid gas seepage, where gas escapes into the open water column, gas hydrate binds gas for some time by incorporating it into its cage. Because of the crystal structure of hydrates, where the cages are positioned in a three-dimensional lattice, under atmospheric conditions many more gas molecules are stored within a given volume than there would be in case of free gas. Hence, the gas composition of a piece of hydrate might give a more realistic idea of the chemistry of seeping gases than a gas sample that was taken within a short time. On the other hand, not all gases can be incorporated into the gas hydrate structure (Sloan and Koh 2007).

Because gas hydrates do not precipitate like sediments onto the sea floor, they are not strata-bound and thus are not necessarily parallel to the bedding (Bohrmann and Torres, 2006). Instead, they flocculate along gas escaping routes in the sediment (Abegg et al., 2007). Subsequently, their macrostructure (shape), texture, microstructure and orientation should mirror gas migration ways. For the Makran accretionary wedge, the gas seeping routs in the subsurface might be inferred from the orientation of gas hydrates.

Many pieces of gas hydrate were sampled during the Meteor Cruise M74/3. All of the hydrates which are brought home for further analysis in the lab were sampled at two seep locations, which are spatially remote from one another: 3 gravity cores were retrieved in northern part of the working area at Flare 2 in about 1000 m water depth, and 2 gravity cores were gained from Flare 5 on the Nascent Ridge in the southern part of the working area in 2900 m water depth. More hydrate containing cores were analyzed on board regarding sedimentological questions. For the coring, a gravity corer was used with either a 6 m or 3 m long core barrel. During coring, inside a core barrel was a soft plastic hose, not a PVC liner that was used for most other coring purposes. The plastic hose can easily be pulled out of the barrel at the end of the core catcher and is easily opened with a knife. Consequently, gas hydrates can be quickly recovered from the core and are swiftly carried into liquid nitrogen (-196 °C), where they are safe from dissociation.

Table 24 gives an overview of the hydrate recovering stations on M74/3.

Table 24: Stations of gas hydrate recovery on M74/3.

St. No.	GC No.	Location	Date	Time	Latitude	Longitude	Water	Recovery
GeoB				(UTC)	N°	E°	depth (m)	Remarks
12303	GC-1	Nascent Ridge	02.11.07	17:00	24°11.749	62°44.309	2860	recovery 4,34 m
12341	GC-23	Nascent Ridge	17.11.07	20:37	24°11.746	62°44.308	2861	recovery 3,60 m
12316-2	GC 9	Flare 2	07.11.07	02:42	24°50.798	63°01.416	1021	recovery 1,03 m
12316-3	GC-11	Flare 2	08.11.07	10:49	24°50.789	63°01.422	1020	recovery 2,18 m
12316-4	GC-12	Flare 2	08.11.08	12:39	24°50.788	63°01.424	1019	recovery 1,63 m
12342-2	GC-25	Flare 2	18.11.07	04:35	24°50.799	63°01.420	1018	recovery ca. 40 cm

Methane is the most common gas that was found at cold seeps during the expedition M74/3 (see Chapter 10.2 – gas analyses) with C1/C2+ proportions of 99 % C1 or more; higher short-chain hydrocarbon homologs C2+ only play a minor role. Accordingly, it is likely that most of the hydrates which were recovered during the cruise are methane hydrates

and thus form sI hydrate. Fig. 119 shows the stability curve for methane hydrate in blue. Also, other stability curves are given here, which all contain methane as the major fraction. However, slight fractions of other light, sI hydrate forming gases are incorporated in the model. For the modeling it is assumed that there are 2 wt.-% of H_2S in the hydrates, because on board Meteor, we could not measure the precise amount of H_2S that is stored in the hydrates. In addition, the stability of hydrates containing 2 wt.-% of CO_2 and of C_2H_6 is modeled. It is likely that the hydrates at Makran contain these gases. The arbitrary amount of 2 wt.-% is chosen in order to calculate with small figures, but significantly enough to obtain a good idea what the trend would be if the compounds were indeed in the hydrates' cages.

Fig. 119 depicts a stability diagram with the gas compounds explained above, that was calculated for the Makran accretionary wedge. The temperature curves as well as the salinity data, which were considered in the model, are from CTD-data obtained during the cruise (see Chapter 8).

The stability diagram in Fig. 119 shows that for pure methane as feeding gas, gas hydrate sI can be expected from 850 m of water depth downwards. If there are 2 wt.-% of C_2H_6 in the feeding gas, the stability does not change much.

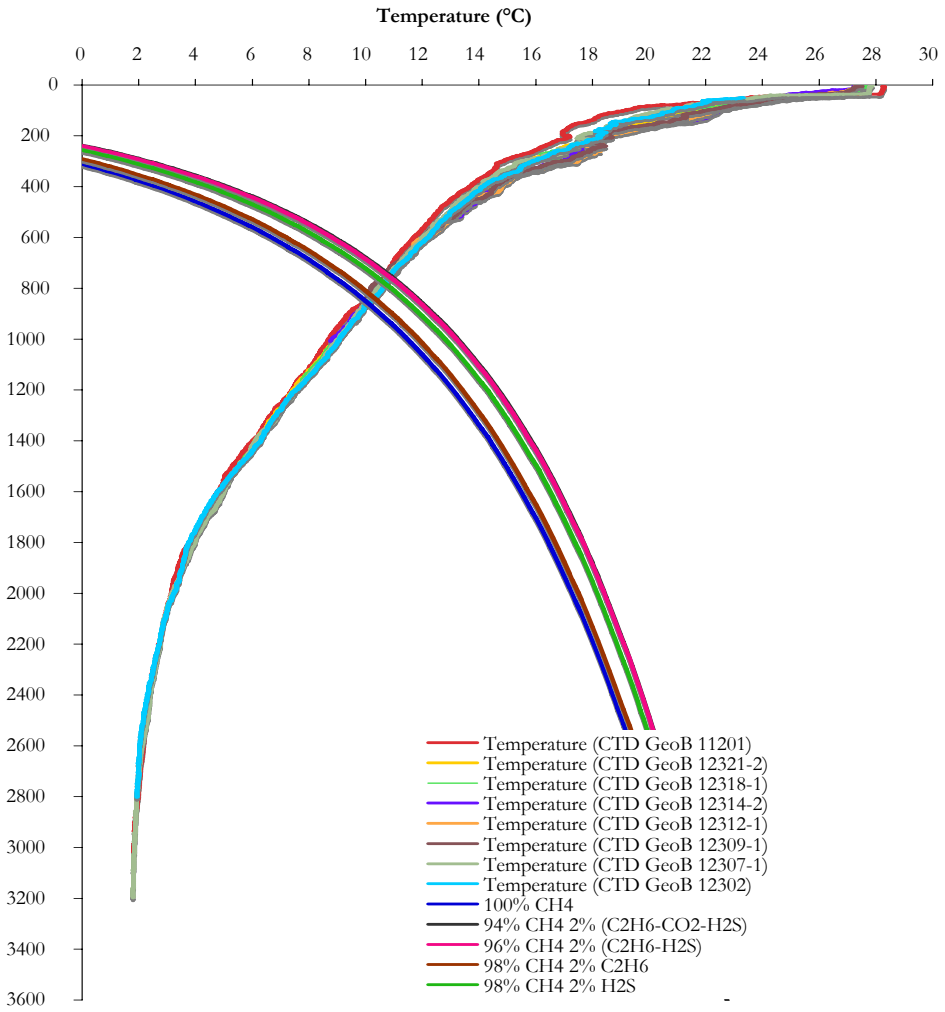

Fig. 119: Stability diagram of gas hydrates and water temperatures at different stations along the Makran accretionary wedge using the calculation software of the Heriot-Watt University, Edinburgh.

Adding H_2S affects the stability significantly: A mixture of 2 wt.-% of C_2H_6, 2 wt.-% of H_2S and 96 wt.-% of CH_4 is stable from about 750 m depth. If there are additionally 2 wt.-% CO_2 present on the expense of methane or, for a third model, if there is only methane and H_2S does not matter much. Those stability curves are quite close.

It is likely that the figures of the minor compounds in the calculations are exaggerated and that there is even more methane present, as evidenced by gas chemistry analyses. This would suggest stability closer to pure methane at about 850 m water depth than shallower. However, H_2S results could not be obtained onboard METEOR.

Gas hydrates occur at different sediment depths at the two Flare sites, where hydrates were sampled (see Chapter 9.2 – core description). At Flare 2 (1000 m water depth), hydrates can be found from 10-12 cm below the sea floor down to the base of the cores. Hydrates from Flare 5 on Nascent Ridge occur below 1.5 m below the sea floor.

Fig. 120: soupy sediments from dissociating gas hydrate (left); platy gas hydrate pieces perpendicular to the bedding (right).

Fig. 121: tube-like gas hydrate (left); bubble fabric of gas hydrate (right).

Pieces of gas hydrate were retrieved from the cores in different sizes and shapes. The soupy, water-stained texture of core segments points to the dissociation of disseminated hydrates, e.g. very small hydrates in the pore space (Fig. 120). Larger pieces of hydrate, which were saved in liquid nitrogen, normally have an irregular shape. There are at least hydrates in two different shapes: platy, chip-like hydrates have about the size of a coin, i.e. 1-3 centimeters in diameter and a few millimeters of thickness. They are oriented along cracks in the sediment, which are (sub-) vertical (Fig. 120). Elongated hydrates mimic the shapes of tubes (Fig. 121), they are thicker than the platy ones. Tube-like hydrates have several cm in

length and 1-2 cm in diameter. As the platy hydrates, they are oriented (sub-) vertically to the bedding.

Some of the retrieved hydrates have a pronounced bubble fabric (Fig. 121). This fabric probably indicates the presence of free gas bubbles within the gas hydrate matrix. It suggests the presence of much gas during hydrate formation, which only partly was incorporated into the hydrate structure. The reasons for that could be manifold: Gases, which cannot form gas hydrate might build a bubble fabric. Alternatively, the fabric could indicate very strong gas seepage, where individual gas bubbles are clad by a hydrate matrix.

The shape of the tube-like hydrates can point to gas ascend paths, where gas hydrates precipitate from the gas phase and water. Accordingly, the hydrates would reflect the orientation of the gas flow ways in the subsurface. The platy hydrates might flocculate along the walls of cracks which work for gas migration. In how far these observations indicate gas flux remains open.

10 Pore Water and Gas Chemistry

10.1 Pore Water Chemistry

(S. Kasten, K. Enneking, D. Fischer, A. Gassner, K. Zonneveld)

The focus of geochemical investigations carried out during this cruise in the frame of RCOM project E1 was a detailed examination of the geochemical processes occurring at seep sites of the Northern Arabian Sea off Makran. Due to the unique setting of these seeps within a pronounced oxygen minimum zone we aimed at determining how the oxygen levels of the bottom water affect (bio)geochemical processes within the seep sediments and control the colonization with various chemosynthetic communities. In particular, we were seeking to determine the efficiency of methane consumption by anaerobic oxidation of methane in the various seep types/habitats and to quantify the fluxes of gases and dissolved pore water constituents across the sediment/water interface – particularly focussing on the cycling of carbon, sulfur and iron. These studies will also involve studying the processes of mineral formation and dissolution in these hydrocarbon-seepage influenced sites and – together with the geology as well as the organic geochemistry group – determine the potential of diagnostic mineral precipitates to reconstruct hydrocarbon seepage in older geologic sequences.

Besides the seep-related investigations we also aimed at studying early diagenetic processes in dependence on bottom water oxygen concentrations by working on gravity and multicorer cores along a depth transect across the continental slope. In close cooperation with the working groups of micropaleontology (K. Zonneveld) as well as organic geochemistry and biogeochemistry (J. Rethemeyer, M. Yoshinaga, P. Rossel) five stations were investigated on a depth transect along the oxygen minimum zone stretching from oxygen depleted conditions 650 m in the North down to the well oxygenated bottom water environment on Nascent Ridge in the south at 2850 m water depth. The aim of these investigations is to determine the processes and rates of degradation of various organic compounds in dependence on oxygen levels in the water column.

For an accurate estimation of the marine carbon sink and for correct interpretation of the fossil record, assessment of the character and influence of selective preservation on the original signal is essential. Furthermore, information is required on how selective degradation might influence and/or overprint the initial signal of OM based proxies and how such “overprint” might be recognised in fossil sediments.

Although it has already been a long known fact that high degradation rates of OM are found in oxygenated deposition environments the detailed relationship between oxygen concentration within the sediment and degradation rates of individual OM components is not known. To increase this knowledge detailed information about the oxygen concentration in the upper few centimetres of the sediment will be compared to variability in the organic matter content, notably the organic walled microfossils (organic-walled dinoflagellate cysts, pollen/spores) and organic geochemical proxies such a TEX86 and Uk37.

Pore water sampling

To prevent a warming of the sediments on board all samples (gravity, multicorer and push cores) were rapidly transferred into the cooling room (4°C) and immediately processed after recovery. Pore water was extracted by means of rhizon samplers (pore size 0.1 µm) or within a glove box under argon atmosphere using Teflon squeezers operated with argon at a pressure of up to 5 bar. At each site two multicorer and push cores were taken for pore water extraction and solid-phase sampling. For the multicorer and push cores two samples of the supernatant bottom water were taken and filtered for subsequent analyses. The remaining bottom water was carefully removed from the multicorer and push core tubes by means of a siphon to avoid destruction of the sediment surface. During subsequent cutting of one of the parallel cores into slices for solid phase sampling, pH and Eh measurements were performed with a minimum depth resolution of 1 cm. At the five stations along the OMZ depth transect an additional MUC core was utilized to perform oxygen measurements with a fiber optic oxygen sensor (FIBOX3) and a micromanipulator.

Gravity cores were cut in 1 m long segments on deck and sealed with plastic caps upon recovery. For sampling, holes were cut into the plastic liner of the segments with a vibro-saw at 20 cm depth resolution and the following samples/measurements were taken/performed: (1) 3 ml syringe samples of wet sediment for methane/hydrocarbon analyses, (2) determination of pH and Eh by means of punch-in electrodes, (3) about 10 ml of wet sediment were taken and stored under argon for subsequent solid-phase analyses, and (4) pore water was retrieved by means of rhizon samplers.

Pore water analyses

Pore water analyses of the following parameters were carried out during this cruise: Eh, pH, ammonium, alkalinity, iron (Fe^{2+}) and hydrocarbons – including methane.

Ammonium was measured using a conductivity method. Alkalinity was calculated from a volumetric analysis by tritration of 1 ml of pore water with 0.01 or 0.05 M HCl, respectively. For the analyses of dissolved iron (Fe^{2+}) sub-samples of 1 ml were taken within the glove box or directly from pore water extracted by rhizons, immediately complexed with 50 µl of "Ferrospectral" and determined photometrically.

For further analyses at the Alfred Wegener Institute for Polar and Marine Research (AWI) in Bremerhaven and at the University of Bremen, aliquots of the remaining pore water samples were diluted 1:2 for phosphate, 1:10 and acidified with $HNO_{3\ (suprapure)}$ for determination of cations (Ca, Mg, Sr, K, Ba, S, Mn, Si, B, Li) by ICP-AES and AAS. Additionally, 1.5 ml subsamples of the pore water were added to a ZnAc solution (600 µl) to fix all hydrogen sulfide present as ZnS for later analysis – including sulfur isotopes. Subsamples for sulfate and chloride determinations were diluted 1:100 and stored frozen for ion chromatography (HPLC) analyses at the University of Bremen and the AWI Bremerhaven. Further aliquots of the pore water were taken and stored for concentrations and $\delta^{13}C$ of DIC and acetate.

A complete overview of sampling procedures and analytical techniques used on board and in the laboratories at the Alfred Wegener Institute and the University of Bremen is available on http://www.uni-bremen.geochemie.de.

Shipboard results - pore water chemistry

During the cruise, 7 gravity cores, 6 multicorer cores and 38 ROV push cores were sampled for pore water and solid phase (Appendix 6). In addition, 1 gravity core (GeoB 123305-1, GC-2) was taken as backup and stored away, without being sampled onboard, for onshore analyses of magnetic susceptibility and other rock magnetic parameters. In addition, samples from 2 KIPS deployments and 4 ISPS casts were taken. All sites sampled geochemically, including parameters analysed on board as well as aliquots of pore-water and solid-phase samples taken and stored for further analyses at the Alfred Wegener Institute (AWI) in Bremerhaven and at the University of Bremen are listed in the appendix.

Five stations were sampled along the oxygen minimum zone depth transect by gravity corer and multicorer – stretching from strongly oxygen-deficient conditions at 600 m water depth down to the better oxygenated site on Nascent Ridge (2850 m). The pore water concentrations of ammonium and alkalinity at the five sites display a clear depth trend with values decreasing with increasing water depth (Figs. 122-126). We attribute the decrease in the amount of these products of organic matter degradation to both increase in oxygen levels in bottom water as well as to the decrease in the input of organic matter to the sea floor with increasing water depth and distance from the more productive shallow sites.

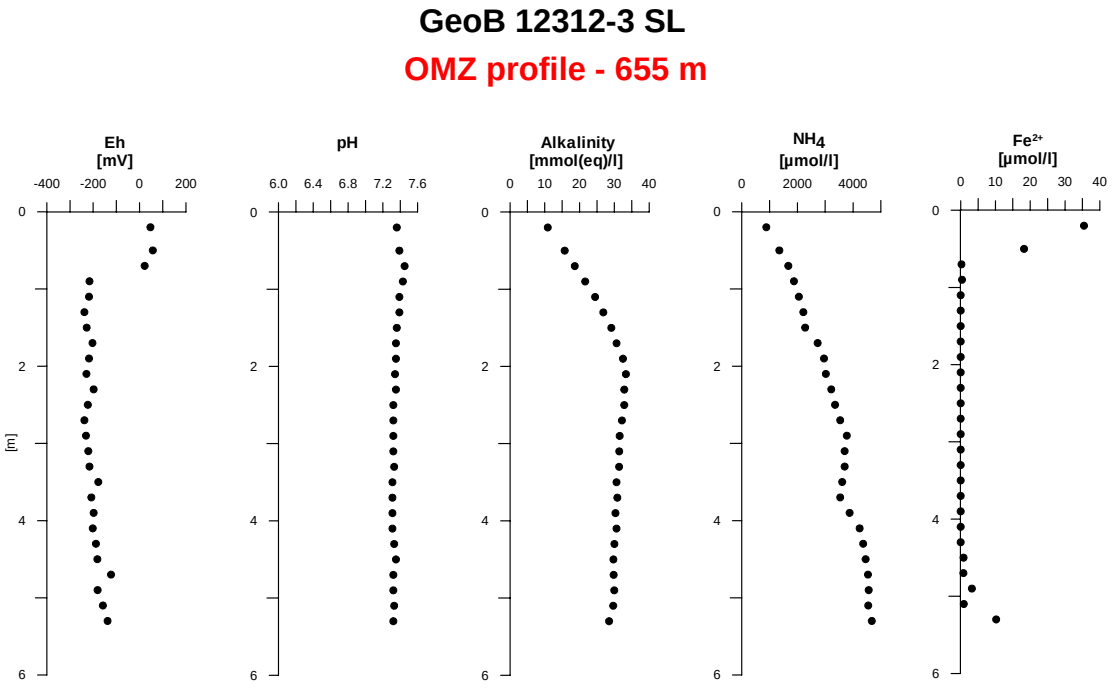

Fig. 122: Pore water concentration profiles for site GeoB 12312-3.

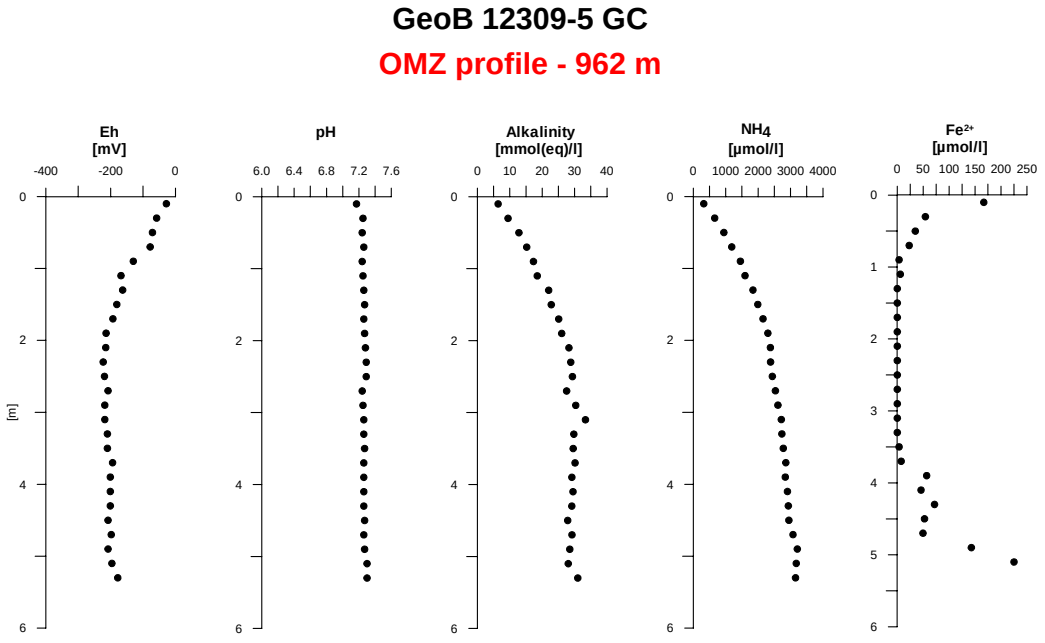

Fig. 123: Pore water concentration profiles for site GeoB 12309-5.

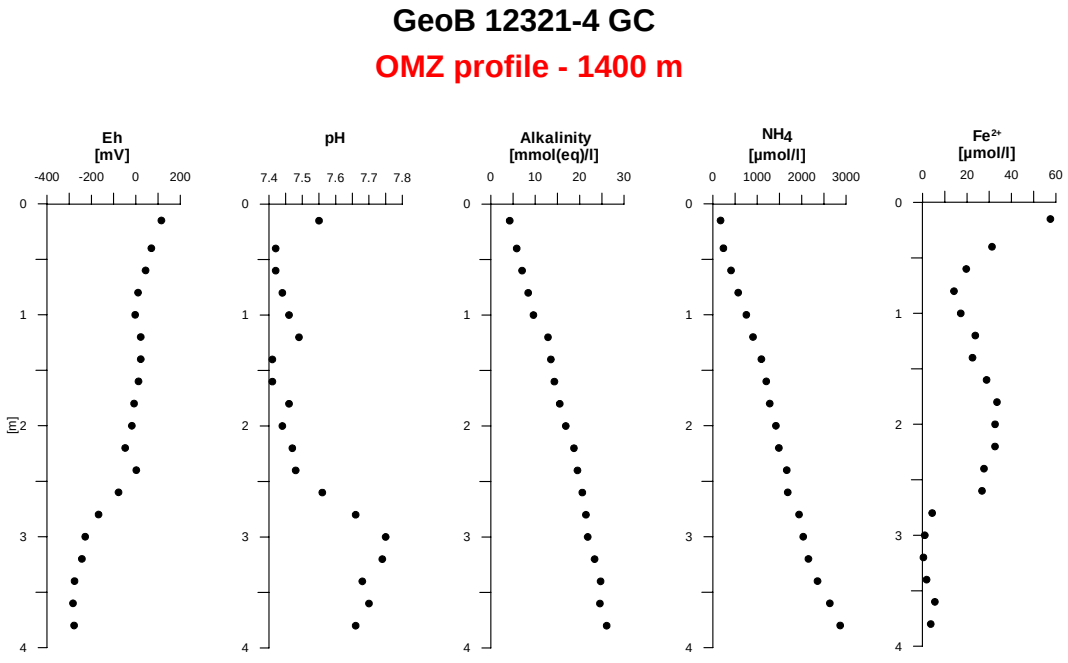

Fig. 124: Pore water concentration profiles for site GeoB 12321-4.

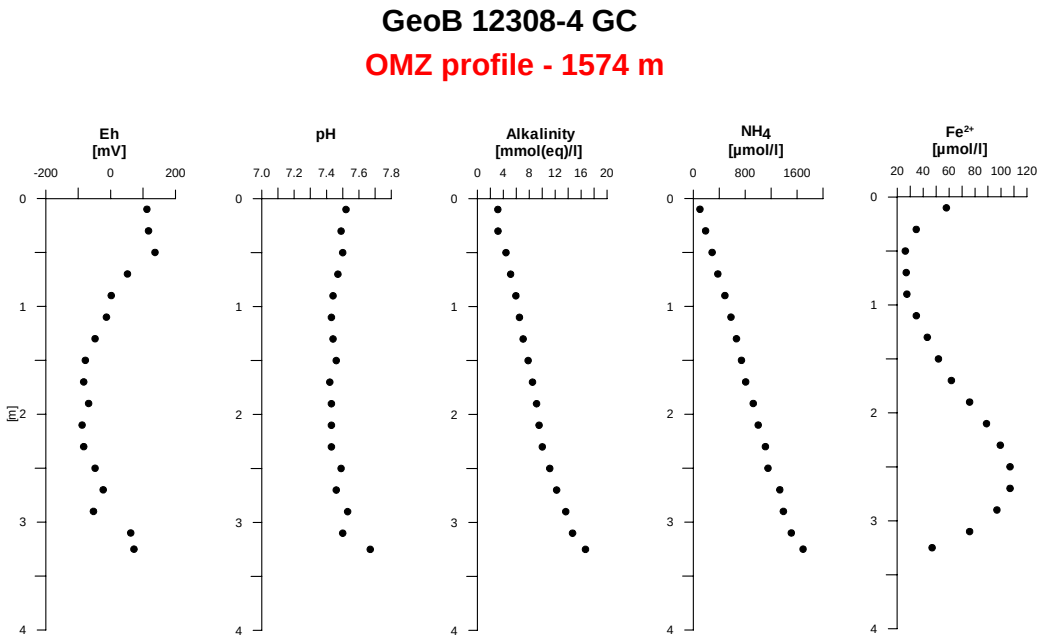

Fig. 125: Pore water concentration profiles for site GeoB 12308-4.

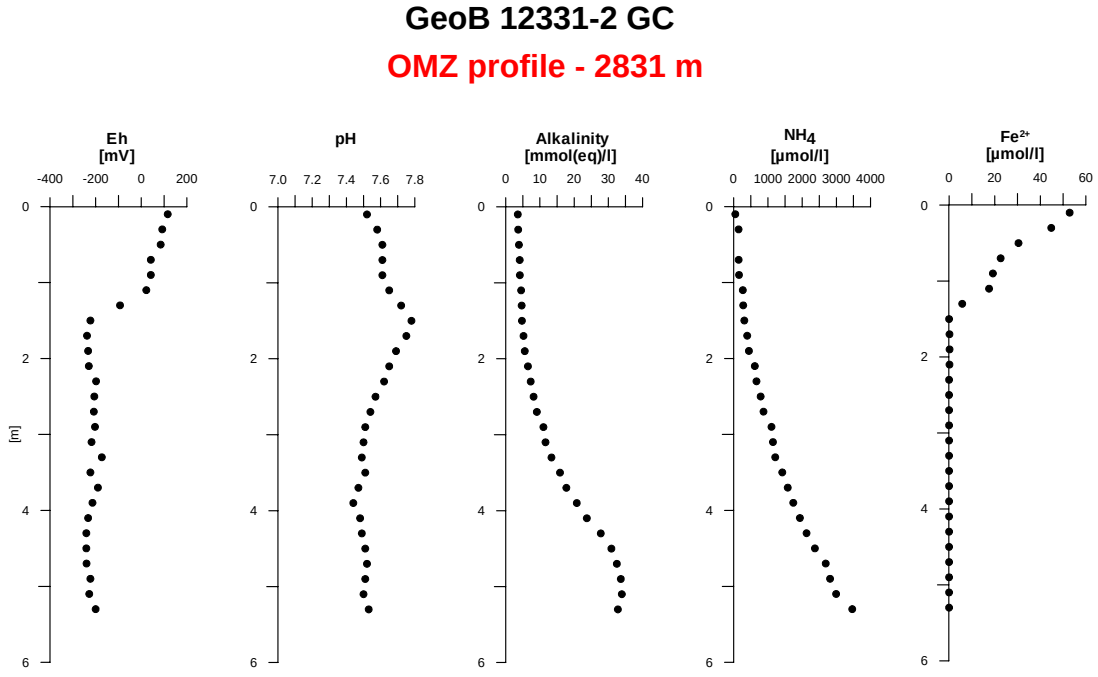

Fig. 126: Pore water concentration profiles for site GeoB 12331-2.

The oxygen penetration depth at the five sampling sites as determined ex-situ by a fiber optic sensor (Fig. 127) as well as the depth of the iron redox boundary increase with water depth owing to the increase in oxygen contents (Fig. 128).

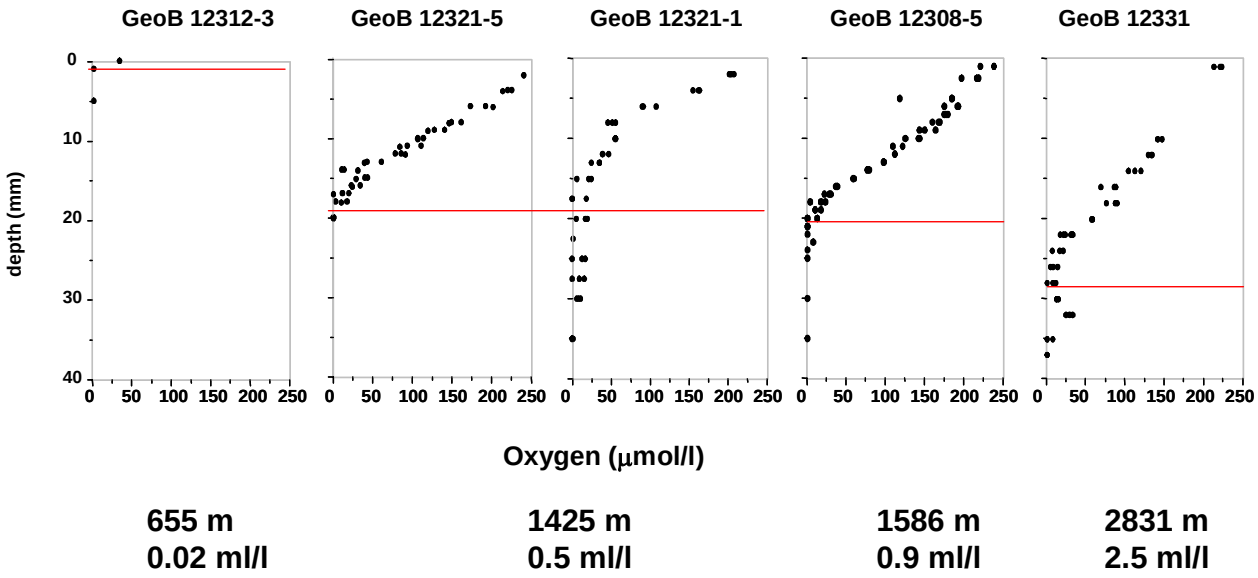

Fig. 127: Pore water oxygen concentration profiles and oxygen penetration depths at the stations sampled along the OMZ profile.

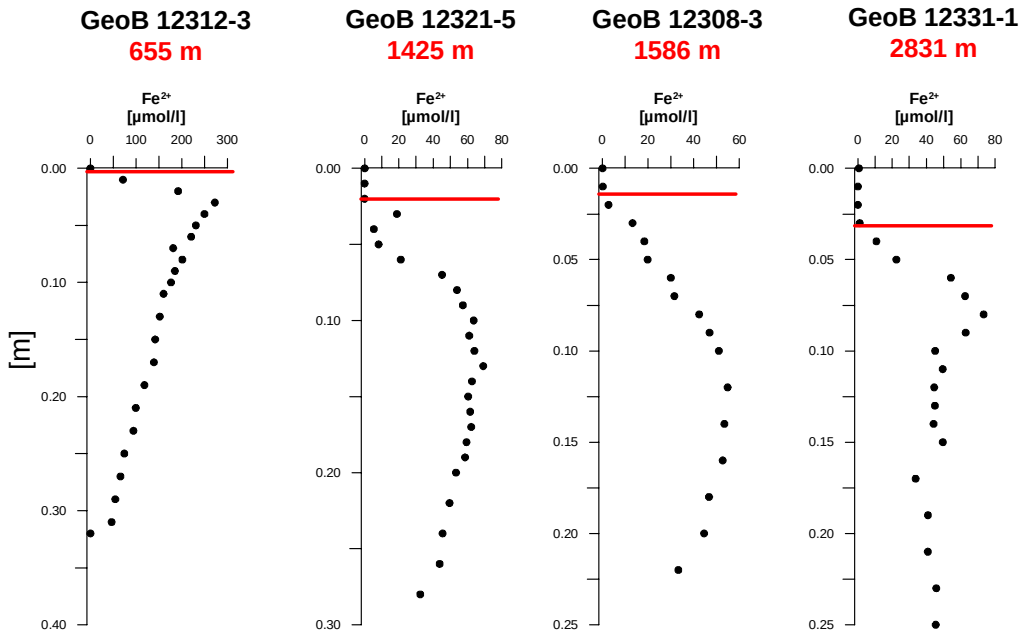

Fig. 128: Pore water iron concentrations at the stations sampled along the OMZ profile.

Surface sediment samples for geochemical investigations of seep sites were taken by ROV push cores at Flares 1, 2, 6, 15 and at Nascent Ridge (Appendix 6). Pore water geochemistry of the seep locations significantly differs from “normal” hemipelagic sediments in that the former are higher in alkalinity due to the process of anaerobic oxidation of methane and lower in ammonium concentrations. In the following we will present selected pore water data from Nascent Ridge and Flare 2 to demonstrate the typical geochemical environments found at the investigated hydrocarbon seeps.

A seep site with several linearly aligned orifices (elongated structure, “bubble curtain”) was sampled on Nascent Ridge at a water depth of 2876 m (during ROV Dive 179 – GeoB 12301-3 and GeoB 12301-5). Push cores were taken close to the bubble orifices as well as at a certain distance to the gas ebullition sites where the sediment surface was inhabited by small tube worms. This site was re-visited during ROV Dive 192 and the two most distinct habitats “close to gas seeps” (GeoB 12339-3, Fig. 129) and “tube worms” (GeoB 12339-5, Fig. 130) were sampled by push cores.

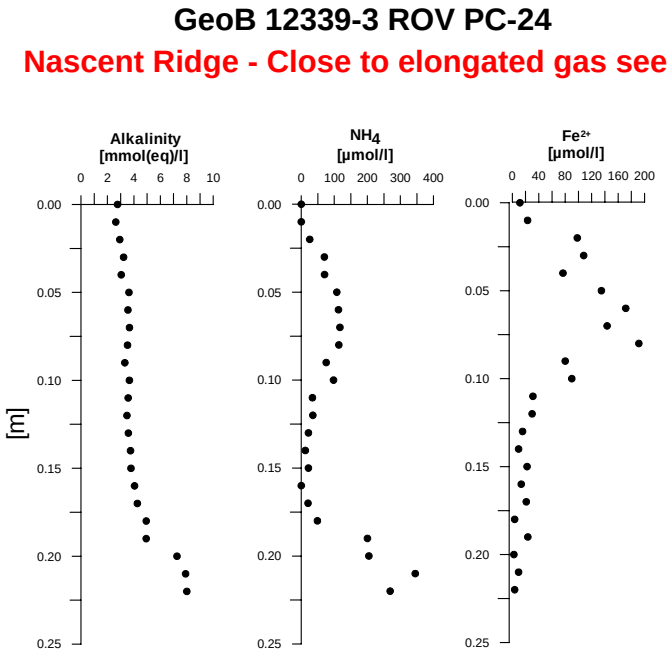

Fig. 129: Pore water concentration profiles for site GeoB 12339-3 at Nascent Ridge.

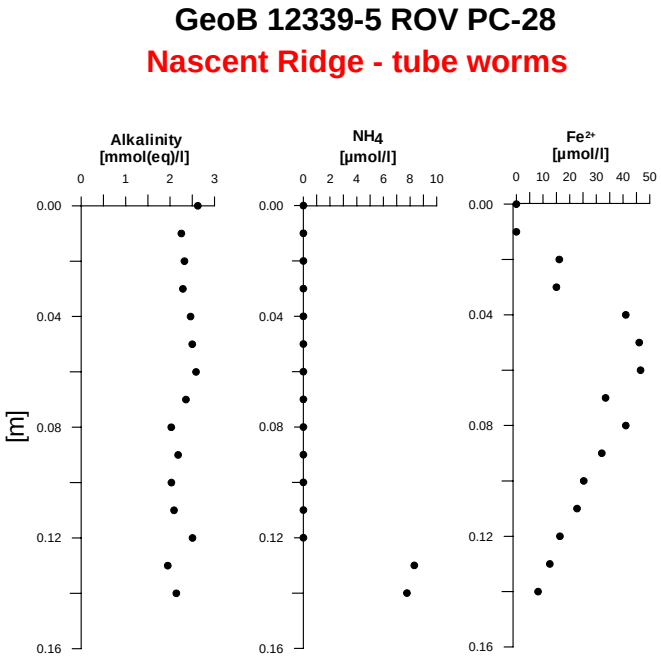

Fig. 130: Pore water concentration profiles for site GeoB 12339-5 at Nascent Ridge.

During ROV Dive 180 (GeoB 12313-5) a gas bubble seep site with a rose-coloured microbial mat in the center (Fig. 131) surrounded by small clams (Fig. 132) was sampled. We suggest that this site represents a comparatively young seep location as no carbonates were found below the central microbial mat. A more mature seep site with carbonates underlying the microbial mat in the center was sampled at Flare 2 during the subsequent ROV Dive 181.

At Flare 2 the clam sites (GeoB 12313-12 and GeoB 12315-4) did not show detectable amounts of ammonium in the upper centimeters while the central microbial mat patch/habitat was characterized by ammonium concentrations which fluctuated around 100 µmol/l close to the sediment surface and which decreased below detection limit further downcore.

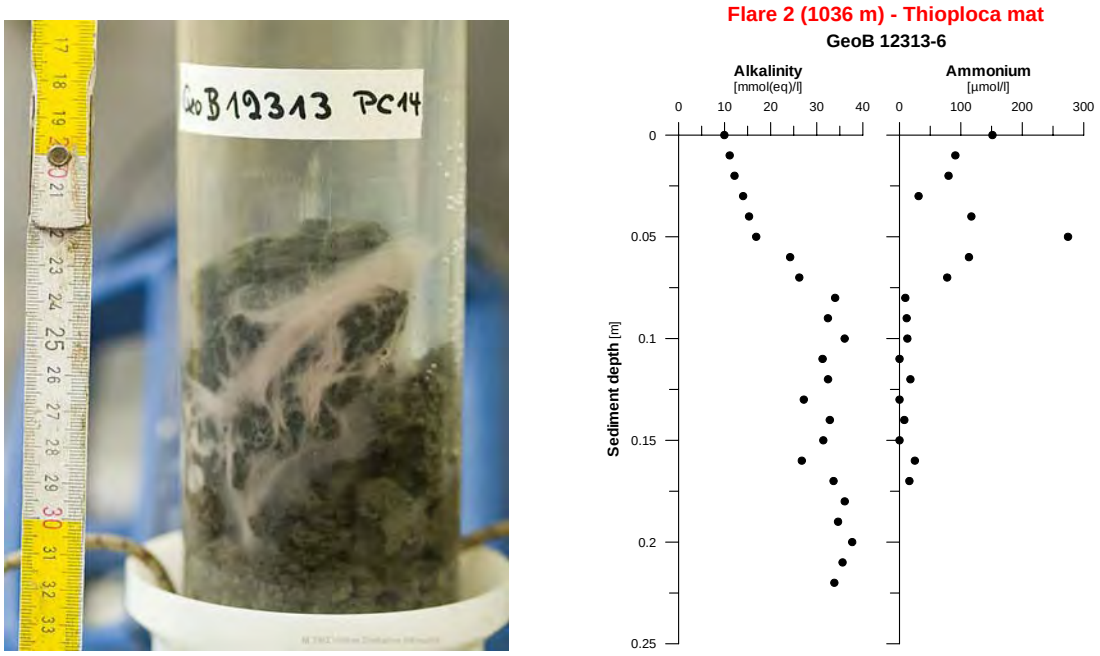

Fig. 131: Pore water concentration profiles for site GeoB 12313-6.

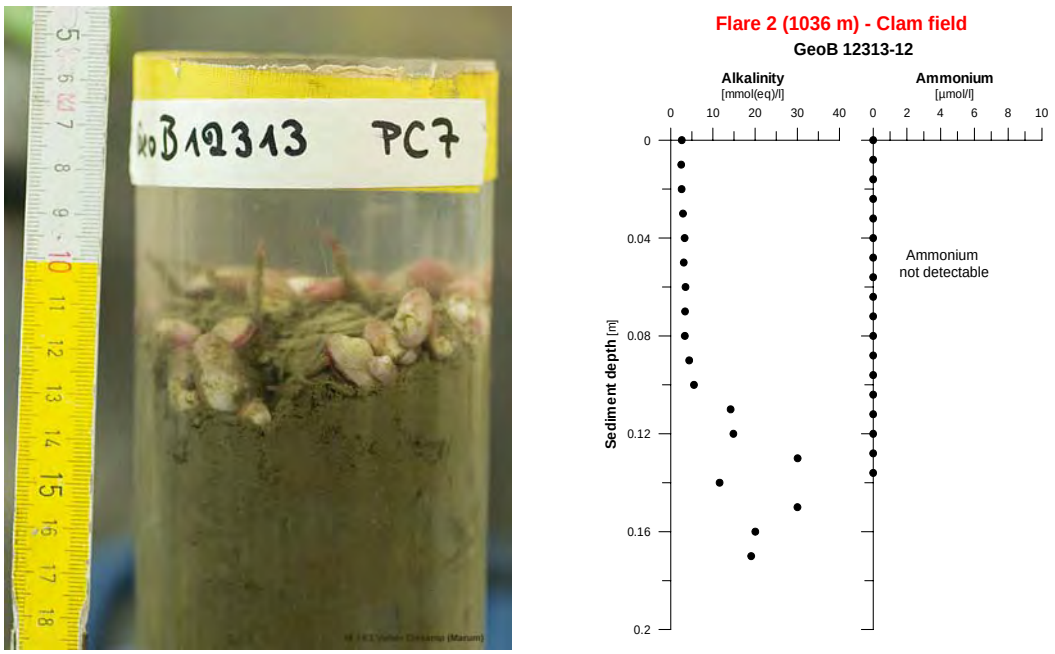

Fig. 132: Pore water concentration profiles for site GeoB 12313-12.

Oxygen measurements in sediment cores

Sedimentary organic matter (OM) in marine environments is by far the largest sink within the global carbon cycle and forms the basis of many proxies used in palaeoceanographic and palaeoclimatic studies. During the last decades it has become clear that preservation is highly selective and that the amount and composition of OM preserved in marine sediments varies largely between regions and deposition environment. It has been shown that this is dependent on the origin of the OM and related to that to the molecular and chemical structure of its components as well as the depositional environment (e.g. oxic or anoxic) and the substrate in which the OM is deposited (e.g. Hedges and Keil 1995).

For an accurate estimation of the marine carbon sink and for correct interpretation of the fossil record, assessment of the character and influence of selective preservation on the original signal is essential. Furthermore, information is required on how selective degradation might influence and/or overprint the initial signal of OM based proxies and how such "overprint" might be recognised in fossil sediments.

Although it has already been a long known fact that high degradation rates of OM are found in oxygenated deposition environments the detailed relationship between oxygen concentration within the sediment and degradation rates of individual OM components is not known. To increase this knowledge detailed information about the oxygen concentration in the upper few centimetres of the sediment will be compared to variability in the organic matter content, notably the organic walled microfossils (organic-walled dinoflagellate cysts, pollen/spores) and organic geochemical proxies such a TEX86 and Uk37.

For this detailed oxygen measurements have been preformed on multicores collected along a transect from deep oceanic sites where bottom waters are well oxygenated towards slope sites where bottom waters have extreme low oxygen concentrations as result of the presence of a strong oxygen minimum zone within the region.

Oxygen measurements have been preformed with a fiber optic oxygen sensor (FIBOX3) using a micromanipulator. Sediments of all cores contained of silty mud.

Oxygen concentrations become depleted within the upper mm of sediment within the OMZ. Within the suboxic zone in the lower part of the OMZ, oxygen penetrates until about 20cm within the cm. Oxygen penetration reaches about 30 mm within core GeoB 12331 received from the Nascent Ridge where bottom waters are well oxygenated.

10.2 Gas Analyses

(T. Pape, J. Rethemeyer)

The distribution of sea floor seeps at the Makran accretionary wedge and their relations to gas-hydrate bearing horizons were previously investigated during SO-90, -122, -124, and -130 cruises (e.g., von Rad et al. 1996, 2000; Grevemeyer et al. 2000; Wiedicke et al. 2001; Delisle and Berner 2002; Delisle 2004). As a result of these studies, submarine gas seepages were mainly attributed to gas accumulations below the gas hydrate stability zone via faults and canyons, and to destabilization of gas hydrates due to tectonic uplift of the upper slope into shallower waters (Delisle and Berner 2002). In addition, gas hydrates at the Makran

accretionary wedge are stable in water depths lower than about 850 m and seepages of free gas were preferentially found in shallow waters of less than 800 m water depth during previous cruises. These observations lead Delisle and Berner (2002) to propose gas hydrates to act as effective seal against upward-directed fluid flow in the study area.

So far, data on concentrations and stable carbon isotopic compositions of methane in the water column (Faber et al. 1994; von Rad et al. 2000; Delisle and Berner 2002), and in sediments (von Rad et al. 1996, 2000) have been published only for some stations at the Makran accretionary wedge. Reported methane concentrations in the water column were always below 700 nL/L (Faber et al. 1994; Delisle and Berner 2002), but much higher concentrations of about 40,000 nL/L were observed in sediments associated to a cold seep area (von Rad et al. 1996) and an inactive mud diapir (von Rad et al. 2000). However, correlations between individual sea floor gas outlets (cold seeps, mud diapirs) and their hydrocarbon sources, as deduced from molecular and isotopic compositions, have not been reported so far.

Delisle and Berner (2002) delineated the extensions of methane plumes sourced from the sea floor and drifting southward in about 600 m water depths. The authors suggest that methane plumes in the OMZ spread over tens of kilometers in length. If those plume dimensions are correct, this would imply strong southward currents and the lack of substantial methane oxidation in the respective water depth range. For a seep site well located within the OMZ (station 154MS, ca. 800 m water depth), Faber et al. (1994) reported a remarkable decrease in methane concentrations in water masses directly above the outlet accompanied by an enrichment in ^{13}C-CH_4. These observations, together with the detection of authigenic carbonates at this site (von Rad et al. 1996) demonstrated that substantial removal of methane within the lower OMZ might be related to the anaerobic oxidation of methane and that molecular oxygen is not necessarily consumed during hydrocarbon degradation. During the same study, substantial concentration increases and ^{13}C-depletions of methane were observed in water depths between about 760 and 720 m (Faber et al. 1994), pointing to an admixture of microbial methane within the OMZ.

Like methane concentrations, the origins of low-molecular weight hydrocarbons (LMWHC) on the Makran accretionary wedge are poorly constraint. High productivity in surface waters in combination with limited ventilation in the oxygen minimum zone between about 100 to 1,200 m water depths lead to rapid deposition (> 1 m/ka; von Rad et al. 2000) of relatively organic-rich slope sediments, which might serve as substrate for the generation of LMWHC. However, $\delta^{13}C$ values of about –44‰ and –62 ‰, determined for methane dissolved in near-bottom waters at two stations (31/32-MS, 154-MS) located in about 1400 and 800 m water depths (Faber et al. 1994), suggests that both, thermocatalytic and biotic processes, might lead to methane production at specific seep sites of the Makran accretionary wedge. For the latter site, microbial carbonate reduction (Whiticar et al. 1986) as the dominant methane generating process could be inferred from stable isotope signatures ($\delta^{13}C$: –77.8‰; δD: –180.8‰) as determined for methane extracted from underlying sediments (153GA; von Rad et al. 1996).

The gas chemical works during M74/3 were performed to determine sources of LMWHC and to characterize their fate in the water column. More specifically the works were directed to the following aspects:

- to correlate hydrocarbon sources and individual geological structures, e.g. cold seeps, mud diapirs
- to analyze the composition of hydrate-bound gases for use in gas hydrate stability modelling
- to characterize molecular fractionations of LMWHC during incorporation into gas hydrate cavities
- to determine the chemical composition and vertical extension of methane anomalies in the water column
- to evaluate the potential impact of hydrocarbon seepage on the OMZ situated between about 100 and 1,200 m water depths during our sampling campaign (chapter 8)
- to collect a comprehensive gas sample set for subsequent on-shore analysis (e.g. $^{13}C/^{12}C$, D/H)

For this, water samples, pieces of gas hydrate and vent gas were recovered during hydrocasts and gravity corer stations as well as ROV dives and analyzed for their concentrations of LMWHC. In addition, for water samples the concentrations of nitrogen, oxygen, and carbon dioxide were followed. Preferential sites of investigation were hydrocarbon seepages feeding flares within the OMZ (e.g. Flare 1, 2, and 15), or in the lower oxic zone (4, 5, 7), as well as several non-seep areas for reference. Here we report on compositions of gas venting from the sea floor, bound in gas hydrates and dissolved in the water column.

Sample preparation and on-board analyses

During M74/3 gas-bearing samples and gases were recovered using a CTD-Water Rosette System, a ROV-operated Gas Bubble Sampler and a conventional Gravity Corer. For an accurate positioning of the rosette during water sampling above gas flares detected (chapters 4 and 5) and during gravity coring, an acoustic transponder system (POSIDONIA, IXSEA) was mounted on the wire 50 m above the tool. Gas and water samples were taken at six flare sites and at six sites remote from gas outlets as a reference. A detailed sample list is shown in Appendix 7.

Fifteen samples of gas venting from the sea floor were collected with the Gas Bubble Sampler (GBS) during eleven dives conducted at four flare sites. Additionally, three pressurized near-bottom water samples were taken with the GBS at three stations. The GBS is a ROV-operated in situ pressure sampling device. It was designed to collect free gas escaping from the sea floor within the gas hydrate stability zone, but enables sampling of gas hydrates generated in the water column or of pure sea water as well. Furthermore, the GBS allows for estimations of gas flux rates by visual observations during ROV dives and by quantitative degassing upon its recovery on deck. Due to its handling with the ROV, samples can be taken very close to the sea floor, e.g. above discrete gas outlets. The GBS first deployment was during cruise M70/3 and it has routinely been used during M72/3a. For technical descriptions refer to the report of cruise M72/3 (Bohrmann et al. 2007). At M74/3 the GBS was deployed 18 times.

Immediately upon recovery, the GBS was connected to a ‘gas manifold’ (Heeschen et al. 2007), and the gas released incrementally for quantification and sub-sampling. Gas sub-

samples were transferred into 20 mL serum glass vials pre-filled with concentrated NaCl solution.

Pieces of gas hydrate were recovered from the area of Flare 2 (ca. 1,020 m water depth) and Flare 5 (ca. 2,860 m) during six deployments of a conventional gravity corer using a 3 m cutting barrel (see chapter 9.1). Hydrate-bound gases were released by controlled dissociation of gas hydrate pieces in gastight syringes under room temperature and transferred into 20 mL serum glass vials.

During M74/3 246 water samples were taken at 14 hydrocast stations with a rosette of 18 10 L Niskin (Hydro-Bios) bottles housed at the University of Bremen. While lowering the rosette, strong generally eastward directed water currents were recognized by means of the USBL underwater navigation at most stations. Speed and accurate directions of those water currents were not analysed during M74/3, however, they appeared to impact water masses down to about 300 to 200 m above sea floor.

Consequently, high-resolution sampling comprising 25 m dephts intervals in water masses up to about 300 m above the gas outlet was performed to characterize the fate of volatiles emitted from the sea floor. For this, the rosette was lowered close to the expected emission site and usually stopped between 10 to 20 m above sea floor. A near-bottom sample was taken and hauling started immediately. In addition to hydrocasts carried out close to gas flares, some water sampling stations remote from known seep sites were performed for reference. For on-board preparation of LMWHCs, oxygen, nitrogen and carbon dioxide, volatiles dissolved in the water samples were extracted by using a headspace technique and/or a vacuum extraction method.

The headspace technique was used for rapid on-board concentration analysis of methane, nitrogen and oxygen dissolved in water samples. Water samples were released from the Niskin bottles into 250 mL serum vials, sealed with butyl-stoppers and immediately stored top-to-bottom in the dark at 4°C. 10 mL of helium (5.0, AirLiquide Deutschland) were introduced by releasing excess amounts of water. The bottles were shaken thoroughly and left for 24 h. During the cruise 245 gas samples were obtained by this method.

The vacuum extraction of dissolved gases was accomplished to obtain gas amounts sufficient for on board quantification of C_{2+} compounds and for onshore stable isotope analysis of hydrocarbons and carbon dioxide. Water samples were transferred from the Niskin bottles via gastight hoses into 1 L glas flasks without headspace and subjected to gas extraction (Lammers and Suess 1994; adopted from Schmitt et al. 1991). For this, a high grade vacuum combined with heating until boiling and repeated short-time ultrasonification was applied to the water samples. Using the vacuum extraction technique, 72 gas samples were prepared from waters of the Makran accretionary wedge

Samples collected at several CTD stations (GeoB 12329, 12337, 12340, 12344, 12347, and 12354) were treated by both methods, for comparison. All gas samples obtained by the above mentioned methods were transferred with a gas-tight syringe into 20 mL glass serum vials prefilled with NaCl solution for i) on board gas chemical analysis and ii) for long-term storage and onshore analysis of stable isotope ratios ($^{1}H/D$, $^{12}C/^{13}C$) of volatile hydrocarbons and CO_2.

For onboard measurements of gas chemical compositions the samples were analyzed with a two-channel HP6890N gas chromatograph (GC). Low-molecular-weight hydrocarbons (C1

to C6) were separated, detected and quantified with a capillary column (OPTIMA-5; 5 µM film thickness; 0.32 mm ID, 50 m length, carrier gas: N2) connected to a Flame Ionisation Detector, while permanent gases (O_2, N_2, CO_2) as well as C1 and C2 hydrocarbons were determined using a packed (Molecular sieve, carrier gas: He) stainless steel column coupled to a Thermal Conductivity Detector. The GC oven temperature program was: initial 45°C held for 4 min; heating with a rate of 15°C min-1 up to 155°C (constant for 2 min), 25°C min-1 up to 240°C (7 min). A PC-operated integration system (GC Chemstation, Agilent Technologies) was used for recording and calculation of the data. Calibrations and performance checks of the analytical system were conducted daily using commercial pure gas standards and gas mixtures (Air Liquide). The coefficient of variation determined for the analytical procedure was lower than 2 %.

Preliminary results and discussion

A total of 540 gas samples were prepared from waters, vent gas and gas hydrates during M74/3 for analysis of their gas composition.

The hydrocarbon compositions of vent gases collected with the GBS at four flare areas were strongly dominated by methane, followed by ethane, propane and occasionally by traces of C4 compounds (Table 25). The molecular ratios (C1 / C2+) suggests that LMWHC emitted at Flare areas 1, 2, and 5 are predominantly of microbial origin (Bernard et al. 1976). A different hydrocarbon composition was found for gas venting from Flare 7 located close to the Sonne fault (Kukowski et al. 2000). Gas samples from that site were characterized by lowest amounts of methane and comparably high portions of ethane and propane. Considering the respective molecular ratios (C1 / C2+) of around 500, an admixture of thermogenic hydrocarbons might be assumed for gases emitted at Flare site 7 (Bernard et al. 1976).

Table 25: Distributions of C_1 to C_4 hydrocarbons [mol - % of C_1 – C_6] in gases analysed during M74/3.

	avg. water depth [m]	methane	ethane	propane	*i*-butane	*n*-butane	C_1 / C_{2+}
vent gas							
Flare 1 (mean, n = 2)	590	99.9752	0.0219	0.0029			4,029
Flare 2 (mean, n = 3)	1,030	99.9755	0.0148	0.0034	0.0021	0.0018	4,078
Flare 7 (mean, n = 2)	1,645	99.8034	0.1772	0.0138	0.0029	0.0015	505
Flare 5 (mean, n = 3)	2,875	99.9439	0.0137	0.0059	0.0048	0.0019	2,756
hydrate-bound gas							
Flare 2 (mean, n = 3)	1,010	99.9786	0.0189	0.0025			4,677
Flare 5	2,860	99.9781	0.0155	0.0024	0.0019		4,561

Calculations of the nominal gas hydrate stability showed that precipitation of pure methane hydrate in the Makran area might be expected in water depths below 850 m (see chap 9.4.3.). Hydrate-bound hydrocarbons at both sites, Flare area 2 and 5, were strongly dominated by methane, followed by ethane and propane (Table 25). While hydrate-bound hydrocarbons at Flare site 2 virtually lacked C_4-isomers and higher homologues, *i*-C_4 was additionally found for the gas hydrate piece from Flare site 5. This correlates with highest amounts of *i*-C_4 found for vent gas of Flare 5. On average, hydrate-bound hydrocarbons are slightly enriched in

methane and ethane but depleted in propane compared to those contained in vent gas from both study sites.

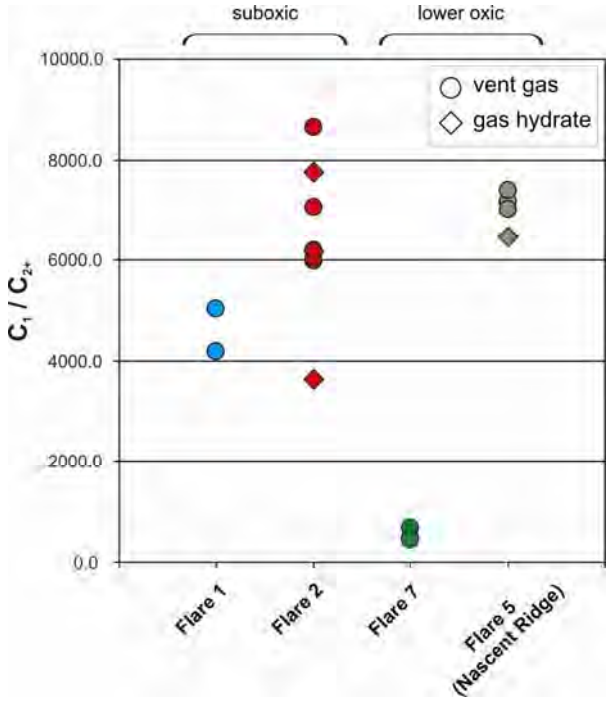

Fig. 133: Molecular ratios of hydrocarbons determined for vent and hydrate-bound gases from flare sites in the suboxic and the lower oxic zone at the Makran accretionary wedge.

In gas samples prepared from the water column C3+ hydrocarbons were virtually absent or below detection limit while using the usual analytical settings. Therefore, we here report on concentrations of methane, as well as oxygen and nitrogen as revealed by on-board headspace analysis of dissolved volatiles in waters from selected hydrocasts.

In Fig. 134 methane and oxygen amounts as well as N_2/O_2 and O_2/CH_4 ratios in the water column above individual hydrocarbon seeps (CTD-23, 604 m water depth, CTD-19, 1,648 m; CTD 21, 2,859 m) as revealed by headspace analysis are shown. Methane profiles clearly showed elevated concentrations in near-bottom waters which can be related to gas emission from the sea floor. Highest methane amounts were found for CTD 21 carried out in the area of Flare 5. For all seep sites assumed background values were reached in waters about 150 to 200 m above the individual seeps, indicating effective methane oxidation in this depths range and/or water current-induced drifting of the methane plume. Corresponding to the trends observed with the oxygen-sensitive sensor (chapter 8), oxygen contents generally decreased with increasing depths from surface water towards the OMZ and increased again in the suboxic water body below about 1,200 m. On a smaller scale, variations in oxygen contents were observed for all three stations in waters close to the seafloor. Moreover, at both stations deployed in the lower oxic zone (CTD 19 and 21), oxygen contents in near-seafloor waters of about 300 m thickness, did not follow the general trend of increasing concentrations with increasing depths, but in average appeared to be constant or even slightly reduced.

N_2/O_2 ratios in surface waters resembled atmospheric values (~ 3.6) and strongly increased towards the OMZ, where up to 15.5 were found. Using headspace gas, we still detected small amounts of molecular oxygen within the OMZ, which corresponds to oxygen profiles

determined with the oxygen sensor mounted to the CTD-rosette system (chapter 8). With increasing water depth N_2/O_2 ratios decreased again to approximate atmospheric values in the lower oxic water column.

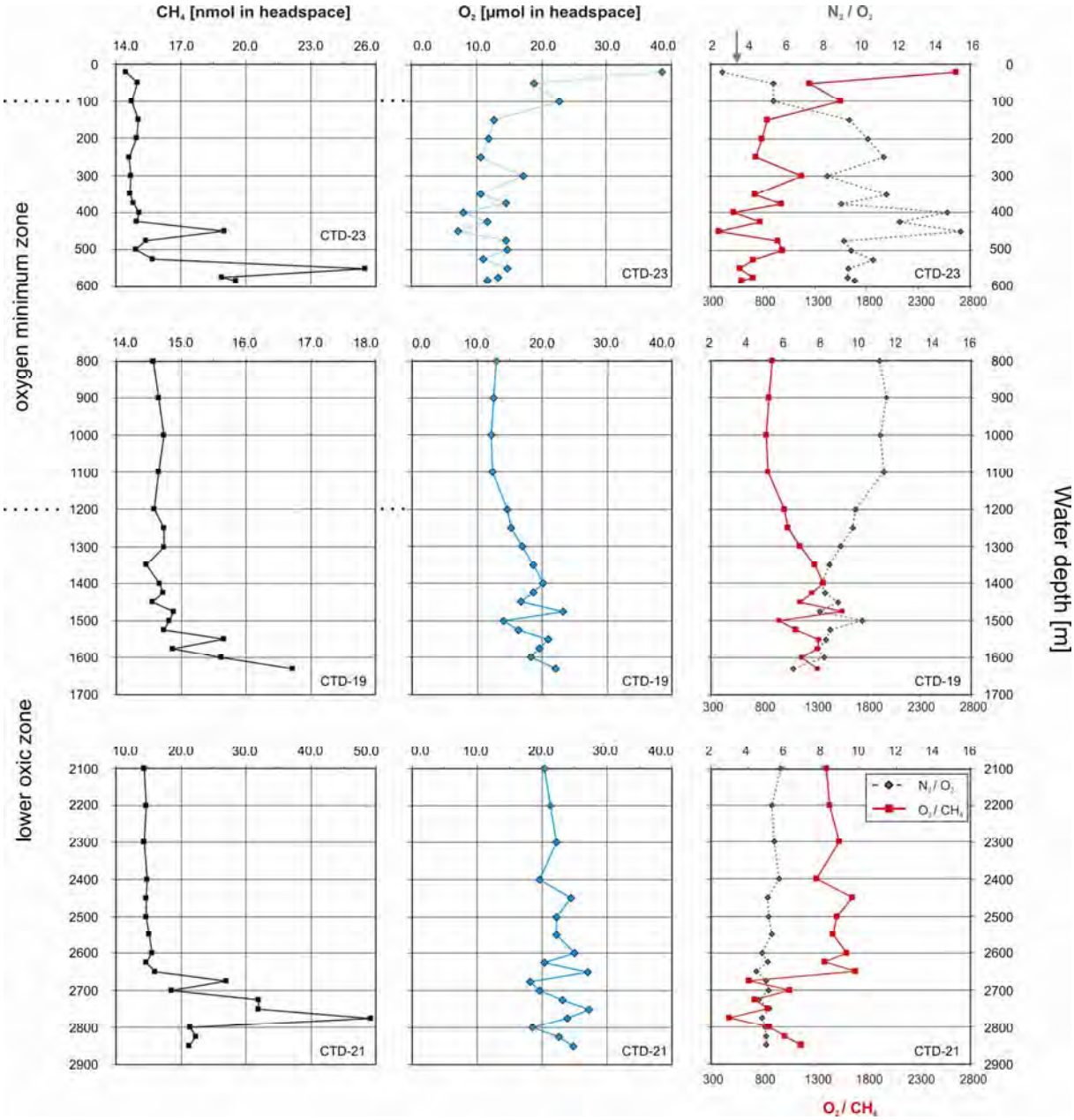

Fig. 134: Distributions of major volatiles in the water column of the Makran accretionary wedge.
left column: CH_4 amounts in headspace gas prepared from three CTD stations indicating seepage at the individual sampling sites. Note the different scales for methane concentrations.
middle column: O_2 amounts in headspace gas prepared from the three CTD stations.
right column: nitrogen - oxygen ratios and oxygen - methane ratios determined for headspace gas from the three CTD stations. The arrow denotes the atmospheric nitrogen - oxygen ratio.

An opposite trend with depth was observed for the O_2/CH_4 ratio, which strongly decreased towards the OMZ and increased again in greater depths. However, hydrocarbon seepage at Flare area 1 (CTD 23) does not seem to greatly affect the O_2/CH_4 ratio in near-bottom waters, suggesting that dissolved O_2 in the OMZ is not rapidly consumed by methane oxidation. If this assumption is correct, it would corroborate the idea of extending methane plumes in the

OMZ as proposed by Delisle and Berner (2002). In contrast, the seeps within the lower oxic zone (CTD 19, CTD 21) appear to have much greater impacts on the O_2/CH_4 ratio. At these stations near-bottom O_2/CH_4 values are considerably lower as those observed in overlying water masses. Low O_2/CH_4 values in these depths range result from admixture of methane emanated from the seafloor and concurrent depletions of O_2 concentrations. Therefore it might be assumed that in the lower oxic zone considerable amounts of oxygen are consumed close to hydrocarbon seeps by aerobic methanotrophy.

Scattering in O_2 and N_2 concentrations (data not shown) and the respective ratios, however, was observed in deeper water masses at the three stations, which are all characterized by high concentrations of methane. Turbulences in the water column might be caused during water collection with the rosette and the greatest impact – as shortest time spans occur during lowering and hauling - might be expected for deeper water masses. An alternative explanation might be an upwelling of ambient water masses induced by rising gas bubbles as recently reported by Sauter et al. (2006) for the water column at the Håkon Mosby mud volcano.

11 Biogeochemistry of the Oxygen Minimum Zone and Seep Sites

11.1 Influence of Oxygen Content and Methane Seepage on the Microbial Carbon Cycling in Sediments from the Pakistan Margin

(M. Y. Yoshinaga, P. Rossel)

The Arabian Sea accounts for approximately 30% of the world's ocean oxygen minimum zone (OMZ) (Helly and Levin, 2004). Sediments underlying OMZs exhibit high carbon burial efficiency and are of global importance not only as sink for atmospheric carbon, but also as source of petroleum and natural gas. Microbes thriving in subsurface sediments are imperative at controlling the fluxes and rates of carbon cycling in these environments. While nitrate, iron and manganese oxides are important electron acceptors for the degradation of organic matter (OM) within the upper anoxic layers of sediments (first millimeters to few meters below the sea floor, mbsf), microbial respiration in deeper sediment layers is largely dominated by sulfate reduction (SR) coupled to either respiration of fresh OM or, in more deeply buried sediments to the anaerobic oxidation of methane (AOM) at the sulfate-methane interface zone (SMI) (e.g. Iversen and Jørgensen, 1985; D'Hondt et al. 2002). The anaerobic degradation of OM is also performed by syntrophic associations of microbes, but involves fermentative breakdown of large organic molecules (e.g. amino acids) to low molecular weight products (such as acetate), which are subsequently respired to CO_2 when coupled to SR, and CH_4 and CO_2 (Megonigal et al., 2004). Acetate and other volatile fatty acids (VFAs) are important metabolic intermediates and can reflect the intensity and route of OM degradation in anoxic sediments. As a major terminal degradation processes in subsurface sediments, methanogenesis occurs below the SMI. The basic approach is to examine the active microbial communities (intact membrane lipids, IPLs) and the low molecular weight products of their metabolism, such as dissolved inorganic carbon (DIC), CH_4, and VFAs

Microbiological investigations using stable carbon isotopes have provided major insights in the global CH_4 budgets through identification and quantification of its sources and sinks (Hinrichs and Boetius, 2002; Conrad, 2005). Similarly to CH_4, pore water VFAs exhibit a wide range of carbon isotopic composition, particularly acetate (-5‰ to -85‰) (Heuer et al., 2006). Given the central role played by VFAs as intermediates in anaerobic metabolism, their isotopic composition can be used to support process-specific information about the microbial carbon flow in marine sediments (Heuer et al., 2006). A very powerful tool to read these subtle *in situ* substrate signatures and their influence on microbial carbon cycling is the study of stable carbon isotopes of specific bacterial or archaeal membrane lipids (e.g. Sturt et al., 2004; Biddle et al., 2006).

Methane seeps are controlled by advective processes that supply, from subsurface sediments, methane by gas bubbles or rising fluids (Judd et al., 2002). This supply of methane can be derived from ancient or recent reservoirs, and from microbial, thermogenic or abiotic sources. Methane contribution can be affected by pressure, temperature, salinity (affect the solubility of methane) and by the rate of methane production and flow through the sediment (Yamamoto et al., 1976). In this system anaerobic oxidation of methane (AOM) is one of the major microbial processes. Previous observations indicate that AOM consume more than 80% of the methane in diffusive systems (Reeburgh, 1996). However in seep areas AOM rates can

be one order of magnitude higher, but due to the limited information of methane from these sites not realistic calculations of the consumption of methane in the sea can be done (Hinrichs and Boetius, 2002).

Base on molecular, GC-amenable lipids and their isotopes it has been shown that AOM is performed by a microbial consortium between methanotrophic archaea (acronym ANME=anaerobic methonotrophs) and sulfate reducing bacteria (SRB). Thus AOM is mainly affected by the magnitude of methane supply and the co-occurrence of sulfate.

Today, three main groups of ANME have been identified: ANME-1, ANME-2 and ANME-3. In detail it has been reported that ANME-1 can occur as single cells (Orphan et al., 2002), while ANME-2 and ANME-3 have closer association with the SRB partner *Desulfosarcina/Desulfococcus* (DSS) and *Desulfobulbus* (DBB) for ANME-1 and ANME-3 systems respectively (Boetius et al., 2000; Niemann et al., 2006).

Several publications have attributed different zonation of AOM communities in relation to the type of sulfide oxidizing community present (Elvert et al., 2005, Treude et al., 2003, Knittel et al., 2005). Variations in AOM community composition in Hydrate Ridge have been associated with different sites; Beggiatoa site was characterized for the high methane flow and the dominance of ANME 2a/DSS consortia, while Calyptogena site presented low to medium methane fluxes and the domination of ANME 2c/DSS (Elvert et al., 2005). However all the lipid biomarkers used to evaluate AOM communities are based on GC-amenable lipids (small derivates from IPLs), which contrary to IPLs, represent the decayed cells. Thus the use of IPLs provides more complete information not only because they are associated to living cells, but also due to their taxonomic specificity.

The influence of different oxygen content, water depth (both affecting type and quality of the organic matter that reach the sea floor) and the occurrence of seepage in the modulation of the microbial community structures performing AOM have not been systematically evaluated. Thus the study area provides a great opportunity to apply multi-approach techniques including lipid biomarker (IPLs and GC-amenable lipids), VFAS, DIC (concentration and isotopes) and molecular techniques (FISH and clone library) from different sites; Calyptogena, Thioploca (white and orange site), gassy seep sites and carbonate fields (Appendix 8) located within and outside of the OMZ (Appendix 8).

This research is aimed at understanding the nature of major carbon transforming processes such as routes of acetate production and consumption, methane consumption and its sources, comparing nearby sites within and outside the OMZ, and at gas-venting sites from the Pakistan continental margin. Employing an interdisciplinary combination of isotopic information from environmental carbon pools (e.g. total organic carbon, VFAs, intact membrane polar lipids) coupled to the geochemical horizons data (e.g. SR zone, alkalinity, etc), together with incubation experiments and molecular phylogenetic analyses, this research proposal has the potential to build up further insights into the microbial carbon cycling in shallow subsurface sediments.

General questions addressed: 1) *How do redox conditions in the water column influence the diagenesis of OM and the size and structure of the microbial community in subsurface sediments?* 2) *How does carbon flow in sediments under the influence of OMZ compared to other sedimentary environments (outside and at the seep site)? 3) Can we observe a zonation*

of the communities performing AOM in the different sites sampled outside and within the OMZ (Calyptogena, white and orange mat, gassy seep) and what are the main environmental factors controlling the distribution of these communities?

Three major zones of sediments (above, at and below the sulfate-methane transition zone, SMTZ) were sampled using gravity corers in and out the OMZ (~ 6 m) and push corers at seeps sites (0.5 m) using the ROV QUEST (see Appendix 8). High-resolution intervals (20 cm for gravity corers and 1 cm for push corers) yielded 20-25 samples for most analytical procedures.
Pore water chemicals: alkalinity, nitrate, ammonium, iron, manganese, hydrogen sulfide and sulfate measurements (AWI group).
Pore water carbon pools: TOC, DIC, CH4, VFAs (acetate, butyrate, others) concentration and stable carbon isotopes.
Microbial lipids: Intact Polar Lipids (IPLs) concentration and stable carbon isotopes.
Microbial phylogenetics: FISH and DNA (t-RFLP and clone library).
Incubation: We will use 1:1 slurries of sediments (collected on board, 500 mL bottles and kept anoxic) and sulfate-free artificial seawater incubation checking for H_2, CH_4 and pore water VFA's concentrations in a time series experiment (2-4 months) at home laboratory.

Gas sampling and measurements on board
Sediment samples were collected on deck at the end caps of every 1 m gravity corer section immediately after recovery. 3 mL syringes were filled with sediments, and samples were stored in a 22 mL gas tight glass vials. This approach was used to check for gas loss due to sample handling and storage. Gas sampling for horizontal intervals (20 cm for gravity corers and 1 cm for push corers) were taken with syringes and kept in 22 mL vials containing 5 mL of NaOH (1M). 5 mL from those vials were transferred to a 22 mL vial containing NaCl for storage.

Methane concentrations were measured on board by gas chromatography coupled to a flame ionization detector (GC-FID, Agilient 6890N). The GC was equipped with Optima 5 (50 m x 320 µm x 5 µm) column and it was used as gas carrier. The oven was programmed to 60˚C for 3 minutes. 50 to 200 µL of samples were injected during each run, and calibration curves were made everyday with methane standards.

Pore water sampling
A sediment squeezer was used to obtain pore water samples. ~50 mL of wet sediments were transferred to the squeezer device, yielding ~20 mL of pore water. Aliquots of 10 mL were used for hydrogen sulfide, sulfate, iron and ammonium concentrations and 10 mL aliquots were transferred to 2 mL vials for DIC and 4 mL vials for acetate concentration and isotopic composition analysis determinations.

IPLs and DNA sampling
For IPLs and DNA, sediments (~50 mL aliquots) were stored in previously muffled aluminum foils and frozen (-20˚C) and later transported in liquid nitrogen to avoid lipid degradation before the analysis in Bremen. In order to screen the composition of bacterial and/or archaeal

communities, we plan to conduct 16S rRNA t-RFLP, and according to these results clone libraries might be used as tool for specific taxonomic determination.

For fluorescence in situ hybridization (FISH) samples we collected 0.5 mL of sediments and transferred into a 2 mL vial containing 1 mL of para-formaldehyde (PFA). This solution was kept in 4˚C for 6-12 hours. Several washing steps with phosphate buffer solution (PBS) were conducted. A final solution of 0.5 mL of PBS and 0.5 mL of Ethanol was added to each sample, which were stored at -20˚C. These samples will be used to quickly assess known microorganisms responsible for the biochemical pathways under investigation using specific probes (e.g. sulfate reducing bacteria and Archaea probes to check for AOM, Boetius et al., 2000).

IPL analyses will be performed with an HPLC-ESI-MS^n using protocols described previously by Sturt et al. (2004) and Biddle et al. (2006) (Fig. 135).

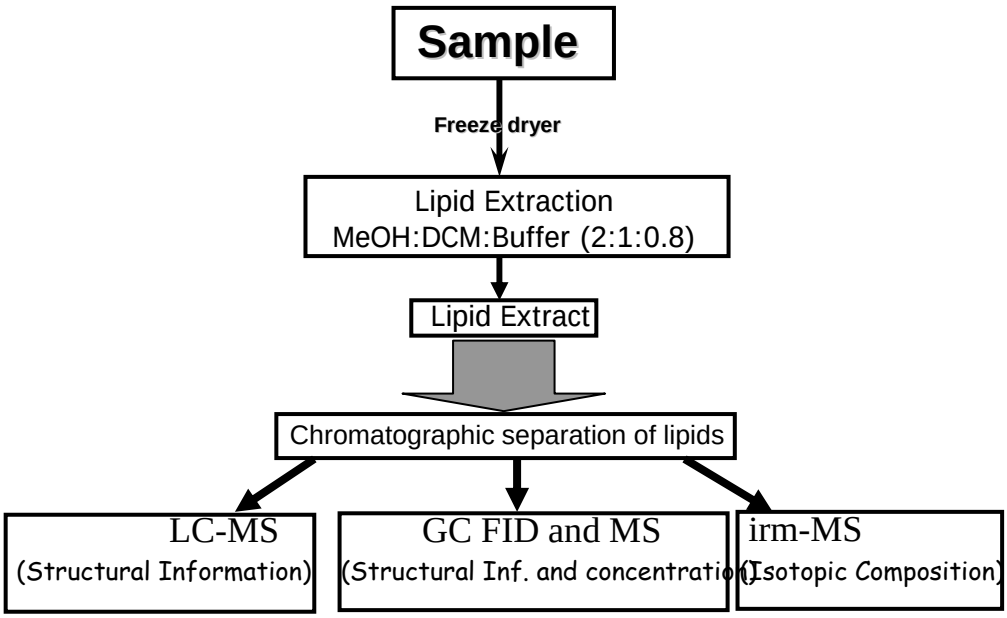

Fig. 135: Analytical procedure that will be used for lipid and isotope analysis in the samples collected.

Preliminary results

A quick assessment of methane concentrations was conducted on board using a GC-FID (Fig. 136). This approach was helpful to select samples for the incubation experiments, meaning that sedimentary horizons were chosen and defined locations of SR, AOM and methanogenesis could be sampled precisely. Gravity corers were taken at 355, 680, 975 and 1500 m and ranged from sediments completely imbedded in oxygen depleted waters to sites with higher oxygen concentrations in bottom waters (see chapter 8. water column work for more details). In addition, sediments sampled below 1000 m with the multicorer were commonly fluffy in the first 5-10 cm, lacking fauna, whereas sediments from 1000 m or deeper stations presented numerous metazoans, for example brittle starts, polychaetes and bryozoans (MY, personal observation).

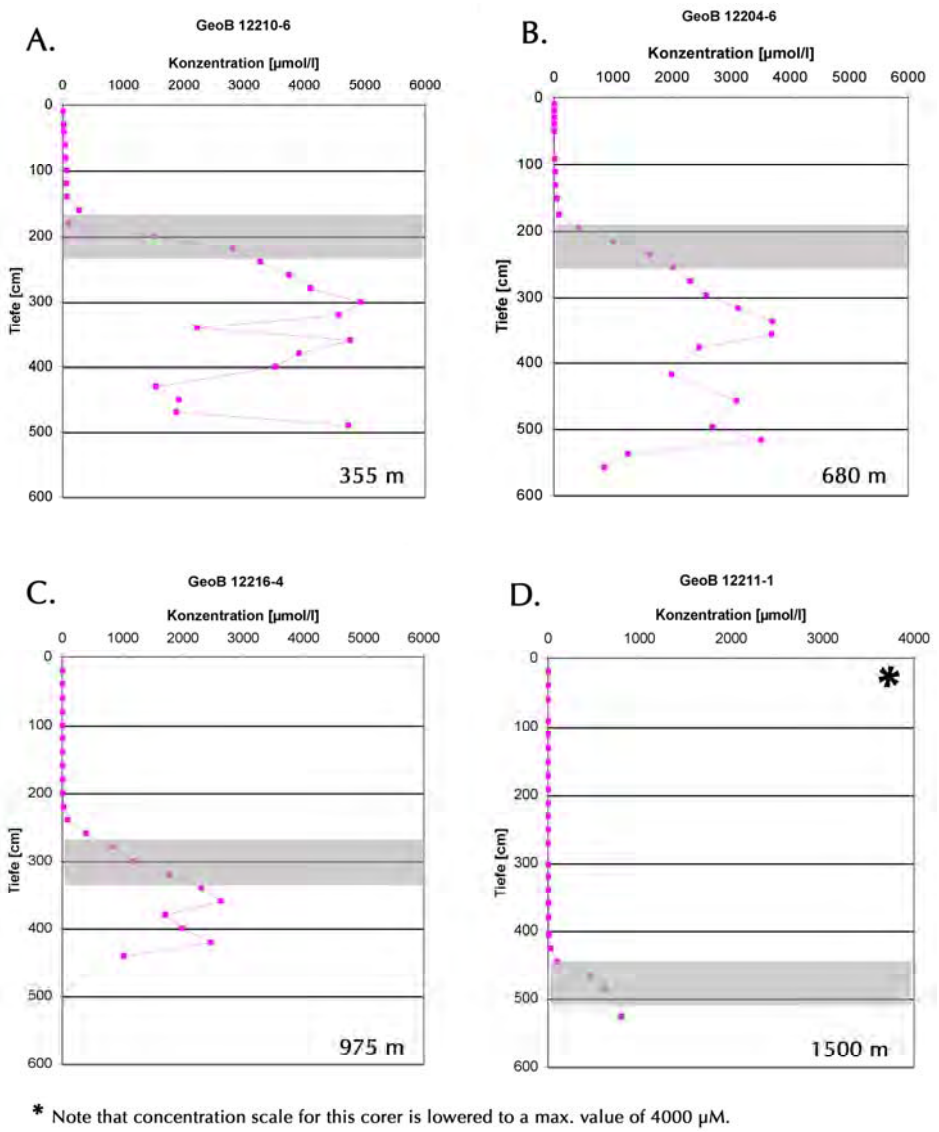

Fig. 136: Methane concentrations from gravity corers recovered from sediments exposed to differential bottom water oxygen content from the Pakistan continental margin. The data showed in this section are not normalized to true values of pore water volume. Alternatively, we assumed 70% of water content in all sediment samples.

In gravity corers, methane concentrations reached a maximum of 5mM. The magnitude of the values found during this cruise was comparable to other high productive areas, for instance the Namibian upwelling system (Niewöhner et al., 1998). The highest values occurred at the shallower stations Geo B 12210-6 (355 m) and Geo B 12204-6 (680 m) (Fig. 136 A and B), whereas lowest values were found at station Geo B 12211-1 (1500 m) (Fig. 136 D). Two important factors determine the accumulation (and preservation) of OM in marine sediments: export fluxes of organic carbon and bottom-water O_2 (e.g. Hartnett et al., 1998; Hedges et al., 1999). These factors are key parameters shaping the early diagenetic reactions in surface sediments (e.g. Wakeham and Canuel 2006), and have major repercussion in the sedimentary anaerobic metabolism, especially to methane production in deep sediment layers. At a first glance, our results strongly suggest the OMZ control in the amount of carbon buried in these sediments. Methanogenic activities driven by high quality and quantity of organic matter in sites within the OMZ produce greater amount of methane compared to sites

exposed to oxygen at the sediment-water interface. Sediments from stations located within the OMZ presented both higher amounts of methane and shallower depths of the so-called SMTZ (Fig. 136, gray rectangles). The depth of the SMTZ is dependent on the methane concentrations and its diffusion upwards (e.g. Niewöhner et al., 1998), and as noted in other marine systems, this factor drives the intensity and magnitude of the AOM and SR (e.g. see Parkes et al., 2007). We expect that patterns in methane concentrations and also in SMTZ, SRZ and MZ positioning within the corers will produce differential signatures in biomarkers (IPL, DNA) and microbial metabolic products (DIC, VFAs) that can be tracked by molecular and isotopic techniques. These tools will allow us to build up solid insights into the subsurface microbial carbon cycling from the study area.

11.2 Organic Matter Degradation/Preservation around the OMZ

(J. Rethemeyer, A. Bahr)

Organic matter (OM) burial in marine sediments is an important long-term sink of carbon out of the more active carbon cycle. One of the most controversial issues in biogeochemistry is the control on the preservation of organic matter (e.g., Hedges and Keil, 1995). The time OM is exposed to oxic conditions during sedimentation and within the sediment is thought to be a major controlling factor on OM preservation and alteration (e.g. Hartnett et al. 1998). ^{14}C based studies of different organic compounds isolated from marine surface sediments indicate the preferential degradation of fresh, labile OM from marine primary production in oxygenated sediments relative to older, stabilized marine and terrigenous compounds, while a greater proportion of 'young', marine compounds was preserved in sediments in contact with oxygen depleted bottom waters (e.g. Mollenhauer and Eglinton, 2007). The selective degradation/preservation of different compounds of sedimentary OM will bias the information on paleoenvironmental conditions that are derived from biomarker compounds. Thus, a proper knowledge of the mechanisms of carbon cycling, and differences in burial efficiency in contrasting redox settings is required.

The high productivity and the intense oxygen minimum zone (OMZ) of the Northern Arabian Sea between 150 and 1200 m lead to the deposition of relatively OM-rich sediments. This provides ideal conditions for the study of the selective degradation/preservation of organic compounds in sediments with oxygenated and oxygen depleted bottom waters. We will isolate key marine and terrestrial biomarker compounds by preparative gas chromatography (GC) and liquid chromatography (LC) from surface sediment cores taken at 4 locations within and below the OMZ (Table 26). Compound-specific ^{13}C and ^{14}C analysis of these compounds will be used to (a) quantify the contribution of different OM sources to surface sediments, (b) estimate timescales of terrigenous OM transport from land to the ocean, and (c) identify preferential degradation of individual compounds and possible effects on paleoenvironmental proxies (e.g. TEX86). The latter will be done by comparison of the abundance and carbon isotopic composition of biomarkers in surface-sediments as well as in down core samples. In addition, the new branched versus isoprenoid tetraether lipid (BIT) index as an indicator for the relative fluvial contribution of terrigenous organic matter to marine sediments will be applied (Hopmans et al., 2004) and individual BIT compounds will

be isolated by LC and ^{14}C dated. Since the interpretation of OM and biomarker degradation respectively requires a proper knowledge of the oxygenation history of the sediments after deposition, we will closely collaborate with S. Kasten et al. (Chapter 10.1).

During Cruise M74/3, near-surface sediments from 4 different stations within and below the OMZ were sampled with a multicorer (Table 26). Two sites were located in the present-day intense OMZ (GeoB 12309 and 12312) at around 960 m (0.03 ml O_2 l^{-1}) and 655 m (0.02 ml O_2 l^{-1}) water depth. The water depth of the stations GeoB 12308 and 12321 was around 1570 m and 1425 m respectively, with suboxic conditions (~0.86 ml O_2 l^{-1}). From each location 2 large tubes of the multicorer were sampled for high-resolution organic geochemical analyses. Most cores were cut into 1 cm segments down to 20 cm core length and the remaining core was sampled in 2 cm intervals. For stations GeoB 12308, 12309 and 12321 additional cores were taken and cut into 2 cm segments. All samples were filled into pre-combusted glass jars, stored and shipped frozen by air cargo to Bremen.

Table 26: Multicorer samples taken for lipid analysis.

GeoB No	Lat. N°	Long. E°	Water depth (m)	Core length (cm)	No of cores	Sampling intervals
12308-3	24°43.115	62°59.504	1574	30	2	0-20 cm: 1cm, 20-30cm: 2 cm
12308-5	24°43.109	62°59.497	1586	30	1	0-30 cm: 2 cm
12309-3	24°59.322	62°59.859	962	34	2	0-20 cm: 1cm, 20-34 cm: 2 cm
12309-4	24°52.292	62°59.839	957	30	2	0-30 cm: 2 cm
12312-3	24°53.072	63°01.641	654	35	2	0-20 cm: 1cm, 20-27 cm: 2 cm
12321-1	24°46.002	62°59.973	1425	28	2	a) 0-28 cm: 2 cm, b) 0-28 cm: 1 cm
12331-1	24°11.507	62°46.502	2831	26	2	0-26 cm: 1 cm

In Bremen, all sample material will be freeze-dried. Aliquots of samples will be taken for analysis of bulk parameters such as total organic carbon, nitrogen and carbonate content, etc.

Sediment samples will then be extracted with organic solvents using a Soxhlet extractor to recover total extractable lipids. These will be separated into different compound classes such as alkanes, ketones, fatty acids, and alcohols using standard methods and analysed by GC and LC/MS. Individual source-specific compounds that occur in sufficient quantities for radiocarbon analysis (>50 µg C of each individual compound), will be isolated using preparative GC and LC and converted to graphite for radiocarbon analyses by accelerator mass spectrometry.

12 Weather Conditions during Leg M74/3

(W. T. Ochsenhirt, DWD)

In the late afternoon of 30 October 2007 R/VMETEOR left Fujairah for a test of the PARASOUND System, which had been equipped with a new software update in the harbour. The weather off Fujairah was calm with south-easterly to easterly winds of 2 Bft under a clear sky.

On 31 October at noon the technician was brought ashore. Then the new Leg M74/3 began and METEOR headed for the area of operation off the coast of Pakistan. We reached this area on 1 November with easterly winds force 2.

Meanwhile a tropical cyclone, which moved from southern India westwards along latitude 12°, had reached the coast of Yemen and southern Oman. Originating from this storm, a southeasterly swell up to 2,5 metre affected METEOR. This swell decreased not before 5 November.

During the following days the weather was generally fair with few clouds and variable winds of 2-4 Bft. With high pressure over northern Oman and northern India there were only small differences of pressure in the Arabian Sea. Light westerly winds predominated, at times the wind direction was variable. The wind speed during daytime was 1-3 Bft, at night 3-4 Bft.

In the northern area of operation on some days for shorter periods wind speeds of Bft. 5 were measured, but in the morning time the wind decreased to force 2.

Some smaller areas of low pressure over India and Pakistan had no influence on the weather in the area of operation. METEOR left this area on 22 November heading for the Maldives. The weather during the cruise was characterized by northerly winds about 3 Bft and a clear sky. Later on the wind veered northeasterly with 3-4 Bft., sometimes 4-5 Bft. South of 07°N the wind veered further easterly with 1-3 Bft. On 27 November in the morning the voyage ended in Male.

13 References

Abegg F, Hohnberg HJ, Pape T, Bohrmann G, Freitag J (in press) Development and application of pressure core sampling systems for the investigation of gas and gas hydrate bearing sediments. Deep Sea Research Part I: Oceanographic Research Papers.

Abegg F, Bohrmann G, Freitag J and Kuhs WF (2007) Fabric of gas hydrate in sediments from Hydrate Ridge - Results from ODP Leg 204 samples. Geo-Marine Letters.

Aloisi G, Pierre C, Rouchy JM, Foucher JP and Woodside J (2000) Methane-related authigenic carbonates of eastern Mediterranean Sea mud volcanoes and their possible relation to gas hydrate destabilisation. Earth and Planetary Science Letters 184(1): 321-338.

Barton ED and Hill AE (1989) Abyssal flow through the Amirante Trench (western Indian Ocean). Deep-Sea Research 36(7): 1121-1126.

Bauer S, Hitchkock GL, and Olson DB (1991) Influence of monsoonally-forced Ekman dynamics upon surface layer depth and plankton biomass distribution in the Arabian Sea. Deep-Sea Research 38(5): 531-553.

Bemis BE, Spero HJ, Bijma J, and Lea DW (1998) Reevaluation of the oxygen isotopic composition of planktonic foraminifera: experimental results and revised paleotemperature equations. Paleoceanography 13(2): 150-160.

Bernard BB, Brooks JM, Sackett WM (1976) Natural gas seepage in the Gulf of Mexico. Earth and Planetary Science Letters 31:48-54.

Berner RA (1989) Biogeochemical cycles of carbon and sulfur and their effect on atmospheric oxygen over phanerozoic time. Palaeogeography. Palaeoclimatology. Palaeoecology 73: 97–122.

Bernstein RE, Byrne RH, Betzer PR and Greco AM (1992. Morphologies and transformations of celestite in seawater: The role of acantharians in strontium and barium geochemistry. Geochim. Cosmochim. Acta, 56: 3276-3279.

Biddle JF, Lipp JS, Lever MA, Lloyd KG, Sørensen KB, Anderson R, Fredricks HF, Elvert M, Kelly TJ, Schrag DP, Sogin ML, Brenchley JE, Teske A, House CH, Hinrichs KU (2006) Heterotrophic Archaea dominate sedimentary subsurface ecosystems off Peru. Proc. Natl. Acad. Sci. 103: 3846-3851.

Boetius A, Ravenschlag K, Schubert CJ, Rickert D, Widdel F, Gieseke A, Amann R, Jorgensen BB, Witte U and Pfannkuche O (2000) A marine microbial consortium apparently mediating anaerobic oxidation of methane. Nature 407(6804): 623-626.

Bohrmann G, Greinert J, Suess E and Torres M (1998) Authigenic carbonates from the Cascadia subduction zone and their relation to gas hydrate stability. Geology 26(7): 647-650.

Bohrmann G, Pape T, participants ac (2007) Report and preliminary results of R/V Meteor cruise M72/3, Istanbul - Trabzon - Istanbul, 17 March - 23 April, 2007. Marine gas hydrates of the Eastern Black Sea. In: Bohrmann G, Pape T (eds) Berichte, Fachbereich Geowissenschaften, Universität Bremen, No. 261, Bremen, p 176.

Bohrmann G and Torres M (2006) Gas hydrates in marine sediments. In Schulz HD and Zabel M., Marine Geochemistry. 481- 512, Springer.

Brock JC, McClain CR, Luther ME, and Hay WW (1991) The phytoplankton bloom in the northwestern Arabian Sea during the southwest monsoon of 1979. Journal of Geophysical Research, C 96(11): 20623-20642.

Brock JC, McClain CR, David R, Anderson M, Prell WLand Hay, WW (1992) Southwest monsoon circulation and environments of recent planktonic foraminifera in the northwestern Arabian Sea. Paleoceanography 7: 700-813.

Bruce JG (1974) Some details of upwelling off the Somali and Arabian coasts. Journal of Marine Research 32: 419-423.

Bruce JG (1979) Eddies off the Somali Coast during the southwest monsoon. Journal of Geophysical Research, C 84(12): 7742-7748.

Campbell KA (2006) Hydrocarbon seep and hydrothermal vent paleoenvironments and paleontology: Past developments and future research directions. Palaeogeography, Palaeoclimatology, Palaeoecology 232(2-4): 362-407.

Conrad R (2005) Quantification of methanogenic pathways using stable carbon isotopic signatures: a review and a proposal. Org. Geochem. 36, 739–752.

Currie RI, Fisher AE and Hargraeves PM (1971) Arabian Sea upwelling. In: "The Biology of the Indian Ocean". (Eds. Zeitzschel B and Gerlach SA) Springer: Berlin.

DeJong KA (1982) Tectonics of the Persian Gulf, Gulf of Oman, and southern Pakistan region. In: Nain AEM, Staehli FG (eds) The Ocean Basins and Margins V 6: The Indian Ocean: 315–351.

Delisle G, Berner U (2002) Gas hydrates acting as cap rock to fluid discharge in the Makran accretionary prism? In: Clift PD, Kroon D, Gaedicke C, Craig J (eds) The Tectonic and Climatic Evolution of the Arabian Sea Region. The Geological Society of London, pp 137-146.

Delisle G (2004) The mud volcanoes of Pakistan. Environmental Geology 46:1024-1029.

D'Hondt S, Rutherford S and Spivack AJ (2002) Metabolic activity of the subsurface biosphere in deep-sea sediments. Science 295, 2067–2070.

Eglinton TI, Benitez-Nelson BC, Pearson A, McNichol AP, Bauer JE, Druffel ERM (1997) Variability in radiocarbon ages of individual organic compounds from marine sediments. Science 277: 796-799.

Elvert M, Hopmans EC, Treude T, Boetius A, Suess E (2005) Spatial variations of methanotrophic consortia at cold methane seeps: implications from a high-resolution molecular and isotopic approach. Geobiology 3: 195-209.

Faber E, Gerling P, Berner U, Sohns E (1994) Methane in ocean waters: Concentration and carbon isotope variability at East Pacific Rise and in the Arabian Sea. Environmental Monitoring and Assessment 31:139-144.

Gnibidenko HS, Svarichevskaya LV (1983) The submarine canyons of Kamchatka. Marine Geology 54: 277-307.

Grevemeyer I, Rosenberger A, Villinger H (2000) Natural gas hydrates on the continental slope off Pakistan: constraints from seismic techniques. Geophysical Journal International 140:295-310.

Harms JC, Cappel HN, Francis, DC (1984) The Makran coast of Pakistan: Its stratigraphy and hydrocarbon potential. In: Haq, BU, Milliman, JD (eds) Marine Geology and

Oceanography of Arabian Sea and Coastal Pakistan. Van Nostrand Reinhold, New York: 3-26.

Hartnett HE, Keil RG, Hedges JI (1998) Influence of oxygen exposure time on organic carbon preservation in continental margin sediments. Nature 391: 572-574.

Hedges JI and Keil RG (1995) Sedimentary organic matter preservation: an assessment and speculative synthesis. Marine Chemistry 49: 81-115.

Hedges JI, Hu FS, Devol AH, Hartnett E, Tsamakis E, Keil RG (1999) Sedimentary organic matter preservation: a test for selective degradation under oxic conditions. Am. J. Sci. 299: 529–555.

Heeschen KU, Hohnberg HJ, Haeckel M, Abegg F, Drews M, Bohrmann G (2007) In situ hydrocarbon concentrations from pressurized cores in surface sediments, Northern Gulf of Mexico. Marine Chemistry 107:498-515.

Helly JJ, Levin LA (2004) Global distribution of naturally occurring marine hypoxia on continental margins. Deep Sea Research. I 51: 1159–1168.

Heuer V, Elvert M, Tille S, Krummen M, Mollar XP, Hmelo LR, Hinrichs KU (2006) Online $\delta^{13}C$ analysis of volatile fatty acids in sediment/porewater systems by liquid chromatography-isotope ratio-mass spectrometry. Limnol. Oceanogr. Methods 4: 346-357.

Hinrichs KU, Boetius A (2002) The anaerobic oxidation of methane: New insights in microbial ecology and biogeochemistry. In Ocean Margin Systems (ed. Wefer G, Billett D, and Hebbeln D), pp. 457-477. Springer-Verlag, Berlin.

Hopmans EC, Weijers JWH, Schefuß E, Herfort L, Sinninghe Damsté JS, Schouten S (2004) A novel proxy for terrestrial organic matter in sediments based on branched and isoprenoid tetraether lipids. Earth and Planetary Science Letters 224: 107-116.

Hovland M, Talbot MR, Qvale H, Olaussen S, and Aasberg L (1987) Methane-related carbonate cements in pockmarks of the North Sea. Journal of Sedimentary Research 57(5): 881-892.

Hunting Survey Corporation Ltd. (1960) Reconnaissance geology of part of West Pakistan. Maracle Press, Oshawa, Ontario, Canada: 550 pp.

Iversen N, Jørgensen BB (1985) Anaerobic methane oxidation rates at the sulfate-methane transition in marine sediments from Kattegat and Skagerrak (Denmark). Limnol. Oceanogr. 30: 944–955.

Jochem FJ, Pollehne F and Zeitzschel (1993) Productivity regime and phytoplankton size structure in the Arabian Sea. Deep-Sea Research 40: 711-735.

Johnson GC, Warren BA and Olson DB (1991a) A deep boundary current in the Arabian Sea. Deep-Sea Research 38: 653-661.

Johnson G. C, Warren BA and Olson DB (1991b) Flow of bottom water in the Somali Basin. Deep-Sea Research 38: 637-652.

Judd AG, Hovland M, Dimitrov LI, García Gil S, Jukes V (2002) The geological methane budget at continental margins and its influence on climate change. Geofluids 2: 109-126.

Knittel K, Lösekann T, Boetius A, Kort R, Amann R (2005) Diversity and distribution of methanotrophic archaea at cold seeps. Applied and Environmental Microbiology 71: 467-479.

Kopp C, Fruehn J, Flueh ER, et al. (2000) Structure of the Makran subduction zone from wide-angle and reflection seismic data. Tectonophysics, Vol. 329, 171-191.

Kukowski N, Schillhorn T, Flueh ER, Huhn K (2000) Newly identified strike-slip plate boundary in the northeastern Arabian Sea. Geology 28(4): 355–358.

Kukowski N, Schillhorn T, Huhn K et al. (2001) Morphotectonics and mechanics of the central Makran accretionary wedge off Pakistan. Marine Geology, Vol.173, 1-19.

Kvenvolden KA (1995) A review of the geochemistry of methane in natural gas hydrate. Organic Geochemistry, 23, 997-1008.

Lammers S, Suess E (1994) An improved head-space analysis method for methane in seawater. Marine Chemistry 47:115-125.

Lu H, Seo YT, Lee JW, Moudrakovski I, Ripmeester JA, Chapman NR, Coffin RB, Gardner G and Pohlman J (2007) Complex gas hydrate from the Cascadia margin. Nature, 445 (7125), 303-306.

Megonigal JP, Hines ME, Visscher PT (2004) Anaerobic metabolism: linkages to trace gases and aerobic processes. *In*: Schlesinger, W.H. (ed), Treatise on Geochemistry Vol. 8, Biogeochemistry. Elsevier-Pergamon, Oxford: 317-424.

Milliman JD, Quraishee GS and Beg MAA (1984) Sediment discharge from the Indus river to the ocean: past, present and future. In: Marine geology and oceanography of Arabian Sea and coastal Pakistan. (Eds. Haq BU and Milliman JD) pp. 65-70. (Van Nostrand Reinhold Company Scientific and Academic Editions: New York).

Mollenhauer G, Eglinton T (2007) Diagenetic and sedimentological controls on the composition of organic matter preserved in California Borderland Basin sediments. Limnology and Oceanography, 52(2): 558-576.

Niemann H, Lösekann T, Beer D, Elvert M, Nadalig T, Knittel K, Amann R, Sauter EJ, Schlüter M, Klages M, Foucher JP, Boetius A (2006) Novel microbial communities of the Haakon Mosby mud volcano and their role as a methane sink. Nature 443: 854-858.

Niewöhner C, Hensen C, Kasten S, Zabel M, Schulz HD (1998) Deep sulfate reduction completely mediated by anaerobic methane oxidation in sediments of the upwelling area off Namibia. Geochimica et Cosmochimica Acta 62, 455-464.

Orphan V, House CH, Hinrichs KU, McKeegan KD, DeLong EF (2002) Multiple archaeal groups mediate methane oxidation in anoxic cold seep sediments. PNAS 99: 7663-7668.

Parkes RJ, Cragg BA, Banning N, Brock F, Webster G et al. (2007) Biogeochemistry and biodiversity of methane cycling in subsurface marine sediments (Skagerrak, Denmark). Environ. Microbiol. 9, 1146–1161.

Peckmann J, Reimer A, Luth U, Luth C, Hansen BT, Heinicke C, Hoefs Jand Reitner J (2001) Methane-derived carbonates and authigenic pyrite from the northwestern Black Sea. Marine Geology 177(1-2): 129-150.

Peckmann J and Thiel V (2004) Carbon cycling at ancient methane-seeps. Chemical Geology 205(3-4): 443-467.

Pierre C and Fouquet Y (2007) Authigenic carbonates from methane seeps of the Congo deep-sea fan. Geo-Marine Letters 27(2): 249-257.

Pratson LF, Haxby WF (1996) What is the slop of the U.S. Continental slope? Geology 24, 3-6.

Qasim SZ (1982) Oceanography of the northern Arabian Sea. Deep-Sea Research 29: 1041-1068.

Reeburgh WS (1996) "Soft spots" in the global methane budget. In Microbial Growth on C1 Compounds (ed. Lidstrom ME and Tabita FR): 334-342. Kluwer Academic Publishers.

Sauter EJ, Muyakshin SI, Charlou J-L, Schluter M, Boetius A, Jerosch K, Damm E, Foucher J-P, Klages M (2006) Methane discharge from a deep-sea submarine mud volcano into the upper water column by gas hydrate-coated methane bubbles. Earth and Planetary Science Letters 243:354-365.

Schmaljohann R, Drews M, Walter S, Linke P, von Rad U, Imhoff SJF (2001) Oxygen minimum zone sediments in the northeastern Arabian Sea off Pakistan: a habitat for the bacterium *Thioploca*. Marine Ecology Progress Series 211: 27-42.

Schmitt M, Faber E, Botz R, Stoffers P (1991) Extraction of methane from seawater using ultrasonic vacuum degassing. Analytical Chemistry 63:529-532.

Schubel JR (1984) Estuarine circulation and sedimentation: an overview. In Marine geology and oceanography of Arabian Sea and coastal Pakistan. (Eds. Haq BU and Milliman JD) pp. 113-36. (Van Nostrand Reinhold Company Scientific and Academic Editions: New York).

Shapiro GI and Meschanov SL (1991) Distribution and spreading of Red Sea Water and salt lens formation in the northwest Indian Ocean. Deep-Sea Research 38: 21-34.

Sloan ED and Koh CA (2007) Clathrate hydrates of natural gases, 3 ed., 752 pp., CRC Press.

Smith SL, Banse K, Cochran JK, Codispoti LA, Ducklow HW, Luther ME, Olson DB, Peterson WT, Prell WL, Surgi N, Swallow JC, and Wishner K (1991) "U.S. JGOFS: Arabian Sea process study". U.S. Planning Report Edn. (Woods Hole Oceanographic Institution: Woods Hole, Massachusetts).

Sondhi VP (1947) The Makran Earthquake, 28 November 1945, the birth of new islands. Indian Minerals 1: 146–154. Ican Association of Petroleum Geologists Memoir 34: 499–518.

Staubwasser M, Sirocko F (2001) On the formation of laminated sediments on the continental margin off Pakistan: the effects of sediment provenance and sediment redistribution. Marine Geology 72: 43-56.

Sturt HF, Summons RE, Smith K, Elvert M, Hinrichs KU, (2004) Intact polar membrane lipids in prokaryotes and sediments deciphered by high-performance liquid chromatography/electrospray ionization multistage mass spectrometry - new biomarkers for biogeochemistry and microbial ecology. Rapid Communications in Mass Spectrometry 18: 617-628.

Treude T, Boetius A, Knittel K, Wallmann K, Jørgensen BB (2003) Anaerobic oxidation of methane above gas hydrates (Hydrate Ridge, OR). Mar. Ecol. Prog. Ser. 264: 1-14.

Underwood MB (1991) Submarine canyons, unconfined turbidity currents, and sedimentary bypassing of forearc region. Review in Aquatic Sciences 4 (2-3): 149-200.

Von Rad U, Rösch H, Berner U, Geyh M, Marchig V and Schulz H (1996) Authigenic carbonates derived from oxidized methane vented from the Makran accretionary prism off Pakistan. Marine Geology 136(1-2): 55-77.

Von Rad U, Doose H, cruise participants (1998) FS. SONNE Cruise Report SO 130, MAKRAN II, Hannover. BGR Rep Arch No 117368.

Von Rad U, Schaaf M, Michels KH, Schulz H, Berger WH, Sirocko F (1999) A 5000-yr Record of Climate Change in Varved Sediments from the Oxygen Minimum Zone off Pakistan, Northeastern Arabian Sea. Quat. Res. 51: 39-53.

Von Rad U, Berner U, Delisle G, Doose-Rolinski H, Fechner N, Linke P, Lückge A, Roeser HA, Schmaljohann R, Wiedicke M, Sonne 122/130 Scientific Parties (2000) Gas and fluid venting at the Makran Accretionary wedge off Pakistan. Geo-Marine Letters 20: 10–19.

Von Stackelberg M and Müller HR (1954) Feste Gashydrate II, Zeitschrift für Elektrochemie, 58, 25-39.

Wakeham SG, Canuel EA (2006) Degradation and preservation of organic matter in marine sediments. In: Hutzinger O (Ed.-in-Chief), The Handbook of Environmental Chemistry Vol. 2: Reactions and Processes. Part N: Marine Organic Matter: Biomarkers, Isotopes and DNA (Volkman JK ed.). Springer-Verlag, Berlin: 295–321.

White RS (1982) Deformation of the Makran Accretionary sediment prism in the Gulf of Oman (north-west Indian Ocean). In: Leggett JK (ed) Trench-forearc geology: sedimentation and tectonics on modern and ancient active margins. Geological Society, London: 351-372.

Whiticar MJ, Faber E, Schoell M (1986) Biogenic methane formation in marine and freshwater environments: CO_2 reduction vs. acetate fermentation - isotope evidence. Geochimica et Cosmochimica Acta 50:693-709.

Wiedicke M, Neben S, Spiess V, (2001) Mud volcanoes at the front of the Makran Accretionary complex, Pakistan. Marine Geology 172: 57–73.

Wyrtki K (1971) Oceanographic atlas of the international Indian Ocean expedition. (National Science Foundation, U.S. Government Printing Office: Washington D.C.).

Wyrtki K (1973) Physical oceanography of the Indian Ocean. In: Zeitschel, B. (ed.), The Biology of the Indian Ocean. Ecological Studies, Vol. 3. Springer-Verlag, Berlin: 18–36.

Yamamoto S, Alcauskas JB, Crozier TE (1976) Solubility of methane in distilled water and seawater. J. Chem. Eng. Data 21(1): 78-80.

Zonneveld KAF (2004) Potential use of stable oxygen isotope composition of *Thoracosphaera heimii* for upper water column (thermocline) temperature reconstruction. Marine Micropaleontology 50(3/4): 307-317.

Zonneveld KAF, Mackensen A and Baumann KH (2007) Stable oxygen isotopes of *Thoracosphaera heimii* (dinophyceae) in relationship to temperature; a culture experiment. Marine Micropaleontology 64: 80-90.

Appendix 1: Station List

RV METEOR cruise M74/3 (Fujairah-Male)							Begin / on seafloor			End / off seafloor			Recovery
Date	St. No.	St. No.			Start Sci:	End Sci:	Latitude	Longitude	Water	Latitude	Longitude	Water	Recovery
	GeoB		Instruments	Location	Program	Program	N°	E°	depth (m)	N°	E°	depth (m)	Remarks
02.11.07	12301	ROV-01	ROV-179	Nascent Ridge	06:22	10:31	24:11.750	62:44.308	2830	24:11.741	62:44.258	2872	dead recovery
	12301-1		GBS-1	Nascent Ridge	09:03		24:11.748	62:44.307	2876				
	12301-2		T-stick-1	Nascent Ridge	09:19	09:38	24:11.750	62:44.309	2876				
	12301-3		PC-1	Nascent Ridge	09:26		24:11.749	62:44.308	2876				PC-11
	12301-4		PC-2	Nascent Ridge	09:29		24:11.749	62:44.308	2876				PC-28
	12301-5		PC-3	Nascent Ridge	09:32		24:11.750	62:44.308	2876				PC-35
	12301-6		PC-4	Nascent Ridge	09:35		24:11.750	62:44.308	2876				PC-29
	12301-7		T-stick-2	Nascent Ridge	09:40	09:55	24:11.750	62:44.308	2876				
	12302	CTD-1		Nascent Ridge	13:12	15:45	24:11.751	62:44.307	2868	24:11.726	62:44.320	2859	15 bottles closed, Posidonia
	12303	GC-1		Nascent Ridge	17:00		24:11.749	62:44.309	2860				recovery 4,34 m; plastic hose; gas hydrates
	12304	CTD-2		Nascent Ridge	18:50	19:15	24:10.423	62:45.901	2960				17 bottles closed
03.11.07	12305	GC-2		Nascent Ridge	02:17		24:10.442	62:45.900	2949				recovery > 6m; liner; no posidonia
	12306	GC-3		Nascent Ridge	06:42		24:11.761	62:44.311	2861				recovery 3,8 m; pore water; posidonia
	12307-1	CTD-3		background deep sea	09:06	11:37	24:06.024	62:52.034	3230				All bottles closed
	12307-2	CTD-4		background deep sea	12:00	12:20	24:05.993	62:52.010	3225				17 bottles closed; exploration depth 150 m
04.11.07	12308-1	CTD-5		OMZ 1590	01:31	18:06	24:43.087	62:59.500	1594				18 bottles closed; Posidonia
	12308-2	CTD-6		OMZ 1590	02:09	02:36	24:43.103	62:59.490	1591				17 bottles closed
	12308-3	MUC-1		OMZ 1590	03:47		24:43.115	62:59.504	1574				liners closed
	12308-4	GC-4		OMZ 1590	05:15		24:43.114	62:59.502	1587				recovery 3,5 m; liner; pore water; no posidonia
	12309-1	CTD-7		OMZ 950	07:33	09:00	24:52.326	62:59.869	955				15 bottles closed
	12309-2	CTD-8		OMZ 950	09:32	09:56	24:52.320	62:59.865	956				18 bottles closed
	12309-3	MUC-2		OMZ 950	10:47		24:52.322	62:59.859	962				all liners closed
	12310	TV-sled-9		Flare 7	15:16	18:50	24:38.613	62:44.803	1669	24:38.366	62:44.334	1664	seep communities found
	12311	TV-sled-10		Flare 6, Pockmark	21:29	00:02	24:35.015	62:56.272	1770	24:33.492	62:56.273	1935	seep communities found at Flare 6, not at Pockmark
05.11.07	12312-1	CTD 9		OMZ 650	02:55	03:55	24:55.051	63:01.166	633				all bottles closed
	12312-2	CTD 10		OMZ 650	04:22	04:39	24:53.068	63:01.644	655				all bottles closed
	12312-3	MUC-3		OMZ 650	05:38		24:53.072	63:01.641	654				all liners closed
	12312-4	GC 5		OMZ 650	06:47		24:53.072	63:01.642	658				recovery 4,5 m; liner; take home; no posidonia
	12312-5	GC 6		OMZ 650	08:19		24:53.071	63:01.643	647				recovery 4 m; liner; pore water; no posidonia
	12313	ROV-02	ROV-180	Flare 2	10:04	15:41	24:50.787	63:01.483	1032	24:50.829	63:01.419	1038	
	12313-1		ISPS	Flare 2	10:39		24:50.787	63:01.419	1023				deployment of ISPS
	12313-2		PC-1	Flare 2	10:49		24:50.787	63:01.419	1023				recovery during ROV-181 / GeoB 12315
	12313-3		GBS-2	Flare 2	11:41		24:50.799	63:01.420	1024				
	12313-4		BC	Flare 2	12:06		24:50.799	63:01.420	1023				
	12313-5		PC-2	Flare 2	14:34		24:50.827	63:01.420	1038				PC-14
	12313-6		PC-3	Flare 2	14:37		24:50.827	63:01.420	1038				PC-3

Appendix 1: Continuation Station List

RV METEOR cruise M74/3 (Fujairah-Male)							Begin / on seafloor			End / off seafloor			Recovery
Date	St. No.	St. No.			Start Sci:	End Sci:	Latitude	Longitude	Water	Latitude	Longitude	Water	
	GeoB		Instruments	Location	Program	Program	N°	E°	depth (m)	N°	E°	depth (m)	Remarks
	12313-7		PC-4	Flare 2	14:41		24:50.827	63:01.419	1038				PC-4
	12313-8		GBS-3	Flare 2	14:57		24:50.827	63:01.419	1038				
	12313-9		Marker 9	Flare 2	15:08		24:50.828	63:01.420	1038				
	12313-10		PC-5	Flare 2	15:20		24:50.828	63:01.420	1038				PC-7
	12313-11		PC-6	Flare 2	15:25		24:50.828	63:01.419	1038				PC-15
	12313-12		PC-7	Flare 2	15:26		24:50.828	63:01.419	1038				PC-33
	12313-13		PC-8	Flare 2	15:34		24:50.829	63:01.419	1038				PC-24
	12313-14		Net	Flare 2	15:38		24:50.829	63:01.419	1038				
	12314-1	GC 7		Flare 2	17:35		24:50.797	63:01.423	960				recovery 1 carbonate; no gas hydrates; posidonia
06.11.07	12314-2	CTD-11		Flare 2	02:06	03:31	24:50.801	63:01.416	1023				Posidonia
	12314-3	CTD-12		Flare 2	04:02	04:17	24:50.796	63:01.402	1019				All bottles closed
	12315	ROV-3	ROV-181	Flare 2	05:14	15:02	24:50.784	63:01.443	1019	24:50.789	63:01.417	1025	
	12315-1		OS	Flare 2	05:36		24:50.753	63:01.436	1025				recovery during ROV-188 / GeoB 12328
	12315-2		GBS-4	Flare 2	06:24		24:50.753	63:01.436	1025				yellow GBS
	12315-3		Carbonate-1	Flare 2	13:22		24:50.784	63:01.422	1025				
	12315-4		PC-1	Flare 2	13:53		24:50.753	63:01.439	1025				PC 36
	12315-5		PC-2	Flare 2	13:57		24:50.753	63:01.439	1025				PC 19
	12315-6		PC-3	Flare 2	14:03		24:50.753	63:01.439	1025				PC 5
	12315-7		PC-4	Flare 2	14:24		24:50.753	63:01.439	1025				PC 28
	12315-8		PC-5	Flare 2	14:29		24:50.753	63:01.439	1025				PC 11
	12315-9		PC-6	Flare 2	14:34		24:50.753	63:01.439	1025				PC 2
	12315-10		PC-7	Flare 2	14:39		24:50.753	63:01.439	1025				PC 23
	12315-11		PC-8	Flare 2	14:51		24:50.789	63:01.417	1025				PC 22
	12315-12		ISPS	Flare 2		14:55	24:50.789	63:01.417	1025				recovery of ISPS (from ROV-180 /GeoB 12313)
	12316-1	GC 8		Flare 2	16:57		24:50.795	63:01.422	1021				recovery 0,3 m; carbonate; no gas hydrates; posidonia
07.11.07	12316-2	GC 9		Flare 2	02:42		24:50.798	63:01.416	1021				recovery 1,03 m; gas hydrates + carbonates; posidonia
	12317	ROV-4	ROV-182	Flare 7	09:30	16:22	24:38.624	62:44.660	1652	24:38.633	62:44.644	1651	
	12317-1		GBS-5	Flare 7	13:56		24:38.649	62:44.254	1654				yellow GBS
	12317-2		PC-1	Flare 7	15:49		24:38.633	62:44.645	1651				PC-14
	12317-3		Clams	Flare 7	16:22		24:38.633	62:44.644	1651				
	12318-1	CTD-13		Flare 7	17:58	19:41	24:38.641	62:44.261	1642				all bottles closed; Posidonia
	12318-2	CTD-14		Flare 7	20:07	20:31	24:38.642	62:44.219	1641				all bottles closed
08.11.07	12309-4	MUC-4		OMZ 950	02:42		24:52.292	62:59.839	957				
	12319	ROV-5	ROV-183	Flare 1	04:37	07:39	24:53.606	63:01.436	575	24:53.631	63:01.422	572	dive terminated earlier than anticipated due to oil leakage
	12319-1		T-stick	Flare 1	06:44	06:54	24:53.629	63:01.418	572				
	12319-2		ISPS	Flare 1	07:23		24:53.631	63:01.423	572				ISPS launched - recovery next dive
	12309-5	GC 10		OMZ 950	09:16		24:52.301	62:59.872	956				recovery 5,60 m; pore water

Appendix 1: Continuation Station List

RV METEOR cruise M74/3 (Fujairah-Male)														
							Begin / on seafloor			End / off seafloor			Recovery	
Date	St. No.	St. No.			Start Sci:	End Sci:	Latitude	Longitude	Water	Latitude	Longitude	Water		
	GeoB		Instruments	Location	Program	Program	N°	E°	depth (m)	N°	E°	depth (m)	Remarks	
	12316-3	GC-11		Flare 2	10:49		24:50.789	63:01.422	1020				recovery 2,18 m; gas hydrates	
	12316-4	GC-12		Flare 2	12:39		24:50.788	63:01.424	1019				recovery 1,63 m; gas hydrates	
	12316-5	GC-13		Flare 2	13:43		24:50.798	63:01.428	1024				no recovery	
09.11.07	12308-5	MUC-5		OMZ 1590	03:02	03:32	24:43.109	62:59.497	1586				bottles closed	
	12320	ROV-6	ROV-184	Flare 1	05:29	15:49	24:53.491	63:01.469	552	24:53.630	63:01.425	580		
	12320-1		T-stick	Flare 1	08:29	08:49	24:53.636	63:01.405	592					
	12320-2		GBS-6	Flare 1	09:23		24:53.636	63:01.406	591				red GBS	
	12320-3		GBS-7	Flare 1	11:17		24:53.633	63:01.405	590				yellow GBS	
	12320-4		PC-1	Flare 1	14:04		24:53.634	63:01.404	551				PC 22	
	12320-5		PC-2	Flare 1	14:08		24:53.634	63:01.404	551				PC 21	
	12320-6		PC-3	Flare 1	14:10		24:53.634	63:01.404	551				PC 20	
	12320-7		PC-4	Flare 1	14:12		24:53.634	63:01.404	551				PC 15	
	12320-8		PC-5	Flare 1	14:22		24:53.634	63:01.404	551				PC 3	
	12320-9		PC-6	Flare 1	14:25		24:53.634	63:01.404	551				PC 29	
	12320-10		PC-7	Flare 1	14:26		24:53.634	63:01.404	551				PC 32	
	12320-11		KIPS-1	Flare 1	14:55		24:53.631	63:01.405	557				bubble site	
	12320-12		KIPS-2	Flare 1	15:17		24:53.631	63:01.405	557				Water column	
	12320-13		PC-8	Flare 1	15:36		24:53.630	63:01.425	580				PC 7	
	12319-2		ISPS	Flare 1		15:38	24:53.630	63:01.425	580				recovery of ISPS (GeoB 12319-2; ROV-183)	
10.11.07	12321-1	MUC-6		OMZ 1400	02:45	03:30	24:46.002	62:59.973	1425				bottles closed	
	12322	ROV-7	ROV-185	Flare 7	06:04	15:28	24:38.664	62:44.273	1657	24:38.555	62:44.376	1653		
	12322-1		KIPS-1	Flare 7	12:26		24:38.643	62:44.261	1652					
	12322-2		KIPS-2	Flare 7	12:34		24:38.643	62:44.261	1652					
	12322-3		BM-1	Flare 7	12:18		24:38.644	62:44.261	1652					
	12322-4		GBS-8	Flare 7	12:56		24:38.644	62:44.260	1652					
	12322-5		PC-1	Flare 7	14:30		24:38.610	62:44.303	1649				PC-11	
	12322-6		PC-2	Flare 7	15:16		24:38.579	62:44.344	1649				PC-19	
	12323	TV-sled-11		Flare 11	21:12	00:45	24:44.180	62:59.432	1484	24:44.30	62:59.071	1478	Flare 11 and 2 carbonate sites found	
11.11.07	12321-2	CTD-15		OMZ 1400	02:02	03:32	24:46.010	62:59.996	1424				all bottles closed	
	12321-3	CTD-16		OMZ 1400	03:59	04:17	24:46.005	62:59.986	1423				All bottles closed	
	12324	ROV-8	ROV-186	Flare 6	06:58	16:43	24:34.957	62:56.289	1790	24:34.816	62:56.302	1822		
	12324-1		ISPS	Flare 6	08:53	16:40	24:34.820	62:56.305	1822					
	12324-2		Carbonate	Flare 6	09:34		24:34.808	62:56.324	1823				3 carbonate pieces	
	12324-3		T-stick-1	Flare 6	12:14	12:15	24:34.809	62:56.325	1823					
	12324-4		T-stick-2	Flare 6	13:28	13:38	24:34.841	62:56.522	1835					
	12324-5		T-stick-3	Flare 6	14:22	14:38	24:34.840	62:56.522	1835					
	12324-6		PC-1	Flare 6	14:47		24:34.840	62:56.522	1835				PC-21	
	12324-7		PC-2	Flare 6	14:55		24:34.839	62:56.521	1835				PC-22	
	12324-8		PC-3	Flare 6	14:56		24:34.840	62:56.521	1835				PC-15	
	12324-9		PC-4	Flare 6	15:00		24:34.840	62:56.521	1835				PC-20	
	12324-10		PC-5	Flare 6	15:34		24:34.841	62:56.525	1836				PC-36	

Appendix 1: Continuation Station List

RV METEOR cruise M74/3 (Fujairah-Male)														
Date	St. No.	St. No.			Start Sci	End Sci	Begin / on seafloor			End / off seafloor			Recovery	
	GeoB		Instruments	Location	Program	Program	N°	E°	depth (m)	N°	E°	depth (m)	Remarks	
	12324-11		PC-6	Flare 6	15:35		24:34.842	62:56.524	1836				PC-7	
	12324-12		PC-7	Flare 6	15:37		24:34.840	62:56.524	1836				PC-5	
	12324-13		PC-8	Flare 6	15:39		24:34.840	62:56.523	1836				PC-17	
	12325	TV-sled-12		Flare 4	20:45	01:55	24:17.832	62:50.341	1951	24:17.983	62:49.669	2186	seep communities and 3 flares found	
12.11.07	12326	ROV-9	ROV-187	Nascent Ridge	05:37	15:49	24:11.771	62:44.324	2526	24:11.744	62:44.306	2860		
	12326-1		ISPS	Nascent Ridge	06:09	15:47	24:11.745	62:44.306	2876					
	12326-2		GBS-9	Nascent Ridge	08:44		24:11.750	62:44.418	2874					
	12326-3		Marker 1	Nascent Ridge	08:59		24:11.749	62:44.418	2874					
	12326-4		GBS-10	Nascent Ridge	09:45		24:11.745	62:44.424	2873					
	12326-5		Marker 8	Nascent Ridge	10:08		24:11.746	62:44.424	2873					
	12326-6		PC-1	Nascent Ridge	14:03		24:11.750	62:44.420	2873				PC-2	
	12326-7		PC-2	Nascent Ridge	14:07		24:11.749	62:44.420	2873				PC-28	
	12326-8		PC-3	Nascent Ridge	14:14		24:11.740	62:44.421	2873				PC-24	
	12326-9		PC-4	Nascent Ridge	14:20		24:11.749	62:44.420	2873				PC-1	
	12326-10		PC-5	Nascent Ridge	15:01		24:11.743	62:44.307	2875				PC-11	
	12326-11		PC-6	Nascent Ridge	15:07		24:11.743	62:44.306	2875				PC-32	
	12326-12		PC-7	Nascent Ridge	15:10		24:11.742	62:44.306	2875				PC-33	
	12326-13		PC-8	Nascent Ridge	15:20		24:11.742	62:44.307	2875				PC-13	
	12327	GC-14		Nascent Ridge	19:23		24:11.747	62:44.428	2860				recovery 2,56 m, no gas hydrates; posidonia	
13.11.07	12328	ROV-10	ROV-188	Flare 2	05:39	15:00	24:50.796	63:01.445	1047	24:50.754	63:01.436	1024		
	12328-1		GBS-11	Flare 2	12:42		24:50.699	63:01.445	1028					
	12328-2		PC-1	Flare 2	14:22		24:50.738	63:01.443	1025				PC-36	
	12328-3		PC-2	Flare 2	14:25		24:50.738	63:01.443	1025				PC-7	
	12328-4		PC-3	Flare 2	14:30		24:50.738	63:01.443	1025				PC-15	
	12328-5		PC-4	Flare 2	14:33		24:50.738	63:01.443	1025				PC-20	
	12328-6		PC-5	Flare 2	14:44		24:50.738	63:01.443	1025				PC-17	
	12328-7		PC-6	Flare 2	14:44		24:50.738	63:01.443	1025				PC-21	
	12328-8		PC-7	Flare 2	14:42		24:50.738	63:01.443	1025				PC-9	
	12328-9		PC-8	Flare 2	14:41		24:50.738	63:01.443	1025				PC-22	
14.11.07	12329-1	CTD-17		OMZ 1000	04:14	05:35	24:50.754	63:01.437	1025				all bottles closed; Posidonia	
	12329-2	CTD-18		OMZ 1000	06:11	06:29	24:50.752	63:01.426	1022				all bottles closed	
	12330	GC-15		Nascent Ridge	12:04		24:11.744	62:44.308	2856				recovery 1,96 m; Posidonia	
	12331-1	MUC-7		Nascent Ridge	14:45		24:11.507	62:46.502	2831				liners full	
	12332	GC-16		Background	19:04		24:17.482	62:57.586	2036				recovery 5,87 m	
15.11.07	12316-6	GC-17		Flare 2	02:49		24:50.781	63:01.411	1004				no recovery; Posidonia	
	12316-7	GC-18		Flare 2	03:49		24:50.780	63:01.410	1019				no recovery; Posidonia	
	12333	ROV-11	ROV-189	Flare 2	05:12	07:12	24:50.745	63:01.448	1029	24:50.800	63:01.421	1024		
	12333-1		BM-2	Flare 2	06:17		24:50.797	63:01.420	1023				bubble escape record (2 sec)	
	12333-2		GBS-12	Flare 2	06:52		24:50.797	63:01.420	1024					
	12334	ROV-12	ROV-190	Flare 3	10:40	11:45	24:37.267	63:02.617	1552	24:37.219	63:02.530	1539	dive terminated earlier than anticipated due to electricity problem	

Appendix 1: Continuation Station List

RV METEOR cruise M74/3 (Fujairah-Male)							Begin / on seafloor			End / off seafloor			Recovery
Date	St. No.	St. No.			Start Sci:	End Sci:	Latitude	Longitude	Water	Latitude	Longitude	Water	Recovery
	GeoB		Instruments	Location	Program	Program	N°	E°	depth (m)	N°	E°	depth (m)	Remarks
	12321-4	GC-19		OMZ 1400	14:48		24:46.002	62:59.980	1419				pore water
	12335	GC-20		Background	16:27		24:43.100	62:59.511	1594				recovery 4,45 m
	12336	GC 21		Background	18:17		24:47.777	63:01.471	1263				recovery 4,47 m
16.11.07	12337-1	CTD-19		Flare 7	02:06	04:29	24:38.650	62:44.248	1648	24:38.610	62:44.540	1639	all bottles closed; Posidonia but probe drifted
	12337-2	CTD-20		Flare 7	04:59	05:15	24:38.649	62:44.237	1650				all bottles closed
	12338	ROV-13	ROV-191	Flare 7	06:29	16:01	24:38.504	62:44.205	1669				
	12338-1		Carbonate-1	Flare 7	07:01		24:38.544	62:44.241	1656				Carbonate, sponges and tube worms
	12338-2		Carbonate-2	Flare 7	07:51		24:38.556	62:44.246	1656				
	12338-3		Carbonate-3	Flare 7	08:10		24:38.556	62:44.246	1656				
	12338-4		Net	Flare 7	08:58		24:38.617	62:44.257	1652				
	12338-5		KIPS-1	Flare 7	10:27		24:38.649	62:44.255	1654				
	12338-6		KIPS-2	Flare 7	10:41		24:38.649	62:44.254	1654				
	12338-7		KIPS-3	Flare 7	10:48		24:38.649	62:44.254	1654				
	12338-8		KIPS-4	Flare 7	11:02		24:38.649	62:44.254	1654				
	12338-9		KIPS-5	Flare 7	11:11		24:38.649	62:44.253	1654				
	12338-10		KIPS-6	Flare 7	11:23		24:38.648	62:44.254	1654				
	12338-11		GBS-13	Flare 7	11:50	14:21	24:38.649	62:44.253	1654	24:11.740	62:44.300	1875	yellow GBS
	12338-12		BC-1	Flare 7	12:40		24:38.650	62:44.253	1654				
	12338-13		Carbonate-4	Flare 7	12:49		24:38.563	62:44.286	1656				
17.11.07	12331-2	GC-22		Nascent Ridge	03:00		24:11.498	62:46.505	2838				pore water
	12339	ROV-14	ROV-192	Nascent Ridge	06:26	14:21	24:11.746	62:44.307	2876	24:11.740	62:44.301	2875	
	12339-1		GBS-14	Nascent Ridge	13:12		24:11.742	62:44.301	2875				yellow GBS
	12339-2		GBS-15	Nascent Ridge	13:38		24:11.742	62:44.301	2875				red GBS; sampled water
	12339-3		PC-1	Nascent Ridge	13:49		24:11.742	62:44.300	2875				PC-24
	12339-4		PC-2	Nascent Ridge	13:51		24:11.742	62:44.302	2875				PC-6
	12339-5		PC-3	Nascent Ridge	14:03		24:11.741	62:44.300	2875				PC-28
	12339-6		PC-4	Nascent Ridge	14:06		24:11.740	62:44.301	2875				PC-11
	12339-7		PC-5	Nascent Ridge	14:09		24:11.741	62:44.300	2875				PC-22
	12339-8		PC-6	Nascent Ridge	14:13		24:11.740	62:44.301	2875				PC-9
	12339-9		PC-7	Nascent Ridge	14:16		24:11.740	62:44.300	2875				PC-13
	12339-10		PC-8	Nascent Ridge	14:18		24:11.740	62:44.301	2875				PC-29
	12340	CTD-21		Nascent Ridge	18:41		24:11.747	62:44.307	2859				all bottles closed; Posidonia
	12341	GC-23		Nascent Ridge	20:37		24:11.746	62:44.308	2861				recovery 3,60 m; Posidonia; hydrates
18.11.07	12342-1	GC-24		Flare 2	02:26		24:50.799	63:01.420	1020				barrel broken: no recovery
	12342-2	GC-25		Flare 2	04:35		24:50.799	63:01.420	1018				hydrates; recovery ca. 40 cm; Posidonia
	12343	ROV-15	ROV-193	Flare 2	05:47	14:22	24:50.705	63:01.453	1031	24:50.692	63:01.450	1030	
	12343-1		T-stick-1	Flare 2	06:08	06:20	24:50.697	63:01.446	1030				
	12343-2		ISPS	Flare 2	06:18	14:15	24:50.696	63:01.446	1030				
	12343-3		GBS-16	Flare 2	09:18		24:50.844	63:01.415	1040				
	12344	CTD-22		Flare 2	16:21	17:55	24:50.837	63:01.412	1011				bottles closed; Posidonia

Appendix 1: Continuation Station List

RV METEOR cruise M74/3 (Fujairah-Male)														
Date	St. No.	St. No.			Start Sci:	End Sci:	Begin / on seafloor			End / off seafloor			Recovery	
	GeoB		Instruments	Location	Program	Program	Latitude N°	Longitude E°	Water depth (m)	Latitude N°	Longitude E°	Water depth (m)	Remarks	
	12345	TV-sled-13		Flare 11	19:56	21:08	24:44.619	62:59.150	1477	24:44.499	62:58.231	1514	clams, carbonate; flare in Parasound	
19.11.07	12346	TV-sled-14		Canyon wall slump	00:04	01:02	24:45.610	63:09.309	1236	24:45.601	63:08.800	1527		
	12347	CTD-23		Flare 1	03:57	04:57	24:53.636	63:01.401	604				all bottles closed; Posidonia	
	12348	ROV-16	ROV-194	Flare 11	08:08	13:08	24:44.515	62:58.639	1465	24:44.548	62:58.914	1463		
	12348-1		Carbonate-1	Flare 11	10:03		24:44.476	62:58.633	1475					
	12348-2		Carbonate-2	Flare 11	10:39		24:44.486	62:58.683	1475					
	12348-3		Carbonate-3	Flare 11	11:09		24:44.520	62:58.731	1469					
	12321-5	MUC-8		OMZ 1400	15:55		24:46.007	62:59.973	1428				all liners full	
	12349	GC-26		Background	17:40		24:52.323	62:59.852	960				recovery 4,25 m	
	12350	GC-27		Background	19:37		24:53.722	63:16.035	353					
20.11.07	12351	GC-28		Flare-1	02:41		24:53.650	63:01.409	592				recovery 3,22 m, pore water	
	12352	ROV-17	ROV-195	Flare 4	07:39	15:27	24:17.909	62:50.412	1946	24:17.929	62:50.098	1983		
	12352-1		Kips-1	Flare 4	10:38		24:17.932	62:50.081	1985				Sample 1	
	12352-2		Kips-2	Flare 4	10:40		24:17.933	62:50.081	1984				Sample 3	
	12352-3		Kips-3	Flare 4	10:47		24:17.934	62:50.081	1984				Sample 4	
	12352-4		Kips-4	Flare 4	11:10		24:17.934	62:50.081	1984				Samples 5, 6	
	12352-5		Kips-5	Flare 4	11:21		24:17.933	62:50.081	1984				Samples 7, 8, 9	
	12352-6		Kips-6	Flare 4	11:28		24:17.934	62:50.082	1984				Samples 10,11	
	12352-7		PC-1	Flare 4	11:41		24:17.933	62:50.082	1984				PC-17	
	12352-8		BC-1	Flare 4	13:57		24:17.930	62:50.098	1983					
	12352-9		T-stick-1	Flare 4	14:28	14:40	24:17.929	62:50.098	1983					
	12352-10		GBS-17	Flare 4	15:15		24:17.929	62:50.097	1983				GBS red	
21.11.07	12353	ROV-18	ROV-196	Flare 15	09:54	16:53	24:48.409	63:59.650	733	24:48.445	63:59.646	734		
	12353-1		Net	Flare 15	11:32		24:48.463	63:59.649	730					
	12353-2		GBS-18	Flare 15	14:07		24:48.458	63:59.649	732				GBS yellow	
	12353-3		PC-1	Flare 15	14:42		24:48.458	63:59.649	732				PC-15	
	12353-4		PC-2	Flare 15	14:44		24:48.457	63:59.649	732				PC-4	
	12353-5		PC-3	Flare 15	14:48		24:48.457	63:59.649	732				PC-6	
	12353-6		PC-4	Flare 15	14:49		24:48.458	63:59.650	732				PC-2	
	12353-7		Carbonate-1	Flare 15	15:22		24:48.457	63:59.654	731					
	12353-8		Carbonate-2	Flare 15	15:34		24:48.459	63:59.654	731					
	12353-9		Carbonate-3	Flare 15	15:54		24:48.467	63:59.650	730					
	12353-10		Carbonate-4	Flare 15	16:09		24:48.467	63:59.647	731					
	12353-11		Carbonate-5	Flare 15	16:30		24:48.445	63:59.644	734					
	12354-1	CTD-24		Flare 15	17:52	18:51	24:48.455	63:59.657	733				all bottles closed	
	12354-2	CTD-25		Flare 15	19:43	20:11	24:48.454	63:59.643	734				all bottles closed	

Appendix 1: Continuation Station List

Abbreviations:

SL: Gravity corer
TV-sled: TV-sled
MUC: Multicorer
MIC: Minicorer
ROV: Remotely operated vehicle QUEST
CTD: CTD with water-sampling rosette

ROV samples / tools:

Push core 1,2,3...
Nets
T-stick 1,2,3
Gas bubble sampler (GBS) 1-2
Bubble catcher (BC)
Marker
In-situ pore water sampler (ISPS)
Osmo-sampler (OS)
Bubble-meter (BM)

Appendix 2: CTD stations

Date	St. No.	St. No.		Start Sci:	End Sci:	Latitude	Longitude	Water										Bottle depth (m)									remarks
	GeoB		Location	Program	Program	N°	E°	depth (m)	1	2	3	4	5	6	7	8	9	10	11	12	13	14	15	16	17	18	
02.11.07	12302	CTD-1	Nascent Ridge	13:12	16:46	24.11.751	62:44.307	2868	2800	2750	2700	2650	2600	2550	2500	2450	2400	2300	2100	1900	1700	1500	1000	500	50	10	Posidonia
02.11.07	12304	CTD-2	Nascent Ridge	18:50	19:15	24:10.423	62:45.901	2960	150	150	150	60	60	60	45	45	45	38	38	38	30	30	30	20	20	20	
03.11.07	12307-1	CTD-3	background deep sea	09:06	11:37	24:06.024	62:52.034	3230	3190	3150	3100	3050	3000	2900	2800	2700	2600	2500	2300	2100	1900	1600	1100	500	10	10	
03.11.07	12307-2	CTD-4	background deep sea	12:00	12:20	24:05.993	62:52.010	3225	150	150	150	80	80	53	53	53	48	48	48	38	38	38	30	30	30	10	
04.11.07	12308-1	CTD-5	OMZ 1590	16:31	18:06	24:43.087	62:59.500	1594	1550	1500	1460	1400	1300	1200	1100	1000	900	800	700	600	500	400	300	200	50	50	Posidonia
04.11.07	12308-2	CTD-6	OMZ 1590	02:09	02:36	24:43.103	62:59.490	1591	150	150	80	80	40	40	40	33	33	33	26	26	26	17	17	17	10	10	
04.11.07	12309-1	CTD-7	OMZ 950	07:33	09:00	24:52.326	62:59.869	955	930	900	850	800	750	692	650	600	550	500	450	400	350	300	250	200	150	150	
04.11.07	12309-2	CTD-8	OMZ 950	09:32	09:56	24:52.320	62:59.865	956	150	150	80	80	68	68	68	46	46	46	35	35	35	20	20	20	10	10	
05.11.07	12312-1	CTD 9	OMZ 650	02:55	03:55	24:55.051	63:01.166	633	630	600	575	550	525	500	475	450	425	400	350	300	248	200	150	100	50	20	
05.11.07	12312-2	CTD 10	OMZ 650	04:22	04:39	24:53.068	63:01.644	655	150	80	80	40	40	40	35	35	35	28	28	28	20	20	20	17	17	17	
06.11.07	12314-2	CTD-11	Flare 2	02:06	03:31	24:50.801	63:01.416	1023	1007	1000	975	850	925	900	850	800	750	700	600	500	400	300	250	200	x	x	Posidonia
06.11.07	12314-3	CTD-12	Flare 2	04:02	04:17	24:50.796	63:01.402	1019	150	80	80	42	42	42	26	26	26	20	20	20	15	15	15	10	10	10	
07.11.07	12318-1	CTD-13	Flare 7	17:58	19:41	24:38.641	62:44.261	1642	1630	1600	1550	1500	1400	1300	1200	1100	1000	900	800	700	600	500	400	300	200	100	Posidonia
07.11.07	12318-2	CTD-14	Flare 7	20:07	20:31	24:38.642	62:44.219	1641	150	80	80	80	64	54	54	38	38	38	29	29	29	15	15	15	10	10	
11.11.07	12321-2	CTD-15	OMZ 1400	02:02	03:32	24:46.010	62:59.996	1424	1400	1350	1300	1249	1200	1150	1100	1000	900	800	700	600	500	400	300	200	100	50	
11.11.07	12321-3	CTD-16	OMZ 1400	03:59	04:17	24:46.005	62:59.986	1423	150	80	80	54	54	54	49	49	49	33	33	33	20	20	20	10	10	10	
14.11.07	12329-1	CTD-17	OMZ 1000	04:14	05:35	24:50.754	63:01.437	1025	1010	980	955	925	900	875	850	825	800	775	750	725	700	675	650	600	400	200	Posidonia
14.11.07	12329-2	CTD-18	OMZ 1000	06:11	06:29	24:50.752	63:01.426	1022	150	80	80	58	58	58	42	42	42	33	33	33	28	28	28	10	10	10	
16.11.07	12337-1	CTD-19	Flare 7	02:06	04:29	24:38.650	62:44.248	1648	1630	1600	1575	1550	1525	1500	1475	1450	1425	1400	1350	1300	1250	1200	1100	1000	900	800	Posidonia but probe dmted
16.11.07	12337-2	CTD-20	Flare 7	04:59	05:15	24:38.649	62:44.237	1650	150	150	68	68	68	35	35	35	28	28	28	28	20	20	20	10	10	10	
17.11.07	12340	CTD-21	Nascent Ridge	17:02	18:40	24:11.747	62:44.307	2859	2850	2825	2800	2775	2750	2725	2700	2675	2650	2625	2600	2550	2500	2450	2400	2300	2200	2100	Posidonia
18.11.07	12344	CTD-22	Flare 2	16:21	17:55	24:50.837	63:01.412	1031	1030	1010	975	950	925	900	875	850	825	800	750	700	650	600	550	500	400	300	Posidonia
19.11.07	12347	CTD-23	Flare 1	03:57	04:57	24:53.636	63:01.401	604	583	575	550	525	500	475	450	425	400	375	350	300	250	200	150	100	50	20	Posidonia
20.11.07	12354-1	CTD-24	Flare 15	17:52	18:51	24:48.465	63:59.657	733	719	700	675	650	625	600	575	550	525	500	450	400	350	300	300	200	100	50	posidonia
20.11.07	12354-2	CTD-25	Flare 15	19:43	20:11	24:48.454	63:59.643	734	150	150	80	80	80	65	65	65	40	40	40	32	32	32	20	20	20	Test fluid	

Appendix 3: Overview of gravity corer (GC) stations

GeoB	GC No.	Area	Lat. [°N]	Long. [°E]	Depth [mbsl]	Comments
12303	GC-1	Nascent Ridge	24:11.749	62:44.309	2860	recovery 4.34 m; plastic hose; gas hydrates
12305	GC-2	Nascent Ridge	24:10.442	62:45.900	2949	recovery > 6 m; liner; no posidonia; taken home
12306	GC-3	Nascent Ridge	24:11.761	62:44.311	2861	recovery 3.8 m; pore water; posidonia
12308-4	GC-4	OMZ 1590	24:43.114	62:59.502	1587	recovery 3.5 m; liner; pore water; no posidonia
12312-4	GC 5	OMZ 650	24:53.072	63:01.642	658	recovery 4.5 m; liner; take home; no posidonia
12312-5	GC 6	OMZ 650	24:53.071	63:01.643	647	recovery 4 m; liner; pore water; no posidonia
12314-1	GC 7	Flare 2	24:50.797	63:01.423	960	recovery 1 carbonate; no gas hydrates; posidonia
12316-1	GC 8	Flare 2	24:50.795	63:01.422	1021	recovery 0.3 m; carbonate; no gas hydrates; posidonia
12316-2	GC 9	Flare 2	24:50.798	63:01.416	1021	recovery 1.03 m; gas hydrates + carbonates; posidonia
12309-5	GC 10	OMZ 950	24:52.301	62:59.872	956	recovery 5.60 m; pore water
12316-3	GC-11	Flare 2	24:50.789	63:01.422	1020	recovery 2.18 m; gas hydrates
12316-4	GC-12	Flare 2	24:50.788	63:01.424	1019	recovery 1.63 m; gas hydrates
12316-5	GC-13	Flare 2	24:50.798	63:01.428	1024	no recovery
12327	GC-14	Nascent Ridge	24:11.747	62:44.428	2860	recovery 2.56 m. no gas hydrates; posidonia
12330	GC-15	Nascent Ridge	24:11.744	62:44.308	2856	recovery 1.96 m; Posidonia
12332	GC-16	Background	24:17.482	62:57.586	2036	recovery 5.87 m
12316-6	GC-17	Flare 2	24:50.781	62:01.411	1004	no recovery; Posidonia
12316-7	GC-18	Flare 2	24:50.780	63:01.410	1019	no recovery; Posidonia
12321-4	GC-19	OMZ 1400	24:46.002	62:59.980	1419	pore water
12335	GC-20	Background	24:43.100	62:59.511	1594	recovery 4.45 m
12336	GC 21	Background	24:47.777	63:01.471	1263	recovery 4.47 m
12331-2	GC-22	Nascent Ridge	24:11.498	62:46.505	2838	pore water
12341	GC-23	Nascent Ridge	24:11.746	62:44.308	2861	recovery 3.60 cm; Posidonia; hydrates
12342-1	GC-24	Flare 2	24:50.799	63:01.420	1020	barrel broken: no recovery
12342-2	GC-25	Flare 2	24:50.799	63:01.420	1018	hydrates; recovery ca. 40 cm; Posidonia
12349	GC-26	Background	24:52.323	62:59.852	960	recovery 4.25 m
12350	GC-27	Background	24:53.722	63:16.035	353	
12351	GC-28	Flare-1	24:53.650	63:01.409	592	recovery 3.22 m. pore water

Appendix 4: Overview of multicorer (MUC) stations

GeoB	MUC No.	Area	Lat. [°N]	Long. [°E]	Depth [mbsl]	Comments
12308-3	MUC-1	OMZ 1590	24:43.115	62:59.504	1574	Liners closed
12309-3	MUC-2	OMZ 950	24:52.322	62:59.859	962	Liners closed
12312-3	MUC-3	OMZ 650	24:53.072	63:01.641	654	Liners closed
12309-4	MUC-4	OMZ 950	24:52.292	62:59.839	957	Liners closed
12308-5	MUC-5	OMZ 1590	24:43.109	62:59.497	1586	Liners closed
12321-1	MUC-6	OMZ 1400	24:46.002	62:59.973	1425	Liners closed
12331-1	MUC-7	Nascent Ridge	24:11.507	62:46.502	2831	Liners closed
12321-5	MUC-8	OMZ 1400	24:46.007	62:59.973	1428	Liners closed

Appendix 5: Recovered carbonate samples, abbreviations: GC: gravity corer, BC: bubble catcher

Station (GeoB)	Flare #	Dive #	Lat N	Long E	depth (mbsl))	tool	depth (cm)	sample type
GeoB12313-4	2	180	24:50.799	63:01.420	1023	ROV (BC)	-	small carbonate nodules within sediment
GeoB12313-5	2	180	24:50.827	63:01.420	1038	push core	3 - 8	small carbonate nodules within sediment
GeoB12313-14 G	2	180	24:50.829	63:01.419	1038	ROV (net)	-	small carbonate nodules within sediment
GeoB12314-1	2		24:50.829	63:01.419	960	GC	0 - 13	massive cavernous carbonate crust
GeoB12315-3	2	181	24:50.753	63:01.439	1023	ROV (arm)	-	thin carbonate crust
GeoB12315-8	2	181	24:50.753	63:01.439	1025	push core	top	small carbonate nodules within sediment
GeoB12316-1A	2		24:50.795	63:01.422	1021	GC	0 - 15	carbonate crust, desintegrated into smaller pieces after recovery
GeoB12316-2	2		24:50.798	63:01.416	1021	GC	5 - 9	1 carbonate piece
GeoB12316-2	2		24:50.798	63:01.416	1021	GC	20 - 26	2 carbonate pieces
GeoB12316-2	2		24:50.798	63:01.416	1021	GC	37	1 carbonate piece
GeoB12316-2	2		24:50.798	63:01.416	1021	GC	42 - 46	3 carbonate pieces
GeoB12316-2	2		24:50.798	63:01.416	1021	GC	52 - 56	6 carbonate pieces
GeoB12316-2	2		24:50.798	63:01.416	1021	GC	60 - 62	7 carbonate pieces
GeoB12316-2	2		24:50.798	63:01.416	1021	GC	70 - 75	2 carbonate pieces
GeoB12316-2	2		24:50.798	63:01.416	1021	GC	80 - 85	8 carbonate pieces
GeoB12316-2	2		24:50.798	63:01.416	1021	GC	87 - 90	2 carbonate pieces
GeoB12316-2	2		24:50.798	63:01.416	1021	GC	97 - 100	2 carbonate pieces
GeoB12316-3	2		24:50.789	63:01.422	1018	GC	10	1 carbonate piece
GeoB12316-3	2		24:50.789	63:01.422	1018	GC	20	2 carbonate pieces
GeoB12316-3	2		24:50.789	63:01.422	1018	GC	25-30	3 carbonate pieces
GeoB12316-3	2		24:50.789	63:01.422	1018	GC	43	1 carbonate piece
GeoB12316-3	2		24:50.789	63:01.422	1018	GC	53	3 carbonate pieces

GeoB12316-3	2		24:50.789	63:01.422	1018	GC	75-79	1 carbonate piece
GeoB12316-3	2		24:50.789	63:01.422	1018	GC	82	1 carbonate piece
GeoB12316-3	2		24:50.789	63:01.422	1018	GC	87-94	2 carbonate pieces
GeoB12316-3	2		24:50.789	63:01.422	1018	GC	101	1 carbonate piece
GeoB12316-3	2		24:50.789	63:01.422	1018	GC	107	1 carbonate piece
GeoB12316-3	2		24:50.789	63:01.422	1018	GC	118-120	3 carbonate pieces
GeoB12316-3	2		24:50.789	63:01.422	1018	GC	148	1 carbonate piece
GeoB12316-3	2		24:50.789	63:01.422	1018	GC	160	3 carbonate pieces
GeoB12316-3	2		24:50.789	63:01.422	1018	GC	192	2 carbonate pieces
GeoB12316-4	2		24:50.788	63:01.424	1019	GC	61	1 clam/carbonate aggregate
GeoB12324-2	6	186	24:34.808	62:56.324	1823	ROV (arm)	-	3 pieces of carbonate crust (two below dead tube worm colony, one above)
GeoB12328-7	2	188	24:50.738	63:01.443	1025	push core	2 - 5	small carbonate nodules within sediment
GeoB12338-1	7	191	24:38.544	62:44.241	1656	ROV (arm)	-	a few pieces of carbonate crust associated with tube worms
GeoB12338-2	7	191	24:38.556	62:44.246	1656	ROV (arm)	-	piece of carbonate crust
GeoB12338-3	7	191	24:38.556	62:44.246	1656	ROV (arm)	-	big piece of carbonate crust
GeoB12338-4	7	191	24:38.617	62:44.257	1652	ROV (net)	-	a few carbonate pieces of slabs associated with mytilids
GeoB12338-13	7	191	24:38.563	62:44.286	1656	ROV (arm)	-	very big carbonate piece densely covered with a faunal assemblage
GeoB12348-1	11	194	24:44.476	62:58.633	1475	ROV (arm)	-	2 pieces of carbonate crust covered with many mytilids (from an area extensively covered with mytilids and white crabs, active site)
GeoB12348-2	11	194	24:44.486	62:58.683	1475	ROV (arm)	-	2 pieces of carbonate crust covered with many mytilids (from an area covered with mainly dead mussel shells, dying site)
GeoB12348-3	11	194	24:44.520	62:58.731	1469	ROV (arm)	-	1 piece of carbonate crust (from an area of exposed crust, subrecent seep site, dead)
GeoB12353-7	15	196	24:48.457	63:59.654	731	ROV (arm)	-	small “precipitate dome” underneath bacterial mat #1 (cap in good conditions)
GeoB12353-8	15	196	24:48.459	63:59.654	731	ROV (arm)	-	small “precipitate dome” underneath bacterial mat #2 (small part)
GeoB12353-9	15	196	24:48.467	63:59.650	730	ROV (arm)	-	small “precipitate dome” underneath bacterial mat #3, (cap in good conditions)
GeoB12353-10	15	196	24:48.467	63:59.647	731	ROV (arm)	-	small “precipitate dome” underneath bacterial mat #4 (big cap)
GeoB12353-11	15	196	24:48.445	63:59.644	734	ROV (arm)	-	massive “tower” of many thin carbonate layers (exposed to the sea water)

Appendix 6: Sites investigated geochemically during this cruise, including parameters analysed on board and aliquots of samples taken and stored for further analyses in the home lab

Station	Area	Water depth	Device	Rhizon	Squeezer	Alk.	NH4	Fe	PO4	HS-*	HS-*	SO4, Cl*	Cations*	CH4	Wet Sed.* (stored under argon)	Remarks
		[m]		Sampling	Sampling				(1:2)	(conc.)	(δ34S)	(1:100)	(1:10)			
GeoB 12301-3	Nascent Ridge	2850	PC-11	X		X	X	X	X			X	X		X	
GeoB 12301-5	Nascent Ridge	2850	PC-36		X	X	X	X		X		X	X		X	squeeze cakes
GeoB 12305-1	Nascent Ridge	2949	GC													core stored
GeoB 12306-1	Nascent Ridge, Gas Hydrates	2861	GC	X		X	X	X		X	X	X	X	X	X	
GeoB 12308-3	Below OMZ, 1574 m	1574	MUC A	X		X	X	X	X			X	X		X	
GeoB 12308-3	Below OMZ, 1574 m	1574	MUC B	X		X	X	X				X	X		X	
GeoB 12308-4	Below OMZ, 1574 m	1574	GC	X		X	X	X				X	X	X	X	
GeoB 12309-3	OMZ, 962 m	962	MUC	X		X	X	X	X			X	X		X	
GeoB 12309-5	OMZ, 962 m	962	GC	X		X	X	X	X	X	X	X	X	X	X	
GeoB 12312-3	OMZ, 655 m	655	MUC	X		X	X	X	X			X	X		X	
GeoB 12312-5	OMZ, 655 m	655	GC	X		X	X	X		X	X	X	X	X	X	
GeoB 12313-5	Thioploca mat	1036	PC-14												X	solid phase
GeoB 12313-6	Thioploca mat	1036	PC-3	X		X	X	X		X	X	X	X			
GeoB 12313-10	Clam field	1036	PC-7												X	solid phase
GeoB 12313-12	Clam field	1036	PC-33	X		X	X	X		X	X	X	X			
GeoB 12313-13	Border of clam field	1036	PC-24	X		X	X	X	X	X		X	X			
GeoB 12315-1	Yellow and white/rose-coloured mat	1025	OS													
GeoB 12315-4	Clam field	1025	PC-36	X		X	X		X	X		X	X			
GeoB 12315-6	Clam field	1025	PC-5												X	solid phase
GeoB 12315-7	Thioploca mat, carbonates below	1025	PC-28	X		X	X		X	X		X	X			
GeoB 12315-8	Thioploca mat, carbonates below	1025	PC-11													
GeoB 12315-9	Thioploca mat, carbonates below	1025	PC-2		X	X	X		X	X		X	X			
GeoB 12319-2	ISPS (Background site)	579	ISPS			X	X	X	X			X				
GeoB 12320-4	White/rose microbial mat	589	PC-22	X		X	X		X	X	X	X	X			
GeoB 12320-5	White/rose microbial mat	589	PC-21		X	X	X			X					X	squeeze cakes
GeoB 12320-8	Yellow microbial mat (center)	589	PC-3		X	X	X			X					X	squeeze cakes

Appendix 6: Continuation

Station	Area	Water depth	Device	Rhizon	Squeezer	Alk.	NH4	Fe	PO4	HS- *	HS- *	SO4, Cl*	Cations*	CH4	Wet Sed.*	Remarks
		[m]		Sampling	Sampling				(1:2)	(conc.)	(δ34S)	(1:100)	(1:10)		(stored under argon)	
GeoB 12320-9	Yellow microbial mat	589	PC-29	X		X	X		X	X	X	X	X			
GeoB 12320-13	ISPS Background site	579	PC-7	X		X	X	X	X	X	X	X	X			
GeoB 12321-4	OMZ, 1400 m	1419	GC	X		X	X	X				X		X		
GeoB 12321-5	OMZ, 1400 m	1428	MUC	X		X	X	X							X	
GeoB 12324-7	Calyptogena field	1835	PC-22	X		X	X	X	X	X	X	X				
GeoB 12324-9	Calyptogena field	1835	PC-20												X	solid phase
GeoB 12324-10	Close to white mat and carbonates	1836	PC-36												X	solid phase
GeoB 12324-11	Close to white mat and carbonates	1836	PC-7	X		X	X	X	X	X	X	X				
GeoB 12326-7	Nascent Ridge, Calyptogena	2873	PC-28					X							X	solid phase
GeoB 12326-8	Nascent Ridge, slimy sediment	2873	PC-24	X				X	X	X						
GeoB 12326-10	Nascent Ridge, ISPS Station, slime	2875	PC-11	X				X	X	X						
GeoB 12326-13	Nascent Ridge, Calypt. and slime	2875	PC-13												X	solid phase
GeoB 12328-2	Area between mat and clams	1025	PC-36												X	solid phase
GeoB 12328-3	Area between mat and clams	1025	PC-7	X		X	X	X	X	X	X	X				
GeoB 12328-4	Small clams	1025	PC-15												X	solid phase
GeoB 12328-5	Small clams	1025	PC-20	X		X	X	X	X	X	X	X				
GeoB 12328-6	Rose-coloured mat	1025	PC-17												X	solid phase
GeoB 12328-8	Rose-coloured mat	1025	PC-9	X		X	X	X		X	X	X				
GeoB 12331-1	OMZ, 2850 Nascent Ridge	2831	MUC	X		X	X	X			X	X			X	
GeoB 12331-2	OMZ, 2850 Nascent Ridge	2831	GC	X		X	X	X		X	X	X		X	X	
GeoB 12338-X	Flare 7	1654	KIPS			X	X					X				
GeoB 12339-3	Close to gas seep, Nascent Ridge	2875	PC-24	X		X	X	X								
GeoB 12339-4	Close to gas seep, Nascent Ridge	2875	PC-6												X	solid phase
GeoB 12339-5	Tube worm site, Nascent Ridge	2875	PC-28	X		X	X	X								
GeoB 12339-10	Tube worm site, Nascent Ridge	2875	PC-29												X	solid phase

Appendix 6: Continuation

Station	Area	Water depth	Device	Rhizon	Squeezer	Alk.	NH4	Fe	PO4	HS- *	HS- *	SO4, Cl*	Cations*	CH4	Wet Sed.* (stored under argon)	Remarks
		[m]		Sampling	Sampling				(1:2)	(conc.)	(δ34S)	(1:100)	(1:10)			
GeoB 12343-2	Flare 2	1030	ISPS	X		X						X				
GeoB 12351-1	Flare 1	592	GC	X		X	X	X		X	X	X		X		
GeoB 12352-X	Flare 4	1985	KIPS			X			X			X	X			
GeoB 12353-3	Flare 15, Rose-coloured mat	732	PC-15	X		X			X	X	X	X	X			
GeoB 12353-4	Flare 15, Rose-coloured mat	732	PC-4												X	solid phase
GeoB 12353-5	Flare 15, Yellow mat	732	PC-6		X	X			X	X		X				squeeze cakes

* for analyses or further processing in the home lab

Appendix 7: List of samples taken for measurements of gas compositions during M74/3. Listing according to water depth.

GeoB No.	Device	Lat. N°	Long. E°	Water depth [m]	Site	Type of sample	No. of samples	No. of sub-samples prepared	Underwater navigation
SUBOXIC ZONE									
Flare 1									
12320-2	GBS-06	24:53.636	63:01.406	591	Flare 1	Gas	1	6	
12320-3	GBS-07	24:53.633	63:01.405	590	Flare 1	Gas	1	8	
12347	CTD-23	24:53.636	63:01.401	604	Flare 1	Water	18	30	deployed
Flare 15									
12353-2	GBS-18	24:48.458	63:59.649	732	Flare 15	Gas	1	4	
12354-1	CTD-24	24:48.455	63:59.657	733	Flare 15	Water	18	30	
Flare 2									
12313-3	GBS-02	24:50.788	63:01.420	1,024	Flare 2	Gas	1	8	
12313-8	GBS-03	24:50.788	63:01.420	1,038	Flare 2	Gas	1	10	
12315-2	GBS-04	24:50.758	63:01.433	1,025	Flare 2	Gas	1	10	
12328-1	GBS-11	24:50.699	63:01.445	1,028	Flare 2	Gas	1	12	
12333-2	GBS-12	24:50.797	63:01.420	1,024	Flare 2	Gas	1	11	
12343-3	GBS-16	24:50.844	63:01.415	1,040	Flare 2	Gas	1	13	
12314-2	CTD-11	24:50.801	63:01.416	1,007	Flare 2	Water	16	16	deployed
12344	CTD-22	24:50.837	63:01.412	1,011	Flare 2	Water	18	30	deployed
12316-2	GC-09	24:50.758	63:01.433	1,021	Flare 2	Gas hydrate	1	15	deployed
12316-3	GC-11	24:50.789	63:01.422	1,020	Flare 2	Gas hydrate	1	3	
12316-4	GC-12	24:50.788	63:01.424	1,019	Flare 2	Gas hydrate	1	8	
12342-2	GC-25	24:50.799	63:01.420	1,018	Flare 2	Gas hydrate	1	3	deployed
Reference stations									
12312-1	CTD-09	24:55.05	63:01.166	663	OMZ	Water	18	18	
12309-1	CTD-07	24:52.326	62:59.869	955	OMZ	Water	18	18	
12329-1	CTD-17	24:50.754	63:01.443	1,010	OMZ	Water	18	28	deployed
LOWER OXIC ZONE									
Flare 7									
12317-1	GBS-05	24:38.649	62:44.254	1,650	Flare 7	Gas	1	12	
12338-11	GBS-13	24:38.649	62:44.253	1,654	Flare 7	Gas	1	6	

Appendix 7: Continuation

GeoB No.	Device	Lat. N°	Long. E°	Water depth [m]	Site	Type of sample	No. of samples	No. of sub-samples prepared	Underwater navigation
12322-3	GBS-08	24:38.644	62:44.260	1,652	Flare 7	Gas / near-bottom water	1	2	
12318-1	CTD-13	24:38.642	62:44.219	1,642	Flare 7	Water	18	18	deployed
12337-1	CTD-19	24:38.648	62:44.248	1,630	Flare 7	Water	18	30	deployed
Flare 4									
12352-10	GBS-17	24:17.929	62:50.097	1,983	Flare 4	Near-bottom water	1	1	
Flare 5 (Nascent Ridge)									
12301-1	GBS-01	24:11.748	62:44.307	2,876	Flare 5	Gas	1	18	
12326-2	GBS-09	24:11.750	62:44.418	2,874	Flare 5	Gas	1	16	
12326-4	GBS-10	24:11.745	62:44.418	2,873	Flare 5	Gas	1	16	
12339-1	GBS-14	24:11.742	62:44.301	2,875	Flare 5	Gas	1	14	
12339-2	GBS-15	24:11.742	62:44.301	2,875	Flare 5	Gas / near-bottom water	1	1	
12302-1	CTD-01	24:11.752	62:44.301	2,861	Flare 5	Water	15	15	deployed
12340	CTD-21	24:11.747	62:44.307	2,859	Flare 5	Water	18	30	deployed
12303	GC-01	24:11.749	62:44.309	2,860	Flare 5	Gas hydrate	1	15	
12341	GC-23	24:11.746	62:44.308	2,861	Flare 5	Gas hydrate	1	12	
Reference stations									
12321-2	CTD-15	24:46.00	62:59.996	1,422	OMZ	Water	18	18	
12308-1	CTD-05	24:43.087	62:59.500	1,594	OMZ	Water	17	17	deployed
12307-1	CTD-03	24:06.024	62:52.634	3,230	deep sea	Water	18	18	
						Sum	**270**	**570**	

CTD: CTD-Rosette Water Sampler; GBS: Gas Bubble Sampler (ROV-based); GC: Gravity Corer; OMZ = Oxygen Minimum Zone.

Appendix 8: Samples for Biogeochemistry Investigations collected during M74-2 and M74-3

Coordinates	Stations	Depth (m)	Area	Instrument	Analysis	Remarks
Lat:24°52.97'N Lon:63°1.6'E	M74-2, GeoB12204-6	680	OMZ	Gravity core (10-557cm)	Pore water, gas, lipids, FISH	SMTZ ~2m
Lat:24°53.71'N Lon:63°16.03'E	M74-2, GeoB12210-6	355	OMZ	Gravity core (10-490cm)	Pore water, gas, lipids, FISH	SMTZ ~2m
Lat:24°52.31'N Lon:62°59.87'E	M74-2, GeoB12216-4	975	Suboxia	Gravity core (20-440cm)	Pore water, gas, lipids, FISH	SMTZ ~2.5m
Lat:24°37.245'N Lon:62°58.549'E	M74-2, GeoB12211-1	1600	Out OMZ	Gravity core (20-526cm)	Pore water, gas, lipids, FISH	SMTZ ~4.5m
Lat:24°11.75'N Lon:62°44.308'E	M74-3, GeoB12301	2876	Nascent Ridge, Out OMZ	Dive 179, PC (1-11cm)	Pore water, gas, lipids, FISH	Gassy seep, recent ridge
Lat:24°50.827'N Lon:63°01.420'E	M74-3, GeoB12313	1038	Flare #2, suboxia	Dive 180, PC (1-17; 1-18cm)	Pore water, gas, lipids, FISH for the PC and Calyptogena tissues and thioploca mat for lipids	Thioploca and Calyptogena site
Lat:24°50.753'N Lon:63°01.439'E	M74-3, GeoB12315	1025	Flare 2, suboxia	Dive 181, PC (1-19cm)	Pore water, gas, lipids, FISH	Collected just from Thioploca
Lat: 24°38.633'N Lon: 63°44.645'E	M74-2, GeoB 12317	1651	Flare 7, Out OMZ	Dive182, PC	Only tissue analysis for lipids and pore water from the gas bubble sampler	Calyptogena site
Lat:24°53.634'N Lon:63°01.404'E	M74-3, GeoB12320	551	Flare 1, OMZ	Dive 184, PC (1-14; 1-21cm)	Pore water, gas, lipids and FISH for the PC, and orange mat and white mat for lipids. Additionally KIPS samples from mat and background site for pore water analysis (35, 31, 28)	Orange and white mat site
Lat:24°34.840'N Lon:62°56.522'E	M74-3, GeoB12324-2	1835	Flare 6, Out OMZ	Dive 186, ROV net	Only sponges in carbonate piece for lipids analysis	Sponges, thioploca and anemones
Lat:24°50.738'N Lon:63°01.443'E	M74-3, GeoB12328	1025	Flare 2, Out OMZ	Dive 188, PC	Collected only mat for lipids analysis	Thioploca
Lat:24°50.795'N Lon:63°01.422'E	M74-3, GeoB12316-1a	1021	Flare 2, Out OMZ	Gravity core (only carbonates)	Brownish mat collected from a carbonate piece of the GC from S.Klapp for IPLs	Gas hydrates from S.Klapp
Lat:24°11.761'N Lon:62°44.311'E	M74-3, GeoB12306-1	2861	Flare 2, Out OMZ	Gravity core (20-360cm)	Pore water, gas, lipids, FISH	Gas hydrates starting at 1.5m
Lat:24°38.643'N Lon:62°44.261'E	M74-3, GeoB12322	1650	Flare 7	Dive 185	Only DIC (concentration and isotopes) and acetate from gas bubble sample T. Pape	White mat site

Appendix 8: Continuation

Coordinates	Stations	Depth (m)	Area	Instrument	Analysis	Remarks
Lat:24°38.649'N Lon:62°44.254'E	M74-3, GeoB12338	1654	Flare 7	Dive 191	Only carbonate with sponges for lipid analysis. KIPS sampler from 6 locations (two bubble streams, background and profile at 20, 50 and 100 cm on top of mussel field)	Carbonate with sponges and barnacles and Bathymodiolus field
Lat:24°44.476'N Lon:62°58.633'E	M74-3, GeoB12348-1	1475	Flare 11	Dive 194	Only Bathymodiolus gills for lipid analysis	Carbonate with mussels
Lat:24°17.933'N Lon:62°52.081'E	M74-3, GeoB12352	1084	Flare 4	Dive 195	KIPS sampler from 6 locations	
Lat:24°48.458'N Lon:63°59.649'E	M74-3, GeoB12353	732	Flare 15	Dive 196, PC (0-12cm)	Pore water, gas, lipids, FISH. Additionally was collected carbonate pieces from GeoB sub numbers 9 and 11 for lipid analysis	Orange and white mat with carbonate structures
Lat:24°53.650'N Lon:63°01.409'E	M74-3, GeoB12351	592	Flare 1	Gravity core (15-310cm)	Pore water, gas, lipids, FISH. Samples for alive sediments for experiment	Orange and white mat

Appendix 9: List of all core descriptions

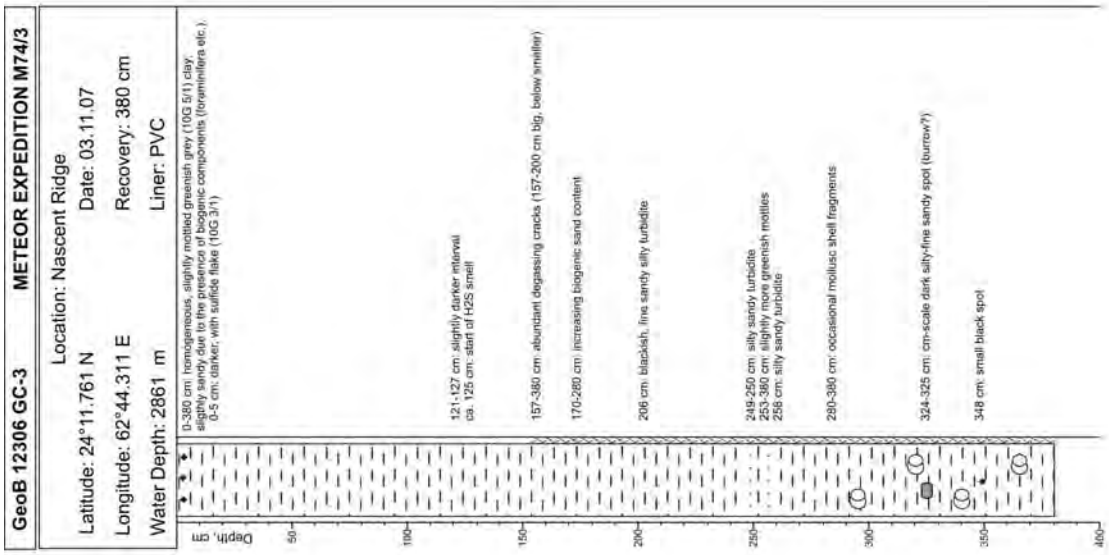

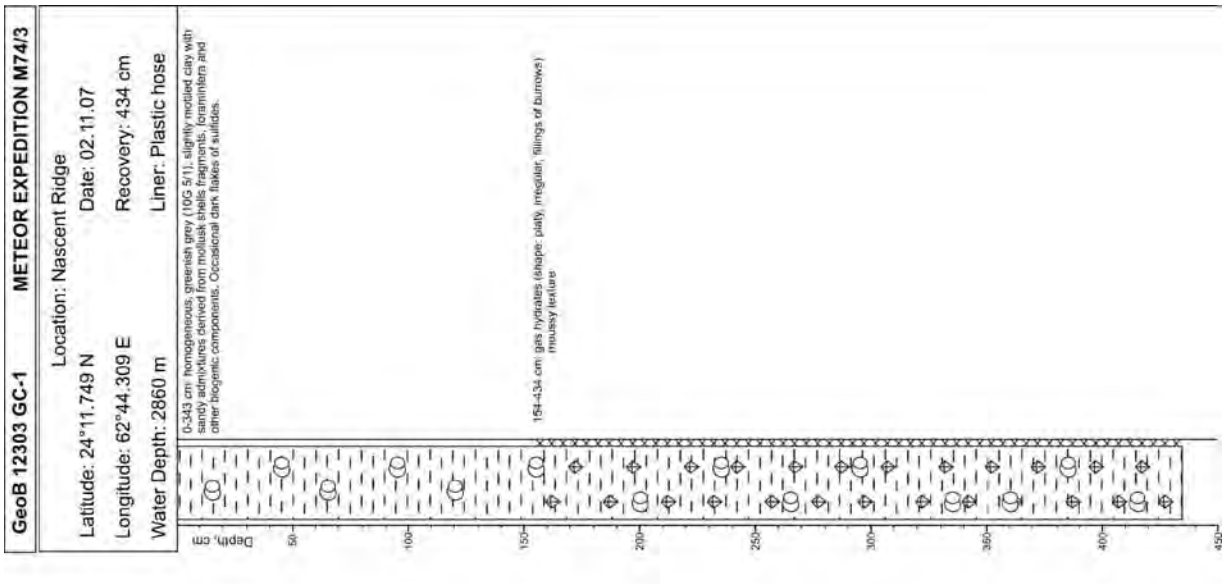

Appendix 9: Continuation

GeoB 12308-3 MUC-1 METEOR EXPEDITION M74/3

Location: Background

Latitude: 24°43.115 N
Longitude: 62°59.504 E
Water Depth: 1574 m

Date: 04.11.07
Recovery: 33 cm
Liner: PVC

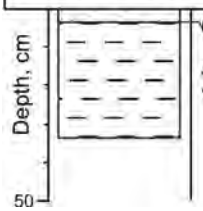

0-4 cm: homogeneous, very soft, olive brown (2.5 Y 4/3) clay (fluff)

4-33 cm: more cohesive, homogeneous, dark greenish grey (10Y 4/1) clay; very slight admixture of sandy components (forams etc.)

GeoB 12308-5 MUC-5 METEOR EXPEDITION M74/3

Location: Background

Latitude: 24°43.109 N
Longitude: 62°59.497 E
Water Depth: 1586 m

Date: 09.11.07
Recovery: 34 cm
Liner: PVC

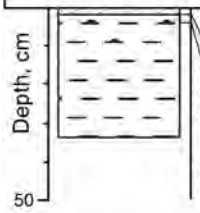

0-0.5 cm: homogeneous, very soft, olive brown (2.5Y 4/3) clay (fluff)

0.5-2 cm: more cohesive, homogeneous, olive brown (2.5Y 4/3) clay; very slight admixture of sandy components (forams etc.)

2-34 cm: cohesive, homogeneous, greyish brown (2.5 YR 5/2) slightly silty to silty clay between 2-12 cm, below 12 cm clay.

Special observation: ball-like, jelly-like organic remain (ca. 2 cm in diam.) with sediment-like filling on top of core. Egg?

GeoB 12309-3 MUC-2 METEOR EXPEDITION M74/3

Location: Background

Latitude: 24°52.322 N
Longitude: 62°59.859 E
Water Depth: 962 m

Date: 04.11.07
Recovery: 35 cm
Liner: PVC

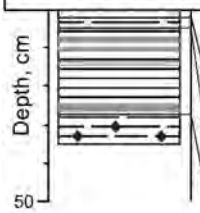

0-1 cm: homogeneous, very soft, olive brown (2.5Y 4/3) clay (fluff) with abundant burrows, tubes and amphiura

1-5.5 cm: faintly laminated olive brown clay; very slight admixture of sandy components

5.5-28.5 cm: distinctly laminated olive grey (5Y 4/2) clay with intercalations of homogenous dark greenish grey (10Y 4/1) layers at 7.5-8.5, 9.5-11,12.7, 13.7 and 25.2-27.5 cm core depth

28.5-35 cm: indistinctly laminated olive grey clay.
29.5-35 cm: sulfide flakes

Appendix 9: Continuation

GeoB 12309-4 MUC-4 METEOR EXPEDITION M74/3

Location: Background

Latitude: 24°52.394 N Date: 08.11.07

Longitude: 62°59.839 E Recovery: 37 cm

Water Depth: 957 m Liner: PVC

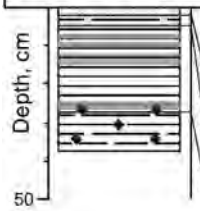

0-1 cm: homogeneous, very soft, olive brown (2.5Y 4/3) clay (fluff) with abundant burrows, tubes and amphiura

1-5 cm: faintly laminated olive brown clay; very slight admixture of sandy components. 3.7 cm: rust-brown layer

5-23 cm: distinctly laminated olive grey (5Y 4/2) clay with intercalations of homogenous dark greenish grey (10Y 4/1) layers at 7.8, 8.0, 9.5-10.2, 11.7-12.2, 13.8, 14.0, 14.5-14.7, 25.7-27.3 cm core depth

23-37 cm: indistinctly laminated to homogeneous olive grey clay.
25.3-37 cm: sulfide flakes
30.3-31.1 cm: darker layers

GeoB 12312-3 MUC-3 METEOR EXPEDITION M74/3

Location: Background

Latitude: 24°53.072 N Date: 05.11.07

Longitude: 63°01.641 E Recovery: 36 cm

Water Depth: 654 m Liner: PVC

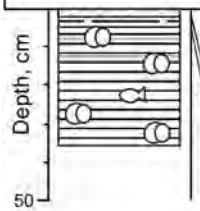

0-1.5 cm: very soft, olive (5Y 5/3) to light olive brown (2.5Y 5/6) silty clay (fluff) with abundant organic constituents

1.5-4 cm: faintly laminated olive brown silty clay

4-36 cm: distinctly laminated olive (5Y5/2) silty clay with pteropod shells, including occasional light coloured mm/thick layers
22.5-23.2 cm: fish remains
30.5 cm: distinct dark layer of silty clay (turbidite?)

GeoB 12314-1 GC-7 METEOR EXPEDITION M74/3

Location: Flare 2

Latitude: 24°50.797 N Date: 05.11.07

Longitude: 63°01.423 E Recovery: ~15 cm

Water Depth: 960 m Liner: Plastic hose

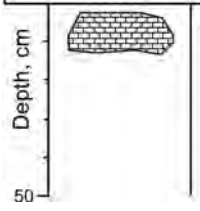

Penetration of corer was blocked by massive carbonate (ca. 15 cm in diameter)

Appendix 9: Continuation

GeoB 12316-1 GC-8 METEOR EXPEDITION M74/3

Location: Flare 2

Latitude: 24°50.795 N Date: 06.11.07

Longitude: 63°01.422 E Recovery: ~30 cm

Water Depth: 1021 m Liner: Plastic hose

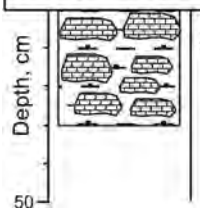

Penetration of corer was blocked by massive carbonate (ca. 30 cm of platy and irregularly shaped carbonates with some clayey sediment)

GeoB 12316-2 GC-2 METEOR EXPEDITION M74/3

Location: Flare 2

Latitude: 24°50.798 N Date: 07.11.07

Longitude: 63°01.416 E Recovery: 103 cm

Water Depth: 1021 m Liner: Plastic hose

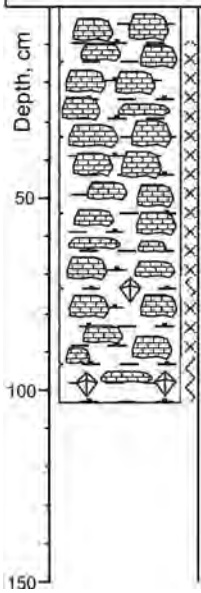

0-103 cm: abundant carbonate pieces (up to ca. 10 cm in size, platy to irregularly shaped) in a matrix of silty-clayey sediment; dark olive grey (10Y 4/1) in the upper 10 cm, below dominantely green grey with some slightly stiffer dark green grey (10Y 4/1 - 10Y 5/1) intervals.
0-11 cm: very soft
11-72 cm: moussy

72-75 cm: soupy, contains small gas hydrates (<1 cm)
75-91 cm: moussy

91-103 cm: soupy, contains small gas hydrates (< 2cm)

Appendix 9: Continuation

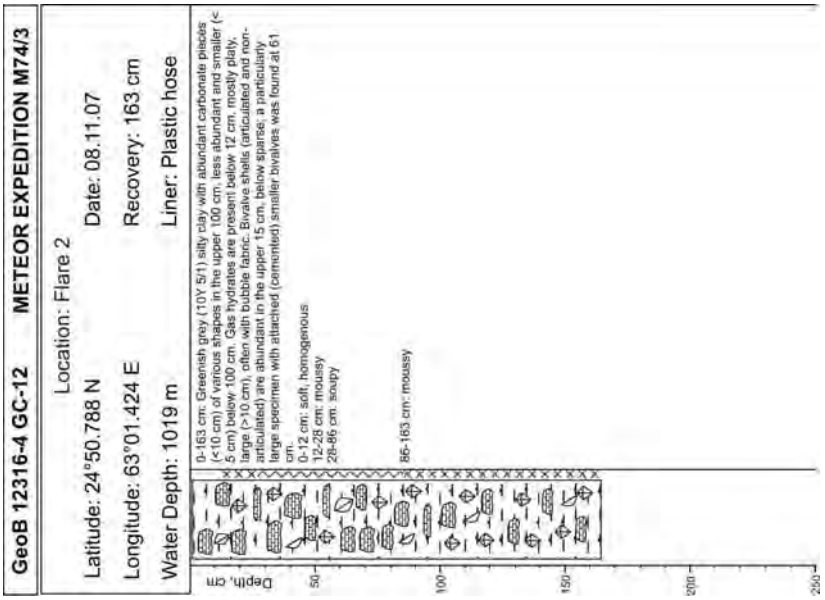

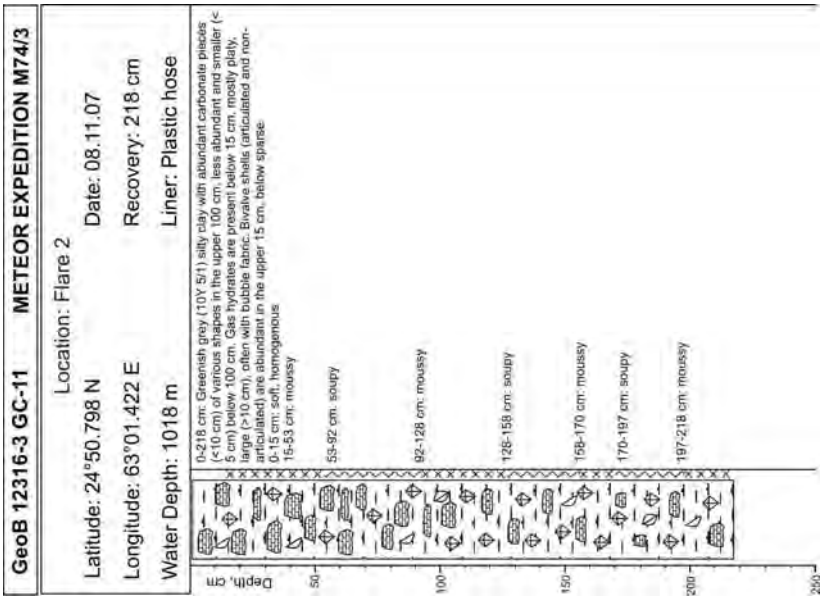

Appendix 9: Continuation

GeoB 12316-5 GC-13 METEOR EXPEDITION M74/3

Location: Flare 2

Latitude: 24°50.798 N
Longitude: 63°01.428 E
Water Depth: 1024 m

Date: 08.11.07
Recovery: -
Liner; Plastic hose

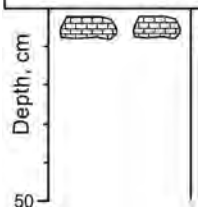

No recovery, due to failure of the core catcher. A few carbonates remained in the liner.

GeoB 12321-1 MUC-6 METEOR EXPEDITION M74/3

Location: Background

Latitude: 24°46.002 N
Longitude: 62°59.973 E
Water Depth: 1425 m

Date: 12.11.07
Recovery: 31.5 cm
Liner: PVC

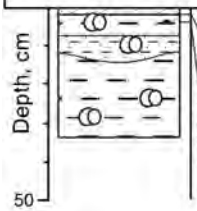

0-0.5 cm: homogeneous, organic-rich, very soft, olive (5Y 5/3) clay (fluff)
0.5-3.5 cm: more cohesive, homogeneous, olive (5Y 5/3) slightly silty clay with a slight admixture of sandy components (forams, mollusc shell fragments, etc.)
3.5-31.5 cm: cohesive, homogeneous, greenish grey (10 Y 5/1) slightly silty to silty clay between 3.5-7.5 cm, below 11.5 cm clay with occasional mollusc shell debris.
7.5-11.5 cm: Olive (5Y 5/2) sandy mud (turbidite) with shell debris; erosive base

GeoB 12321-5 MUC METEOR EXPEDITION M74/3

Location: Background

Latitude: 24°46.007 N
Longitude: 62°59.973 E
Water Depth: 1428 m

Date: 19.11.07
Recovery: 31 cm
Liner: PVC

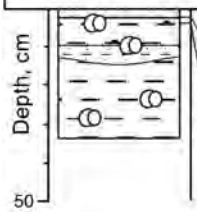

0-2 cm: homogeneous, organic-rich, very soft, olive (5Y 5/3) clay (fluff)
2-4 cm: more cohesive, homogeneous, olive (5Y 5/3) slightly silty clay with a slight admixture of sandy components (forams, mollusc shell fragments, etc.)
4-31 cm: cohesive, homogeneous, greenish grey (10 Y 5/1) slightly silty to silty clay between 3.5-7.5 cm, below 11.5 cm clay with occasional mollusc shell debris.
10-12 cm: Olive (5Y 5/2) sandy mud (turbidite) with shell debris; erosive base

Appendix 9: Continuation

GeoB 12324-13 PC17 **METEOR EXPEDITION M74/3**

Location: Flare 6

Latitude: 24°34.840 N
Longitude: 62°56.523 E
Water Depth: 1836 m

Date: 11.11.07
Recovery: 18 cm
Liner: PVC

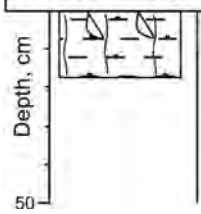

0-18 cm: dark greenish grey (10Y 4/1), slightly silty to silty clay with abundant vertical polychaete burrows. Small-sized bivalve hash in 2 cm core depth.

GeoB 12324-6 PC21 **METEOR EXPEDITION M74/3**

Location: Flare 6

Latitude: 24°34.840 N
Longitude: 62°56.522 E
Water Depth: 1835 m

Date: 11.11.07
Recovery: ~10 cm
Liner: PVC

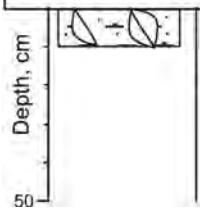

0-10 cm: dark greenish grey (10Y 4/1), slightly fine sandy silty clay with 3 vesicomyid clams with ca. 7 cm length; 2 articulated, 1 disarticulated, all in life position. Some faint banding with lighter and darker layers is visible.
10 cm core depth: dark interval with mm-sized shell hash.

GeoB 12326-11 PC32 **METEOR EXPEDITION M74/3**

Location: Nascent Ridge

Latitude: 24°11.743 N
Longitude: 62°44.306 E
Water Depth: 2875 m

Date: 12.11.07
Recovery: 17 cm
Liner: PVC

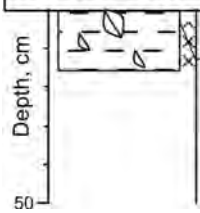

0-3.5 cm: soft dark greenish grey (10Y 4/1), bivalve (6 cm long) in living position

3.5-17 cm: patchy mottled, dark greenish grey (10Y 3-4/1) to greenish black (10Y 2/1) clay, cohesive, some small (<cm) bivalve shell hash. Moussy structure.

Very strong H2S and fishy odor.

Appendix 9: Continuation

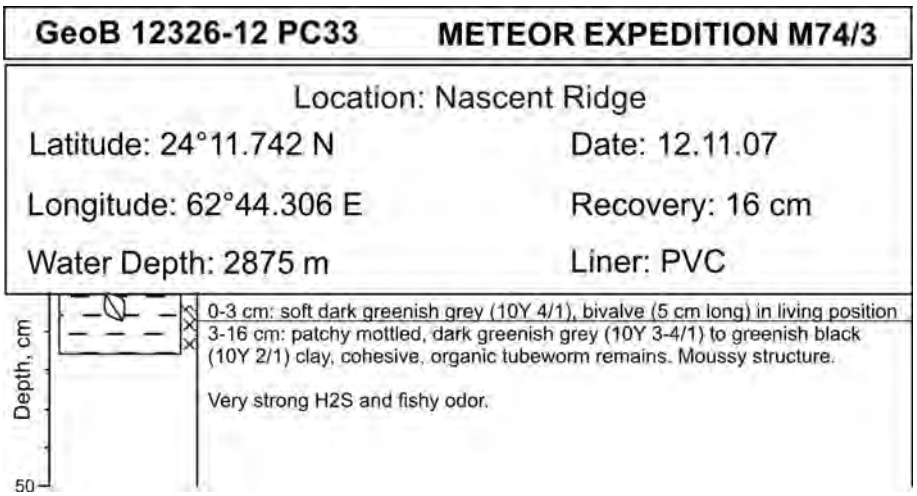

Appendix 9: Continuation

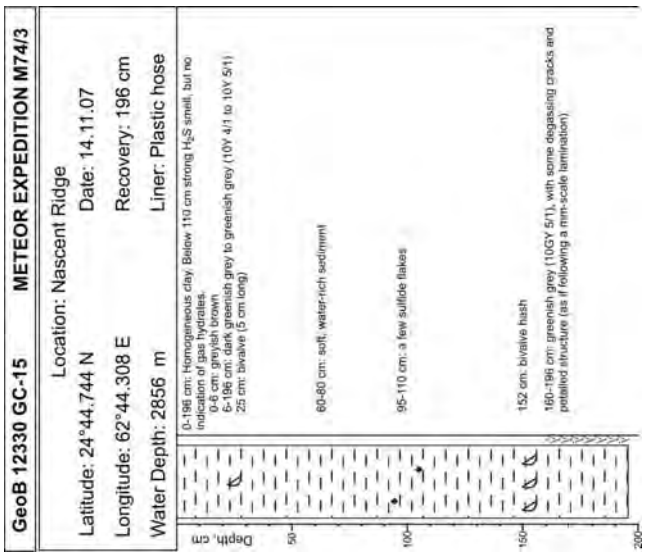

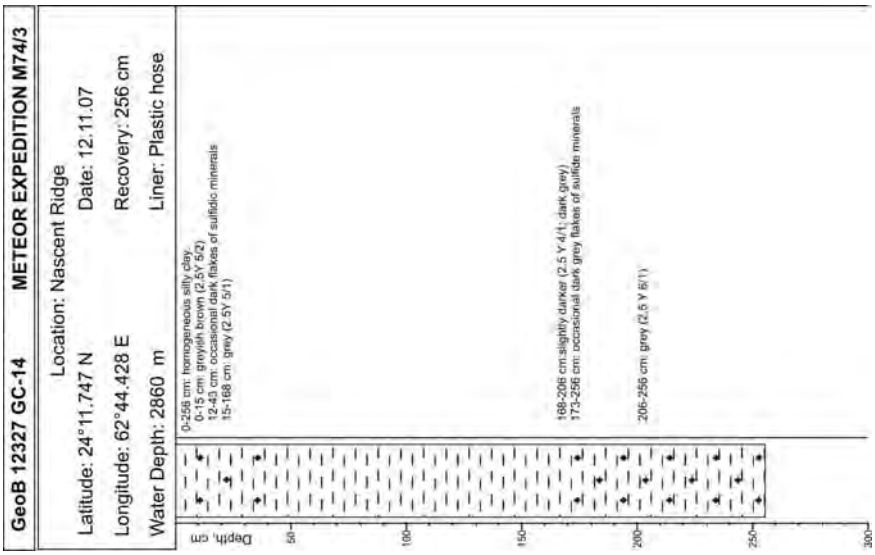

Appendix 9: Continuation

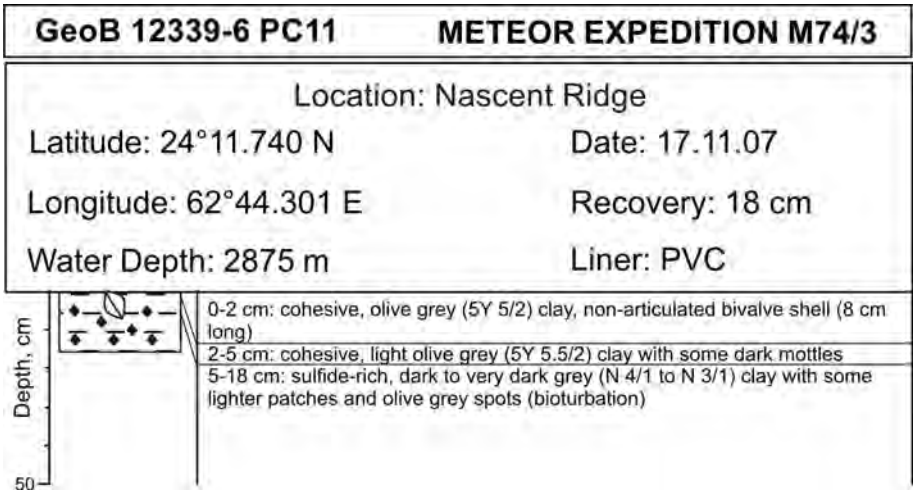

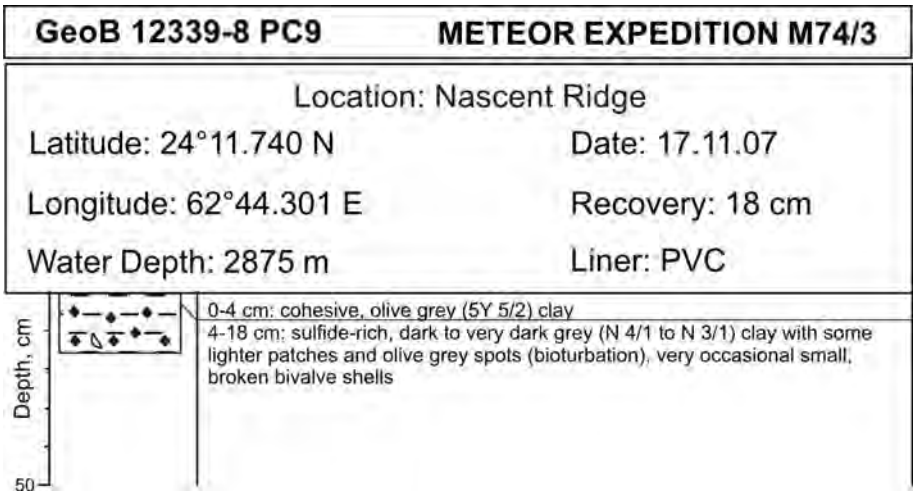

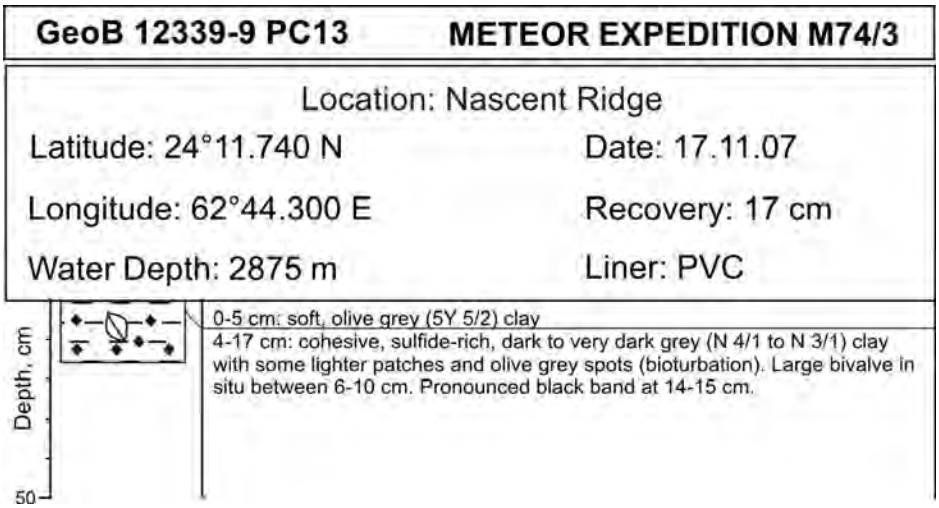

Appendix 9: Continuation

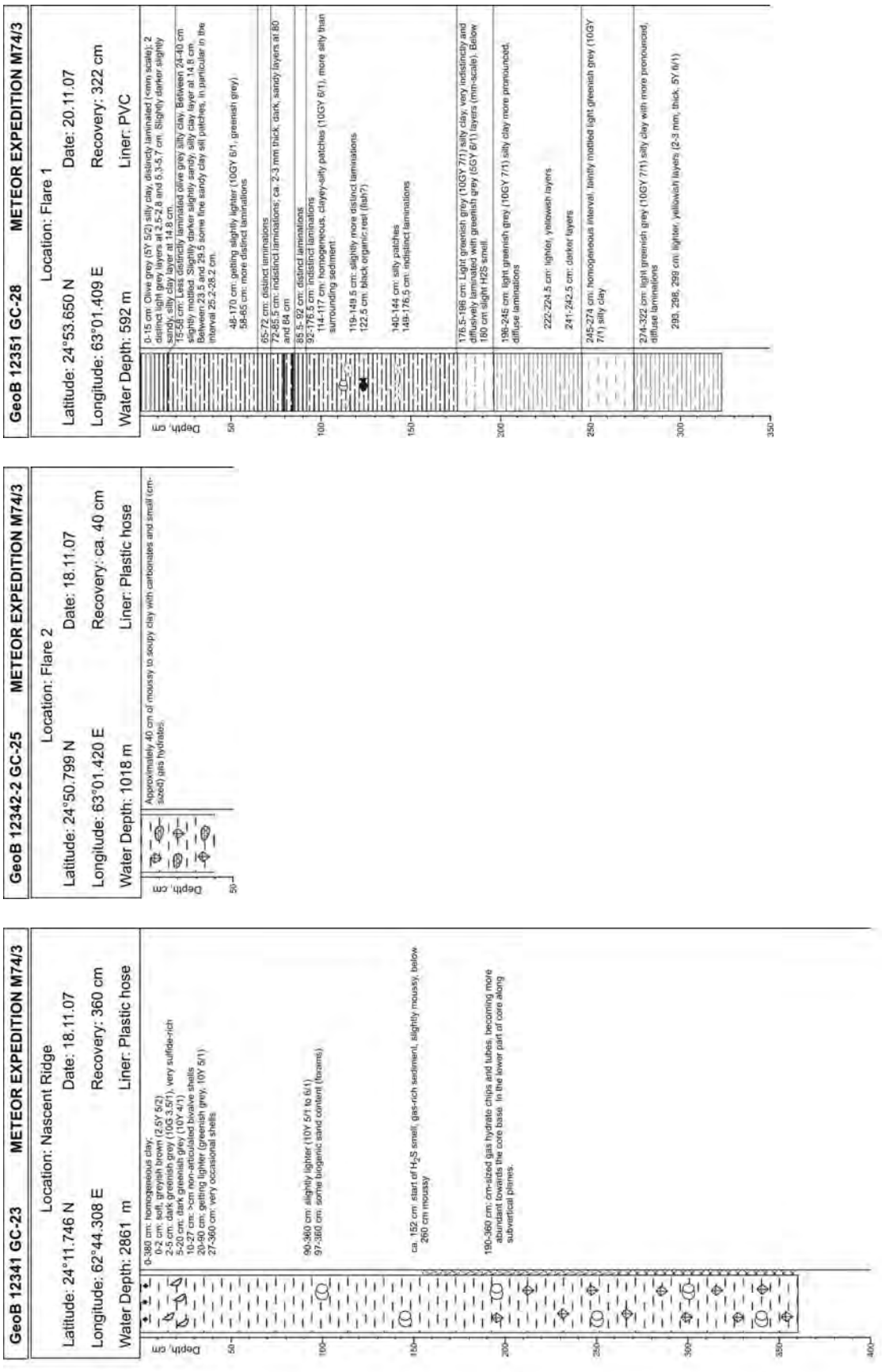

Appendix 9: Continuation

Lithological symbols used

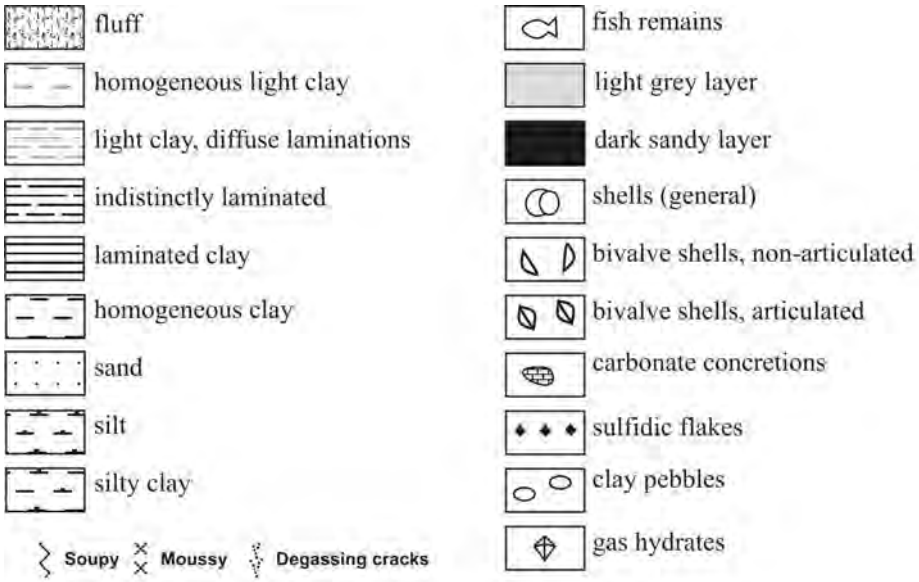

Publications of this series:

No. 1 **Wefer, G., E. Suess and cruise participants**
Bericht über die POLARSTERN-Fahrt ANT IV/2, Rio de Janeiro - Punta Arenas, 6.11. - 1.12.1985.
60 pages, Bremen, 1986.

No. 2 **Hoffmann, G.**
Holozänstratigraphie und Küstenlinienverlagerung an der andalusischen Mittelmeerküste.
173 pages, Bremen, 1988. (out of print)

No. 3 **Wefer, G. and cruise participants**
Bericht über die METEOR-Fahrt M 6/6, Libreville - Las Palmas, 18.2. - 23.3.1988.
97 pages, Bremen, 1988.

No. 4 **Wefer, G., G.F. Lutze, T.J. Müller, O. Pfannkuche, W. Schenke, G. Siedler, W. Zenk**
Kurzbericht über die METEOR-Expedition No. 6, Hamburg - Hamburg, 28.10.1987 - 19.5.1988.
29 pages, Bremen, 1988. (out of print)

No. 5 **Fischer, G.**
Stabile Kohlenstoff-Isotope in partikulärer organischer Substanz aus dem Südpolarmeer (Atlantischer Sektor). 161 pages, Bremen, 1989.

No. 6 **Berger, W.H. and G. Wefer**
Partikelfluß und Kohlenstoffkreislauf im Ozean.
Bericht und Kurzfassungen über den Workshop vom 3.-4. Juli 1989 in Bremen.
57 pages, Bremen, 1989.

No. 7 **Wefer, G. and cruise participants**
Bericht über die METEOR - Fahrt M 9/4, Dakar - Santa Cruz, 19.2. - 16.3.1989.
103 pages, Bremen, 1989.

No. 8 **Kölling, M.**
Modellierung geochemischer Prozesse im Sickerwasser und Grundwasser.
135 pages, Bremen, 1990.

No. 9 **Heinze, P.-M.**
Das Auftriebsgeschehen vor Peru im Spätquartär. 204 pages, Bremen, 1990. (out of print)

No. 10 **Willems, H., G. Wefer, M. Rinski, B. Donner, H.-J. Bellmann, L. Eißmann, A. Müller, B.W. Flemming, H.-C. Höfle, J. Merkt, H. Streif, G. Hertweck, H. Kuntze, J. Schwaar, W. Schäfer, M.-G. Schulz, F. Grube, B. Menke**
Beiträge zur Geologie und Paläontologie Norddeutschlands: Exkursionsführer.
202 pages, Bremen, 1990.

No. 11 **Wefer, G. and cruise participants**
Bericht über die METEOR-Fahrt M 12/1, Kapstadt - Funchal, 13.3.1990 - 14.4.1990.
66 pages, Bremen, 1990.

No. 12 **Dahmke, A., H.D. Schulz, A. Kölling, F. Kracht, A. Lücke**
Schwermetallspuren und geochemische Gleichgewichte zwischen Porenlösung und Sediment im Wesermündungsgebiet. BMFT-Projekt MFU 0562, Abschlußbericht. 121 pages, Bremen, 1991.

No. 13 **Rostek, F.**
Physikalische Strukturen von Tiefseesedimenten des Südatlantiks und ihre Erfassung in Echolotregistrierungen. 209 pages, Bremen, 1991.

No. 14 **Baumann, M.**
Die Ablagerung von Tschernobyl-Radiocäsium in der Norwegischen See und in der Nordsee.
133 pages, Bremen, 1991. (out of print)

No. 15 **Kölling, A.**
Frühdiagenetische Prozesse und Stoff-Flüsse in marinen und ästuarinen Sedimenten.
140 pages, Bremen, 1991.

No. 16 **SFB 261 (ed.)**
1. Kolloquium des Sonderforschungsbereichs 261 der Universität Bremen (14.Juni 1991):
Der Südatlantik im Spätquartär: Rekonstruktion von Stoffhaushalt und Stromsystemen.
Kurzfassungen der Vorträge und Poster. 66 pages, Bremen, 1991.

No. 17 **Pätzold, J. and cruise participants**
Bericht und erste Ergebnisse über die METEOR-Fahrt M 15/2, Rio de Janeiro - Vitoria,
18.1. - 7.2.1991. 46 pages, Bremen, 1993.

No. 18 **Wefer, G. and cruise participants**
Bericht und erste Ergebnisse über die METEOR-Fahrt M 16/1, Pointe Noire - Recife,
27.3. - 25.4.1991. 120 pages, Bremen, 1991.

No. 19 **Schulz, H.D. and cruise participants**
Bericht und erste Ergebnisse über die METEOR-Fahrt M 16/2, Recife - Belem, 28.4. - 20.5.1991.
149 pages, Bremen, 1991.

No. 20 **Berner, H.**
Mechanismen der Sedimentbildung in der Fram-Straße, im Arktischen Ozean und in der Norwegischen See. 167 pages, Bremen, 1991.

No. 21 **Schneider, R.**
Spätquartäre Produktivitätsänderungen im östlichen Angola-Becken: Reaktion auf Variationen im Passat-Monsun-Windsystem und in der Advektion des Benguela-Küstenstroms.
198 pages, Bremen, 1991. (out of print)

No. 22 **Hebbeln, D.**
Spätquartäre Stratigraphie und Paläozeanographie in der Fram-Straße. 174 pages, Bremen, 1991.

No. 23 **Lücke, A.**
Umsetzungsprozesse organischer Substanz während der Frühdiagenese in ästuarinen Sedimenten.
137 pages, Bremen, 1991.

No. 24 **Wefer, G. and cruise participants**
Bericht und erste Ergebnisse der METEOR-Fahrt M 20/1, Bremen - Abidjan, 18.11.- 22.12.1991.
74 pages, Bremen, 1992.

No. 25 **Schulz, H.D. and cruise participants**
Bericht und erste Ergebnisse der METEOR-Fahrt M 20/2, Abidjan - Dakar, 27.12.1991 - 3.2.1992.
173 pages, Bremen, 1992.

No. 26 **Gingele, F.**
Zur klimaabhängigen Bildung biogener und terrigener Sedimente und ihrer Veränderung durch die Frühdiagenese im zentralen und östlichen Südatlantik. 202 pages, Bremen, 1992.

No. 27 **Bickert, T.**
Rekonstruktion der spätquartären Bodenwasserzirkulation im östlichen Südatlantik über stabile Isotope benthischer Foraminiferen. 205 pages, Bremen, 1992. (out of print)

No. 28 **Schmidt, H.**
Der Benguela-Strom im Bereich des Walfisch-Rückens im Spätquartär. 172 pages, Bremen, 1992.

No. 29 **Meinecke, G.**
Spätquartäre Oberflächenwassertemperaturen im östlichen äquatorialen Atlantik.
181 pages, Bremen, 1992.

No. 30 **Bathmann, U., U. Bleil, A. Dahmke, P. Müller, A. Nehrkorn, E.-M. Nöthig, M. Olesch, J. Pätzold, H.D. Schulz, V. Smetacek, V. Spieß, G. Wefer, H. Willems**
Bericht des Graduierten Kollegs. Stoff-Flüsse in marinen Geosystemen.
Berichtszeitraum Oktober 1990 - Dezember 1992. 396 pages, Bremen, 1992.

No. 31 **Damm, E.**
Frühdiagenetische Verteilung von Schwermetallen in Schlicksedimenten der westlichen Ostsee.
115 pages, Bremen, 1992.

No. 32 **Antia, E.E.**
Sedimentology, Morphodynamics and Facies Association of a mesotidal Barrier Island Shoreface (Spiekeroog, Southern North Sea). 370 pages, Bremen, 1993.

No. 33 **Duinker, J. and G. Wefer (ed.)**
Bericht über den 1. JGOFS-Workshop. 1./2. Dezember 1992 in Bremen. 83 pages, Bremen, 1993.

No. 34 **Kasten, S.**
Die Verteilung von Schwermetallen in den Sedimenten eines stadtbremischen Hafenbeckens.
103 pages, Bremen, 1993.

No. 35 **Spieß, V.**
Digitale Sedimentographie. Neue Wege zu einer hochauflösenden Akustostratigraphie.
199 pages, Bremen, 1993.

No. 36 **Schinzel, U.**
Laborversuche zu frühdiagenetischen Reaktionen von Eisen (III) - Oxidhydraten in marinen Sedimenten.189 pages, Bremen, 1993.

No. 37 **Sieger, R.**
CoTAM - ein Modell zur Modellierung des Schwermetalltransports in Grundwasserleitern.
56 pages, Bremen, 1993. (out of print)

No. 38 **Willems, H. (ed.)**
Geoscientific Investigations in the Tethyan Himalayas. 183 pages, Bremen, 1993.

No. 39 **Hamer, K.**
Entwicklung von Laborversuchen als Grundlage für die Modellierung des Transportverhaltens von Arsenat, Blei, Cadmium und Kupfer in wassergesättigten Säulen. 147 pages, Bremen, 1993.

No. 40 **Sieger, R.**
Modellierung des Stofftransports in porösen Medien unter Ankopplung kinetisch gesteuerter Sorptions- und Redoxprozesse sowie thermischer Gleichgewichte. 158 pages, Bremen, 1993.

No. 41 **Thießen, W.**
Magnetische Eigenschaften von Sedimenten des östlichen Südatlantiks und ihre paläozeanographische Relevanz. 170 pages, Bremen, 1993.

No. 42 **Spieß, V. and cruise participants**
Report and preliminary results of METEOR-Cruise M 23/1, Kapstadt - Rio de Janeiro, 4.-25.2.1993. 139 pages, Bremen, 1994.

No. 43 **Bleil, U. and cruise participants**
Report and preliminary results of METEOR-Cruise M 23/2, Rio de Janeiro - Recife, 27.2.-19.3.1993 133 pages, Bremen, 1994.

No. 44 **Wefer, G. and cruise participants**
Report and preliminary results of METEOR-Cruise M 23/3, Recife - Las Palmas, 21.3. - 12.4.1993 71 pages, Bremen, 1994.

No. 45 **Giese, M. and G. Wefer (ed.)**
Bericht über den 2. JGOFS-Workshop. 18../19. November 1993 in Bremen.
93 pages, Bremen, 1994.

No. 46 **Balzer, W. and cruise participants**
Report and preliminary results of METEOR-Cruise M 22/1, Hamburg - Recife, 22.9. - 21.10.1992.
24 pages, Bremen, 1994.

No. 47 **Stax, R.**
Zyklische Sedimentation von organischem Kohlenstoff in der Japan See: Anzeiger für Änderungen von Paläoozeanographie und Paläoklima im Spätkänozoikum.
150 pages, Bremen, 1994.

No. 48 **Skowronek, F.**
Frühdiagenetische Stoff-Flüsse gelöster Schwermetalle an der Oberfläche von Sedimenten des Weser Ästuares. 107 pages, Bremen, 1994.

No. 49 **Dersch-Hansmann, M.**
Zur Klimaentwicklung in Ostasien während der letzten 5 Millionen Jahre:
Terrigener Sedimenteintrag in die Japan See (ODP Ausfahrt 128). 149 pages, Bremen, 1994.

No. 50 **Zabel, M.**
Frühdiagenetische Stoff-Flüsse in Oberflächen-Sedimenten des äquatorialen und östlichen Südatlantik. 129 pages, Bremen, 1994.

No. 51 **Bleil, U. and cruise participants**
Report and preliminary results of SONNE-Cruise SO 86, Buenos Aires - Capetown, 22.4. - 31.5.93
116 pages, Bremen, 1994.

No. 52 **Symposium: The South Atlantic: Present and Past Circulation.**
Bremen, Germany, 15 - 19 August 1994. Abstracts. 167 pages, Bremen, 1994.

No. 53 **Kretzmann, U.B.**
^{57}Fe-Mössbauer-Spektroskopie an Sedimenten - Möglichkeiten und Grenzen.
183 pages, Bremen, 1994.

No. 54 **Bachmann, M.**
Die Karbonatrampe von Organyà im oberen Oberapt und unteren Unteralb (NE-Spanien, Prov. Lerida): Fazies, Zyklo- und Sequenzstratigraphie. 147 pages, Bremen, 1994. (out of print)

No. 55 **Kemle-von Mücke, S.**
Oberflächenwasserstruktur und -zirkulation des Südostatlantiks im Spätquartär.
151 pages, Bremen, 1994.

No. 56 **Petermann, H.**
Magnetotaktische Bakterien und ihre Magnetosome in Oberflächensedimenten des Südatlantiks.
134 pages, Bremen, 1994.

No. 57 **Mulitza, S.**
Spätquartäre Variationen der oberflächennahen Hydrographie im westlichen äquatorialen Atlantik.
97 pages, Bremen, 1994.

No. 58 **Segl, M. and cruise participants**
Report and preliminary results of METEOR-Cruise M 29/1, Buenos-Aires - Montevideo, 17.6. - 13.7.1994
94 pages, Bremen, 1994.

No. 59 **Bleil, U. and cruise participants**
Report and preliminary results of METEOR-Cruise M 29/2, Montevideo - Rio de Janiero
15.7. - 8.8.1994. 153 pages, Bremen, 1994.

No. 60 **Henrich, R. and cruise participants**
Report and preliminary results of METEOR-Cruise M 29/3, Rio de Janeiro - Las Palmas
11.8. - 5.9.1994. Bremen, 1994. (out of print)

No. 61 **Sagemann, J.**
Saisonale Variationen von Porenwasserprofilen, Nährstoff-Flüssen und Reaktionen in intertidalen Sedimenten des Weser-Ästuars. 110 pages, Bremen, 1994. (out of print)

No. 62 **Giese, M. and G. Wefer**
Bericht über den 3. JGOFS-Workshop. 5./6. Dezember 1994 in Bremen.
84 pages, Bremen, 1995.

No. 63 **Mann, U.**
Genese kretazischer Schwarzschiefer in Kolumbien: Globale vs. regionale/lokale Prozesse.
153 pages, Bremen, 1995. (out of print)

No. 64 **Willems, H., Wan X., Yin J., Dongdui L., Liu G., S. Dürr, K.-U. Gräfe**
The Mesozoic development of the N-Indian passive margin and of the Xigaze Forearc Basin in southern Tibet, China. – Excursion Guide to IGCP 362 Working-Group Meeting "Integrated Stratigraphy". 113 pages, Bremen, 1995. (out of print)

No. 65 **Hünken, U.**
Liefergebiets - Charakterisierung proterozoischer Goldseifen in Ghana anhand von Fluideinschluß - Untersuchungen. 270 pages, Bremen, 1995.

No. 66 **Nyandwi, N.**
The Nature of the Sediment Distribution Patterns in ther Spiekeroog Backbarrier Area, the East Frisian Islands. 162 pages, Bremen, 1995.

No. 67 **Isenbeck-Schröter, M.**
Transportverhalten von Schwermetallkationen und Oxoanionen in wassergesättigten Sanden. - Laborversuche in Säulen und ihre Modellierung -. 182 pages, Bremen, 1995.

No. 68 **Hebbeln, D. and cruise participants**
Report and preliminary results of SONNE-Cruise SO 102, Valparaiso - Valparaiso, 95.
134 pages, Bremen, 1995.

No. 69 **Willems, H. (Sprecher), U.Bathmann, U. Bleil, T. v. Dobeneck, K. Herterich, B.B. Jorgensen, E.-M. Nöthig, M. Olesch, J. Pätzold, H.D. Schulz, V. Smetacek, V. Speiß. G. Wefer**
Bericht des Graduierten-Kollegs Stoff-Flüsse in marine Geosystemen.
Berichtszeitraum Januar 1993 - Dezember 1995. 45 & 468 pages, Bremen, 1995.

No. 70 **Giese, M. and G. Wefer**
Bericht über den 4. JGOFS-Workshop. 20./21. November 1995 in Bremen. 60 pages, Bremen, 1996. (out of print)

No. 71 **Meggers, H.**
Pliozän-quartäre Karbonatsedimentation und Paläozeanographie des Nordatlantiks und des Europäischen Nordmeeres - Hinweise aus planktischen Foraminiferengemeinschaften.
143 pages, Bremen, 1996. (out of print)

No. 72 **Teske, A.**
Phylogenetische und ökologische Untersuchungen an Bakterien des oxidativen und reduktiven marinen Schwefelkreislaufs mittels ribosomaler RNA. 220 pages, Bremen, 1996. (out of print)

No. 73 **Andersen, N.**
Biogeochemische Charakterisierung von Sinkstoffen und Sedimenten aus ostatlantischen Produktions-Systemen mit Hilfe von Biomarkern. 215 pages, Bremen, 1996.

No. 74 **Treppke, U.**
Saisonalität im Diatomeen- und Silikoflagellatenfluß im östlichen tropischen und subtropischen Atlantik. 200 pages, Bremen, 1996.

No. 75 **Schüring, J.**
Die Verwendung von Steinkohlebergematerialien im Deponiebau im Hinblick auf die Pyritverwitterung und die Eignung als geochemische Barriere. 110 pages, Bremen, 1996.

No. 76 **Pätzold, J. and cruise participants**
Report and preliminary results of VICTOR HENSEN cruise JOPS II, Leg 6, Fortaleza - Recife, 10.3. - 26.3. 1995 and Leg 8, Vítoria - Vítoria, 10.4. - 23.4.1995.
87 pages, Bremen, 1996.

No. 77 **Bleil, U. and cruise participants**
Report and preliminary results of METEOR-Cruise M 34/1, Cape Town - Walvis Bay, 3.-26.1.1996.
129 pages, Bremen, 1996.

No. 78 **Schulz, H.D. and cruise participants**
Report and preliminary results of METEOR-Cruise M 34/2, Walvis Bay - Walvis Bay, 29.1.-18.2.96
133 pages, Bremen, 1996.

No. 79 **Wefer, G. and cruise participants**
Report and preliminary results of METEOR-Cruise M 34/3, Walvis Bay - Recife, 21.2.-17.3.1996.
168 pages, Bremen, 1996.

No. 80 **Fischer, G. and cruise participants**
Report and preliminary results of METEOR-Cruise M 34/4, Recife - Bridgetown, 19.3.-15.4.1996. 105 pages, Bremen, 1996.

No. 81 **Kulbrok, F.**
Biostratigraphie, Fazies und Sequenzstratigraphie einer Karbonatrampe in den Schichten der Oberkreide und des Alttertiärs Nordost-Ägyptens (Eastern Desert, N'Golf von Suez, Sinai). 153 pages, Bremen, 1996.

No. 82 **Kasten, S.**
Early Diagenetic Metal Enrichments in Marine Sediments as Documents of Nonsteady-State Depositional Conditions. Bremen, 1996.

No. 83 **Holmes, M.E.**
Reconstruction of Surface Ocean Nitrate Utilization in the Southeast Atlantic Ocean Based on Stable Nitrogen Isotopes. 113 pages, Bremen, 1996.

No. 84 **Rühlemann, C.**
Akkumulation von Carbonat und organischem Kohlenstoff im tropischen Atlantik: Spätquartäre Produktivitäts-Variationen und ihre Steuerungsmechanismen. 139 pages, Bremen, 1996.

No. 85 **Ratmeyer, V.**
Untersuchungen zum Eintrag und Transport lithogener und organischer partikulärer Substanz im östlichen subtropischen Nordatlantik. 154 pages, Bremen, 1996.

No. 86 **Cepek, M.**
Zeitliche und räumliche Variationen von Coccolithophoriden-Gemeinschaften im subtropischen Ost-Atlantik: Untersuchungen an Plankton, Sinkstoffen und Sedimenten. 156 pages, Bremen, 1996.

No. 87 **Otto, S.**
Die Bedeutung von gelöstem organischen Kohlenstoff (DOC) für den Kohlenstoffffluß im Ozean. 150 pages, Bremen, 1996.

No. 88 **Hensen, C.**
Frühdiagenetische Prozesse und Quantifizierung benthischer Stoff-Flüsse in Oberflächensedimenten des Südatlantiks. 132 pages, Bremen, 1996.

No. 89 **Giese, M. and G. Wefer**
Bericht über den 5. JGOFS-Workshop. 27./28. November 1996 in Bremen. 73 pages, Bremen, 1997.

No. 90 **Wefer, G. and cruise participants**
Report and preliminary results of METEOR-Cruise M 37/1, Lisbon - Las Palmas, 4.-23.12.1996. 79 pages, Bremen, 1997.

No. 91 **Isenbeck-Schröter, M., E. Bedbur, M. Kofod, B. König, T. Schramm & G. Mattheß**
Occurrence of Pesticide Residues in Water - Assessment of the Current Situation in Selected EU Countries. 65 pages, Bremen 1997.

No. 92 **Kühn, M.**
Geochemische Folgereaktionen bei der hydrogeothermalen Energiegewinnung. 129 pages, Bremen 1997.

No. 93 **Determann, S. & K. Herterich**
JGOFS-A6 "Daten und Modelle": Sammlung JGOFS-relevanter Modelle in Deutschland. 26 pages, Bremen, 1997.

No. 94 **Fischer, G. and cruise participants**
Report and preliminary results of METEOR-Cruise M 38/1, Las Palmas - Recife, 25.1.-1.3.1997, with Appendix: Core Descriptions from METEOR Cruise M 37/1. Bremen, 1997.

No. 95 **Bleil, U. and cruise participants**
Report and preliminary results of METEOR-Cruise M 38/2, Recife - Las Palmas, 4.3.-14.4.1997. 126 pages, Bremen, 1997.

No. 96 **Neuer, S. and cruise participants**
Report and preliminary results of VICTOR HENSEN-Cruise 96/1. Bremen, 1997.

No. 97 **Villinger, H. and cruise participants**
Fahrtbericht SO 111, 20.8. - 16.9.1996. 115 pages, Bremen, 1997.

No. 98 **Lüning, S.**
Late Cretaceous - Early Tertiary sequence stratigraphy, paleoecology and geodynamics of Eastern Sinai, Egypt. 218 pages, Bremen, 1997.

No. 99 **Haese, R.R.**
Beschreibung und Quantifizierung frühdiagenetischer Reaktionen des Eisens in Sedimenten des Südatlantiks. 118 pages, Bremen, 1997.

No. 100 **Lührte, R. von**
Verwertung von Bremer Baggergut als Material zur Oberflächenabdichtung von Deponien - Geochemisches Langzeitverhalten und Schwermetall-Mobilität (Cd, Cu, Ni, Pb, Zn). Bremen, 1997.

No. 101 **Ebert, M.**
Der Einfluß des Redoxmilieus auf die Mobilität von Chrom im durchströmten Aquifer.
135 pages, Bremen, 1997.

No. 102 **Krögel, F.**
Einfluß von Viskosität und Dichte des Seewassers auf Transport und Ablagerung von Wattsedimenten (Langeooger Rückseitenwatt, südliche Nordsee). 168 pages, Bremen, 1997.

No. 103 **Kerntopf, B.**
Dinoflagellate Distribution Patterns and Preservation in the Equatorial Atlantic and Offshore North-West Africa. 137 pages, Bremen, 1997.

No. 104 **Breitzke, M.**
Elastische Wellenausbreitung in marinen Sedimenten - Neue Entwicklungen der Ultraschall Sedimentphysik und Sedimentechographie. 298 pages, Bremen, 1997.

No. 105 **Marchant, M.**
Rezente und spätquartäre Sedimentation planktischer Foraminiferen im Peru-Chile Strom.
115 pages, Bremen, 1997.

No. 106 **Habicht, K.S.**
Sulfur isotope fractionation in marine sediments and bacterial cultures.
125 pages, Bremen, 1997.

No. 107 **Hamer, K., R.v. Lührte, G. Becker, T. Felis, S. Keffel, B. Strotmann, C. Waschkowitz, M. Kölling, M. Isenbeck-Schröter, H.D. Schulz**
Endbericht zum Forschungsvorhaben 060 des Landes Bremen: Baggergut der Hafengruppe Bremen-Stadt: Modelluntersuchungen zur Schwermetallmobilität und Möglichkeiten der Verwertung von Hafenschlick aus Bremischen Häfen. 98 pages, Bremen, 1997.

No. 108 **Greeff, O.W.**
Entwicklung und Erprobung eines benthischen Landersystemes zur *in situ*-Bestimmung von Sulfatreduktionsraten mariner Sedimente. 121 pages, Bremen, 1997.

No. 109 **Pätzold, M. und G. Wefer**
Bericht über den 6. JGOFS-Workshop am 4./5.12.1997 in Bremen. Im Anhang:
Publikationen zum deutschen Beitrag zur Joint Global Ocean Flux Study (JGOFS), Stand 1/1998.
122 pages, Bremen, 1998.

No. 110 **Landenberger, H.**
CoTReM, ein Multi-Komponenten Transport- und Reaktions-Modell. 142 pages, Bremen, 1998.

No. 111 **Villinger, H. und Fahrtteilnehmer**
Fahrtbericht SO 124, 4.10. - 16.10.199. 90 pages, Bremen, 1997.

No. 112 **Gietl, R.**
Biostratigraphie und Sedimentationsmuster einer nordostägyptischen Karbonatrampe unter Berücksichtigung der Alveolinen-Faunen. 142 pages, Bremen, 1998.

No. 113 **Ziebis, W.**
The Impact of the Thalassinidean Shrimp *Callianassa truncata* on the Geochemistry of permeable, coastal Sediments. 158 pages, Bremen 1998.

No. 114 **Schulz, H.D. and cruise participants**
Report and preliminary results of METEOR-Cruise M 41/1, Málaga - Libreville, 13.2.-15.3.1998.
Bremen, 1998.

No. 115 **Völker, D.J.**
Untersuchungen an strömungsbeeinflußten Sedimentationsmustern im Südozean. Interpretation sedimentechographischer Daten und numerische Modellierung. 152 pages, Bremen, 1998.

No. 116 **Schlünz, B.**
Riverine Organic Carbon Input into the Ocean in Relation to Late Quaternary Climate Change.
136 pages, Bremen, 1998.

No. 117 **Kuhnert, H.**
Aufzeichnug des Klimas vor Westaustralien in stabilen Isotopen in Korallenskeletten.
109 pages, Bremen, 1998.

No. 118 **Kirst, G.**
Rekonstruktion von Oberflächenwassertemperaturen im östlichen Südatlantik anhand von Alkenonen. 130 pages, Bremen, 1998.

No. 119 **Dürkoop, A.**
Der Brasil-Strom im Spätquartär: Rekonstruktion der oberflächennahen Hydrographie während der letzten 400 000 Jahre. 121 pages, Bremen, 1998.

No. 120 **Lamy, F.**
Spätquartäre Variationen des terrigenen Sedimenteintrags entlang des chilenischen Kontinentalhangs als Abbild von Klimavariabilität im Milanković- und Sub-Milanković-Zeitbereich.
141 pages, Bremen, 1998.

No. 121 **Neuer, S. and cruise participants**
Report and preliminary results of POSEIDON-Cruise Pos 237/2, Vigo – Las Palmas, 18.3.-31.3.1998. 39 pages, Bremen, 1998

No. 122 **Romero, O.E.**
Marine planktonic diatoms from the tropical and equatorial Atlantic: temporal flux patterns and the sediment record. 205 pages, Bremen, 1998.

No. 123 **Spiess, V. und Fahrtteilnehmer**
Report and preliminary results of RV SONNE Cruise 125, Cochin – Chittagong, 17.10.-17.11.1997. 128 pages, Bremen, 1998.

No. 124 **Arz, H.W.**
Dokumentation von kurzfristigen Klimaschwankungen des Spätquartärs in Sedimenten des westlichen äquatorialen Atlantiks. 96 pages, Bremen, 1998.

No. 125 **Wolff, T.**
Mixed layer characteristics in the equatorial Atlantic during the late Quaternary as deduced from planktonic foraminifera. 132 pages, Bremen, 1998.

No. 126 **Dittert, N.**
Late Quaternary Planktic Foraminifera Assemblages in the South Atlantic Ocean: Quantitative Determination and Preservational Aspects. 165 pages, Bremen, 1998.

No. 127 **Höll, C.**
Kalkige und organisch-wandige Dinoflagellaten-Zysten in Spätquartären Sedimenten des tropischen Atlantiks und ihre palökologische Auswertbarkeit. 121 pages, Bremen, 1998.

No. 128 **Hencke, J.**
Redoxreaktionen im Grundwasser: Etablierung und Verlagerung von Reaktionsfronten und ihre Bedeutung für die Spurenelement-Mobilität. 122 pages, Bremen 1998.

No. 129 **Pätzold, J. and cruise participants**
Report and preliminary results of METEOR-Cruise M 41/3, Vítoria, Brasil – Salvador de Bahia, Brasil, 18.4. - 15.5.1998. Bremen, 1999.

No. 130 **Fischer, G. and cruise participants**
Report and preliminary results of METEOR-Cruise M 41/4, Salvador de Bahia, Brasil – Las Palmas, Spain, 18.5. – 13.6.1998. Bremen, 1999.

No. 131 **Schlünz, B. und G. Wefer**
Bericht über den 7. JGOFS-Workshop am 3. und 4.12.1998 in Bremen. Im Anhang: Publikationen zum deutschen Beitrag zur Joint Global Ocean Flux Study (JGOFS), Stand 1/ 1999. 100 pages, Bremen, 1999.

No. 132 **Wefer, G. and cruise participants**
Report and preliminary results of METEOR-Cruise M 42/4, Las Palmas - Las Palmas - Viena do Castelo; 26.09.1998 - 26.10.1998. 104 pages, Bremen, 1999.

No. 133 **Felis, T.**
Climate and ocean variability reconstructed from stable isotope records of modern subtropical corals (Northern Red Sea). 111 pages, Bremen, 1999.

No. 134 **Draschba , S.**
North Atlantic climate variability recorded in reef corals from Bermuda. 108 pages, Bremen, 1999.

No. 135 **Schmieder, F.**
Magnetic Cyclostratigraphy of South Atlantic Sediments. 82 pages, Bremen, 1999.

No. 136 **Rieß, W.**
In situ measurements of respiration and mineralisation processes – Interaction between fauna and geochemical fluxes at active interfaces. 68 pages, Bremen, 1999.

No. 137 **Devey, C.W. and cruise participants**
Report and shipboard results from METEOR-cruise M 41/2, Libreville – Vitoria, 18.3. – 15.4.98. 59 pages, Bremen, 1999.

No. 138 **Wenzhöfer, F.**
Biogeochemical processes at the sediment water interface and quantification of metabolically driven calcite dissolution in deep sea sediments. 103 pages, Bremen, 1999.

No. 139 **Klump, J.**
Biogenic barite as a proxy of paleoproductivity variations in the Southern Peru-Chile Current. 107 pages, Bremen, 1999.

No. 140 **Huber, R.**
Carbonate sedimentation in the northern Northatlantic since the late pliocene. 103 pages, Bremen, 1999.

No. 141 **Schulz, H.**
Nitrate-storing sulfur bacteria in sediments of coastal upwelling. 94 pages, Bremen, 1999.

No. 142 **Mai, S.**
Die Sedimentverteilung im Wattenmeer: ein Simulationsmodell. 114 pages, Bremen, 1999.

No. 143 **Neuer, S. and cruise participants**
Report and preliminary results of Poseidon Cruise 248, Las Palmas - Las Palmas, 15.2.-26.2.1999. 45 pages, Bremen, 1999.

No. 144 **Weber, A.**
Schwefelkreislauf in marinen Sedimenten und Messung von in situ Sulfatreduktionsraten. 122 pages, Bremen, 1999.

No. 145 **Hadeler, A.**
Sorptionsreaktionen im Grundwasser: Unterschiedliche Aspekte bei der Modellierung des Transportverhaltens von Zink. 122 pages, 1999.

No. 146 **Dierßen, H.**
Zum Kreislauf ausgewählter Spurenmetalle im Südatlantik: Vertikaltransport und Wechselwirkung zwischen Partikeln und Lösung. 167 pages, Bremen, 1999.

No. 147 **Zühlsdorff, L.**
High resolution multi-frequency seismic surveys at the Eastern Juan de Fuca Ridge Flank and the Cascadia Margin – Evidence for thermally and tectonically driven fluid upflow in marine sediments. 118 pages, Bremen 1999.

No. 148 **Kinkel, H.**
Living and late Quaternary Coccolithophores in the equatorial Atlantic Ocean: response of distribution and productivity patterns to changing surface water circulation. 183 pages, Bremen, 2000.

No. 149 **Pätzold, J. and cruise participants**
Report and preliminary results of METEOR Cruise M 44/3, Aqaba (Jordan) - Safaga (Egypt) – Dubá (Saudi Arabia) – Suez (Egypt) - Haifa (Israel), 12.3.-26.3.-2.4.-4.4.1999. 135 pages, Bremen, 2000.

No. 150 **Schlünz, B. and G. Wefer**
Bericht über den 8. JGOFS-Workshop am 2. und 3.12.1999 in Bremen. Im Anhang: Publikationen zum deutschen Beitrag zur Joint Global Ocean Flux Study (JGOFS), Stand 1/ 2000. 95 pages, Bremen, 2000.

No. 151 **Schnack, K.**
Biostratigraphie und fazielle Entwicklung in der Oberkreide und im Alttertiär im Bereich der Kharga Schwelle, Westliche Wüste, SW-Ägypten. 142 pages, Bremen, 2000.

No. 152 **Karwath, B.**
Ecological studies on living and fossil calcareous dinoflagellates of the equatorial and tropical Atlantic Ocean. 175 pages, Bremen, 2000.

No. 153 **Moustafa, Y.**
Paleoclimatic reconstructions of the Northern Red Sea during the Holocene inferred from stable isotope records of modern and fossil corals and molluscs. 102 pages, Bremen, 2000.

No. 154 **Villinger, H. and cruise participants**
Report and preliminary results of SONNE-cruise 145-1 Balboa – Talcahuana, 21.12.1999 – 28.01.2000. 147 pages, Bremen, 2000.

No. 155 **Rusch, A.**
Dynamik der Feinfraktion im Oberflächenhorizont permeabler Schelfsedimente. 102 pages, Bremen, 2000.

No. 156 **Moos, C.**
Reconstruction of upwelling intensity and paleo-nutrient gradients in the northwest Arabian Sea derived from stable carbon and oxygen isotopes of planktic foraminifera. 103 pages, Bremen, 2000.

No. 157 **Xu, W.**
Mass physical sediment properties and trends in a Wadden Sea tidal basin. 127 pages, Bremen, 2000.

No. 158 **Meinecke, G. and cruise participants**
Report and preliminary results of METEOR Cruise M 45/1, Malaga (Spain) - Lissabon (Portugal), 19.05. - 08.06.1999. 39 pages, Bremen, 2000.

No. 159 **Vink, A.**
Reconstruction of recent and late Quaternary surface water masses of the western subtropical Atlantic Ocean based on calcareous and organic-walled dinoflagellate cysts. 160 pages, Bremen, 2000.

No. 160 **Willems, H. (Sprecher), U. Bleil, R. Henrich, K. Herterich, B.B. Jørgensen, H.-J. Kuß, M. Olesch, H.D. Schulz,V. Spieß, G. Wefer**
Abschlußbericht des Graduierten-Kollegs Stoff-Flüsse in marine Geosystemen. Zusammenfassung und Berichtszeitraum Januar 1996 - Dezember 2000. 340 pages, Bremen, 2000.

No. 161 **Sprengel, C.**
Untersuchungen zur Sedimentation und Ökologie von Coccolithophoriden im Bereich der Kanarischen Inseln: Saisonale Flussmuster und Karbonatexport. 165 pages, Bremen, 2000.

No. 162 **Donner, B. and G. Wefer**
Bericht über den JGOFS-Workshop am 18.-21.9.2000 in Bremen: Biogeochemical Cycles: German Contributions to the International Joint Global Ocean Flux Study. 87 pages, Bremen, 2000.

No. 163 **Neuer, S. and cruise participants**
Report and preliminary results of Meteor Cruise M 45/5, Bremen – Las Palmas, October 1 – November 3, 1999. 93 pages, Bremen, 2000.

No. 164 **Devey, C. and cruise participants**
Report and preliminary results of Sonne Cruise SO 145/2, Talcahuano (Chile) - Arica (Chile), February 4 – February 29, 2000. 63 pages, Bremen, 2000.

No. 165 **Freudenthal, T.**
Reconstruction of productivity gradients in the Canary Islands region off Morocco by means of sinking particles and sediments. 147 pages, Bremen, 2000.

No. 166 **Adler, M.**
Modeling of one-dimensional transport in porous media with respect to simultaneous geochemical reactions in CoTReM. 147 pages, Bremen, 2000.

No. 167 **Santamarina Cuneo, P.**
Fluxes of suspended particulate matter through a tidal inlet of the East Frisian Wadden Sea (southern North Sea). 91 pages, Bremen, 2000.

No. 168 **Benthien, A.**
Effects of CO2 and nutrient concentration on the stable carbon isotope composition of C37:2 alkenones in sediments of the South Atlantic Ocean. 104 pages, Bremen, 2001.

No. 169 **Lavik, G.**
Nitrogen isotopes of sinking matter and sediments in the South Atlantic. 140 pages, Bremen, 2001.

No. 170 **Budziak, D.**
Late Quaternary monsoonal climate and related variations in paleoproductivity and alkenone-derived sea-surface temperatures in the western Arabian Sea. 114 pages, Bremen, 2001.

No. 171 **Gerhardt, S.**
Late Quaternary water mass variability derived from the pteropod preservation state in sediments of the western South Atlantic Ocean and the Caribbean Sea. 109 pages, Bremen, 2001.

No. 172 **Bleil, U. and cruise participants**
Report and preliminary results of Meteor Cruise M 46/3, Montevideo (Uruguay) – Mar del Plata (Argentina), January 4 – February 7, 2000. Bremen, 2001.

No. 173 **Wefer, G. and cruise participants**
Report and preliminary results of Meteor Cruise M 46/4, Mar del Plata (Argentina) – Salvador da Bahia (Brazil), February 10 – March 13, 2000. With partial results of METEOR cruise M 46/2. 136 pages, Bremen, 2001.

No. 174 **Schulz, H.D. and cruise participants**
Report and preliminary results of Meteor Cruise M 46/2, Recife (Brazil) – Montevideo (Uruguay), December 2 – December 29, 1999. 107 pages, Bremen, 2001.

No. 175 **Schmidt, A.**
Magnetic mineral fluxes in the Quaternary South Atlantic: Implications for the paleoenvironment. 97 pages, Bremen, 2001.

No. 176 **Bruhns, P.**
Crystal chemical characterization of heavy metal incorporation in brick burning processes. 93 pages, Bremen, 2001.

No. 177 **Karius, V.**
Baggergut der Hafengruppe Bremen-Stadt in der Ziegelherstellung. 131 pages, Bremen, 2001.

No. 178 **Adegbie, A. T.**
Reconstruction of paleoenvironmental conditions in Equatorial Atlantic and the Gulf of Guinea Basins for the last 245,000 years. 113 pages, Bremen, 2001.

No. 179 **Spieß, V. and cruise participants**
Report and preliminary results of R/V Sonne Cruise SO 149, Victoria - Victoria, 16.8. - 16.9.2000. 100 pages, Bremen, 2001.

No. 180 **Kim, J.-H.**
Reconstruction of past sea-surface temperatures in the eastern South Atlantic and the eastern South Pacific across Termination I based on the Alkenone Method. 114 pages, Bremen, 2001.

No. 181 **von Lom-Keil, H.**
Sedimentary waves on the Namibian continental margin and in the Argentine Basin – Bottom flow reconstructions based on high resolution echosounder data. 126 pages, Bremen, 2001.

No. 182 **Hebbeln, D. and cruise participants**
PUCK: Report and preliminary results of R/V Sonne Cruise SO 156, Valparaiso (Chile) - Talcahuano (Chile), March 29 - May 14, 2001. 195 pages, Bremen, 2001.

No. 183 **Wendler, J.**
Reconstruction of astronomically-forced cyclic and abrupt paleoecological changes in the Upper Cretaceous Boreal Realm based on calcareous dinoflagellate cysts. 149 pages, Bremen, 2001.

No. 184 **Volbers, A.**
Planktic foraminifera as paleoceanographic indicators: production, preservation, and reconstruction of upwelling intensity. Implications from late Quaternary South Atlantic sediments. 122 pages, Bremen, 2001.

No. 185 **Bleil, U. and cruise participants**
Report and preliminary results of R/V METEOR Cruise M 49/3, Montevideo (Uruguay) - Salvador (Brasil), March 9 - April 1, 2001. 99 pages, Bremen, 2001.

No. 186 **Scheibner, C.**
Architecture of a carbonate platform-to-basin transition on a structural high (Campanian-early Eocene, Eastern Desert, Egypt) – classical and modelling approaches combined. 173 pages, Bremen, 2001.

No. 187 **Schneider, S.**
Quartäre Schwankungen in Strömungsintensität und Produktivität als Abbild der Wassermassen-Variabilität im äquatorialen Atlantik (ODP Sites 959 und 663): Ergebnisse aus Siltkorn-Analysen. 134 pages, Bremen, 2001.

No. 188 **Uliana, E.**
Late Quaternary biogenic opal sedimentation in diatom assemblages in Kongo Fan sediments. 96 pages, Bremen, 2002.

No. 189 **Esper, O.**
Reconstruction of Recent and Late Quaternary oceanographic conditions in the eastern South Atlantic Ocean based on calcareous- and organic-walled dinoflagellate cysts. 130 pages, Bremen, 2001.

No. 190 **Wendler, I.**
Production and preservation of calcareous dinoflagellate cysts in the modern Arabian Sea. 117 pages, Bremen, 2002.

No. 191 **Bauer, J.**
Late Cenomanian – Santonian carbonate platform evolution of Sinai (Egypt): stratigraphy, facies, and sequence architecture. 178 pages, Bremen, 2002.

No. 192 **Hildebrand-Habel, T.**
Die Entwicklung kalkiger Dinoflagellaten im Südatlantik seit der höheren Oberkreide. 152 pages, Bremen, 2002.

No. 193 **Hecht, H.**
Sauerstoff-Optopoden zur Quantifizierung von Pyritverwitterungsprozessen im Labor- und Langzeit-in-situ-Einsatz. Entwicklung - Anwendung – Modellierung. 130 pages, Bremen, 2002.

No. 194 **Fischer, G. and cruise participants**
Report and Preliminary Results of RV METEOR-Cruise M49/4, Salvador da Bahia – Halifax, 4.4.-5.5.2001. 84 pages, Bremen, 2002.

No. 195 **Gröger, M.**
Deep-water circulation in the western equatorial Atlantic: inferences from carbonate preservation studies and silt grain-size analysis. 95 pages, Bremen, 2002.

No. 196 **Meinecke,G. and cruise participants**
Report of RV POSEIDON Cruise POS 271, Las Palmas - Las Palmas, 19.3.-29.3.2001. 19 pages, Bremen, 2002.

No. 197 **Meggers, H. and cruise participants**
Report of RV POSEIDON Cruise POS 272, Las Palmas - Las Palmas, 1.4.-14.4.2001. 19 pages, Bremen, 2002.

No. 198 **Gräfe, K.-U.**
Stratigraphische Korrelation und Steuerungsfaktoren Sedimentärer Zyklen in ausgewählten Borealen und Tethyalen Becken des Cenoman/Turon (Oberkreide) Europas und Nordwestafrikas. 197 pages, Bremen, 2002.

No. 199 **Jahn, B.**
Mid to Late Pleistocene Variations of Marine Productivity in and Terrigenous Input to the Southeast Atlantic. 97 pages, Bremen, 2002.

No. 200 **Al-Rousan, S.**
Ocean and climate history recorded in stable isotopes of coral and foraminifers from the northern Gulf of Aqaba. 116 pages, Bremen, 2002.

No. 201 **Azouzi, B.**
Regionalisierung hydraulischer und hydrogeochemischer Daten mit geostatistischen Methoden. 108 pages, Bremen, 2002.

No. 202 **Spieß, V. and cruise participants**
Report and preliminary results of METEOR Cruise M 47/3, Libreville (Gabun) - Walvis Bay (Namibia), 01.06 - 03.07.2000. 70 pages, Bremen 2002.

No. 203 **Spieß, V. and cruise participants**
Report and preliminary results of METEOR Cruise M 49/2, Montevideo (Uruguay) - Montevideo, 13.02 - 07.03.2001. 84 pages, Bremen 2002.

No. 204 **Mollenhauer, G.**
Organic carbon accumulation in the South Atlantic Ocean: Sedimentary processes and glacial/interglacial Budgets. 139 pages, Bremen 2002.

No. 205 **Spieß, V. and cruise participants**
Report and preliminary results of METEOR Cruise M49/1, Cape Town (South Africa) - Montevideo (Uruguay), 04.01.2001 - 10.02.2001. 57 pages, Bremen, 2003.

No. 206 **Meier, K.J.S.**
Calcareous dinoflagellates from the Mediterranean Sea: taxonomy, ecology and palaeoenvironmental application. 126 pages, Bremen, 2003.

No. 207 **Rakic, S.**
Untersuchungen zur Polymorphie und Kristallchemie von Silikaten der Zusammensetzung $Me_2Si_2O_5$ (Me:Na, K). 139 pages, Bremen, 2003.

No. 208 **Pfeifer, K.**
Auswirkungen frühdiagenetischer Prozesse auf Calcit- und Barytgehalte in marinen Oberflächen-sedimenten. 110 pages, Bremen, 2003.

No. 209 **Heuer, V.**
Spurenelemente in Sedimenten des Südatlantik. Primärer Eintrag und frühdiagenetische Überprägung. 136 pages, Bremen, 2003.

No. 210 **Streng, M.**
Phylogenetic Aspects and Taxonomy of Calcareous Dinoflagellates. 157 pages, Bremen 2003.

No. 211 **Boeckel, B.**
Present and past coccolith assemblages in the South Atlantic: implications for species ecology, carbonate contribution and palaeoceanographic applicability. 157 pages, Bremen, 2003.

No. 212 **Precht, E.**
Advective interfacial exchange in permeable sediments driven by surface gravity waves and its ecological consequences. 131 pages, Bremen, 2003.

No. 213 **Frenz, M.**
Grain-size composition of Quaternary South Atlantic sediments and its paleoceanographic significance. 123 pages, Bremen, 2003.

No. 214 **Meggers, H. and cruise participants**
Report and preliminary results of METEOR Cruise M 53/1, Limassol - Las Palmas – Mindelo, 30.03.2002 - 03.05.2002. 81 pages, Bremen, 2003.

No. 215 **Schulz, H.D. and cruise participants**
Report and preliminary results of METEOR Cruise M 58/1, Dakar – Las Palmas, 15.04..2003 – 12.05.2003. Bremen, 2003.

No. 216 **Schneider, R. and cruise participants**
Report and preliminary results of METEOR Cruise M 57/1, Cape Town – Walvis Bay, 20.01. – 08.02.2003. 123 pages, Bremen, 2003.

No. 217 **Kallmeyer, J.**
Sulfate reduction in the deep Biosphere. 157 pages, Bremen, 2003.

No. 218 **Røy, H.**
Dynamic Structure and Function of the Diffusive Boundary Layer at the Seafloor. 149 pages, Bremen, 2003.

No. 219 **Pätzold, J., C. Hübscher and cruise participants**
Report and preliminary results of METEOR Cruise M 52/2&3, Istanbul – Limassol – Limassol, 04.02. – 27.03.2002. Bremen, 2003.

No. 220 **Zabel, M. and cruise participants**
Report and preliminary results of METEOR Cruise M 57/2, Walvis Bay – Walvis Bay, 11.02. – 12.03.2003. 136 pages, Bremen 2003.

No. 221 **Salem, M.**
Geophysical investigations of submarine prolongations of alluvial fans on the western side of the Gulf of Aqaba-Red Sea. 100 pages, Bremen, 2003.

No. 222 **Tilch, E.**
Oszillation von Wattflächen und deren fossiles Erhaltungspotential (Spiekerooger Rückseitenwatt, südliche Nordsee). 137 pages, Bremen, 2003.

No. 223 **Frisch, U. and F. Kockel**
Der Bremen-Knoten im Strukturnetz Nordwest-Deutschlands. Stratigraphie, Paläogeographie, Strukturgeologie. 379 pages, Bremen, 2004.

No. 224 **Kolonic, S.**
Mechanisms and biogeochemical implications of Cenomanian/Turonian black shale formation in North Africa: An integrated geochemical, millennial-scale study from the Tarfaya-LaAyoune Basin in SW Morocco. 174 pages, Bremen, 2004. Report online available only.

No. 225 **Panteleit, B.**
Geochemische Prozesse in der Salz- Süßwasser Übergangszone. 106 pages, Bremen, 2004.

No. 226 **Seiter, K.**
Regionalisierung und Quantifizierung benthischer Mineralisationsprozesse. 135 pages, Bremen, 2004.

No. 227 **Bleil, U. and cruise participants**
Report and preliminary results of METEOR Cruise M 58/2, Las Palmas – Las Palmas (Canary Islands, Spain), 15.05. – 08.06.2003. 123 pages, Bremen, 2004.

No. 228 **Kopf, A. and cruise participants**
Report and preliminary results of SONNE Cruise SO175, Miami - Bremerhaven, 12.11 - 30.12.2003. 218 pages, Bremen, 2004.

No. 229 **Fabian, M.**
Near Surface Tilt and Pore Pressure Changes Induced by Pumping in Multi-Layered Poroelastic Half-Spaces. 121 pages, Bremen, 2004.

No. 230 **Segl, M. , and cruise participants**
Report and preliminary results of POSEIDON cruise 304 Galway – Lisbon, 5. – 22. Oct. 2004. 27 pages, Bremen 2004

No. 231 **Meinecke, G. and cruise participants**
Report and preliminary results of POSEIDON Cruise 296, Las Palmas – Las Palmas, 04.04 – 14.04.2003. 42 pages, Bremen 2005.

No. 232 **Meinecke, G. and cruise participants**
Report and preliminary results of POSEIDON Cruise 310, Las Palmas – Las Palmas, 12.04 – 26.04.2004. 49 pages, Bremen 2005.

No. 233 **Meinecke, G. and cruise participants**
Report and preliminary results of METEOR Cruise 58/3, Las Palmas - Ponta Delgada, 11.06 - 24.06.2003.
50 pages, Bremen 2005.

No. 234 **Feseker, T.**
Numerical Studies on Groundwater Flow in Coastal Aquifers. 219 pages. Bremen 2004.

No. 235 **Sahling, H. and cruise participants**
Report and preliminary results of R/V POSEIDON Cruise P317/4, Istanbul-Istanbul , 16 October - 4 November 2004. 92 pages, Bremen 2004.

No. 236 **Meinecke, G. und Fahrtteilnehmer**
Report and preliminary results of POSEIDON Cruise 305, Las Palmas (Spain) - Lisbon (Portugal), October 28th – November 6th, 2004. 43 pages, Bremen 2005.

No. 237 **Ruhland, G. and cruise participants**
Report and preliminary results of POSEIDON Cruise 319, Las Palmas (Spain) - Las Palmas (Spain), December 6th – December 17th, 2004. 50 pages, Bremen 2005.

No. 238 **Chang, T.S.**
Dynamics of fine-grained sediments and stratigraphic evolution of a back-barrier tidal basin of the German Wadden Sea (southern North Sea). 102 pages, Bremen 2005.

No. 239 **Lager, T.**
Predicting the source strength of recycling materials within the scope of a seepage water prognosis by means of standardized laboratory methods. 141 pages, Bremen 2005.

No. 240 **Meinecke, G.**
DOLAN - Operationelle Datenübertragung im Ozean und Laterales Akustisches Netzwerk in der Tiefsee. Abschlußbericht. 42 pages, Bremen 2005.

No. 241 **Guasti, E.**
Early Paleogene environmental turnover in the southern Tethys as recorded by foraminiferal and organic-walled dinoflagellate cysts assemblages. 203 pages, Bremen 2005.

No. 242 **Riedinger, N.**
Preservation and diagenetic overprint of geochemical and geophysical signals in ocean margin sediments related to depositional dynamics. 91 pages, Bremen 2005.

No. 243 **Ruhland, G. and cruise participants**
Report and preliminary results of POSEIDON cruise 320, Las Palmas (Spain) - Las Palmas (Spain), March 08th - March 18th, 2005. 57 pages, Bremen 2005.

No. 244 **Inthorn, M.**
Lateral particle transport in nepheloid layers – a key factor for organic matter distribution and quality in the Benguela high-productivity area. 127 pages, Bremen, 2006.

No. 245 **Aspetsberger, F.**
Benthic carbon turnover in continental slope and deep sea sediments: importance of organic matter quality at different time scales. 136 pages, Bremen, 2006.

No. 246 **Hebbeln, D. and cruise participants**
Report and preliminary results of RV SONNE Cruise SO-184, PABESIA, Durban (South Africa) – Cilacap (Indonesia) – Darwin (Australia), July 08th - September 13th, 2005. 142 pages, Bremen 2006.

No. 247 **Ratmeyer, V. and cruise participants**
Report and preliminary results of RV METEOR Cruise M61/3. Development of Carbonate Mounds on the Celtic Continental Margin, Northeast Atlantic. Cork (Ireland) – Ponta Delgada (Portugal), 04.06. – 21.06.2004. 64 pages, Bremen 2006.

No. 248 **Wien, K.**
Element Stratigraphy and Age Models for Pelagites and Gravity Mass Flow Deposits based on Shipboard XRF Analysis. 100 pages, Bremen 2006.

No. 249 **Krastel, S. and cruise participants**
Report and preliminary results of RV METEOR Cruise M65/2, Dakar - Las Palmas, 04.07. – 26.07.2005. 185 pages, Bremen 2006.

No. 250 **Heil, G.M.N.**
Abrupt Climate Shifts in the Western Tropical to Subtropical Atlantic Region during the Last Glacial. 121 pages, Bremen 2006.

No. 251 **Ruhland, G. and cruise participants**
Report and preliminary results of POSEIDON Cruise 330, Las Palmas – Las Palmas, November 21th – December 03rd, 2005. 48 pages, Bremen 2006.

No. 252 **Mulitza , S. and cruise participants**
Report and preliminary results of METEOR Cruise M65/1, Dakar – Dakar, 11.06.- 1.07.2005. 149 pages, Bremen 2006.

No. 253 **Kopf, A. and cruise participants**
Report and preliminary results of POSEIDON Cruise P336, Heraklion - Heraklion, 28.04. – 17.05.2006. 127 pages, Bremen, 2006.

No. 254 **Wefer, G. and cruise participants**
Report and preliminary results of R/V METEOR Cruise M65/3, Las Palmas - Las Palmas (Spain), July 31st - August 10th, 2005. 24 pages, Bremen 2006.

No. 255 **Hanebuth, T.J.J. and cruise participants**
Report and first results of the POSEIDON Cruise P342 GALIOMAR, Vigo – Lisboa (Portugal), August 19th – September 06th, 2006. Distribution Pattern, Residence Times and Export of Sediments on the Pleistocene/Holocene Galician Shelf (NW Iberian Peninsula). 203 pages, Bremen, 2007.

No. 256 **Ahke, A.**
Composition of molecular organic matter pools, pigments and proteins, in Benguela upwelling and Arctic Sediments. 192 pages, Bremen 2007.

No. 257 **Becker, V.**
Seeper - Ein Modell für die Praxis der Sickerwasserprognose. 170 pages, Bremen 2007.

No. 258 **Ruhland, G. and cruise participants**
Report and preliminary results of Poseidon cruise 333, Las Palmas (Spain) – Las Palmas (Spain), March 1st – March 10th, 2006. 32 pages, Bremen 2007.

No. 259 **Fischer, G., G. Ruhland and cruise participants**
Report and preliminary results of Poseidon cruise 344, leg 1 and leg 2, Las Palmas (Spain) – Las Palmas (Spain), Oct. 20th –Nov 2nd & Nov. 4th – Nov 13th, 2006. 46 pages, Bremen 2007.

No. 260 **Westphal, H. and cruise participants**
Report and preliminary results of Poseidon cruise 346, MACUMA. Las Palmas (Spain) – Las Palmas (Spain), 28.12.2006 – 15.1.2007. 49 pages, Bremen 2007.

No. 261 **Bohrmann, G., T. Pape, and cruise participants**
Report and preliminary results of R/V METEOR Cruise M72/3, Istanbul – Trabzon – Istanbul, March 17th – April 23rd, 2007. Marine gas hydrates of the Eastern Black Sea. 130 pages, Bremen 2007.

No. 262 **Bohrmann, G., and cruise participants**
Report and preliminary results of R/V METEOR Cruise M70/3, Iraklion – Iraklion, 21 November – 8 December 2006. Cold Seeps of the Anaximander Mountains / Eastern Mediterranean. 75 pages, Bremen 2008.

No. 263 **Bohrmann, G., Spiess, V., and cruise participants**
Report and preliminary results of R/V Meteor Cruise M67/2a and 2b, Balboa -- Tampico -- Bridgetown, 15 March -- 24 April, 2006. Fluid seepage in the Gulf of Mexico. Bremen 2008.

No. 264 **Kopf, A., and cruise participants**
Report and preliminary results of Meteor Cruise M73/1: LIMA-LAMO (Ligurian Margin Landslide Measurements & Observatory), Cadiz, 22.07.2007 – Genoa, 11.08.2007. 170 pages, Bremen 2008.

No. 265 **Hebbeln, D., and cruise participants**
Report and preliminary results of RV Pelagia Cruise 64PE284. Cold-water Corals in the Gulf of Cádiz and on Coral Patch Seamount (NE Atlantic). Portimão - Portimão, 18.02. - 09.03.2008. 90 pages, Bremen 2008.

No. 266 **Bohrmann, G., and cruise participants**
Report and preliminary results of R/V Meteor Cruise M74/3, Fujairah – Male, 30 October - 28 November, 2007. Cold Seeps of the Makran subduction zone (Continental margin of Pakistan). 161 pages, Bremen 2008.